SYNTHESIS AND CHARACTERIZATION OF GROUP-13-BRIDGED [1]- AND [1.1]METALLACYCLOPHANES

A Thesis Submitted to the College of

Graduate Studies and Research

in Partial Fulfillment of the Requirements

for the Degree of Doctor of Philosophy

in the Department of Chemistry

University of Saskatchewan

Saskatoon

By

CLINTON LUND

© Copyright Clinton Laine Lund, October, 2008. All rights reserved.

Permission to Use

In presenting this thesis in partial fulfilment of the requirements for a Postgraduate degree from the University of Saskatchewan, I agree that the Libraries of this University may make it freely available for inspection. I further agree that permission for copying of this thesis in any manner, in whole or in part, for scholarly purposes may be granted by the professor or professors who supervised my thesis work or, in their absence, by the Head of the Department or the Dean of the College in which my thesis work was done. It is understood that any copying or publication or use of this thesis or parts thereof for financial gain shall not be allowed without my written permission. It is also understood that due recognition shall be given to me and to the University of Saskatchewan in any scholarly use which may be made of any material in my thesis.

Requests for permission to copy or to make other use of material in this thesis in whole or part should be addressed to:

Head of the Department of Chemistry

University of Saskatchewan

Saskatoon, Saskatchewan (S7N 5C9)

Canada

ABSTRACT

The synthesis and characterization of the first aluminum- and gallium-bridged [1]chromarenophanes, [1]vanadarenophanes and [1]molybdarenophanes are described; these compounds belong to a class of compounds referred to as [1]metallacyclophanes. [1]Metallacyclophanes are strained, ring-tilted complexes that have a propensity to undergo ring-opening polymerizations (ROPs). On the basis of using bulky, intramolecularly coordinating ligands, the [1]metallacyclophanes described within have been synthesized and characterized. By exploring known transition-metal catalyzed ROP methodologies, a serendipitous discovery has been made. The gallium-bridged [1]molybdarenophane undergoes ring-opening reactions catalyzed by σ donors such as thf and PEt_3 or by π donors such as 1,5-cyclooctadiene. Known transition-metal catalyzed ROP methodologies proved to be unsuccessful with the aluminum- and gallium-bridged [1]metallarenophanes, possibly due to steric overprotection.

The synthesis and characterization of the first [1.1]metallarenophanes is described. By utilizing ligands with dimethylamine-donor functionalities, aluminum- and gallium-bridged unstrained [1.1]chromarenophanes and [1.1]molybdarenophanes have been isolated. Gallium-bridged [1.1]metallarenophanes have been determined to be Class II compounds through investigations by cyclic voltammetry. Aluminum-bridged [1.1]metallarenophanes can not be successfully characterized by electrochemical measurements because of their acute sensitivity towards oxygen and moisture. All isolated [1.1]metallarenophanes adopt *anti* conformations in the solid state.

Several new reactive aluminum, gallium and indium and compounds have been prepared that incorporate bulky donor ligands.

All new compounds have been characterized by NMR spectroscopy, X-ray crystallography, mass spectrometry and elemental analysis. When comparing solid-state structures of [1]metallarenophanes, some generalizations can be made. For a given [1]metallarenophane gallium-bridged compounds are always more tilted when compared to their respective aluminum-bridged compound for reasons that still remain unknown. If the bridging element is kept constant, the tilt angles are found to increase in the order of Mo > V > Cr for the [1]metallarenophanes, which can be attributed directly to their respective metallic radii.

ACKNOWLEDGMENTS

I am grateful to Professor Jens Müller for providing motivation, support and guidance during my studies as a graduate student.

I would like to thank the University of Saskatchewan and Department of Chemistry for providing me the opportunity to study here and providing financial support; the members of my committee for providing support; the staff at the SSSC for providing assistance when needed and in particular, Dr. J. Wilson Quail for providing expertise in solving crystal structures.

Also, I would like to acknowledge all members of the Müller research group past and present for their support. In particular, I would like to acknowledge Dr. Jörg Schachner for making my experience in the lab an enjoyable one.

To my wife Vanessa, I would like to thank you for providing support over the last five years. I would also like to thank my parents Laine and Lana, brother Darcy and sister Paula for supporting me for so long.

LIST OF FIGURES

Figure page

Figure 1-1. Illustration of a [1]metallarenophane. 1
Figure 1-2. Illustration of the tilt angles in a [1]metallarenophane. 2
Figure 1-3. Illustration of the spirocyclic sila[1]CAP **1j**. 10
Figure 1-4. Illustration of diphenylsila[1]VAP (**2d**). 12
Figure 1-5. Chemical illustrations of silicon-bridged [1]VAPs **2i**, **2j** and **2k**. 13
Figure 1-6. Known 1,1′-disubstituted di(benzene)molybdenum compounds. 14
Figure 1-7. Known [2]CAPs **1p**, **1q** and **1r**. 15
Figure 1-8. Cycloheptatrienyl-cyclopentadienyl sandwich complexes. 18
Figure 1-9. Illustration of benzenecyclopentadienylmanganese (**7**). 19
Figure 1-10. Illustrations of troticenophanes **4d**, **4e** and **4f** (*o*-Xy = 2,6-dimethylphenyl). 23
Figure 1-11. Illustration of sila[1]trovacenophanes **5c** and **5d**. 24
Figure 1-12. Illustration of silicon-bridged [1]metallarenocenophane **7b**. 26
Figure 1-13. Illustration of disila[2]trovacenophane **5e**. 26
Figure 1-14. Illustration of [3]trochrocenophane **6l**. 28
Figure 1-15. Two isomers of [4]trochrocenophanes **6m** and **6n**. 28
Figure 1-16. [2]FCP **8h** isolated from the equimolar reaction of $[Pt(cod)_2]$ and dimethylsila[1]FCP (**8a**). 39
Figure 1-17. Copolymer generated from the thermal ROP of **8a** and **1a**. 45
Figure 1-18. [2]Troticenophanes **4g** and **4h** isolated from a platinum insertion reaction. 48
Figure 1-19. *Syn* and *anti* isomers of [1.1]metallocenophanes and *exo*/*endo* substituents (R_{exo}/R_{endo}). 51
Figure 1-20. *Syn* and *anti* isomers of a [1.1]FCP depicting the proximity of α and α′ protons on Cp rings. 51
Figure 1-21. Conformational analogy of the *syn* and *anti* conformations of [1.1]FCPs to the *boat* and *chair* conformation of cyclohexane (eq = equatorial, ax = axial) (adapted from ref. 76). 52
Figure 1-22. Illustration of dimercura[1.1]FCP **9b** from its solid-state structure. 53
Figure 1-23. Illustration of dibora[1.1]FCP **10a**. 54
Figure 1-24. Schematic representation of the dialumina[1.1]FCP **10d**. 56
Figure 1-25. Known galla[1.1]FCPs **10e**, **10f**, **10g** and **10h**. 57
Figure 1-26. Dicarba[1.1]FCPs prepared to study the proposed *syn*-to-*syn* isomerization in [1.1]FCPs. 62
Figure 1-27. Illustrations of the dicarba[1.1]FCPs **11k** and **11l** with interannular propyl linkers in α- and β-positions. 65
Figure 1-28. Illustration of dicarba[1.1]FCP **11o** and **11p**. 67
Figure 1-29. Illustration of lithium coordination to the dicarba[1.1]FCP **11a**. 68
Figure 2-1. Molecular structure of (Pytsi)$AlEt_2$ (**2**) with thermal ellipsoids drawn at a 50% probability level. 97

Figure 2-2. Molecular structure of $[(Pytsi)AlMe]^+[MeB(C_6F_5)_3]^-$ (**3**) with thermal ellipsoids drawn at a 50% probability level. 99
Chart 2-1. a) Cation of $[(Pytsi)AlMe(thf)]^+[MeB(C_6F_5)_3]^-$ (**3**·thf) b) NMR time-averaged molecular symmetry of the cation of $[(Pytsi)AlMe(thf)]^+[MeB(C_6F_5)_3]^-$ (**3**·thf). 102
Figure 2-S1. ^1H NMR spectrum of $[(Pytsi)AlMe]^+[MeB(C_6F_5)_3]^-$ (**3**) in C_7D_8 at 225 K. 111
Figure 2-S2. ^{13}C NMR spectrum of $[(Pytsi)AlMe]^+[MeB(C_6F_5)_3]^-$ (**3**) in C_7D_8 at 225 K. 111
Figure 2-S3. ^{27}Al NMR spectrum of $[(Pytsi)AlMe]^+[MeB(C_6F_5)_3]^-$ (**3**) in C_7D_8 at 225 K. 112
Figure 2-S4. ^{19}F NMR spectrum of $[(Pytsi)AlMe]^+[MeB(C_6F_5)_3]^-$ (**3**) in C_7D_8 at 225 K. 112
Figure 3-1. Intramolecularly coordinating ligands. 116
Figure 3-2. Molecular structure of (Pytsi)AlClMe (**1**) with thermal ellipsoids at the 50% probability level. 119
Figure 3-3. Molecular structure of (Pytsi)Al*t*BuCl (**2**) with thermal ellipsoids at the 50% probability level. 119
Figure 3-4. Molecular structure of {[dimethyl(6-methylpyrid-2-yl)silyl]bis(trimethylsilyl)methyl}dimethylaluminum (**3**) with thermal ellipsoids at the 50% probability level. 123
Figure 3-5. Molecular structure of {[dimethyl(6-phenylpyrid-2-yl)silyl]bis(trimethylsilyl)methyl}dimethylaluminum (**4**) with thermal ellipsoids at the 50% probability level 124
Figure 3-6. Molecular structure of {{[6-(2,6-diisopropylphenyl)pyrid-2yl]dimethylsilyl}bis(trimethylsilyl)methyl}-dimethylaluminum (**5**) with thermal ellipsoids at the 50% probability level. 124
Figure 4-1. ER_x-bridged ferrocenophane. 139
Figure 4-2. Molecular structure of (Pytsi)$GaCl_2$ (**1**) with thermal ellipsoids at the 50% probability level. 140
Figure 4-3. Molecular framework structure of (Pytsi)Ga[1]FCP (**2**). 143
Figure 4-4. Common set of tilt angles to describe [1]ferrocenophanes. 143
Figure 4-5. Assignment of the Cp protons via NOE experiment (R = $SiMe_3$): δ = 4.08 (H_a), 4.45 ($H_{a'}$), 4.61 (H_b), 4.65 ($H_{b'}$). 144
Figure 4-6. Molecular structure of (Pytsi)$InCl_2$ (**3**) with thermal ellipsoids at the 50% probability level. 146
Figure 4-7. Molecular structure of indium-bridged ferrocenophane (**4**) with thermal ellipsoids at the 50% probability level. 148
Figure 4-8. Assignment of the ^1H NMR peaks for indium-bridged ferrocenophane (**4**) (R and R′ = $SiMe_3$; none-primed groups R and Me_a are on the same side of the ferrocene moiety; primed groups R′ and $Me_{a'}$ are on the opposite side of the ferrocene moiety (see experimental for details). 150
Figure 5-1. A view of the molecule of (Pytsi)InI_2 (**II**), with displacement ellipsoids drawn at the 50% probability level. 163
Figure 6-1. Al- and Ga[1]FCP [Pytsi = $C(SiMe_3)_2SiMe_2(2\text{-}C_5H_4N)$] 171

Figure 6-2. Intramolecularly coordinating ligands. 171
Figure 6-3. Molecular structure of (Me_2NCH_2tsi)$AlCl_2$ (**2a**) with thermal ellipsoids at the 50% probability level. 173
Figure 6-4. Molecular structure of (Me_2Ntsi)Al[1]FCP (**4a**) with thermal ellipsoids at the 50% probability level. 177
Figure 6-5. Set of angles to describe deformations in [1]metallocenophanes and [1]metallarenophanes. 177
Figure 6-6. Molecular structure of (Me_2Ntsi)Al[1]CAP (**5a**) with thermal ellipsoids drawn at 50% probability level. 181
Figure 6-7. Molecular structure of (Me_2Ntsi)Al[1]VAP (**6a**) with thermal ellipsoids drawn at 50% probability level. 181
Figure 6-S1. Molecular structure of (Me_2Ntsi)Ga[1]FCP (**4b**) with thermal ellipsoids at the 50% probability level. 191
Figure 6-S2. Molecular structure of (Me_2Ntsi)Ga[1]CAP (**5b**) with thermal ellipsoids drawn at 50% probability level. 192
Figure 6-S3. Molecular structure of (Me_2Ntsi)Ga[1]VAP (**6b**) with thermal ellipsoids drawn at 50% probability level. H atoms and ½ benzene are omitted for clarity. 192
Figure 7-1. [1]Metallacyclophanes. 197
Figure 7-2. ^{1}H NMR spectra in the region of the arene protons of (Me_2Ntsi)Al[1]MAP (**2a**) at 25 ºC (bottom), of (Me_2Ntsi)Ga[1]MAP (**2b**) at 25 ºC (middle), and (Me_2Ntsi)Ga[1]MAP (**2b**) at –10 ºC (top) taken in C_7D_8 (small singlet at δ 4.58 (r.t) and 4.61 (–10 ºC) is due to [Mo(C_6H_6)$_2$]). 199
Figure 7-3. Molecular structure of (Me_2Ntsi)Al[1]MAP (**2a**) with thermal ellipsoids at the 50% probability level. 200
Figure 7-4. Molecular structure of (Me_2Ntsi)Ga[1]MAP (**2b**) with thermal ellipsoids at the 50% probability level. 201
Figure 7-5. Common angles to describe [1]metallacylophanes. 201
Figure 7-6. ^{1}H NMR spectrum in the region of the arene protons of Ph_2Si[1]MAP (**2c**) at 25 ºC. 204
Figure 7-7. Molecular structure of Ph_2Si[1]MAP (**2c**) with thermal ellipsoids at the 50% probability level. 204
Figure 7-8. Molecular structure of [(η^6-C_6H_6)Mo{η^6-C_6H_5[GaPh(Me_2Ntsi)]} (**3b**) with thermal ellipsoids at the 50% probability level. 206
Figure 7-S1. ^{1}H NMR spectrum of Ph_2Si[1]MAP (**2c**) at 25 ºC in C_6D_6 (bottom), and of the arene protons (top). Solvent peak is mark with *. 219
Figure 7-S2. ^{13}C NMR spectrum of Ph_2Si[1]MAP (**2c**) at 25 ºC in C_6D_6 (* spike at the carrier frequency). 220
Figure 8-1. Isomerism in [1.1]metallocenophanes. 225
Figure 8-2. Molecular structure of Ar′Al[1.1]CAP (**2a**) with thermal ellipsoids at the 50% probability level. 227
Figure 8-3. Molecular structure of (p-*t*BuAr′)Ga[1.1]CAP (**4b**) with thermal ellipsoids at the 50% probability level. 231
Figure 8-4. Molecular structure of (p-*t*BuAr′)Al[1.1]MAP (**5a**) with thermal ellipsoids at the 50% probability level. 231

Figure 8-5. Cyclic voltammogram of (p-*t*BuAr′)Ga[1.1]CAP (**4b**) in thf/0.1 M $[Bu_4N][PF_6]$ using a glassy carbon working electrode at a scan rate of 100 mV/s. 236
Figure 8-6. Cyclic voltammogram of (p-*t*BuAr′)Ga[1.1]MAP (**5b**) in thf/0.1 M $[Bu_4N][PF_6]$ using a glassy carbon working electrode at a scan rate of 100 mV/s. 236
Figure 8-7. Illustration of two pairs of inner α protons pointing towards each other. Drawing is based on the experimentally determined molecular structure of compound (p-tBuAr′)Ga[1.1]CAP (**4b**) (ligand p-*t*BuAr′ removed for clarity). 238
Figure 8-S1. Molecular structure of (p-*t*BuAr′)Al[1.1]CAP (**4a**) with thermal ellipsoids at the 50% probability level.....249
Figure 8-S2. Molecular structure of (p-*t*BuAr′)Ga[1.1]MAP (**5b**) with thermal ellipsoids at the 50% probability level.....249
Figure 8-S3. Cyclic voltammogram of $[(C_5H_5)_2Fe]$ (solid line), $[(C_6H_6)_2Cr]$ (dashed line) and $[(C_6H_6)_2Mo]$ (dotted line).....250
Figure 9-1. Two different isomers of [1.1]ferrocenophanes.....255
Figure 9-2. Intramolecularly coordinating ligands used for the synthesis of heavier group-13-bridged metallacyclophanes.....256
Figure 9-3. The first [1.1]CAPs (M = Cr; E = Al or Ga) and [1.1]MAPsmolybdarenophanes (M = Mo; E = Al or Ga), and the first Ar′In[1.1]FCP (**1c**).[8].....256
Figure 9-4. Molecular structure of $(Me_2Ntsi)InCl_2$ (**2a**) with thermal ellipsoids at the 50% probability level (only one of two dimers is shown).....258
Figure 9-5. Molecular structure of $(Me_2Ntsi)InI_2$ (**2b**) with thermal ellipsoids at the 50% probability level.....258
Figure 9-6. Molecular structure of (Me_2Ntsi)In[1.1]FCP (**3**) with thermal ellipsoids at the 50% probability level.....261
Figure 9-7. Illustration of an *anti*-to-*anti* degenerate isomerization of (Me_2Ntsi)In[1.1]FCP (**3**).....263
Figure 9-8. Cp region of selected ^{1}H NMR spectra of compound (Me_2Ntsi)In[1.1]FCP (**3**) (500 MHz; toluene-d_8). 265
Figure 9-9. Left side: Assignment of Cp protons in Ar′In[1.1]FCP (**1c**) by NOE experiments. Right side: Cp region of an EXSY spectrum of **1c** (small signal at 3.99 ppm corresponds to ferrocene). 266
Figure 9-10. Cyclic voltammogram of (Me_2Ntsi)In[1.1]FCP (**3**) in thf / 0.1M $[Bu_4N][PF_6]$ using a glassy carbon working electrode at a scan rate of 100 mV/s. 268
Figure 9-11. Illustration of the proximity between methyl groups of the Me_2Ntsi ligand and α protons of the ferrocene moieties (see double-headed arrows) in the (MeN_2tsi)In[1.1]FCP (**3**) (left side) and the galla[1]ferrocenophane $[(Me_2Ntsi)Ga(\eta^5\text{-}C_5H_4)_2Fe]$[22] (right side). 269
Figure 9-S1. ^{1}H NMR spectrum of compound (MeN_2tsi)In[1.1]FCP (**3**) at 25˚C (C_6D_6; 500 MHz). 279
Figure 9-S2. ^{1}H NMR spectrum of compound (MeN_2tsi)In[1.1]FCP (**3**) at –30˚C (C_7D_8; 500 MHz). 280
Figure 9-S3. Cyclic voltammogram of compound (MeN_2tsi)In[1.1]FCP (**3**) (solid line) and ferrocene (dotted line) in thf / 0.1M $[Bu_4N][ClO_4]$ using a glassy carbon working electrode at a scan rate of 100 mV/s.....281

Figure 10-1. Intramolecular coordinating ligands utilized in this Ph.D. project. 282
Figure 10-2. Novel compounds equipped with Pytsi-type ligands prepared during this Ph.D. project: (a) compounds incorporating AlMe moieties; (b) compounds incorporating EX_2 moieties.....283
Figure 10-3. Novel [1]metallarenophanes prepared during this Ph.D. project.....285
Figure 10-4. Compound $(Me_2NCH_2tsi)AlCl_2$ prepared during this Ph.D. project.....286
Figure 10-5. Novel [1.1]metallarenophanes prepared during this Ph.D. project.....288
Figure 10-6. Compound $(Me_2Ntsi)InCl_2$ synthesized during this Ph.D. project. 289

LIST OF SCHEMES

Scheme page

Scheme 1-1. Generation of a metallarenophane by the dilithiation route. 3
Scheme 1-2. Generation of a metallocenophane by the fly-trap route. 4
Scheme 1-3. Known group-4-bridged [1]metallarenophanes. 6
Scheme 1-4. Known bora[1]CAPs. 7
Scheme 1-5. Conversion of sila[1]CAP **1l** into **1m** by reductive coupling. 10
Scheme 1-6. Chemical reaction for the preparation of the disilane linked [1]CAP **1n.** 11
Scheme 1-7. Preparation of [4]CAP **1w** by an insertion reaction. 16
Scheme 1-8. Preparation of [1]troticenophanes. 22
Scheme 1-9. Thermal ROP of dimethylsila[1]ferrocenophane (**8a**). 32
Scheme 1-10. Anionic ROP mechanism of a [1]FCP (adapted from ref. 51). 34
Scheme 1-11. Cationic ROP of [2]FCP **8c**. 34
Scheme 1-12. Proposed cationic ROP mechanism of [2]FCP **8c** using $MeOSO_2CF_3$ as a cationic initiator (taken from ref. 62). 35
Scheme 1-13. Proposed cationic ROP mechanism of stanna[1]FCP **8e** (taken from refs. 10 and 63). 36
Scheme 1-14. Transition-metal catalyzed ROP of sila[1]FCP **8a**. 37
Scheme 1-15. Synthesis of [2]FCP **8g** from the insertion of $Pt(PEt_3)_2$ into the Si–C bond of [1]FCP **8a**. 38
Scheme 1-16. Proposed mechanism for the heterogenous transition-metal catalyzed ROP of dimethylsila[1]FCP (**8a**) with a platinum(0) source (taken from ref. 69). 41
Scheme 1-17. Photo-controlled ROP of bimetallic phospha[1]FCPs monomers under broad-band irradiation. 42
Scheme 1-18. UV irradiated phospha[1]FCPs in the presence of excess $P(OMe)_3$ inducing a η^5 to η^1 haptotropic shift. 42
Scheme 1-19. UV-irradiated phospha[1]FCP **8k** in the presence of an excess of PMe_3 generating a zwitterionic piano-stool-type complex **8q**. 43
Scheme 1-20. Proposed mechanism for the photo-controlled ROP of phospha[1]FCPs (taken from ref. 73). 43
Scheme 1-21. UV irradiated dimethylsila[1]FCP (**8a**) in the presence of dppe generating a piano-stool-type complex **8r** where one Cp undergoes η^5 to η^1 haptotropic shift. 44
Scheme 1-22. Transition-metal catalyzed ROP of [1]CAPs. 47
Scheme 1-23. Reactions of dilithioferrocene·2/3 tmeda with $(Pytsi)AlCl_2$ in toluene generating a [1]FCP (**10d**) and in hexane generating a [1.1]FCP (**10b**). 55
Scheme 1-24. Acid catalyzed formation of dicarba[1.1]FCPs **11a** and **11b**. 58
Scheme 1-25. Synthetic route to **11c** from a methyl substituted bis(fulvenyl)ferrocene. 59
Scheme 1-26. Friedel–Crafts route to dicarba[1.1]FCP **11d**. 60
Scheme 1-27. Preparation of two isolable isomers of dicarba[1.1]FCP **11a**. 61

Scheme 1-28. Conformational exchange in α- and β-substituted [1.1]FCPs (adapted from refs. 120 and 121). 64
Scheme 1-29. Three-step reaction of dicarba[1.1]FCP with a protic acid generating H_2. 66
Scheme 1-30. Preparation of dicarba[1.1]FCPs **11m** and **11n** from reaction of **11d** and Lawesson's reagent. 66
Scheme 1-31. Illustration for proton transfer between the methylene group and the carbanion in dicarba[1.1]FCP **11a**. 68
Scheme 1-32. Synthetic route to disila[1.1]FCP **11q**. 70
Scheme 1-33. Palladium catalyzed ring-opening dimerization of sila[1]FCP **11w** to yield the disila[1.1]FCP **11v**. 72
Scheme 1-34. Proposed nucleophilically assisted ROP of stanna[1]FCPs (taken from ref. 98). 74
Scheme 1-35. Preparation of dicarba[1.1]RCPs **12d** and **12e**. 76
Scheme 1-36. Illustration of a chiral diphospha[1.1]FCP **14a**. 78
Scheme 3-1. Synthesis of aluminum dimethyl compounds equipped with Pytsi-like ligands **3**–**5**. 122
Scheme 3-2. Synthesis of the lithiopyridine for {{[6-(2,6-diisopropylphenyl)pyrid-2yl]dimethylsilyl}bis(trimethylsilyl)methyl}-dimethylaluminum (**5**). 122
Scheme 5-1. Synthesis of (Pytsi)Al[1]FCP and (Pytsi)Ga[1]FCP. 161
Scheme 5-2. Synthesis of an indium-bridged ferrocenophane. 161
Scheme 6-1. Synthesis of aluminum- and gallium-bridged [1]metallacyclophanes. 174
Scheme 7-1. Synthesis of aluminum- and gallium-bridged [1]MAPs. 198
Scheme 8-1. Synthesis of aluminum- and gallium-bridged [1.1]metallarenophanes. 229
Scheme 10-1. Unsuccessful synthesis of [1]metallarenophanes using (Pytsi)ECl_2. 284

LIST OF TABLES

Table page

Table 1-1. Selected parameters of known sila[1]CAPs.....9
Table 1-2. Summary of known sila[1]VAPs.....13
Table 1-3. Structural details and properties of the trometallocenes.....19
Table 1-4. Selected structural details of bora[1]trometallocenophanes.....21
Table 1-5. Selected structural parameters of group-14-bridged [1]troticenophanes.....22
Table 1-6. Selected structural data of group-14-bridged [1]trochrocenophanes.....25
Table 1-7. Selected structural parameters of heteroleptic [2]metallacyclophanes.....27
Table 2-1. Crystal and structural refinement data for compounds (Pytsi)$AlMe_2$ (**1**), (Pytsi)$AlEt_2$ (**2**), and $[(Pytsi)AlMe]^+[MeB(C_6F_5)_3]^-$ (**3**).....98
Table 3-1. Crystal and structural refinement data for aluminum dimethyl compounds equipped with Pytsi-like ligands **1**–**5**.....120
Table 4-1. Crystal and structural refinement data for compounds (Pytsi)$GaCl_2$ (**1**), (Pytsi)$InCl_2$ (**3**), and indium-bridged ferrocenophane (**4**).....142
Table 5-1. Selected geometric parameters for (Pytsi)InI_2 (**II**) (Å,°).....165
Table 6-1. Crystal and structural refinement data for compounds (Me_2NCH_2tsi)$AlCl_2$ (**2a**), (Me_2Ntsi)Al[1]FCP (**4a**), and (Me_2Ntsi)Ga[1]FCP (**4b**).....176
Table 6-2. Crystal and structural refinement data for [1]CAPs **5a**–**b** and [1]VAPs **6a**–**b**.....180
Table 6-3. Deformation angles α, θ, and δ [º] of [1]CAP **5** and [1]VAP **6** (see Figure 6-5).....182
Table 7-1. Crystal and structural refinement data for compounds (Me_2Ntsi)Al[1]MAP (**2a**), (Me_2Ntsi)Ga[1]MAP (**2b**), Ph_2Si[1]MAP (**2c**), and [(η^6-C_6H_6)Mo{η^6-C_6H_5[GaPh(Me_2Ntsi)]}(**3b**).....202
Table 8-1. Crystal and structural refinement data for compounds Ar′Al[1.1]CAP (**2a**), (p-*t*BuAr′)Al[1.1]CAP (**4a**),(p-*t*BuAr′)Ga[1.1]CAP (**4b**), and (p-*t*BuAr′)Al[1.1]MAP (**5a**), (p-*t*BuAr′)Ga[1.1]MAP (**5b**).....232
Table 9-1. Crystal and structural refinement data for compounds (Me_2Ntsi)$InCl_2$ (**2a**), (Me_2Ntsi)$InCl_2$ (**2b**), and (Me_2Ntsi)In[1.1]FCP (**3**).....262
Table 10-1. Tilt angles α determined from the solid-state structures of [1]metallarenophanes synthesized during this Ph.D. project.....286

LIST OF ABBREVIATIONS

Abbreviation

[1]CAP	[1]chromarenophane
[1]FCP	[1]ferrocenophane
[1]MAP	[1]molybdarenophane
[1]VAP	[1]vanadarenophane
[1.1]CAP	[1.1]chromarenophane
[1.1]FCP	[1.1]ferrocenophane
[1.1]MAP	[1.1]molybdarenophane
[1.1]RFCP	[1.1]ruthenoferrocenophane
[1.1]RCP	[1.1]ruthenocenophane
Ar′	2-(Me_2NCH_2)C_6H_4
Cht	cycloheptatrienyl
CN	coordination number
cod	1,5-cyclooctadiene
Cp	cyclopentadienyl
Cy	cyclohexyl
dba	dibenzylideneacetone
Dipp	2,6-diisopropylphenyl
dme	1,2-dimethoxyethane
dmf	N,N-dimethylformamide
dppe	bis(diphenylphosphino)ethane
DSC	differential scanning calorimetry
FcLi	ferrocenyllithium
GPC	gel permeation chromatography
Me_2Ntsi	–$C(SiMe_3)_2SiMe_2NMe_2$
Men	menthyl
Mes	mesitylene
Mes*	2,4,6-*t*BuC_6H_2
M_n	number average molecular weight
M_w	weight average molecular weight
MS	mass spectrometry
o-Xy	2,6-dimethylphenyl
pmdta	N,N,N′,N″,N″-pentamethyldiethylenetriamine
Pytsi	–$C(SiMe_3)(SiMe_2C_6H_4N$-2)
p-*t*BuAr′	5-*t*Bu-2-(Me_2NCH_2)C_6H_3
ROP	ring-opening polymerization
SAXS	small-angle X-ray scattering
tmeda	N,N,N′,N′-tetramethylethylenediamine
VT-NMR	variable temperature nuclear magnetic resonance

TABLE OF CONTENTS

page

Permission to Use i

ABSTRACT ii

ACKNOWLEDGMENTS iv

LIST OF FIGURES v

LIST OF SCHEMES x

LIST OF TABLES xii

LIST OF ABBREVIATIONS xiii

TABLE OF CONTENTS xiv

INTRODUCTION 1

1.1 [1]Metallarenophanes and Related Compounds 1
1.1.1 Group-4-Bridged [1]Metallarenophanes 5
1.1.2 Group-13-Bridged [1]Metallarenophanes 6
1.1.3 Group-14-Bridged [1]Metallarenophanes 8
1.1.4 Unsuccessful Attempts to Prepare [1]Molybdarenophanes 13
1.1.5 [n]Metallarenophanes with n > 1 14
1.2 [1]Metallacyclophanes and Related Compounds 18
1.2.1 Group-13-Bridged Heteroleptic [1]Metallacyclophanes 20
1.2.2 Group-14-Bridged Heteroleptic [1]Metallacyclophanes 21
1.2.3 Heteroleptic [n]Metallacyclophanes with n > 1 26
1.3 ROP of [1]Metallacyclophanes 29
1.3.1 Thermal ROP 44
1.3.2 Transition-Metal Catalyzed ROP 46
1.3.3 Anionic ROP 49
1.3.4 Photocontrolled ROP 49
1.4 [1.1]Metallacyclophanes 50
1.4.1 Group-12-Bridged [1.1]Metallocenophanes 53
1.4.2 Group-13-Bridged [1.1]Metallocenophanes 54

1.4.3 Group-14-Bridged [1.1]Metallocenophanes 58
1.4.4 Group-15-Bridged [1.1]Metallocenophanes 77
1.4.5 Group-16-Bridged [1.1]Metallocenophanes 79
1.5 Electrochemistry of [1.1]Metallocenophanes 80
1.6 Research Objectives 83
1.7 References 86

PUBLICATION 1 92

2. Synthesis and Characterization of Neutral and Cationic Intramolecularly Coordinated Aluminum Compounds. Structural Determination of $[(Pytsi)AlMe]^{+}[MeB(C_6F_5)_3]^{-}$ (Pytsi = $C(SiMe_3)_2SiMe_2(2\text{-}C_5H_4N)$) 94
2.1 Abstract 94
2.2 Introduction 95
2.3 Results and Discussion 96
2.4 Conclusions 103
2.5 Experimental Section 104
2.6 References 109
2.7 Supporting Information 111

PUBLICATION 2 113

3. Synthesis and Characterization of Intramolecularly Coordinated Alanes with New Sterically Demanding *Trisyl*-Based Ligands 115
3.1 Abstract 115
3.2 Introduction 116
3.3 Results and Discussion 117
3.4 Conclusion 124
3.5 Experimental 125
3.6 References 134

PUBLICATION 3 136

4. Synthesis and Characterization of Heavier Group-13 Element Ferrocenophanes: The First Gallium-Bridged [1]Ferrocenophane and an Unusual Indium Species 138
4.1 Abstract 138
4.2 Introduction 138
4.2 Results and Discussion 139
4.4 Conclusions 151
4.5 Experimental Section 152
4.6 References 156

PUBLICATION 4 158

5. A Monomeric Four-fold Coordinated Indium Dihalide with an Unusual Coordination Geometry 160

5.1 Comment 160
5.2 Experimental 163
5.3 References 166

PUBLICATION 5 168

6. [1]Ferrocenophanes, [1]Chromarenophanes, and [1]Vanadarenophanes with Aluminium and Gallium in Bridging Positions 170
6.1 Abstract 170
6.2 Introduction 171
6.3 Results and Discussion 172
6.3.1 [1]Ferrocenophanes 175
6.3.2 [1]Chromarenophanes and [1]Vanadarenophanes. 178
6.4 Conclusions 183
6.5 Experimental Section 184
6.6 References 189
6.7 Supporting Information 191

PUBLICATION 6 193

7. [1]Molybdarenophanes: Strained Metallarenophanes with Aluminum, Gallium and Silicon in Bridging Positions 195
7.1 Abstract 195
7.2 Introduction 196
7.3 Results and Discussions 197
7.4 Summary and Conclusion 208
7.5 Experimental Section 210
7.6 References 216
7.7 Supporting Information 219

PUBLICATION 7 221

8. Synthesis and Characterization of Aluminum- and Gallium-Bridged [1.1]Chromarenophanes and [1.1]Molybdarenophanes 223
8.1 Abstract 223
8.2 Introduction 224
8.3 Results and Discussion 226
8.3.1 Solid-state structures of **2a**, **4a**,**b** and **5a**,**b**. 229
8.3.2 NMR spectroscopy of **2a**, **4a**,**b** and **5a**,**b**. 232
8.3.3 Electrochemistry of **4a**,**b** and **5a**,**b** 234
8.4 Conclusion 237
8.5 Experimental Section 238
8.6 References 247
8.7 Supporting Information 249

PUBLICATION 8 251

9. The Dynamic Indium-Bridged [1.1]Ferrocenophane [$(Me_2Ntsi)In(C_5H_4)_2Fe]_2$ ... 253
9.1 Abstract ... 253
9.2 Introduction ... 254
9.3 Results and Discussion ... 256
9.3.1 Preparation and characterization of indium dihalides **2a** and **2b** ... 257
9.3.2 Synthesis and solid-state structure of diinda[1.1]ferrocenophane **3**. ... 259
9.3.3 NMR spectroscopy of diinda[1.1]ferrocenophane **3**. ... 262
9.3.4 Cyclic voltammetry of diinda[1.1]ferrocenophane **3**. ... 267
9.4 Conclusion ... 268
9.5 Experimental Section ... 271
9.5.1 General Procedures. ... 271
9.5.2 Electrochemistry. ... 272
9.6 References ... 277
9.7 Supporting Information ... 279

SUMMARY and CONCLUSIONS ... 282

CHAPTER 1
INTRODUCTION

1.1 [1]Metallarenophanes and Related Compounds

Metallarenophanes and metallocenophanes belong to a general class of compounds called metallacyclophanes. Metallacyclophanes are compounds that contain a sandwich complex (or multiple sandwich complexes) with interannular bridging elements and are referred to as *ansa* complexes. One specific type of a metallacyclophane is a [n]metallarenophane. [n]Metallarenophanes consist of a metallarene, that is, a sandwich complex consisting of two benzene rings that are π-bound to a transition-metal M in a η^6-fashion with a number n of bridging elements E σ-bound to the benzene rings such that an interannular bridge is formed between to two benzene rings. The bridging element may have ligands R_x attached in a σ-bound or π-bound fashion. An example of a [1]metallarenophane is depicted below (Figure 1-1).

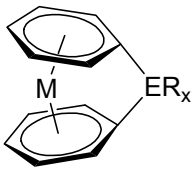

Figure 1-1. Illustration of a [1]metallarenophane.

The introduction of bridging elements in a metallarenophane leads to distortion of the coplanar arrangement of the benzene rings normally found in the parent sandwich complex, resulting in a tilt of the benzene rings towards the bridging element. As a result of the ring tilt, a series of tilt angles can be defined (Figure 1-2): δ (ring centroid-metal-ring centroid), θ (*ipso* carbon-element E-*ipso* carbon), α (angle between the planes of the arenes) and β (angle between

the plane of the arene and *ipso* carbon-element E bond). As a result of this tilt, the *ipso* carbons are brought closer to the transition-metal and there is significant bond angle distortion at the *ipso* carbon-bridging element bond. The distortions can be illustrated and quantified by the tilt angle α which can be determined from the solid-state structure using single-crystal X-ray crystallography (Figure 1-2).

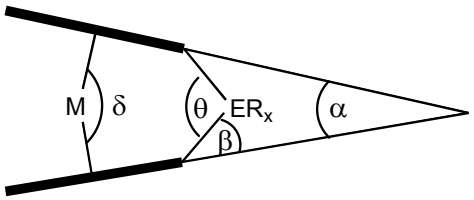

Figure 1-2. Illustration of the tilt angles in a [1]metallarenophane.

The angle α is directly related to the number and size of the bridging elements in the interannular bridge. For a constant bridging element E, the value of α is inversely proportional to the value n. In addition, the value of the tilt angle α is inversely proportional to the atomic radius of the bridging element. That is, the smaller the bridging element in the interannular bridge, the larger the value of the tilt angle α will be.

^{13}C NMR spectroscopy can be a useful qualitative tool for the indirect measure of ring strain in a metallarenophane by observing the chemical shift of the arene carbon that is π-bound to the transition-metal and σ-bound to the bridging element (the *ipso* carbon). The general trend for main-group-bridged [1]metallarenophanes is the chemical shift of *ipso* carbon is shifted upfield when compared to the carbon resonance of the parent metallarene. The values obtained from the ^{13}C NMR spectroscopy provide qualitative evidence that some degree of ring strain is present. The ^{13}C NMR chemical shifts of *ipso* carbons are not quantitatively related to the tilt angle α. For example, the ^{13}C NMR chemical shift (C_6D_6) of bis(benzene)chromium (**1**) is δ

74.8[1] and its solid-state structure possesses coplanar arene rings ($\alpha = 0°$), whereas the *ipso* carbon shifts and tilt angles α for some chromarenophanes (CAPs) are δ 39.5 and $\alpha = 16.6(3)°$ for dimethylsila[1]CAP[2] (**1a**) and δ 36.4 and $\alpha = 14.4(2)°$ for diphenylgerma[1]CAP[3] (**1b**). If a quantitative relationship existed, the *ipso* carbon shift from the arene of **1a** would be expected to be shifted further upfield compared to the *ipso* carbon shift from the arene in **1b**, because the tilt angle in **1a** is larger compared to the tilt angle in **1b**. Thus *ipso* carbon shifts are only a qualitative measure for determining that some degree of ring strain exists.

There are two general routes for preparing [1]metallacyclophanes (compounds that contain a single element interannular bridge between two aromatic rings of any size in a sandwich complex). The first established synthetic route is the dilithiation route where the parent sandwich complex is dilithiated with two equivalents of an alkyllithium source followed by a salt metathesis reaction involving the dilithiated sandwich complex with an element dihalide. An example of the dilithiation route involving an element dihalide is depicted below (Scheme 1-1).

Scheme 1-1. Generation of a metallarenophane by the dilithiation route.

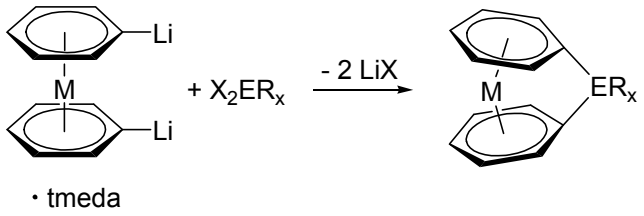

The second and less preferred route is commonly referred to as the fly-trap route. The fly-trap route is a common method used in preparing metallocenophanes. In the fly-trap route an element dicyclopentadienide compound is dilithiated using an alkyllithium source, generating a dilithiobis(cyclopentadienyl)element compound; combining this dilithio salt with a transition-metal dihalide MX_2 results in the formation of a [1]metallocenophane (Scheme 1-2).

Scheme 1-2. Generation of a metallocenophane by the fly-trap route.

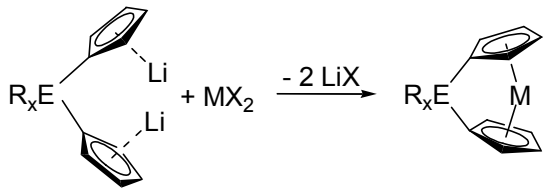

The dilithiation route is usually the preferred route because yields for the intended metallacyclophanes tend to be higher compared to metallacyclophanes prepared by the fly-trap route. The fly-trap route often produces other products including oligomers and polymers due to polycondensation-type reactions, thereby lowering the conversion to the intended [1]metallacyclophane.

All metallarenophanes prepared to date have been prepared by the dilithiation route. The successful dilithiation of sandwich complexes is often accomplished by use of an alkyllithium reagent in the presence of coordinating bases like N,N,N′,N′-tetramethylethylenediamine (tmeda) or N,N,N′,N″,N″-pentamethyldiethylenetriamine (pmdta). Interestingly, some of these dilithiated sandwich complexes have been characterized by ^{1}H NMR spectroscopy, mass spectrometry or X-ray crystallography with the dilithiated sandwich complexes forming adducts with tmeda, pmdta or thf. For example, a crystal structure of a 3:2 adduct of dilithioferrocene with tmeda[4] has been reported, whereas dilithiobis(benzene)metal complexes form 1:1 adducts with tmeda (where the metal = chromium[5], vanadium[6] and molybdenum[7]).

One potential application of [1]metallacyclophanes is the synthesis of organometallic polymers by ring-opening polymerization (ROP). ROP will be discussed in some detail later, but a brief description here is beneficial to the subsequent discussion of metallarenophanes. ROP is a process where polymers are generated from monomers through ring-opening reactions. The first example of thermal ROP of a metallacyclophane was reported by Manners *et. al* in 1992;

strained dimethylsila[1]ferrocenophane undergoes ROP upon heating to 130 °C to yield high molecular weight poly(ferrocenylsilanes)[8] (equation 1-1).

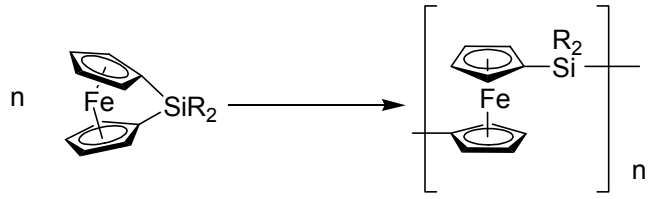

(1-1)

Because reviews on the synthesis and characterization,[9] as well as the ROP[10] of ferrocenophanes and [1]ruthenocenophanes have been published recently and a comprehensive overview of these compounds is beyond the scope of this theses, metallocenophane examples will only be included to explain the ROP methodologies discussed later in chapter 1.3. The subsequent sections will provide an overview on the synthesis, characterization and ROP of [1]CAPs, vanadarenophanes ([1]VAPs) and heteroleptic metallacyclophanes. There are no known [1]molybdarenophanes ([1]MAPs) to report.

1.1.1 Group-4-Bridged [1]Metallarenophanes

Of the ample possibilities there have only been three reported group-4-bridged metallarenophanes to date. Elschenbroich *et al*. prepared two zirconium-bridged [1]CAPs and a single zirconium-bridged [1]VAP, all in low yields (11–14%).[11] [1]CAPs were prepared from reactions of dilithiobis(benzene)chromium·tmeda (**1c**) and a respective metal dichloride compound [ER_x = $Zr(C_5H_4tBu)_2$ (**1d**), $ZrCp_2$ (**1e**)] and the analogous vanadium complex was prepared from the reaction of dilithiobis(benzene)vanadium·tmeda (**2a**) (generated in situ from bis(benzene)vanadium (**2**), butyllithium and tmeda) with bis(*tert*-butylcyclopentadienyl)zirconium dichloride [ER_x = $Zr(C_5H_4tBu)_2$ (**2b**)] (Scheme 1-3).

Scheme 1-3. Known group-4-bridged [1]metallarenophanes.

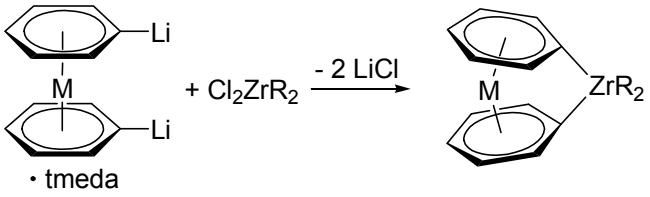

1c M = Cr
2a M = V

1d M = Cr R = C_5H_4tBu
1e M = Cr R = Cp
2b M = V R = C_5H_4tBu

Compound **1d** was characterized by ^{1}H NMR and ^{13}C NMR spectroscopy (biphenyl-d_{12}) and it is important to note that the *ipso* carbon resonance was found at δ 174.4. This shift is significantly downfield from the resonance of the parent bis(benzene)chromium (δ 74.8[1]). As mentioned earlier, the chemical shift of the *ipso* carbon from a [1]metallarenophane is usually shifted upfield when compared to the resonance of the parent compound. Therefore, the resonance of δ 174.4 is shifted in a direction opposite to what is usually observed for main-group-bridged [1]metallarenophanes. The reason for this downfield shift is unknown; a similar phenomenon was observed for zirconium-bridged [1]ferrocenophanes ([1]FCPs).[12,13] Compound **1e** was insoluble in all common solvents and therefore could only be identified by mass spectrometry and element analysis. Compound **2b** was characterized by single-crystal X-ray analysis and possesses the smallest tilt angle α of 5.1° known for [1]metallarenophanes.

There are no titanium or hafnium-bridged [1]metallarenophanes known, to date.

1.1.2 Group-13-Bridged [1]Metallarenophanes

The only known group-13-bridged [1]metallarenophanes contain boron as a bridging element. In addition, these boron-bridged species are the only known examples of [1]metallarenophanes with a bridging atom found in the second row. Boron-bridged [1]CAPs

were prepared by reaction of dilithiobis(benzene)chromium·tmeda (**1c**) with bulky dichloro(dialkylamino)boranes [ER_x = $BN(SiMe_3)_2$ (**1f**), $BNiPr_2$ (**1g**), $BN(SiMe_3)(iPr)$ (**1h**)] in moderate yields (42–48%) (Scheme 1-4).[14]

Scheme 1-4. Known bora[1]CAPs.

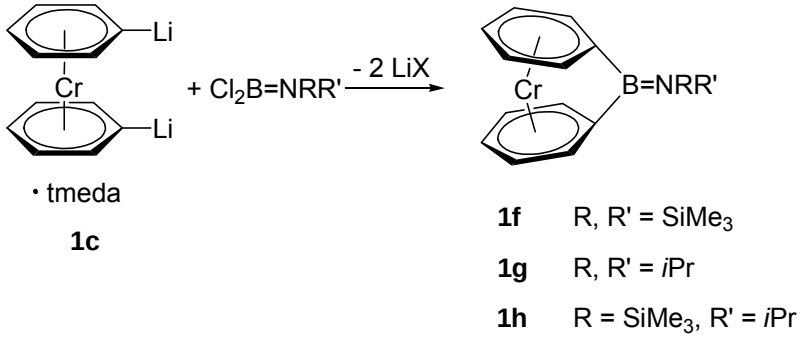

1c

1f R, R' = $SiMe_3$

1g R, R' = *i*Pr

1h R = $SiMe_3$, R' = *i*Pr

Compounds **1f–1h** were reported to be extremely sensitive to air and moisture and decompose readily in polar solvents (MeOH, CH_2Cl_2, dmf, dme) (dmf = N,N-dimethylformamide, dme = 1,2-dimethoxyethane) with formation of bis(benzene)chromium and various phenylborane species. The solid-state structure of **1h** revealed a molecule with approximate C_s symmetry and a relatively large tilt angle α of 26.6(3)°.

Braunschweig *et al*. recently reported on the synthesis and characterization of a boron-bridged [1]VAP prepared by reaction of dilithiobis(benzene)vanadium·tmeda (**2a**) with [bis(trimethysilyl)amino]dichloroborane [ER_x = $BN(SiMe_3)_2$ (**2c**)] in good yield (75%).[15] For compound **2c**, the tilt angle α of 31.12(7)° is the largest known for [1]metallarenophanes. As discussed earlier, the tilt angle α is in inversely proportional to a bridging elements atomic radius and the large tilt angle is expected because of the small covalent radius of boron (CN = 3, r = 0.82 Å) (CN = coordination number).[16]

When this project was undertaken, aluminum-, gallium- and indium-bridged [1]metallarenophanes were unknown in the literature.

1.1.3 Group-14-Bridged [1]Metallarenophanes

To date, [1]metallarenophanes bridged by a single carbon atom are unknown, presumably due to the small covalent radius of carbon (CN = 4, r = 0.77 Å)[16] that would lead to a highly unfavorable and strained species. As with all [1]metallacyclophanes, the silicon- and germanium-bridged [1]metallarenophanes have been predominantly explored. The [1]metallarenophanes bridged by tin or lead atoms are unknown. The tin- or lead-bridged [1]metallarenophanes would presumably be difficult to isolate, due to thermal sensitivity, similar to what had been reported for their [1]ferrocenophane cousins.[17]

The first reported [1]metallarenophanes were a [1]CAP and a [1]VAP with silicon as a bridging element and were prepared by Elschenbroich *et al*.[6] After failed attempts to prepare the diphenylsila[1]CAP (**1i**) by cocondensation of tetraphenylsilane with chromium atoms, **1i** was prepared by reaction of dilithiobis(benzene)chromium·tmeda (**1c**) with dichlorodiphenylsilane in moderate yield (42%). The *ipso* carbon from the benzene π-bound to chromium and σ-bound to silicon was found to resonate at δ 37.7 in the ^{13}C NMR spectrum, an up-field shift of δ 37.1 from the parent bis(benzene)chromium (δ 74.8) (**1**), a certain indication that a strained complex had been prepared. To verify the complex was indeed a [1]metallarenophane, **1i** was characterized by single-crystal X-ray crystallography. From the solid-state structure of **1i**, a tilt angle α of 14.4° was determined; a much smaller tilt angle than that reported for the bora[1]CAP **1h** (26.6(3)°)[14]. However, the much smaller tilt angle in **1i** is not a surprise given the covalent radius of silicon (CN = 4, r = 1.17 Å) is much larger than that of boron (CN = 3, r = 0.82 Å).[16] In addition, the *ipso* C(arene)–Si–*ipso* C(arene) bond angle of 96.0(2)° (Figure 1-2) is significantly smaller than the ideal tetrahedral angle of 109.5°. All other C–Si–C bond angles only deviate slightly from the ideal geometry (109.5 ± 4°). Compound **1i** was found to be very sensitive to oxygen and

moisture, such that addition of thf / 5% H_2O results in instantaneous cleavage of the Si–C bonds producing bis(benzene)chromium and several siloxanes. NMR spectra of **1i** with broadened signals were observed after accidental introduction of air to samples containing **1i**. The authors speculated that small amounts of paramagnetic Cr(I) species were generated and cause the signal broadening. Some other sila[1]CAPs have been prepared from the reaction of dilithiobis(benzene)chromium·tmeda with an appropriate silicon dichloride and are summarized in Table 1-1.

Table 1-1. Selected parameters of known sila[1]CAPs.

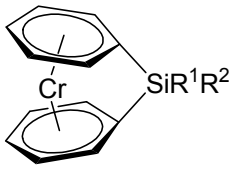

Compound	R^1	R^2	α[a]	*ipso*-C[b]	Ref
1a	Me	Me	16.6(3)	39.5[d]	2
1i	Ph	Ph	14.4	37.7[c]	6
1j	*cyclo*-$(CH_2)_3$		[e]	39.3[c]	18
1k	Me	Et	[e]	39.5[c]	19
1l	Cl	Ph	[e]	39.7[c]	20

[a] °, [b] ppm, [c] C_6D_6, [d] $CDCl_3$, [e] Solid-state structure not determined.

Dimethylsila[1]CAP (**1a**) is only the second sila[1]CAP to be characterized by single-crystal X-ray crystallography to date. The tilt angle α of 16.6(3)° for **1a** is slighter larger than that for **1i** (α = 14.4°) and the θ bond angle of 92.9(3)° for **1a** is substantially smaller than the ideal tetrahedral bond angle. The compounds **1j**–**1l** were not characterized by X-ray crystallography, but their identities were corroborated through their respective *ipso* carbon chemical shifts. Compound **1j** contains a single silicon interannular bridge with silicon in a spiro position (Figure 1-3).

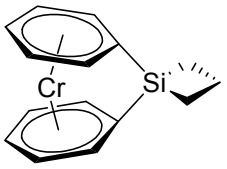

1j

Figure 1-3. Illustration of the spirocyclic sila[1]CAP **1j**.

Compound **1l** is the only sila[1]CAP that contains a silicon–halide bond. Elschenbroich *et al*. took advantage of this fact and linked two sila[1]CAPs together by reductive coupling with lithium naphthalenide resulting in compound **1m** (Scheme 1-5). Single crystals of **1m** were not obtained because of their poor solubility in common organic solvents. Consequently, the identity of compound **1m** was confirmed by mass spectrometry, NMR spectroscopy and elemental analysis. The observed $[M]^+$ signal and the *ipso* carbon resonance at δ 35.2 corroborate that **1m** was formed from the reductive coupling of **1l** (19% yield).

Scheme 1-5. Conversion of sila[1]CAP **1l** into **1m** by reductive coupling.

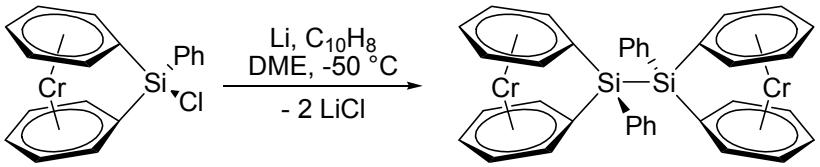

1l **1m**

They also prepared a sila[1]CAP containing a cyclic disilane (Scheme 1-6).[18] Compound **1n** was isolated as a brown powder and analyzed by mass spectrometry and NMR spectroscopy. The $[M]^+$ peak was observed in the mass spectrum and the *ipso* carbon resonance was shifted upfield (δ 39.30) when compared to the carbon resonance of bis(benzene)chromium.

Scheme 1-6. Chemical reaction for the preparation of the disilane linked [1]CAP **1n.**

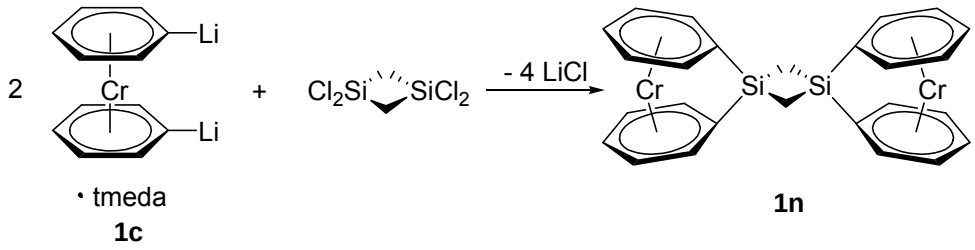

Two germanium-bridged [1]CAPs have been prepared by Elschenbroich *et al*. [ER_x = $GeMe_2$ (**1o**), $GePh_2$ (**1b**)].[3] The identities of **1o** and **1b** were confirmed by ^{13}C NMR spectroscopy with their respective *ipso* carbon resonances of δ 37.5 (**1o**) and 36.4 (**1b**). In addition, the $[M]^+$ ion of **1o** and **1b** were present in their respective mass spectra, corroborating that the [1]CAPs were formed. The tilt angle α of 14.4(2)° from the solid-state structure of **1b** is surprisingly identical (within experimental error) to the tilt angle reported for the diphenylsila[1]CAP **1i**. Based solely on the covalent radius of a four-coordinate group-14-bridging element, the silicon- (r = 1.17 Å)[16] bridged [1]CAP **1i** would be expected to have a marginally larger tilt angle than the germanium- (r = 1.22 Å)[16] bridged [1]CAP **1b**.

The first [1]VAP that was synthesized and characterized contains a silicon atom in the interannular bridge [ER_x = $SiPh_2$ (**2d**)] (Figure 1-4).[6] The identity of compound **2d** was confirmed by mass spectrometry and elemental analysis; the $[M]^+$ ion was observed in the mass spectrum. Because of the paramagnetic vanadium centre, compound **2d** could not be characterized by NMR spectroscopy.

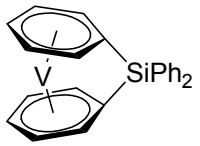

2d

Figure 1-4. Illustration of diphenylsila[1]VAP (**2d**).

The preparation and characterization of several other sila[1]VAPs have been reported from the reaction of dilithiobis(benzene)vanadium·tmeda (**2a**) with an appropriate silicon dichloride and are summarized in Table 1-2.

The identities of compounds **2e**–**2g** were confirmed by mass spectrometry and by elemental analysis. In all cases, the $[M]^+$ signal was observed. The only sila[1]VAP (in Table 1-2) that has been characterized by single-crystal X-ray crystallography is compound **2h** with a tilt angle α of 19.9°. This tilt angle is substantially larger than that determined for dimethylsila[1]CAP (**1a**) (α = 16.6(3)°), due to the larger metal atom radius of vanadium (CN = 12, 1.35 Å)[16] when compared to chromium (CN = 12, 1.29 Å)[16]. The arene(centroid)–metal distance is 1.614(6) Å[21] in $Cr(C_6H_6)_2$ and 1.66 Å[22] in $V(C_6H_6)_2$; introduction of the same interannular bridge will cause the arene rings in a [1]VAP to tilt more towards one another compared to analogous [1]CAP, assuming that the *ipso* carbon-bridging element bonds are comparable in length.

Table 1-2. Summary of known sila[1]VAPs.

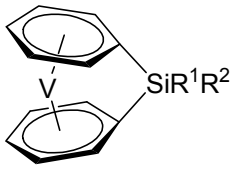

Compound	R^1	R^2	$\alpha^{[a]}$	Ref
2d	Ph	Ph	[b]	6
2e	*i*Pr	Me	[b]	15
2f	Ph	Cl	[b]	20
2g	4-propylphenyl	Cl	[b]	20
2h	*cyclo*-$(CH_2)_3$		19.9	18,20

[a] °, [b] Solid-state structure not determined.

Elschenbroich *et al*. also prepared some sila[1]VAPs analogous to the sila[1]CAPs **1m** and **1n** described above. Compounds **2i** and **2j** contain a silicon–silicon bond and compound **2k** contains a cyclic disilane (Figure 1-5). Compound **2j** was characterized by single-crystal X-ray crystallography and its tilt angle α of 20.8° is slightly larger than that determined for **2h** (α = 19.9°).

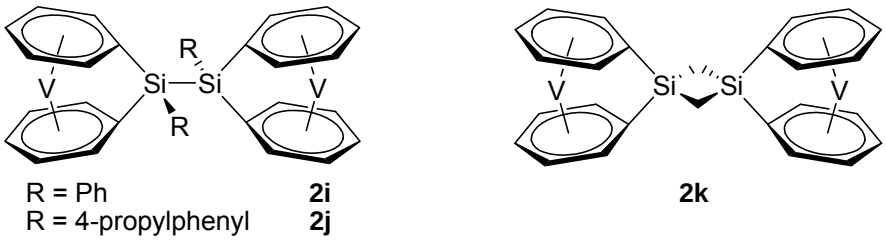

Figure 1-5. Chemical illustrations of silicon-bridged [1]VAPs **2i**, **2j** and **2k**.

1.1.4 Unsuccessful Attempts to Prepare [1]Molybdarenophanes

When this project was undertaken, not a single example of a [1]MAP was known in the literature. Several attempts to prepare [1]MAPs have been reported in the literature, but in all cases, 1,1′-substituted bis(benzene)molybdenum complexes were isolated. This section is a summary of published work dealing with attempts to prepare the elusive [1]MAPs. Bis(benzene)molybdenum (**3**) can be dilithiated utilizing butyllithium in the presence of tmeda to

produce dilithiobis(benzene)molybdenum·tmeda (**3a**). The reaction of **3a** with a stoichiometric amount of borane ($Cl_2BN(SiMe_3)_2$ or $Br_2BN(SiMe_3)_2$) produces the 1,1′-substituted di(benzene)molybdenum derivatives **3b** and **3c** respectively (Figure 1-6).[7] Likewise, the reactions of dichlorosilanes with **3a** result in 1,1′-substituted derivatives [ER_x = $SiMe_2Cl$ (**3d**)[23], $Si\textit{i}Pr_2Cl$ (**3e**)[7]] (Figure 1-6). It was proposed by Braunschweig *et al.* that the preparation and isolation of a bora[1]MAP would be unlikely whereas, the isolation of sila[1]MAP would be possible but thermal lability prevented its isolation from the above reactions.[7]

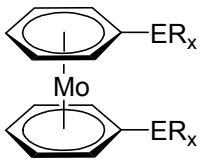

ER_x = $B[N(SiMe_3)_2]Cl$ **3b**
ER_x = $B[N(SiMe_3)_2]Br$ **3c**
ER_x = $SiMe_2Cl$ **3d**
ER_x = $Si\textit{i}Pr_2Cl$ **3e**

Figure 1-6. Known 1,1′-disubstituted di(benzene)molybdenum compounds.

1.1.5 [n]Metallarenophanes with n > 1

Several [n]metallarenophanes are known where the interannular bridge is composed of two, three or four atoms. Generally, the degree of strain is reduced as the number and size of the bridging atoms in the interannular bridge increase. The [n]metallarenophanes with n > 1 are weakly to moderately tilted compounds with values for α of generally less than 10° and are usually resistant to ROP reactions.

There are three known examples of [2]CAPs published in the literature where the interannular bridges are composed of B–B,[14] Si–Si[24] or Ge–Ge[3] linkages (Figure 1-7). Dibora[2]CAP **1p** was prepared from the stoichiometric reaction of the diborane $Br_2B_2(NMe_2)_2$ with dilithiobis(benzene)chromium·tmeda (**1c**). Likewise, **1q**, a [2]CAP possessing a silicon–silicon interannular bridge, was prepared from the reaction of **1c** with $ClMe_2Si–SiMeCl$. The

digerma[2]CAP **1r** was prepared by the reductive coupling of bis[bromodimethyl(η^6-phenyl)germane]chromium (**1s**) with sodium naphthalenide.

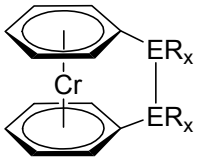

$ER_x = BNMe_2$ **1p**
$ER_x = SiMe_2$ **1q**
$ER_x = GeMe_2$ **1r**

Figure 1-7. Known [2]CAPs **1p**, **1q** and **1r**.

The [2]CAPs are moderately tilted molecules with tilt angles α of 10.1(3) and 2.78(12)° for **1p** and **1q**, respectively. Even though it was reported that **1p** could be polymerized using an anionic initiator, polymerization of [2]metallarenophanes has not been explored intensively. The main reason for preparing [2]metallarenophanes is because their heteroatom-heteroatom bonds are prone to undergo oxidative addition reactions with low-valent transition-metals. For example, Braunschweig *et al*. have generated bis(boryl)-metal moieties by addition of transition-metal complexes to diboranes,[25] and similarly prepared the [3]CAP **1t** ($R_xE–ER_x–ER_x$ = $Me_2NB–Pt(PEt_3)_2–BNMe_2$) by treating **1p** with a stoichiometric amount of $[Pt(PEt_3)_3]$.[26] The solid-state structure of **1t** revealed a molecule with an expected small tilt angle α of 4.2°.

Elschenbroich *et al*.[27] reported on the synthesis of the triphospha[3]CAP **1u** ($R_xE–ER_x–ER_x$ = PhP–PPh–PPh). Surprisingly, **1u** was prepared from dichlorophenylphosphine and **1c** in low yield. They reported **1u** could be prepared in higher yield by treating bis(chlorobenzene)chromium with $K_2[P(C_6H_5)]_3$·thf (16%). Compound **1u** is the only [n]metallarenophane with an element from group-15 in a bridging position to date.

The isolation of four [4]CAPs [$R_xE–ER_x–ER_x–ER_x$ = $Me_2NB–C(Me)–C(Me)–BNMe_2$ **(1u)**[26], $Me_2NB–C(H)–C(Me)–BNMe_2$ **(1v)**[26], $Me_2NB–N(Ph)–N(Ph)–BNMe_2$ **(1w)**[28], $Me_2Si–$

C(H)(Me)–C(H)(Me)–$SiMe_2$ (**1x**)[24]] was achieved through transition-metal catalyzed insertion reactions of unsaturated compounds into the bonds between the bridging elements of [2]chromarenophanes. The synthesis of **1w** is depicted in Scheme 1-7.

Scheme 1-7. Preparation of [4]CAP **1w** by an insertion reaction.

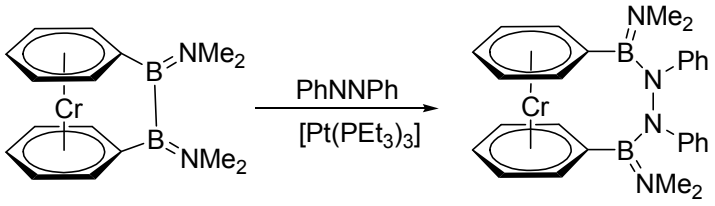

1p **1w**

Compounds **1u**, **1v** and **1x** were prepared by an analogous route to that shown in Scheme 1-7. The [4]chromarenophanes **1u** and **1w** were characterized by single-crystal X-ray crystallography and the benzene rings were nearly co-planar [α = 2.03(9) (**1u**) and 1.98(2)° (**1w**)].

The carbon-bridged [n]CAPs with n = 4 and 5 are the only known examples of [n]CAPs that contain exclusively carbon interannular bridges. A tetracarba[4]CAP [$_x$RE–ER_x–ER_x–ER_x = CH_2–CH_2–CH_2–CH_2 (**1y**)][29,30] and a pentacarba[5]CAP [R_xE–ER_x–ER_x–ER_x–ER_x = CH_2–CH_2–CH_2–CH_2–CH_2 (**1z**)][30] were prepared by condensing chromium vapour into 1,4-dipenylbutane and 1-5-diphenylpentane, respectively. Both compounds were poorly characterized but their identities were confirmed by mass spectrometry and elemental analysis.

Two examples of [n]MAPs have been published in the literature. A [2]MAP was successfully prepared from the reaction of 1,1′-dilithiobis(benzene)molybdenum·tmeda (**3a**) with the disilane $ClMe_2Si$–$SiMe_2Cl$ to yield the [2]MAP **3f** (R_xE–ER_x = Me_2Si–$SiMe_2$).[7] Compound **3f** is the first and only example of a [2]MAP known in the literature. The authors reported that **3f** "is thermally unstable and decomposes within 2h in benzene solutions to yield the free ligand

$PhMe_2Si–SiMe_2Ph$ and black molybdenum metal". Based on the results described within the Ph.D. theses on hand (see Chapter 7), it is very unlikely that compound **3f** is thermally unstable. One can speculate that the decomposition occurs through accidental introduction of oxygen into the sample containing **3f**. This speculation is based on common knowledge that di(benzene)metal complexes are known to be very sensitive to oxygen.

A [3]molybdarenophane [$R_xE–ER_x–ER_x$ = $Me_2Si–O–SiMe_2$ (**3g**)] was obtained in low yield from the reaction of **3a** with Cl_2SiMe_2 upon addition of water and subsequent crystallization from hexane (5% yield).[23] Compound **3g** was the first characterized [n]molybdarenophane and is only one of two [n]molybdarenophanes (n = 2, 3) that are known.

1.2 [1]Metallacyclophanes and Related Compounds

Recently, a new class of strained complexes was discovered which incorporate heteroleptic sandwich complexes. These [1]metallacyclophanes are derived from cycloheptatrienyl-cyclopentadienyl sandwich compounds, [(η^7-C_7H_7)(η^5-C_5H_5)M] (M = Ti (**4**), V **(5)**, Cr (**6**)) (Figure 1-8).

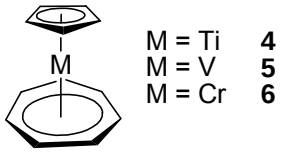

Figure 1-8. Cycloheptatrienyl-cyclopentadienyl sandwich complexes.

The cycloheptatrienyl-cyclopentadienyl sandwich complexes are often referred to as trometallocenes where the prefix tro refers to the tropyllium cation. According to this nomenclature **4** is named troticene, **5** is named trovacene and **6** is named trochrocene. Complexes **4**, **5** and **6** are 16-, 17- and 18-electron complexes, respectively, with their structural details and relevant properties reported in Table 1-3. Compound **4** was first prepared in 1970 by Van Oven *et al*.[31] with details of the solid-state structure being reported by Zeinstra and co-worker,[32] whereas **5** was first prepared by King *et al*.[33] and the solid-state structure was reported by Engetbretson *et al.*[34] Compound **6** was first prepared by Fisher *et al*.[35] and characterized by single-crystal X-ray crystallography by Lyssenko *et al*.[36] In **4, 5** and **6** the cyclopentadienyl (Cp) and cycloheptatrienyl (Cht) rings are π-bound to the metal centre and are co-planar. The $Cp_{centroid}$–metal distances are 1.982, 1.917 and 1.830 Å for **4**, **5** and **6**, respectively, and the $Cht_{centroid}$–metal distances are 1.487, 1.464, and 1.434 Å for **4**, **5** and **6**, respectively.[36]

Both rings of compounds **4**, **5**, **6** can be lithiated by addition of 2 equivalents of an alkyllithium in the presence of tmeda to produce the dilithio derivatives [(η^7-C_7H_6Li)Ti(η^5-C_5H_4Li)]·2tmeda (**4a**)[37], [(η^7-C_7H_6Li)V(η^5-C_5H_4Li)]·tmeda (**5a**)[38] and [(η^7-C_7H_6Li)Cr(η^5-C_5H_4Li)]·tmeda (**6a**)[39], respectively.

Table 1-3. Structural details and properties of the trometallocenes.

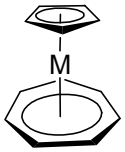

Compound	M	^{1}H NMR[a]		^{13}C NMR[a]		$Cp_{centroid}$ – M[b]	$Cht_{centroid}$ – M[b]	Metal Atomic radius[c]	Ref
		Cp	Cht	Cp	Cht				
4	Ti	4.90	5.47	94.9	84.3	1.982	1.487	1.448	36,40
5	V					1.917	1.464	1.35	36
6	Cr	3.66	5.45	75.37	87.09	1.830	1.434	1.29	36,41

[a] C_6D_6, ppm, [b] Å, [c] Å, CN =12. [16]

[1]Metallacyclophanes can also be prepared from the manganese-containing sandwich complex [(η^6-C_6H_6)(η^5-C_5H_5)Mn] (**7**) (Figure 1-9). Complex **7** was first prepared by Fischer *et al.*[42] and fully characterized by Herberhold *et al*.[43]

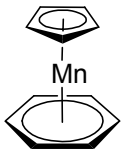

7

Figure 1-9. Illustration of benzenecyclopentadienylmanganese (**7**).

Compound **7** contains a manganese atom sandwiched between a coplanar benzene and Cp ring separated by a distance of 3.27 Å in the solid state. As expected, the ^{1}H NMR spectrum of **7** in C_6D_6 consists of two signals, a resonance at δ 3.83 corresponding to the Cp ligand and a

resonance at δ 4.50 for the C_6H_6 ligand. Consistently, the ^{13}C NMR spectrum (C_6D_6) displays two resonances at δ 69.6 (Cp) and 72.9 (C_6H_6). Compound **7** can be dilithiated using two equivalents of butyllithium in the presence of pmdta to produce [(η^6-C_6H_5Li)(η^5-C_5H_4Li)Mn]·pmdta (**7a**).[44]

Chapters 1.2.1 and 1.2.2 below will summarize all known [1]metallacyclophanes prepared from dilithiated heteroleptic sandwich complexes (**4a**–**7a**).

1.2.1 Group-13-Bridged Heteroleptic [1]Metallacyclophanes

Only three examples of boron-bridged heteroleptic [1]metallacyclophanes have been published in the literature. A bora[1]trovacenophane was prepared by reaction of **5a** with $(Me_3Si)_2NBCl_2$ to produce **5b** [ER_x = $BN(SiMe_3)_2$].[45] Utilizing an analogous procedure, two bora[1]trochrocenophanes [ER_x = $BN(SiMe_3)_2$ (**6b)**, $BN(SiMe_3)$(*t*Bu) (**6c**)] were prepared from **6a** and $(Me_3Si)_2NBCl_2$ and (*t*Bu)$(Me_3Si)NBCl_2$, respectively.[41]

The bora[1]metallacyclophanes **5b** and **6b** were characterized by multi-nuclear NMR spectroscopy and by single-crystal X-ray crystallography with some structural parameters being summarized in Table 1-4.

Compounds **5b** and **6b** possess similar boron–carbon and boron–nitrogen bond lengths, but rather different tilt angles α of 28.23 and 23.87°, respectively, a result of the larger covalent radius of vanadium (CN = 12, r = 1.35 Å)[16] compared to chromium (CN = 12, r = 1.29 Å)[16]. The authors noted the tilt angle for **6b** is surprisingly smaller than anticipated. A similar boron-bridged [1]CAP **1h** [ER_x = $BN(SiMe_3)$(*i*Pr)] possesses a tilt angle of 26.6(3)°.[14] The separation between the arene rings of 3.224 Å in $[Cr(C_6H_6)_2]$[21] and 3.264 Å in [(η^7-C_7H_7)(η^5-C_5H_5)Cr][36] are very similar. Therefore, the tilt angle α in **6b** and **1h** should be likewise very similar.

Interestingly, the authors did not mention that the ring$_{centroid}$–chromium distances are shorter in the strained bora[1]trochrocenophane (Cp$_{centroid}$–Cr = 1.808 Å, Cht$_{centroid}$–Cr = 1.409 Å) than in the parent trochrocene (Cp$_{centroid}$–Cr = 1.830 Å, Cht$_{centroid}$–Cr = 1.434 Å)[36].

Table 1-4. Selected structural details of bora[1]trometallocenophanes.

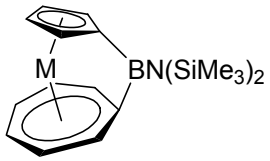

Compound	M	Cp$_{centroid}$ – M[a]	Cht$_{centroid}$ – M[a]	B–Cp[a]	B–Cht[a]	B–N[a]	α[b]	Ref
5b	V	[c]	[c]	1.6209(17)	1.6170(17)	1.4075(16)	28.23	45
6b	Cr	1.808	1.409	1.629(4)	1.620(4)	1.399(4)	23.87(13)	41

[a] Å, [b] °, [c] not reported.

To date, aluminum-, gallium- and indium-bridged heteroleptic [1]metallacyclophanes are unknown in the literature.

1.2.2 Group-14-Bridged Heteroleptic [1]Metallacyclophanes

There are a significant number of publications dealing with group-14-bridged heteroleptic [1]metallacyclophanes. [1]Troticenophanes with silicon[40] and germanium[46] as bridging elements have been published by Tamm *et al*. Troticenophanes **4b** (ER$_x$ = SiMe$_2$) and **4c** (ER$_x$ = GeMe$_2$) were prepared from **4a** and an equimolar amount of Cl$_2$SiMe$_2$ and Cl$_2$GeMe$_2$, respectively (Scheme 1-8).

Scheme 1-8. Preparation of [1]troticenophanes.

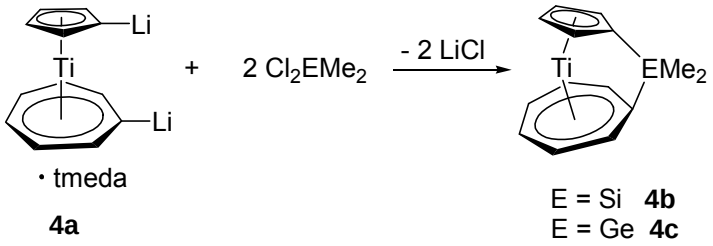

Compounds **4b** and **4c** were fully characterized by multinuclear NMR spectroscopy and by single-crystal X-ray analysis and the structural parameters are summarized in Table 1-5.[40, 46] The solid-state structures revealed highly-tilted molecules with tilt angles α of 24.1 for **4b** and 22.9° for **4c**. The *ipso* carbon resonances in the respective ^{13}C NMR spectrum for **4b** and **4c** were shifted upfield in relation to the resonances of the parent troticene [**4b**: δ = 83.6 (Cp), 61.6 (Cht); **4c**: 81.6 (Cp), 58.8 (Cht); **4**: 94.9 (Cp), 84.3 (Cht]. $Cp_{centroid}$–Ti and $Cht_{centroid}$–Ti bonds are slightly longer in the strained compounds **4b** and **4c** compared to the parent compound **4**. The authors did not comment on these structural details, but interestingly, this is opposite to what was observed for the bora[1]trochrocenophane **6b** ($Cp_{centroid}$–Cr = 1.808 and $Cht_{centroid}$–Cr = 1.409 Å) where the $ring_{centroid}$–Cr distances contract slightly when an interannular bridge is introduced to trochrocene ($Cp_{centroid}$–Cr = 1.830 and $Cht_{centroid}$–Cr = 1.434 Å).

Table 1-5. Selected structural parameters of group-14-bridged [1]troticenophanes.

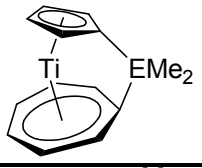

Compound	E	$Cp_{centroid}$ – M[a]	$Cht_{centroid}$ – M[a]	α[b]	*ipso*-C_5H_4[c]	*ipso*-C_7H_6[c]	Ref
4b	Si	1.988	1.496	24.1	83.6	61.6	40
4c	Ge	1.990	1.492	22.9	81.6	58.8	46

[a] Å, [b] °, [c] C_6D_6, ppm.

Since troticene **4** and its *ansa*-derivatives **4b** and **4c** both possess 16 valence electrons, it should be possible to coordinate an additional two-electron donor to the titanium centre. In **4b** and **4c** the bending of two rings creates a gap at the titanium centre making space available for coordination of small donor ligands. To test whether coordination of additional ligands was possible, **4b** was treated with either an atmosphere of carbon monoxide (50 bar) or solutions of 2,6-dimethylphenylisocyanide or *tert*-butylisocyanide which resulted in complexes **4d, 4e** and **4f**, respectively (Figure 1-10).[40]

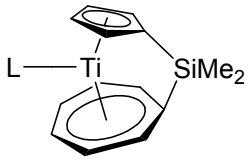

L = CO **4d**
L = CN-*o*-Xy **4e**
L = CN-CMe$_3$ **4f**

Figure 1-10. Illustrations of troticenophanes **4d**, **4e** and **4f** (*o*-Xy = 2,6-dimethylphenyl).

The solid-state structure of **4f** reveals a molecule that is quite structurally different from **4b**. The Cht$_{centroid}$–Cr distance of 1.649 Å in **4f** is significantly longer than that of 1.496 Å in **4b**. The Cht ring in **4f** is slightly puckered with two of the Cht carbons not lying in the plane of the ring, whereas, in **4b** this ring is planar. Unfortunately, the authors did not report quantitative data on how far these two carbons lie outside the plane of the ring. The authors described the bonding mode between the Cht ring and the titanium centre in **4f** as an "open η^5-bonding mode".[40] They suggested that utilizing stronger coordinating ligands might cause the Cht to undergo complete η^7 to η^5 interconversion providing titanocene-like complexes.

The only group-14-bridged [1]trovacenophanes were published by Elschenbroich *et al.* with silicon as an interannular bridge.[38] Compounds **5c** (ER_x = $SiMe_2$) and **5d** (ER_x = $SiPh_2$)

were prepared by treatment of [(η^7-C_7H_6Li)V(η^5-C_5H_4Li)]·tmeda (**5a**) with equimolar amounts of Cl_2SiMe_2 and Cl_2SiPh_2, respectively (Figure 1-11).

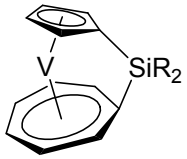

R = Me **5c**
R = Ph **5d**

Figure 1-11. Illustration of sila[1]trovacenophanes **5c** and **5d**.

A tilt angle of $\alpha = 17.3°$ for complex **5d** was determined from its solid-state structure. As expected, this angle is significantly smaller than that reported for bora[1]trovacenophane **5b** (28.23°). This large difference can be attributed to differences in covalent radius between boron (CN = 3, r = 0.82 Å)[16] and silicon (CN = 4, r = 1.17 Å)[16].

Several group-14-bridged [1]trochrocenophanes have been reported by Braunschweig *et al*. with either silicon or germanium as bridging elements.[41,47] [1]Trochrocenophane were prepared by addition of equimolar amounts of silicon dichlorides or germanium dichlorides to a slurry of [(η^7-C_7H_6Li)Cr(η^5-C_5H_4Li)]·tmeda (**6a**) resulting in **6c** (ER_x = $SiMe_2$), **6d** (ER_x = Si*i*Pr_2), **6e** (ER_x = SiMe(*i*Pr)), **6f** (ER_x = Si(*cyclo*-$CH_2)_3$) and **6g** (ER_x = $GeMe_2$), respectively.

All compounds were characterized by X-ray crystallography (except **6e**) and multinuclear NMR spectroscopy; tilt angles α and *ipso* carbon shifts are given in Table 1-6. The compounds **6c**–**6g** are strained with the Cp and Cht rings tilted towards one another with tilt angles α in the range of 15.1–16.3°. As expected, the *ipso* carbon resonances of the strained compounds **6c**–**6g** are shifted upfield compared to the carbon resonances of the parent trochrocene **6** [δ 75.37 (Cp),

87.09 (Cht)]; i.e. the shifts of the *ipso*-C_5H_4 range from δ 49.9–54.5 and those of the *ipso*-C_7H_6 range from δ 60.1–61.4.

Table 1-6. Selected structural data of group-14-bridged [1]trochrocenophanes.

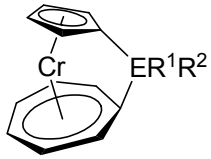

Compound	E	R^1	R^2	α[a]	*ipso*-C_5H_4[b]	*ipso*-C_7H_6[b]	Ref
6c	Si	Me	Me	15.6(1)	51.66	60.10	47
6d	Si	*i*Pr	*i*Pr	15.8(1)	51.67	60.17	47
6e	Si	Me	*i*Pr	[c]	51.39	60.10	47
6f	Si	*cyclo*-$(CH_2)_3$		16.33(17)	49.9	60.2	47
6g	Ge	Me	Me	15.07(17)	54.49	61.35	41

[a] °, [b] C_6D_6, ppm, [c] Solid-state structure not determined.

The stanna[1]trochrocenophane **6h** (ER_x = $SnMes_2$) was prepared in very low yield (1%) by addition of dichlorodimesitylstannane to a slurry containing the dilithium derivative **6b**.[41] ^{13}C NMR data support the proposed structure of compound **6h**, because the resulting *ipso* carbon shifts of δ 70.36 (Cp) and 74.43 (Cht) were shifted upfield compared to the resonances of the parent trochrocene **6** [δ 75.37 (Cp), 87.09 (Cht)].

Only one example of a group-14-bridged [1]metallacyclophane that incorporates the manganese sandwich complex **7** with silicon as a bridging element is known.[44] The sila[1]metallacyclophane **7b** (ER_x = Si*i*Pr_2) was prepared from *i*Pr_2SiCl_2 and a slurry of [(η^6-C_6H_5Li)(η^5-C_5H_4Li)Mn]·pmdta (**7a**) (Figure 1-12).

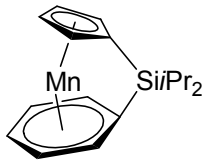

7b

Figure 1-12. Illustration of silicon-bridged [1]metallarenocenophane **7b**.

Compound **7b** is the first example of a [1]metallarenocenophane; a metallarenocenophane that contains a metal in the +1 oxidation state sandwiched between a benzene and a Cp ring linked by a bridging element. The molecular structure of **7b** possesses a tilt angle α of 16.97(14)°. As expected, the *ipso* carbon resonances for **7b** of δ 37.3 (Cp) and 38.2 (C_6H_6) are upfield compared to the resonances of the parent compound **7** of δ 69.6 (Cp) and 72.9 (C_6H_6).

1.2.3 Heteroleptic [n]Metallacyclophanes with n > 1

There are several published examples of heteroleptic [n]metallacyclophanes with n = 2, 3 and 4. [2]Metallacyclophanes are usually prepared by one of two common routes. The first route involves addition of $XR_xE–ER_xX$ (X = Cl, Br) to a dilithiated sandwich complex. Several [2]metallacyclophanes have been prepared by this route including compound **5e** (Figure 1-13) and their structural parameters are summarized in Table 1-7.

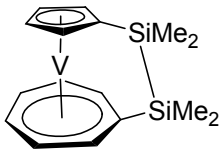

5e

Figure 1-13. Illustration of disila[2]trovacenophane **5e**.

Table 1-7. Selected structural parameters of heteroleptic [2]metallacyclophanes.

Compound	Cp–M(C_nH_{n-1})	ER_x–ER_x	α[a]	*ipso*-C_5H_4[b]	*ipso*-C_nH_{n-1}[b]	Ref
5e	V(C_7H_6)	Me_2NB–$BNMe_2$	11.4	[c]	[c]	45
5f	V(C_7H_6)	Me_2Si–$SiMe_2$	3.8	[c]	[c]	38
6i	Cr(C_7H_6)	Me_2NB–$BNMe_2$	8.9	[c]	[c]	39
6j	Cr(C_7H_6)	Me_2Si–$SiMe_2$	2.60(15)	81.4	91.4	47
7c	Mn(C_6H_5)	Me_2NB–$BNMe_2$	11.26(12)	[c]	[c]	44

[a] °, [b] C_6D_6, ppm, [c] Not observed.

The [2]metallacyclophanes listed in Table 1-7 are moderately tilted and are resistant to ROP. Heteroleptic [2]metallacyclophanes have also been prepared and isolated by adding a platinum(0) compound such as [$Pt(PEt_3)_3$] to a strained [1]metallacyclophane. Two [2]troticenophanes have been prepared by this route [R_xE–ER_x = $(Et_3P)_2Pt$–$SiMe_2$ (**4g**), $(Et_3P)_2Pt$–$GeMe_2$ (**4h**)]. The solid-state structure of compound **4g** reveals a molecule with a two atom interannular bridge and the Cht and Cp rings are moderately tilted towards one another (α = 13.5°).[46] The analogous [2]trovacenophane **5g** [R_xE–ER_x = $(Et_3P)_2Pt$–$SiMe_2$] was prepared from [$Pt(PEt_3)_3$] and **5c**.[48] Revealed by single-crystal X-ray analysis, **5g** is moderately strained with a tilt angle α of 10.6°. [2]Trochrocenophane **6k** [ER_x = R_xE–ER_x = $(Et_3P)_3Pt$–$SiMe_2$] was prepared from the stoichiometric reaction of $Pt(PEt_3)_3$ with sila[1]trochrocenophane **6c**.[47] A tilt angle α of 7.51(7)° was determined from the solid-state structure of **6k**. For complexes **4g**, **4h**, **5g** and **6k** the platinum regioselectively inserts into the bridging element–Cht *ipso* carbon bond. The use of transition-metal(0) compounds for ROP will be discussed in Chapter 1.3.

B–B bonds are prone to undergo oxidative addition reactions with low-valent transition-metals generating bis(boryl)-metal moities.[25] Braunschweig *et al.* have taken advantage of this fact and prepared the first heteroleptic [3]trometallocenophane by reaction of [$Pt(PEt_3)_3$] with the dibora[2]trochrocenophane **6i** generating the [3]trochrocenophane **6l** [R_xE–ER_x–ER_x = $(Me_2N)B$–$Pt(PEt_3)_2$–$B(NMe_2)$] (Figure 1-14).[39]

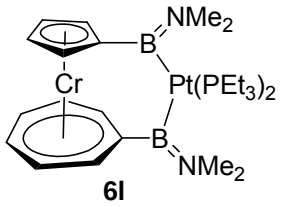

6l

Figure 1-14. Illustration of [3]trochrocenophane **6l**.

The tilt angle α of 3.48(15)° in **6l** shows a marked reduction in the ring strain when compared to the [2]trochrocenophane **6i** (α = 8.9°). What makes the diborane **6l** very interesting is the fact that diboranes have been used in the transition-metal catalyzed diboration of alkynes[49] and, therefore, **6l** can be equated to an intermediate in these type of reactions.

Two heteroleptic [4]metallacyclophanes isomers **6m** and **6n** were prepared in a 3:1 ratio from the [$Pd(PPh_3)_4$] catalyzed insertion of propyne into the Si–Si bond of disila[2]trochrocenophane **6j**[24] (Figure 1-15). Similar reactions have been observed with a disila[2]ferrocenophane using various alkynes and [$Pd(PPh_3)_4$] as a catalyst source.[50] The tilt angle of 4.27(10)° in **6m** indicates the molecule is only slightly strained.

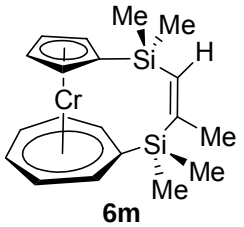

6m

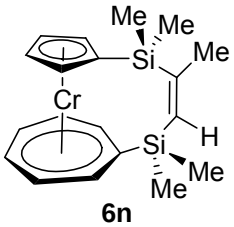

6n

Figure 1-15. Two isomers of [4]trochrocenophanes **6m** and **6n**.

1.3 ROP of [1]Metallacyclophanes

As mentioned earlier, strained [1]metallacyclophanes can be utilized as monomers to prepare organometallic polymers. Organometallic polymers are of interest because of the close proximity of metals in the polymer chain and these polymers could potentially be utilized as semi-conductors or as conducting polymers. Some interesting properties for these polymeric materials include electrochromic behaviour and electronic communication between metal centres.[51]

There are currently two routes known by which organometallic polymers can be prepared: polycondensation and ROP. The former is a step-growth process involving condensation reactions between multi-functional monomers where small molecules are eliminated such as H_2O or LiCl during each condensation reaction. In polycondensations, polymer weights increase slowly such that many species with varying chain lengths will be present at any given time and only near the end of the polycondensation process will be high-molecular weight polymers be generated from long chains reacting with other long chains. During polycondensation reactions, monomers can react with other monomers, dimers, trimers and so on. Two requirements make it very difficult to achieve high molecular weight organometallic polymers from polycondensations. These are precise stoichiometry between reactants and second, high purity levels of organometallic monomers used. The second requirement is often difficult to achieve, for example, dilithioferrocene, a common starting material for polycondensations, is often isolated as a solid not greater than 95% pure. Because of these stringent requirements polycondensations have only found limited success in production of

organometallic polymers. In order to obtain high-molecular-weight polymers from polycondensations the small-molecule byproduct often needs to be removed during the reaction to allow it to go to completion.

ROP is a process where strained cyclic monomers are polymerized through a chain growth or addition polymerization mechanism. In this process an initiator is first required to react with the monomer generating a reactive centre that can attack another monomer and generate a new reactive centre thus generating a propagating chain where a new reactive centre is generated in every subsequent step. The initiator does not get incorporated into the propagating chain of the polymer, but it is sometimes incorporated as an end group, so these polymers have the same composition as the starting monomer. The compounds that are present at any monomer conversion rate are high-molecular weight polymers along with un-reacted monomers, a small concentration of propagating chains, initiator, but no intermediate oligomers.[10] ROP allows for the preparation of high molecular weight polymers because high purity levels of the starting monomers and exact stoichiometric amounts are not required, assuming that any impurity does not react with the reactive propagating centre. Polymer growth by ROP is dependent on maintaining a reactive centre since un-reacted monomers do not react with other un-reacted monomers. The exclusion of adventitious moisture is therefore necessary because it leads to premature chain termination and quenching of the initiator.

Some ROPs are living polymerizations meaning that once all starting monomer has been consumed, the remaining ends of the polymer chain continue to be active or "living" such that addition of new monomer allows for the polymerization to resume without the need for new initiator to be added. A living polymerization is defined as "the creation of polymer chains without significant irreversible chain transfer or chain termination".[52] Only with very meticulous

care in avoiding moisture and very pure starting monomers can living polymerizations be achieved. Living polymerizations allow co-block or star polymers to be accessed. A co-block polymer consists of alternating blocks of different repeating units where each of the blocks is the composed of the same repeating unit. Co-block polymers allow for the combination of polymers with different desirable properties.

There are several known methodologies for generating polymers from ROP of [1]metallacyclophanes. The one common requirement for ROP reactions is the need for an initiator. Initiators that have successfully been employed in ROP reactions of [1]metallacyclophanes include heat (thermal ROP), anions (anionic ROP), cations (cationic ROP), transition metals (transition-metal catalyzed ROP) and photons (photo-controlled ROP). [1]Ferrocenophanes ([1]FCPs) have been at the forefront of development for ROP and, therefore, they will be used as examples to describe ROP methodologies. The discussion on [1]FCPs will not be comprehensive because a review on ROP methodologies for [1]FCPs was published recently by Rehahn *et al*.[10] and a comprehensive discussion of [1]FCPs and ROP methodologies is beyond the scope of this theses.

Interestingly, the first attempts to prepare poly(ferrocenylsilane)s in the 1960s were made by utilizing polycondensation routes involving the condensation of $FeCl_2$ with $Li_2[(C_5H_4)_2SiMe_2]$[53]or 1,1′-dilithioferrocene with silicon dihalides.[54] Unfortunately, both methods only produced low-molecular weight polymers. About 30 years later, the discovery that [1]ferrocenophanes undergo ROP upon heating at elevated temperatures (130 °C) to produce high-molecular weight poly(ferrocenylsilanes) was reported by Manners *et al*. in 1992[8] (Scheme 1-9). The process has been coined “thermal ROP”. The polymerization of dimethylsila[1]ferrocenophane (**8a**) was followed by differential scanning calorimetry (DSC) to

obtain an estimate of the strain energy present in the monomer. An endothermic peak at 78 °C was measured which corresponds to melting of the monomer and an exothermic peak was observed over the range of 120–170 °C corresponding to the exothermic ROP of the ferrocenophane. Through integration of the peak area of the exothermic peak, a strain energy of ca. 80 kJ mol^{-1} was determined. The resulting polymer was analyzed by gel permeatation chromatography (GPC) and a weight average molecular weight (M_w) of 5.2 x 10^5 and a number average molecular weight (M_n) of 3.4 x 10^5 were determined corresponding to a polydispersity index (PDI) of 1.53.

Scheme 1-9. Thermal ROP of dimethylsila[1]ferrocenophane (**8a**).

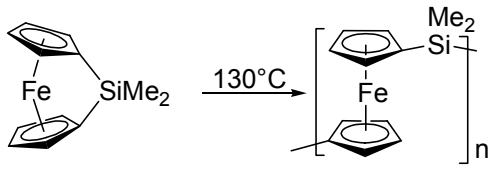

8a

Several years later a paper was published dealing with the mechanistic aspects of the thermal ROP of [1]FCPs.[55] Manners *et al*. were able to demonstrate that thermal ROP proceeds through the *ipso* carbon–Si bond cleavage. Addition of radical traps to the ROPs did not hinder the reactions so homolytic bond cleavage could be excluded and, consequently, a heterolytic bond cleavage was proposed to occur. The authors suggested that the heterolytic bond cleavage would lead to small population of zwitterionic species with a positively charged silicon and a negatively charged Cp. The negatively charged Cp ring could then initiate chain propagation by attack on uncleaved Si–Cp bonds. In the review by Rehann *et al.,* the auhors claim thermal ROP of [1]FCPs does not generate a carbanionic centre because monomers bearing chlorosilyl groups produce high-molecular weight polymers.[10] It is not clear what this claim was based on as there was no experimental evidence or explanation presented in the review.

The first publication on anionic ROP was published by Seyferth *et al*. even though at the time the authors did not realize it.[56,57] They reported that the reaction of $PhPCl_2$ with dilithioferrocene·2/3 tmeda produces a phenylphospha[1]FCP (**8b**), whereas, carrying out the reaction under slightly different conditions led to high-molecular weight polymers ($M_w = 10^5$). The latter reaction was assumed to proceed via a polycondensation type reaction at the time. Manners *et al*. later proposed that poly(ferrocenylphosphines) with substantial molecular mass are more likely to result from a chain-growth process.[58] That is, the phenylphospha[1]FCP is generated *in situ* and reacts with an anionic initiator such as dilithioferrocene to generate high-molecular-weight polymers. In fact, Manners *et al*. demonstrated a living high molecular weight polymer ($M_n = 3.6 \times 10^4$) could be generated by adding catalytic amounts of butyllithium to the phenylphospha[1]FCP in a ratio of 1:100.[58]

The first report on anionic ROP of [1]FCPs was published by Manners *et al*. in 1994.[59] Sila[1]FCP (**8a**) was polymerized by the catalytic initiator ferrocenyllithium (FcLi) (1:10) producing poly(ferrocenylsilane) ($M_w = 9500$, $M_n = 8000$). Shortly thereafter, Manners *et al*. reported on the first example of living anionic ROP of **8a**, utilizing catalytic amounts of FcLi, butyllithium or phenyllithium.[60] The two main requirements for generating the living polymers were very high purity of monomers and the absolute exclusion of moisture.

An anionic ROP is believed to involve nucleophilic attack at the bridging element E, generating a Cp anion that can participate in chain propagation and the propagating chains can be terminated by addition of end-capping agents such as chlorotrimethylsilane or H_2O (Scheme 1-10).[51]

Scheme 1-10. Anionic ROP mechanism of a [1]FCP (adapted from ref. 51).

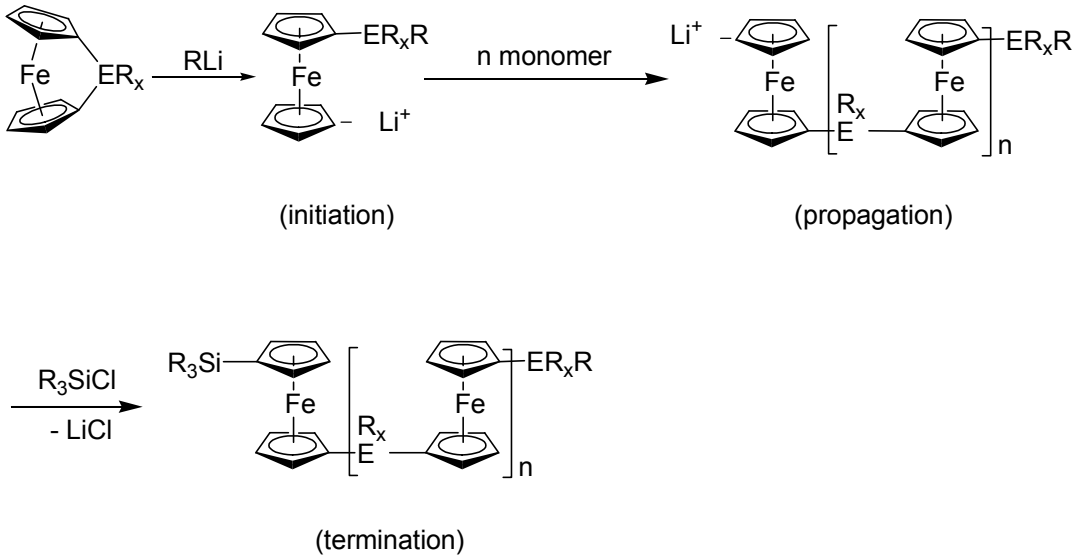

The first example of cationic ROP of [1]FCPs was reported by Manners *et al*. when carbathio[2]FCP **8c** was polymerized using the cationic initiators such as methyl triflate ($MeOSO_2CF_3$) or $BF_3{\cdot}OEt_2$ (Scheme 1-11).[61]

Scheme 1-11. Cationic ROP of [2]FCP **8c**.

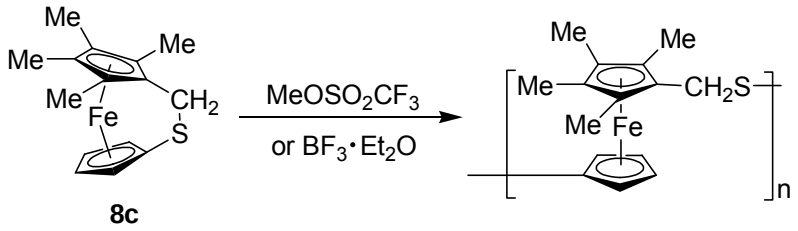

Unfortunately, resulting polymers from the cationic ROP of **8c** were insoluble in common organic solvents and therefore could not be analyzed by GPC. However, some C_6D_6 soluble material could be analyzed by NMR spectroscopy, which were identified as oligomeric materials possessing the $[(\eta^5\text{-}C_5Me_4)Fe(\eta^5\text{-}C_5H_4)CH_2S]_n$ unit, consistent with the proposed structure of the polymeric material. The cationic ROP of **8c** was believed to proceed through an initial methylation step, generating a propagating cationic sulfur centre (Scheme 1-12). To

unravel the cationic ROP mechanism, a detailed study on the cationic ROP of **8c** was untertaken a few years later.[62] A solution containing the carbathio[2]FCP was treated with excess of CF_3OSO_2Me in an attempt to isolate an intermediate such as a cationic S-methylated derivative **8d** (Scheme 1-12) or a ring-opened analogue, but only polymeric materials could be isolated, implying that the propagation step of the ROP occurs more rapidly than the initiation step (methylation step). Treatment of **8c** with equimolar amounts of $BF_3{\cdot}Et_2O$ in the presence of the proton trap 2,6-di-*tert*-butylpyridine inhibited the ROP process, whereas when **8c** was treated with CF_3OSO_2Me in the presence of the same proton trap no inhibition was observed, suggesting that the initiation step involves methylation when utilizing CF_3OSO_2Me and protonation when using $BF_3{\cdot}Et_2O$ in the form of either trace amounts of HF or $H[BF_3(OH)]$.

Scheme 1-12. Proposed cationic ROP mechanism of [2]FCP **8c** using $MeOSO_2CF_3$ as a cationic initiator (taken from ref. 62).

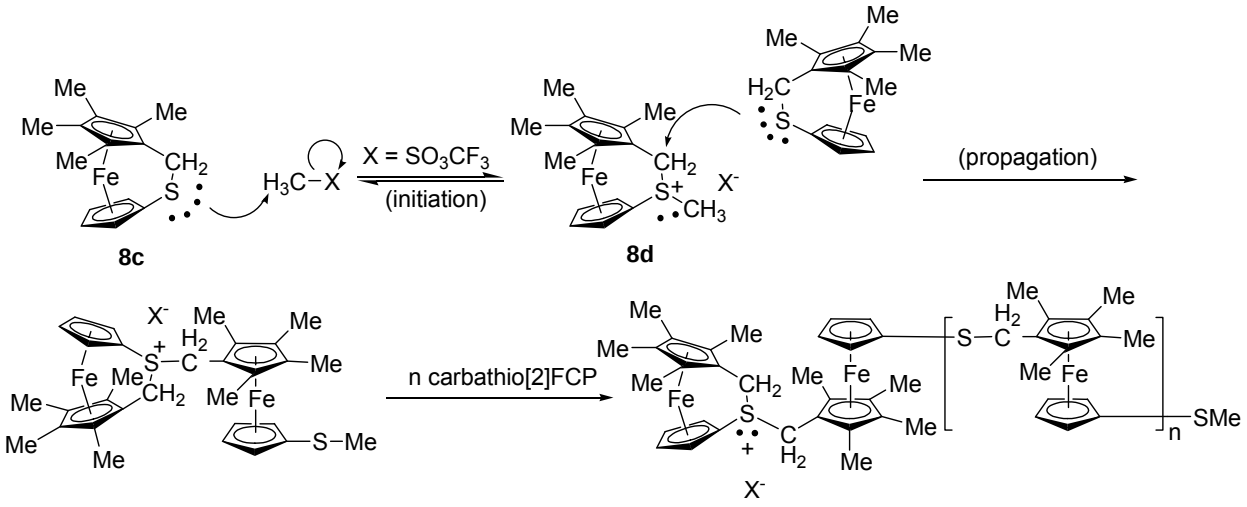

Manners *et al*. polymerized the tin-bridged [1]FCP **8e** by utilizing catalytic amounts of cationic initiators like CF_3SO_3H, CF_3SO_3Me and $CF_3SO_3SnBu_3$, and a mechanism was proposed for this cationic ROP (Scheme 1-13).[63] The initial step involves a rapid reaction of **8e** with the triflate species generating a neutral ring-opened tin-triflate species, which can react with **8e** via a

chain-growth process through a pentacoordinate tin intermediate generating poly(ferrocenylstannanes). If excess triflate anions are present in the reaction mixture, the propagation is inhibited. Based on this observation, they suggested that the propagating tin centre is cationic or cation-like (Scheme 1-13).

Scheme 1-13. Proposed cationic ROP mechanism of stanna[1]FCP **8e** (taken from refs. 10 and 63).

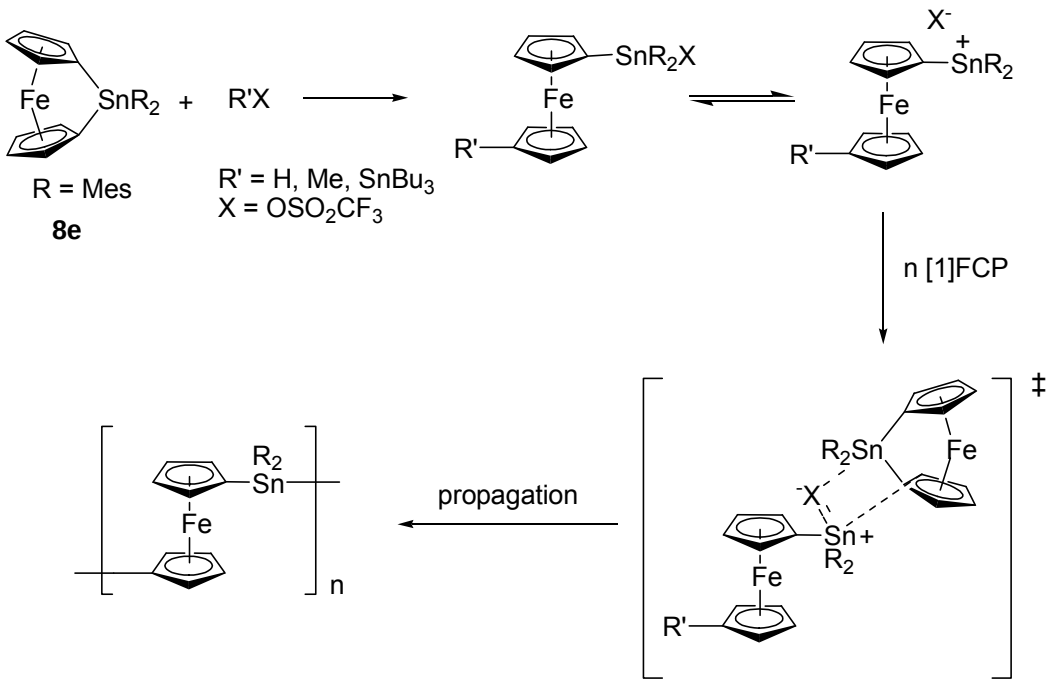

The first examples of transition-metal catalyzed ROP of a [1]FCPs was reported independently by two groups in 1995. The Manners group reported that dimethylsila[1]FCP **8a** readily undergoes ROP when catalytic amounts of transition-metal complexes are added.[64] They found that addition of either $[Rh(cyclooctene)_2(\mu\text{-}Cl)]_2$, $[Pd(cod)Cl_2]$ (cod = 1,5-cyclooctadiene), $PdCl_2$ or $PtCl_2$ (0.01 – 0.10 equivalents) to **8a** led to a rapid increase in solution viscosity and conversion to polyferrocenyl(silane) (Scheme 1-14). When 0.01 equivalents of $[Pd(cod)Cl_2]$ were added to **8a** and stirred for 24 h, poly(ferrocenylsilane) was generated with polymer weights M_w = 132300 and M_n = 122500 as determined by GPC. Interestingly, the transition-

metal complexes $[Rh(cod)(\mu\text{-}Cl)]_2$ $[Rh(PPh_3)_3Cl]$, $[Pd(PPh_3)_2Cl_2]$, $[Pd(CH_3CN)_2Cl_2]$, $[Pd(PPh_3)_3]$ and $[Pd(PPh_3)_3]$ did not catalyze the ROP of **8a** at room temperature. For transition-metal catalyzed ROP to occur, it was believed that the initial step was a ligand dissociation from the transition-metal and when complexes with phosphines were utilized, this dissociation was not believed to occur. The transition-metal catalyzed ROP was proposed to proceed through an initial oxidative addition of the Si–C bond to the transition-metal centre, followed by chlorine transfer from the metal to silicon, generating a growing chain end and repetitive oxidative addition/reductive elimination steps for chain propagation. The above mechanism was proposed based entirely on an earlier proposed mechanism for the homogenous transition-metal catalyzed ROP of sila- and disilacyclobutanes using Pd, Pt and Rh complexes.[65] The transition-metal catalyzed ROP route has advantages over the anionic ROP route in that the starting monomer does not need to be exceptionally pure and the careful exclusion of moisture is not required.

Scheme 1-14. Transition-metal catalyzed ROP of sila[1]FCP **8a**.

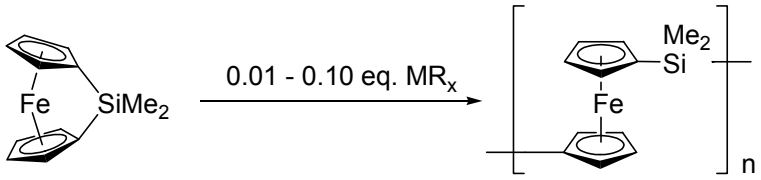

MR_x = $[Rh(cyclooctene)_2(\mu\text{-}Cl_2)]_2$, $[Pd(cod)Cl_2]$, $PdCl_2$, $PtCl_2$

In an independent report, Tanaka *et al*. reported that **8a** and dimethylgerma[1]FCP (**8f**) readily undergo ROP when catalytic amounts of either $[Pt(cod)_2]$, $[Pt(cod)Cl_2]$, $[Pt_2(dba)_3]$ (dba = dibenzylideneacteone), $[Pd(dba)_2]$ or $[Pd(cod)Cl_2]$ are added.[66] For example, addition of 0.02 equivalents of $[Pt(cod)_2]$ to **8a** led to quantitative conversion of polyferrocenylsilane in 3 h with a molecular weight M_w of 1.7×10^6 and PDI of 2.8.

Studies to discern whether the initial step in transition-metal catalyzed ROP was indeed an oxidative addition step were undertaken by Manners *et al* in 1996.[67] Stoichiometric additions of $[Pt(PEt_3)_3]$ to **8a** at 60 °C for 4h led to complete conversion of the [2]FCP **8g** where the platinum had inserted into Si–C bond, providing evidence that such a step can occur (Scheme 1-15). The identity of **8g** was confirmed by single-crystal X-ray analysis, showing that it was still slightly strained ($\alpha = 11.6(3)°$). To test whether **8g** could act as a catalyst, it was added to **8a** and the mixture heated with stirring. No observable changes were seen through monitoring of the mixture by ^{1}H NMR spectroscopy corroborating their earlier findings that phosphine derivatives of group-9 and -10 metals do not polymerize [1]FCPs.

Scheme 1-15. Synthesis of [2]FCP **8g** from the insertion of $Pt(PEt_3)_2$ into the Si–C bond of [1]FCP **8a**.

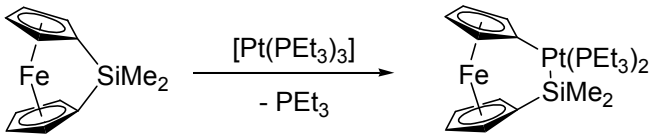

8a **8g**

Because **8g** did not act as precatalyst for ROPs, Manners *et al*. set out to prepare and characterize an active precatalyst for ROPs of [1]FCP. From equimolar mixtures of **8a** and $[Pt(cod)_2]$, a [2]FCP (**8h**) was isolated where one cod ligand had dissociated from the platinum metal (Figure 1-16).[68] The catalytic reaction of **8a** with $[Pt(cod)_2]$ generates poly(ferrocenylsilane). Therefore, **8h** was expected to be an active precatalyst in ROPs of [1]FCPs and indeed, this proved to be the case. A mixture of **8a** and **8h** (350:1) were stirred together at room temperature for 21 h and poly(ferrocenylsilane) was generated ($M_w = 2 \times 10^6$, $M_n = 1 \times 10^6$).

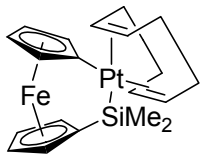

8h

Figure 1-16. [2]FCP **8h** isolated from the equimolar reaction of [Pt(cod)$_2$] and dimethylsila[1]FCP (**8a**).

In 2001, a study was undertaken to elucidate the mechanism by which transition-metal catalyzed ROPs of [1]FCPs operate.[69] Experimental evidence supported a mechanism with a heterogenous colloidal platinum catalyst. Up to this point, it was assumed these reactions progressed through homogenous catalysis in an analogous fashion that had been observed for the ROP of cyclic carbosilanes.[65] In a homogenous reaction for the transition-metal catalyzed ROP of a [1]FCP, a ferrocenophane fragment from the precatalyst should be is incorporated into the polymer at a terminal position. To answer the question whether the transition-metal catalyzed ROP of [1]FCPs proceeds through homogenous or heterogenous reactions several oligo- and polyferrocene model compounds were examined. The first reactions were carried out with the precatalyst **8h** (Figure 1-16) and sila[1]FCP **8i** (ER_x = SiMePh) in the presence of varying amounts of Et_3SiH. It has been demonstrated that addition of Et_3SiH to transition-metal catalyzed ROP of [1]FCPs allows for excellent chain-length control (M_n = 2000–45000) and yields a Et_3Si end-capped polymer.[70] The reactions should generate a polymer with a Me_2Si group incorporated into it and should contain a Et_3Si end-group if the reaction is homogenous in nature. The resulting polymers (M_n = 5000) did possess Et_3Si end-groups, however, $SiMe_2$ was not incorporated into the polymer. Similarly, **8a** was reacted with a catalytic amount of (cod)Pt(*t*Bu)$_2$Sn[2]FCP (**8j**) and stirred for 24 h in the presence of Et_3SiH generating a polymer that showed no ferrocenylstannane resonances.[69] A second test to help validate that the reactions

are heterogenous was carried out by adding mercury to the ROP reactions involving a catalytic amount of [Pt(cod)$_2$] and **8a**, because mercury is a well-known poison for heterogenous platinum forming an inactive alloy.[71] This reaction was strongly inhibited by the presence of mercury that even after two weeks only 40% of the starting monomer had been converted to polymer. So the evidence suggested that transition-metal catalyzed ROP of [1]FCPs involves heterogenous reactions, but the authors could not entirely rule out that a homogenous catalyst has some role in these transformations. A proposed mechanism for heterogenous transition-metal catalyzed ROP of [1]FCPs is given below in Scheme 1-16. The initial step is believed to be ligand dissociation followed by insertion of a $L_{n-1}Pt$ moiety into the Si–C bond generating a [2]FCP. Next, reductive elimination and ligand dissociation generates colloidal platinum. The colloidal platinum can insert into the Si–C bond of **8a**, thereby generating a propagating chain through subsequent oxidative insertion and reductive elimination reactions. These reactions are referred to as transition-metal catalyzed ROP. The actual identity of the propagating species is unknown, but it has commonly been simplified as a ring incorporating the transition metal for proposed ROP mechanisms like that shown in Scheme 1-16.

Scheme 1-16. Proposed mechanism for the heterogenous transition-metal catalyzed ROP of dimethylsila[1]FCP (**8a**) with a platinum(0) source (taken from ref. 69).

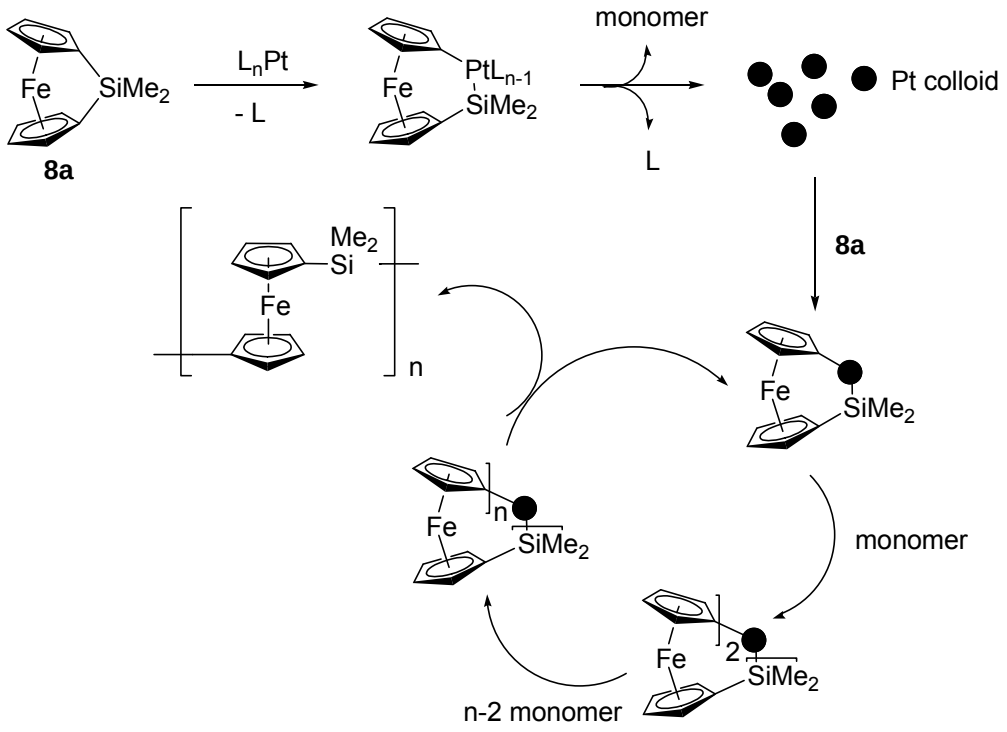

Photo-controlled ROP of [1]FCPs was discovered in 2000 by Miyoshi *et al*. when phospha[1]FCPs were polymerized through initiation by UV light.[72] The monomers chosen were bimetallic phosphorus-bridged [1]FCPs with phosphorus coordinated to organometallic fragments [Mn(η^5-C_5H_5)$(CO)_2$], [Mn(η^5-C_5H_4Me)$(CO)_2$] or [W$(CO)_5$]. When thf or acetonitrile solutions containing the monomer were irradiated for 10 min, a polymer was produced with molecular weights ranging from M_w = 3700 to 30000 and M_n = 2000 to 22000 (Scheme 1-17). ^{31}P NMR spectra of the resulting polymers only showed a single sharp signal. Consequently, the reactions were regioselective producing polymers of different lengths but with the same repeating units. Irradiation of solutions of CH_2Cl_2, 1,2-dichloroethane, benzene or CCl_4 containing the monomers results in loss of the regioselectivity, producing very complex

mixtures. No explanation was give for the differences in reactivity observed. It is important to note, that this is the only report where metalized [1]FCPs undergo ROP.

Scheme 1-17. Photo-controlled ROP of bimetallic phospha[1]FCPs monomers under broad-band irradiation.

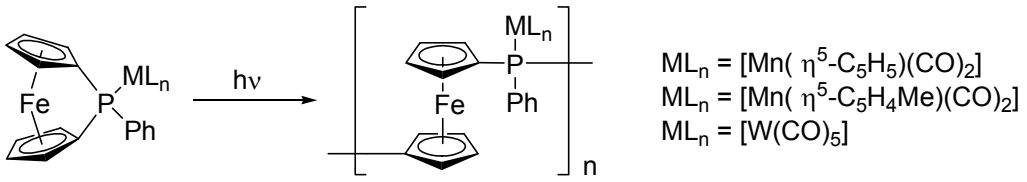

To gain insight into the mechanism of photo-controlled ROP, Miyoshi *et al*. irradiated solutions containing phospha[1]FCPs in the presence of an excess amount of $P(OMe)_3$ generating complexes where the Cp ligands undergo a η^5 to η^1 haptotropic shift (Scheme 1-18)**.**[73]

Scheme 1-18. UV irradiated phospha[1]FCPs in the presence of excess $P(OMe)_3$ inducing a η^5 to η^1 haptotropic shift.

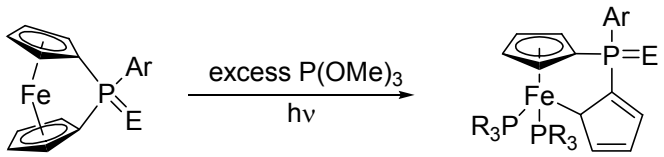

8k	E = S, Ar = Ph,	**8n**
8l	E = nothing, Ar = Ph,	**8o**
8m	E = nothing, Ar = Mes,	**8p**

The ring-slipped complexes readily undergo ROP when refluxed in thf for 24 h. Only low molecular weight polymers (M_w = 300–10000) were generated which was believed to be due to the presence of the strongly coordinating $P(OMe)_3$ that could depress smooth propagation of the polymeric chain. Interestingly, if $P(OMe)_3$ is replaced by a stronger coordinating ligand PMe_3, the η^1-Cp ring containing complex is not observed. Instead, the Cp ring dissociates completely

from the iron centre and through a replacement by 3 PMe_3 ligands, a zwitterionic piano-stool-type complex is generated (Scheme 1-19).

Scheme 1-19. UV-irradiated phospha[1]FCP **8k** in the presence of an excess of PMe_3 generating a zwitterionic piano-stool-type complex **8q**.

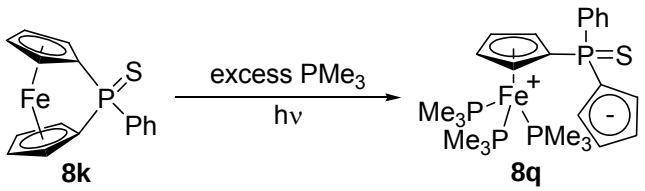

8k **8q**

These results support a mechanism where the initiation step is the intermolecular combination of two reactive ring-slipped intermediates where the η^1-Cp ring of one molecule attacks the iron centre of the another molecule displacing the Cp ring from the iron centre and generating a zwitterionic propagating chain. This propagating chain can then react with any remaining monomer (Scheme 1-20).

Scheme 1-20. Proposed mechanism for the photo-controlled ROP of phospha[1]FCPs (taken from ref. 73).

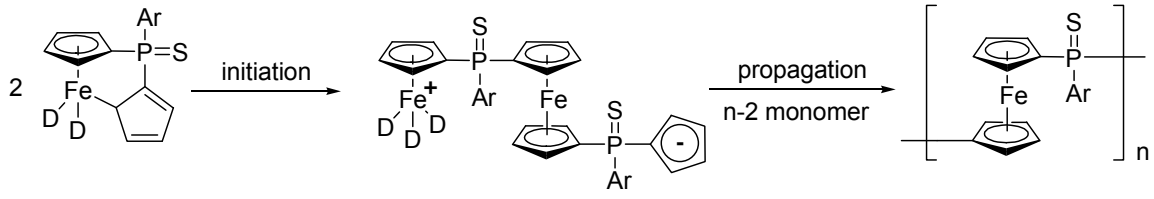

Manners *et al*. demonstrated that photo-controlled induced haptotropic shifts are reversible.[74] Ring slippage in dimethylsila[1]FCP **8a** can be induced by irradiating it with UV light in the presence of one equivalent bis(diphenylphosphino)ethane (dppe) producing a complex where one Cp ligand has slipped from a η^5 to η^1 coordination generating a piano-stool-type complex (Scheme 1-21). By heating **8r** in C_6D_6 at 70 °C, complete phosphine dissociation occurs resulting in quantitative retroconversion to **8a**.

Scheme 1-21. UV irradiated dimethylsila[1]FCP (**8a**) in the presence of dppe generating a piano-stool-type complex **8r** where one Cp undergoes η^5 to η^1 haptotropic shift.

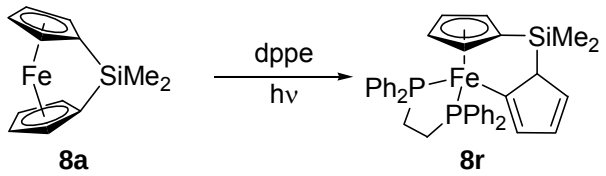

8a **8r**

A variation of the photo-controlled ROP methodology utilizes a combination of anionic initiation and UV irradiation to allow the preparation of living polymers and this variation has be coined photo-controlled living polymerization.[52,75] Manners *et al*. produced living polymers from the reaction of catalytic amounts of MCp (M = Li, Na) with **8a** by irradiating samples with UV light. Neither UV light nor anionic initiator alone causes ROP to occur. A mechanism was proposed where the monomer reacts with MCp in the presence of UV light through a Fe–Cp bond cleavage, generating a propagating chain. Irradiation of the monomer weakens the Fe–Cp bond allowing for nucleophilic attack at the iron centre to generate a propagating chain.

From the above mentioned methodologies for the ROP of [1]FCPs, only a limited number of reports on the application of these methodologies to [1]metallarenophanes or heteroleptic [1]metallacyclophanes have been reported. The following sections will highlight these reports, which include thermal ROP, anionic ROP and transition-metal-catalyzed ROP.

1.3.1 Thermal ROP

Almost every [1]FCP that has been prepared to date is known to undergo thermal ROP. Attempts to carry out analogous thermal ROP reactions on [1]CAPs to produce homo-polymers have been thwarted by the propensity of the chromium–arene bonds of [1]CAPs to break upon heating generating R_xEPh_2 fragments and a chromium metal mirror. For example, heating of dimethylsila[1]CAP (**1a**) or the bora[1]CAP **1f** [ER_x = $BN(SiMe_3)_2$] above 180 °C leads to

formation of a chromium metal mirror along with Me_2SiPh_2 or $(Me_3Si)_2NBPh_2$, respectively.[2] The [1]CAPs do not melt upon heating before the aforementioned deposition of chromium metal occurs above 180 °C. However, Manners *et al*. demonstrated that **1a** could be co-polymerized with dimethylsila[1]FCP (**8a**) by heating the mixture (Figure 1-17).[2] A sealed tube containing an equimolar ratio of **1a** and **8a** was heated to 140 °C for 72 h producing an immobile black solid which was readily soluble in C_6D_6. From the ^{1}H NMR spectrum, a ratio of Cr:Fe was determined to be 1:4.6 through comparison of the relative intensities of the resonances corresponding to the arene and Cp groups. Molecular weights of the resulting co-polymer could not be determined by GPC, presumably due to an acute air sensitivity of the polymeric material. Because methanol is known to react with sila[1]CAPs producing $Si(OH)_x$, Cr and C_6H_6 groups,[6] treatment of this polymer leads to a controlled decomposition of the material with the poly(ferrocenylsilane) remaining intact. From the polymer decomposition a precipitate formed in the brown solution which was separated by filtration. A ^{1}H NMR spectrum of the soluble fraction in C_6D_6 revealed resonances at 4.28 and 4.11 ppm consistent with poly(ferrocenylsilane), which was analyzed by GPC ($M_w = 2.0 \times 10^3$ and $M_n = 0.9 \times 10^3$). Based on the initial Cr:Fe ratio a minimum molecular weight of 2.4×10^3 was estimated for the initial co-polymer.

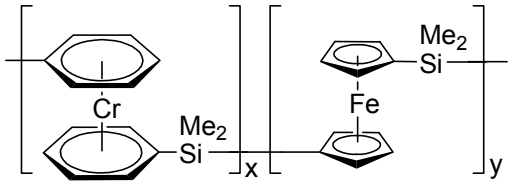

Figure 1-17. Copolymer generated from the thermal ROP of **8a** and **1a**.

Very recently, it was reported that [1]VAPs undergo thermal ROP. Braunschweig *et al*. prepared polymeric materials, in low yield, which contain di(benzene)vanadium units linked by

either Si(*i*Pr)(Me) or $BN(SiMe_3)_2$ fragments by heating [1]VAPs **2e** [ER_x = Si(*i*Pr)(Me)] and **2c** [ER_x = $BN(SiMe_3)_2$].[15] DSC was used to quantify the amount of ring strain present in **2c** and **2e**; endothermic peaks characteristic of melting were observed in thermograms (**2c**: 131 °C; **2e**: 199 °C) and exothermic peaks were observed at higher temperatures (**2e**: 169 °C, ΔH = 92 kJ mol^{-1}; **2c**: 204 °C, ΔH = 18 kJ mol^{-1}). No attempts to determine the molecular weight of the polymer were made, but it was simply inferred that the exothermic ring-opening process results in simultaneous polymerization of the monomers.

The thermal ROP of group-14-bridged [1]troticenophanes has been reported by Tamm *et al*.[40,46] A DSC trace of **4b** (ER_x = $SiMe_2$) shows a melt endotherm at 155 °C and exothermic peak at 170 °C (ΔH = 36 kJ mol^{-1}), while that for **4c** (ER_x = $GeMe_2$) only displays an exothermic peak at 130 °C (ΔH = 45 kJ mol^{-1}). No attempts were made to determine molecular weight for the polymers. The authors simply stated that they were concentrating on another aspect of the strained complexes, namely the addition of two-electron donors to **4b** and **4c** (see Chapter 1.2.2).

Elschenbroich *et al* reported that diphenylsila[1]trovacenophane (**5d**) withstands heating up to 280 °C without change.[38]

1.3.2 Transition-Metal Catalyzed ROP

Transition-metal catalyzed ROP of [1]metallarenophanes and heteroleptic [1]metallacyclophanes is the most successfully applied ROP methodology to date. In 2004, Manners *et al*. reported that the silicon-bridged [1]CAPs **1a** (ER_x = $SiMe_2$) and **1k** (ER_x = SiMeEt) were susceptible to transition-metal catalyzed ROP.[19] By treating the monomers with catalytic amounts (0.3 mol%) of Karstedt's Pt(0) catalyst [$Pt_2(CH_2{=}CHSiMe_2)_2O)_3$], homopolymers of poly(chromarenylsilane) could be generated (Scheme 1-22). Molecular weight

determination of polymers by GPC was prevented by the air sensitivity of the polymers. To estimate the molecular weight of poly(chromarenylsilane), **1k** was treated with Karstedt's catalyst in the presence of an end-capping group $HSiPh_2Cl$, which allowed for an approximate molecular weight determination of polymers by ^1H NMR spectroscopy. By integrating the signals belonging to the phenyl end-group and comparing these integrals to integrals of the arene signals of bis(benzene)chromium repeating units, a molecular weight of 4.1×10^3 was estimated.

Scheme 1-22. Transition-metal catalyzed ROP of [1]CAPs.

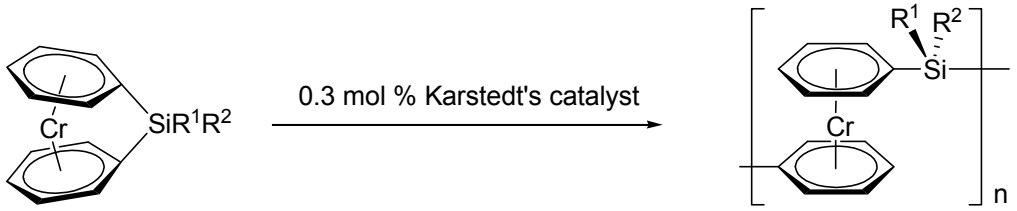

1a $R^1, R^2 = Me$

1k $R^1 = Me, R^2 = Et$

A transition-metal catalyzed ROP of the silicon-bridged [1]VAP **2e** (ER_x = Si*i*PrMe) was reported by Braunschweig *et al*.[15] Treatment of **2e** with Karstedt's catalyst (5 mol%) produced polymeric material that was characterized by small-angle X-ray scattering (SAXS) providing a polymer weight M_w of 28000.

To test whether a [1]metallacyclophane is prone to undergo transition-metal catalyzed ROP, a monomer can be treated with stoichiometric amounts of a platinum(0) complex such as $[Pt(PEt_3)_3]$. The platinum selectively inserts into the *ipso* carbon bridging element bond and retains two triethylphoshine ligands resulting in the formation of a [2]metallacyclophane, which can often be isolated. For example, Tamm *et al*. reported that dimethylsila[1]troticenophane **(4b)** and dimethylgerma[1]troticenophane (**4c**) react with stoichiometric amounts of $[Pt(PEt_3)_3]$ to produce [2]troticenophanes [$R_xE–ER_x$ = $(Et_3P)_2Pt–SiMe_2$ (**4g**), $(Et_3P)_2Pt–GeMe_2$ (**4h**)] (Figure 1-

18). [46,48] Interestingly, **4g** could be utilized as a single-source catalyst in ROP reactions of strained sandwich molecules. For example, when **4b** is treated with 3 mol% of **4g** in C_6D_6 and the mixture is heated for 64 h at 80 °C, oligomers can be detected with molecular weights of 6000 corresponding to 23 repeating units.

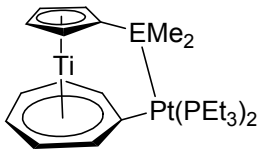

4g E = Si
4h E = Ge

Figure 1-18. [2]Troticenophanes **4g** and **4h** isolated from a platinum insertion reaction.

[2]Trovacenophane **5g** [$R_xE–ER_x$ = $(Et_3P)_2Pt–SiMe_2$] was isolated from the reaction of [1]troticenophane **5c** (ER_x = $SiMe_2$) and [$Pt(PEt_3)_3$],[48] and [2]trochrocenophane **6k** [$R_xE–ER_x$ = $(Et_3P)_2Pt–SiMe_2$] was isolated from an analogous reaction of [1]troticenophane **6c** (ER_x = $SiMe_2$) and [$Pt(PEt_3)_3$].[47] In all cases that involve heteroleptic [1]metallacyclophanes, platinum regioselectively inserts into the *ipso* carbon–Si bond at the Cht ring. If **6c** is treated with catalytic amounts of Karstedt's catalyst, an air-sensitive polymer can be produced. The polymer was characterized by GPC and has a moderate molecular weight ($M_w = 6.4 \times 10^3$, $M_n = 4.0 \times 10^3$, PDI = 1.6).

The heteroleptic diisopropylsila[1]metallarenocenophane (**7b**), containing a manganese sandwiched between a benzene ring and, a Cp ring, undergoes ROP when reacted with Karstedt's catalyst over 3 days, produces oligomeric and polymeric materials.[44] These materials were poorly characterized; a ^{1}H NMR spectrum with broad signals different from the spectrum obtained from **7b** was enough to conclude that polymers were produced.

1.3.3 Anionic ROP

In an attempt to prepare homopolymers containing bis(benzene)chromium, dimethylsila[1]CAP (**1a**) was treated with the anionic initiator MeLi.[2] From a ^{1}H NMR spectrum of a stoichiometric reaction of **1a** and MeLi, followed by quenching with Me_3SiCl, bis[(trimethylsilyl)benzene]chromium was identified as the only product, demonstrating that **1a** could be ring-opened stoichiometrically. Any attempts to make the reactions catalytic with lower concentrations (10%) of MeLi produced inconclusive data because the mixtures could not successfully be characterized by GPC, presumably because the mixtures were very sensitive to oxygen and moisture.

However, co-polymers could be generated by anionic ROP of equimolar mixtures of **1a** and dimethylsila[1]FCP (**8a**) (10 mol% BuLi). According to ^{1}H NMR spectroscopy the resulting polymer contained a Cr:Fe ratio of 1:1.6. By methanol treatment, the poly(ferrocenylsilane) part could be separated and GPC revealed an estimated molecular weight M_w of the co-polymer of at least 1.2×10^4.

Bora[1]CAP **1f** [ER_x = $BN(SiMe_3)_2$] undergoes ring-opening upon treatment with BuLi generating dimers that were characterized by MALDI TOF mass spectrometry.[14]

1.3.4 Photocontrolled ROP

Manners *et al*. reported on their attempts to induce photo-controlled ROP of dimethylsila[1]trochrocenophane (**6c**) by reaction with NaCp or dppe using UV light as an initiator, however, polymers were not obtained.[47]

1.4 [1.1]Metallacyclophanes

[1.1]Metallacyclophanes are members of the class of compounds called [m.n]metallacyclophanes. A [m.n]metallacyclophane can be described as a molecule composed of two (or more) sandwich complex moieties and two (or more) bridging element moieties in such a way that a single molecule is formed. For example, a [1.1]ferrocenophane ([1.1]FCP) would possess two ferrocene moieties connected by two single element bridges E. [1.1]FCPs are known either as *anti* or *syn* isomers (Figure 1-19). In the *anti* conformation, bridging elements are found on opposite sides of the sandwich complexes, whereas in the *syn* conformation, bridging elements occupy the same side with one bridging moiety situated above the other. In addition, the ligands on the bridging elements can occupy either an *exo* position, which is approximately perpendicular to the aromatic rings, or an *endo* position, which is approximately parallel with the aromatic rings. The main factor affecting whether a *syn* or an *anti* isomer is generated, seems to be dependent on bridging element size. Introduction of smaller bridging elements like boron and carbon usually prefer a *syn* conformation, whereas, for larger bridging elements, *anti* isomers are usually observed. However, it is important to note that this just a general trend and in some cases, *syn* and *anti* isomers with identical bridging elements have been characterized.

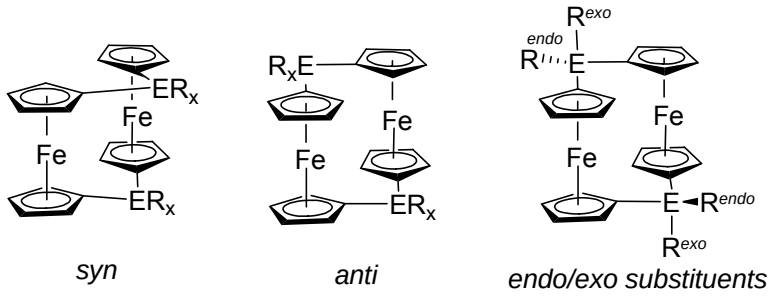

Figure 1-19. *Syn* and *anti* isomers of [1.1]metallocenophanes and *exo*/*endo* substituents (R_{exo}/R_{endo}).

There are two types of steric repulsions that can affect whether a molecule will adopt a *syn* or an *anti* conformation. The first is the repulsion between the inner hydrogen atoms at α and α′ positions on the aromatic rings (Figure 1-20). Whereas an *anti* isomer is rigid and not able to relieve this repulsion, a *syn* isomer can twist to reduce it.

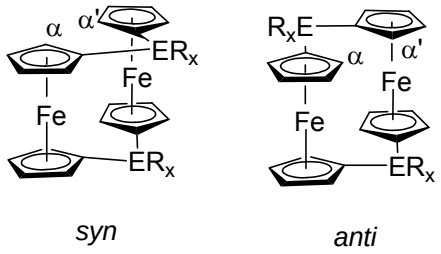

Figure 1-20. *Syn* and *anti* isomers of a [1.1]FCP depicting the proximity of α and α′ protons on Cp rings.

The second repulsion arises from the interaction of the ER_x groups in the *syn* isomer. When ER_x groups are large, formation of a molecule with a *syn* geometry would be unfavorable because of steric repulsions between ER_x. As mentioned earlier, the general rules of thumb for [1.1]metallocenophanes are: if ER_x is small, a *syn* isomer will be preferred and if ER_x is large, an *anti* isomer will be preferred.

A simplification of [1.1]metallocenophane conformations can be made with an analogy to cyclohexane conformations.[76] The *syn* conformation of [1.1]FCPs resemble the *boat* conformation in cyclohexane and the *anti* conformation of [1.1]FCPs resemble that of the *chair* conformation (Figure 1-21).

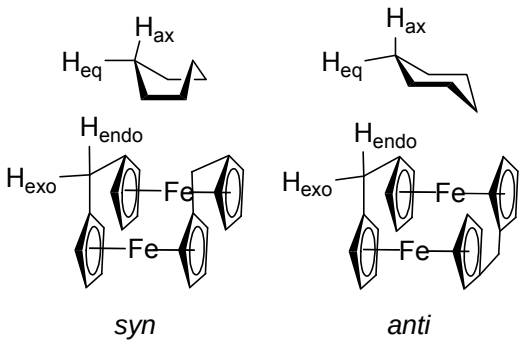

Figure 1-21. Conformational analogy of the *syn* and *anti* conformations of [1.1]FCPs to the *boat* and *chair* conformation of cyclohexane (eq = equatorial, ax = axial) (adapted from ref. 76).

When this project was undertaken, [1.1]FCPs, [1.1]ruthenocenophanes ([1.1]RCPs) and [1.1]ruthenoferrocenophanes ([1.1]RFCPs) were the only known examples of [1.1]metallacyclophanes, with the first example, a dicarba[1.1]FCP being reported by Nesmeyanov in 1956.[77] [1.1]Metallacyclophanes have been markedly less explored than their [1]metallacyclophane counterparts. The group of hetero-atom containing [1.1]ferrocenophanes are known with the bridging elements from group 12 (Hg[78-80]), 13 (B,[81] Al,[82-84] Ga,[84-87], In[84]), 14 (Si,[64,88-94] Sn,[56,63,95-98] Pb[99]), and 15 (P,[72,100-102] As[103]). The knowledge about [1.1]ruthenocenophanes and mixed Ru-Fe [1.1]metallocenophanes is mainly limited to carbon-bridged species. The only known hetero-atom-bridged [1.1]ruthenocenophane (E = $SiMe_2$) was published in 1995 by Herberhold *et al*. [1.1]Metallocenophanes serve as model compounds for the investigation of metal-metal interactions, which can be studied by cyclic voltammetry.

Information gained from these investigations can be applied to polymers with similar compositions.

The following sections will describe known [1.1]FCPs, [1.1]RCPs and [1.1]RFCPs to provide an overview of all known [1.1]metallacyclophanes. A brief discussion on the metal-metal interactions in [1.1]metallacyclophanes will be presented in the electrochemistry section using the Robin and Day classification system (Chapter 1.5).[104]

1.4.1 Group-12-Bridged [1.1]Metallocenophanes

In 1983, Lemonska *et al*. synthesized two dimercura[1.1]FCPs where (N,N′-dimethyaminomethyl)ferrocene or ferrocene were utilized.[78] By adding equimolar amounts of dilithioferrocene or bis(dimethylaminomethyl)dilithioferrocene to $HgCl_2$, dimercura[1.1]FCPs **9a** (ER_x = Hg) and **9b** (ER_x = Hg) (Figure 1-22) could be isolated in yields of 5% and 40%, respectively. The solid-state structure of **9b** revealed two independent molecules in the unit cell with both molecules adopting *syn* geometries where the C–Hg–C bond angle are 177.1(3)° and 176.6(3)°. The dimethylamino groups were found to be weakly coordinated to the Hg atoms in both molecules (Hg–N = 3.049(6) Å and 2.922(6) Å; Figure 1-22).

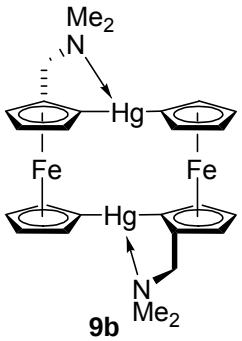

9b

Figure 1-22. Illustration of dimercura[1.1]FCP **9b** from its solid-state structure.

Interestingly, both iron centres in **9b** can be oxidized by addition of two equivalents of ferrocenium tetrafluoroborate or ferrocenium hexafluorophosphate.[79] The dications produced are even stable enough to be isolated and characterized by X-ray crystallography.[80] The [1.1]FCP in $[\mathbf{9b}]^{2+}[Ph_3BCN^-]_2$ adopts a *syn* conformation with a C–Hg–C bond angle of 179.5(6)°. The Hg–N bond of 2.83(1) Å in the dication is markedly shorter than the Hg–N bond length in neutral **9b**.

1.4.2 Group-13-Bridged [1.1]Metallocenophanes

The only known boron-bridged [1.1]FCP [$ER_x = BMe_2^-$ (**10a**)] was published by Wagner *et al*. and was prepared from equimolar reactions of dilithioferrocene with 1,1′-bis(dimethylboryl)ferrocene.[81] Compound **10a** was isolated as a salt with its anion adopting a twisted *syn* geometry in the solid state with two lithium atoms incorporated into the compound (Figure 1-23). In **10a**, one lithium cation is coordinated by two crown ether molecules, whereas the second lithium cation is found situated inside the ferrocenophane cavity between the boron atoms. The lithium–boron distances were 2.314(6) and 2.309(6) Å, respectively. It was suggested that the lithium cation was trapped inside the cavity by electrostatic interactions with the two anionic borates.

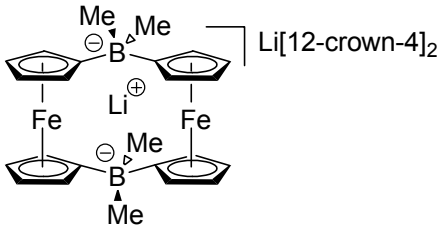

10a

Figure 1-23. Illustration of dibora[1.1]FCP **10a**.

During the course of my Ph.D. work, Müller *et al*. reported on the isolation of a dialumina[1.1]FCP **10b** (ER_x = AlCl·tmeda) in 9% yield by treatment of (Pytsi)$AlCl_2$ [Pytsi = –$C(SiMe_3)_2(SiMe_2)C_6H_4N$-2] with dilithioferrocene·2/3 tmeda when carried out in hexane (Scheme 1-23).[82] Conversely, if the reaction is carried out in toluene, (Pytsi)Al[1]FCP (**10d**) is formed (Scheme 1-23).[105] It remains unknown how **10b** is generated from the above reaction. In an attempt to optimize the synthesis of **10b**, dilithioferrocene·2/3 tmeda was reacted with equimolar amounts of $AlCl_3$, but these reactions proved to be unsuccessful.

Scheme 1-23. Reactions of dilithioferrocene·2/3 tmeda with (Pytsi)$AlCl_2$ in toluene generating a [1]FCP (**10d**) and in hexane generating a [1.1]FCP (**10b**).

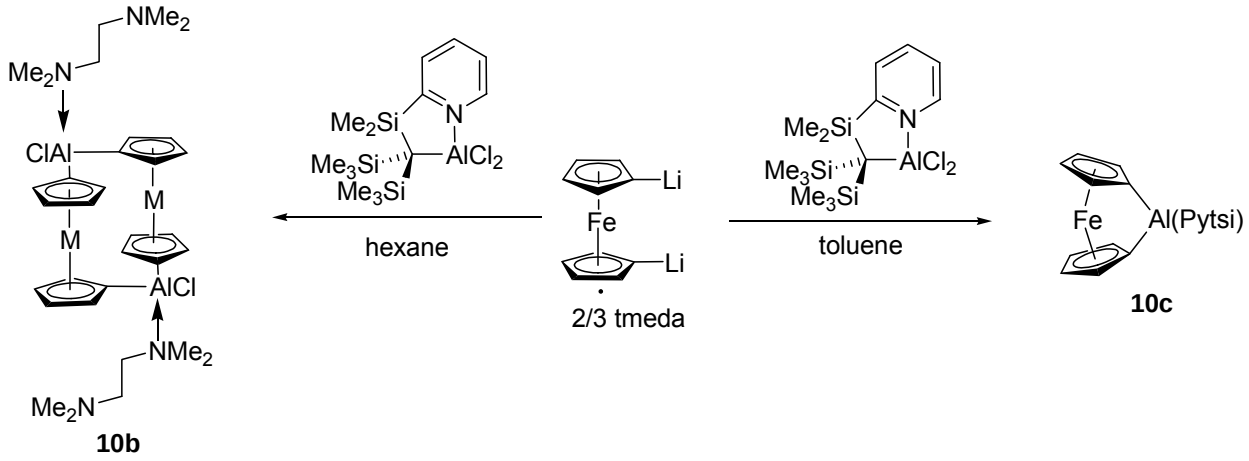

In two independent publications, the Braunschweig and the Müller groups reported on the synthesis of a dialumina[1.1]FCP [ER_x = AlAr′ (**10d**)] utilizing the intramolecularly coordinating Ar′ ligand [Ar′ = 2-$(Me_2NCH_2)C_6H_4$] (Figure 1-24).[83,84] Within the framework of a short communication, Braunschweig *et al*. characterized **10d** by NMR spectroscopy, single-crystal X-ray crystallography, elemental analysis and mass spectrometry, whereas, Müller and co-workers published **10d** as part of a full article, together with results for an analogous gallium and indium-bridged [1.1]FCP. A single-crystal X-ray structural determination of **10d** revealed a molecule in an *anti* conformation.

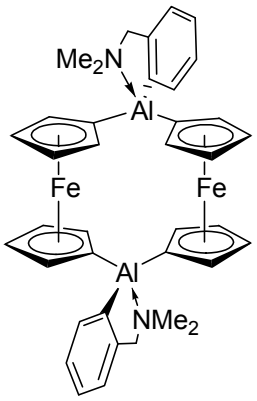

10d

Figure 1-24. Schematic representation of the dialumina[1.1]FCP **10d**.

Several groups have isolated and characterized digalla[1.1]FCPs to date (Figure 1-25). The first digalla[1.1]FCPs were published in two separate publications by Jutzi *et al*.[86] and by Uhl *et al*.[85] Jutzi and co-workers reported that **10e** [ER_x = GaMe(C_6H_5N)] could be isolated as a byproduct from the reaction of 1,1′-bis(trichlorostannyl)ferrocene with trimethylgallium after addition of pyridine.[86] They later reported that **10f** (ER_x = GaMe) could be generated in 46% yield by dissolving 1,1′-bis(dimethylgallyl)ferrocene in diethyl ether and toluene and letting the solution sit at 6 °C for 24 h during which time **10f** crystallized out.[87] The solid-state structures of **10e** and **10f** revealed molecules in *anti* conformations. The ^{1}H NMR spectra (DMSO-d_6) of **10e** and **10f** revealed a pair of signals with the same chemical shift in the Cp region (δ 4.05, 4.18) indicative of a D_{2h} symmetrical species. To explain the ^{1}H NMR spectra for **10e** and **10f**, it was proposed by Jutzi *et al*. that the *anti* and *syn* isomers are in equilibrium and readily interconvert, so that on the NMR time scale, **10e** and **10f** appear as time-averaged D_{2h} symmetrical species. The authors did not obtain any evidence of this proposed *syn* isomer in solution. However, one can conclude from the NMR spectra that a fast degenerate *anti*-to-*anti* isomerization occurs in solution and this would explain why the [1.1]FCPs appear to be D_{2h} symmetrical species.

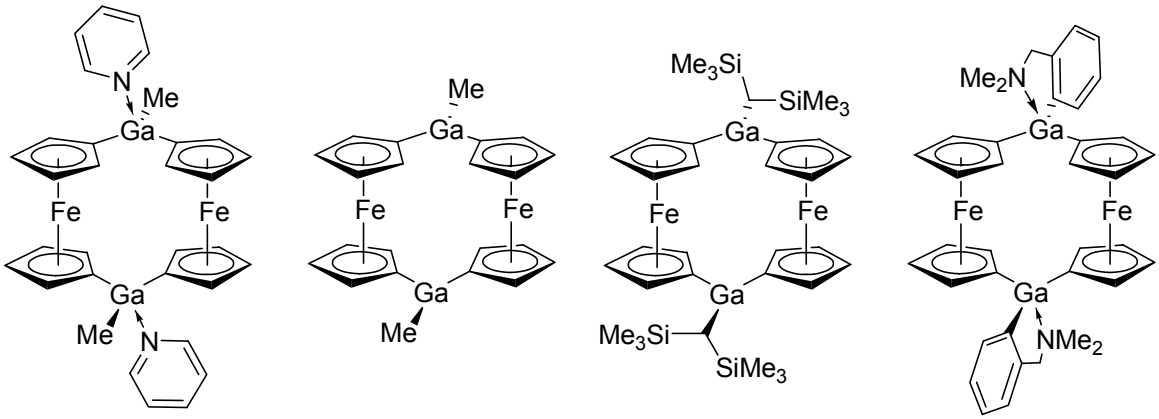

10e **10f** **10g** **10h**

Figure 1-25. Known galla[1.1]FCPs **10e**, **10f**, **10g** and **10h**.

The digalla[1.1]FCP **10g** [ER_x = $GaCH(SiMe_3)_2$] was synthesized from the reaction of $[Li(thf)][Cl_3GaCH(SiMe_3)_2]$ with a slurry of dilithioferrocene in 47% yield.[85] Compound **10g** was characterized by X-ray crystallography revealing a [1.1]FCP with two unsaturated three-fold coordinate gallium atoms in an *anti* conformation. The ^{1}H NMR spectra of **10g** (in C_6D_6) revealed a pair of signals in the Cp region (δ 4.59, 4.40) indicative of a D_{2h} symmetrical species. Even though the authors did not suggest it, it is probable that a fast *anti*-to-*anti* isomerization occurs in solution like that observed for **10e** and **10f**. A fast interconversion between the isomers would be plausible explanation for the observed spectrum of **10g**.

A digalla[1.1]FCP [ER_x = GaAr′ (**10h**)] was synthesized and characterized by Müller *et al*. in 2006.[84] The solid-state structure of compound **10h** revealed a molecule in an *anti* conformation. Unexpectedly, a ^{1}H NMR spectrum (C_6D_6) of **10h** showed four signals in the Cp region (δ 3.99, 4.37, 4.48, 5.07) interpreted as being caused by a time-averaged C_{2h} symmetrical species indicating the solid-state structures and molecular structure in solution are similar when

taking into account the fast inversion of the five-membered rings of the coordinated Ar′ ligand (Figure 1-24).

The only diinda[1.1]FCP **10i** (ER_x = InAr′) was published by Müller *et al*. utilizing the intramolecularly coordinating Ar′ ligand.[84] The solid-state structure of **10i** revealed a molecule in an *anti* conformation. Compound **10i** is isostructural with **10d** and **10h**. Similar to what was observed for **10d** and **10h**, the ^{1}H NMR spectrum of **10i** shows four signals in the Cp region (δ 4.04, 4.45, 4.53, 4.97),

To date, group-13-bridged [1.1]ruthenocenophanes are unknown.

1.4.3 Group-14-Bridged [1.1]Metallocenophanes

Dicarba[1.1]ferrocenophanes were first reported by Nesmeyanov *et al*. in 1956 by the acid-catalyzed condensation reactions of aldehydes with ferrocene (Scheme 1-24).[77] Dicarba[1.1]FCPs **11a** (ER_x = CH_2) and **11b** (ER_x = CHPh) were prepared in yields of 65–75% and 30–37%, respectively, and were characterized by cryoscopic measurements and CHN analysis.

Scheme 1-24. Acid catalyzed formation of dicarba[1.1]FCPs **11a** and **11b**.

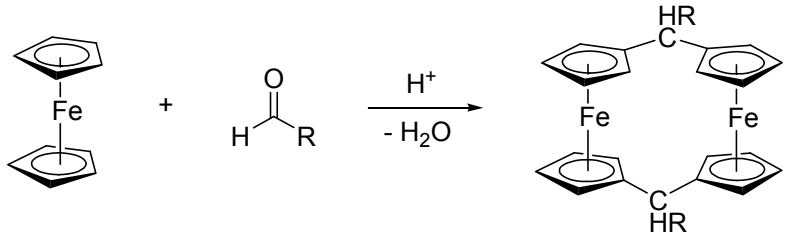

11a R = H
11b R = Ph

Incorrectly cited throughout the literature as the first example of a dicarba[1.1]FCP is a publication by Watts in 1966. He synthesized dicarba[1.1]FCP **11c** (ER_x = $CHCH_3$) from

ferrocene, disubstituted with fulvene groups, by consecutive treatment of $LiAlH_4$ and $FeCl_2$ in 14–20% yield (Scheme 1-25).[106] A proposed molecular structure of **11c** was based on ^1H NMR spectroscopic and mass spectrometric data. The ^1H NMR spectrum revealed four signals with relative intensities of 6:2:12:4 and were assigned to the CH_3, CH and the α and β protons of the Cp groups, whereas the mass spectrum revealed the M^+ peak. Because the methyl groups are equivalent on the NMR time scale, using geometric arguments that the interaction of inner α protons in the *syn* geometry would be unfavorable by being to close to one another (~ 0.8 Å), Watts proposed that **11c** adopted an *anti* conformation with the methyl occupying *exo* positions. A year later, the solid-state structure of **11c** revealed a molecule that adopts a *syn* conformation with the methyl groups occupying *exo* positions.[107] To relieve the interaction of inner α protons, the ferrocene moieties are twisted relative to one another by an angle of 31°, allowing the two inner α protons to be separated by a distance of 2.03 Å. After the solid-state structure was determined, Watts revised his reasoning and proposed that the *syn* isomer would be highly flexible in solution and a fast *syn*-to-*syn* isomerization could occur that would render the methyl groups equivalent on the NMR time scale.[108]

Scheme 1-25. Synthetic route to **11c** from a methyl substituted bis(fulvenyl)ferrocene.

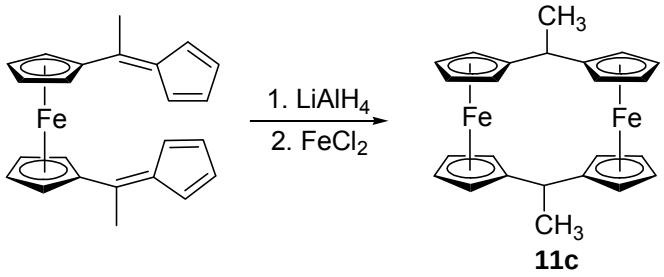

11c

Another route to prepare dicarba[1.1]FCPs was first published Nesmeyanov *et al*. in 1958 and later by Watts *et al*. in 1967 involving the aluminum chloride catalyzed intramolecular Friedel–Crafts cyclization reaction between 1,1′-bis(chloroformyl)ferrocene and ferrocene to

afford a dicarba[1.1]FCP [ER_x = CO (**11d**)] (Scheme 1-26).[108,109] The identity of **11d** was confirmed by observation of M^+ peak of **11d** in the mass spectrum. Compound **11d**, along with other carbonylated derivatives, could also be prepared by treating 1,1′-bis(chloromercura)ferrocene with lithium palladium(II) chloride under carbon monoxide pressure (50 atm).[110] Cowan *et al*. reported that **11d** can be synthesized in 10% yield by reaction of dilithioferrocene with dimethylcarbamyl chloride.[111]

Scheme 1-26. Friedel–Crafts route to dicarba[1.1]FCP **11d**.

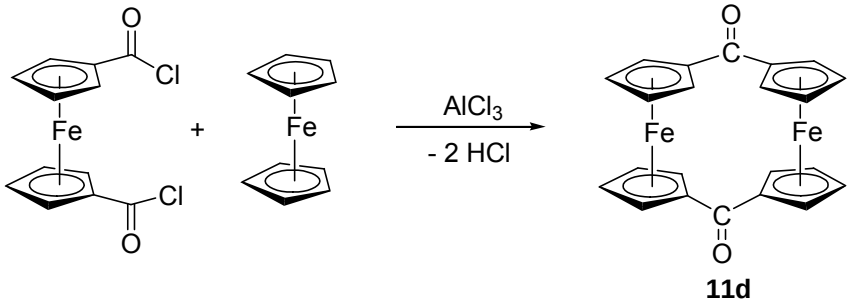

11d

Watts reported on a new route to prepare compound **11a** by addition of $FeCl_2$ to dilithiobis(cyclopentadienyl)methane.[112] The dianion was generated by addition of two equivalents of butyllithium. In a similar fashion, the dicarba[1.1]FCPs **11e** (ER_x = CMe_2) and **11f** (ER_x = CPh_2) were prepared from reactions of respective dianions with $FeCl_2$. Similar to compound **11a**, the [1.1]FCP **11e** exhibits a *syn* conformation in the solid state.[113] Even though the positions of the two methyl groups in **11e** could produce different isomers, only the *endo-exo* species was found.[114] To relieve any interactions between the inner α protons on the Cp rings, the ferrocene moieties are twisted relative to one another by an angle of 22°. Independent from work of Watts, Katz *et al*. reported on the dilithiation of bis(cyclopentadienyl)methane and subsequent reaction with $FeCl_2$ generating the dicarba[1.1]FCP **11a** along with tricarba[1.1.1]FCP, tetracarba[1.1.1.1]FCP and pentacarba[1.1.1.1.1]FCP.[115] The identities of

these oligomers were confirmed by elemental analysis, ^{1}H NMR spectroscopy and mass spectrometry.

In 1981, an improved synthesis of **11a** was reported by Mueller-Westerhoff.[116] By treating bis(fulvenyl)ferrocene with Li[BHEt$_3$] or Li[BHBu$_3$], a dilithium salt was generated, and subsequent addition of $FeCl_2$ gave the product. Compound **11a** was isolated as a pure product in yields of 30–45%. In addition, treatment of bis(fulvenyl)ferrocene with two equivalents of MeLi generated a dilithio derivative. A reaction of $FeCl_2$ with this dilithio moiety produced **11c** in 71% yield.[117] Preparation of **11c** by this route allows two *syn* isomers to be prepared, the *exo-exo* and *exo-endo* isomers in a ratio of 1:2 (Scheme 1-27). The isomers could be separated through multiple crystallizations in hexane. By the previous routes the *exo-exo* isomer was the only isomer isolated.[106]

Scheme 1-27. Preparation of two isolable isomers of dicarba[1.1]FCP **11a**.

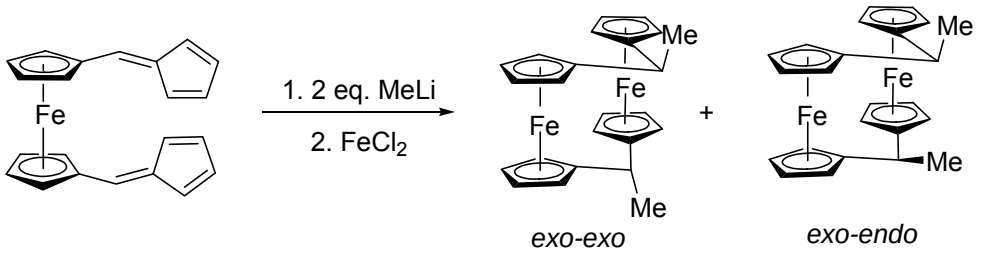

Mueller-Westerhoff *et al*. reported that a tetrafluoroborate salt of **11a** could be prepared by hydride abstraction from the methylene bridge using triphenylcarbenium (trityl) tetrafluoroborate.[118] The molecule was found to adopt a *syn* conformation in the solid state with tilt angles α of –6.6° and –7.5° for the ferrocene moieties, meaning the Cp rings are tilted away from the bridging element. Hendrickson *et al*. reported on solid-state structure of the mixed valence derivative of **11c**, where the iron atoms are in +II and +III oxidation states.[119] The mixed valence derivative was prepared by addition of iodine to **11c** generating a cationic

[1.1]ferrocenophane with a I_3^- counteranion. The mixed valence derivative of **11c** retains a *syn* conformation in the solid state.

Mueller-Westerhoff attempted to provide experimental evidence that a *syn*-to-*syn* isomerization occurs with dicarba[1.1]FCPs in solution. They prepared several derivatives of **11a**, with one of Cp rings substituted with alkyl groups (Figure 1-26), and analyzed them by ^{1}H NMR spectroscopy.[120]

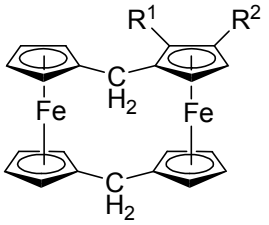

11a $R^1 = R^2 = H$
11g $R^1 = COMe$, $R^2 = H$
11h $R^1 = H$, $R^2 = COMe$
11i $R^1 = Et$, $R^2 = H$
11j $R^1 = H$, $R^2 = Et$

Figure 1-26. Dicarba[1.1]FCPs prepared to study the proposed *syn*-to-*syn* isomerization in [1.1]FCPs.

To undergo a *syn*-to-*syn* interconversion, molecular models predicted that α substituents on the Cp rings would come into close contact in an intermediate structure between two *syn* isomers (Scheme 1-28). Introducing bulky groups in an α position should therefore inhibit this interconversion while introducing bulky groups in a β position should have no effect on this interconversion. The *syn*-to-*syn* interconversion of [1.1]FCP occuring through a "*twist*" intermediate with bulky groups in either α or β positions is depicted in Scheme 1-28. ^{1}H NMR spectra of **11g** and **11i** revealed the methylene protons at each carbon are not equivalent (Figure 1-26). This result is not surprising, given the fact that, these protons are not symmetrically equivalent. The authors argued that a fast *endo-exo* site exchange does not occur in the α-substituted [1.1]FCPs. They based this argument on the fact that the methylene protons in **11g** and **11i** appear as overlapping multiplets. Given the fact the left and right structures depicted in

Scheme 1-28 are diastereomers, even a fast *syn*-to-*syn* interconversion would not render these protons at each methylene carbon equivalent. The methylene protons on each carbon in β-substituted complexes **11h** and **11j** appear as two coincidental singlets separated by 0.12 and 0.02 ppm, respectively. Because the methylene protons appear as singlets, the authors stated that an *endo*-*exo* site exchange occurs in **11h** and **11j**. It is very likely that a fast *syn*-to-*syn* interconversion occurs in these β-substituted dicarba[1.1]FCPs, but it is only coincidence that two singlets are observed for the four inequivalent methylene protons. It would make more sense to evaluate symmetrically substituted [1.1]FCPs so that the both endo (or exo) positions are equivalent. It was proposed earlier that the *syn*-to-*syn* interconversion barrier in **11a** was unusually small (< 10 kJ/mol).[117,121] They concluded that *syn*-to-*syn* interconversion of [1.1]FCPs occurs through an intermediate "*twist*" conformation with the two ferrocene moieties perpendicular to one another. Introduction of the α substituents renders the *syn*-to-*syn* interconversion unfavorable and the β substituents have no effect on this interconversion.

It was demonstrated that *exo* and *endo* protons of **11a** are distinguishable from one another at low temperature by ^{1}H NMR spectroscopy.[122] At room temperature, the methylene protons of **11a** appear as a singlet, the *endo* and *exo* protons readily interconvert rendering them equivalent on the NMR time scale. By lowering the temperature below 150 K, the singlet splits into two singlets, such that, at 133 K the signals are well separated from one another. From the coalescence temperature of 150 K, the free energy of activation for interconversion was estimated to be 28 kJ/mol. The conformational interconversion in **11a** was examined by computational calculations at the MM2′ level of theory.[123] A global minimum for the *syn* isomer was determined and a *syn*-to-*syn* interconversion was determined to proceed through a species with an *anti*-like conformation as a transition state, which was 26.32 kJ/mol higher in energy

than the *syn* isomer. This result is in good agreement with experimentally estimated value of 28 kJ/mol.

Scheme 1-28. Conformational exchange in α- and β-substituted [1.1]FCPs (adapted from refs. 120 and 121).

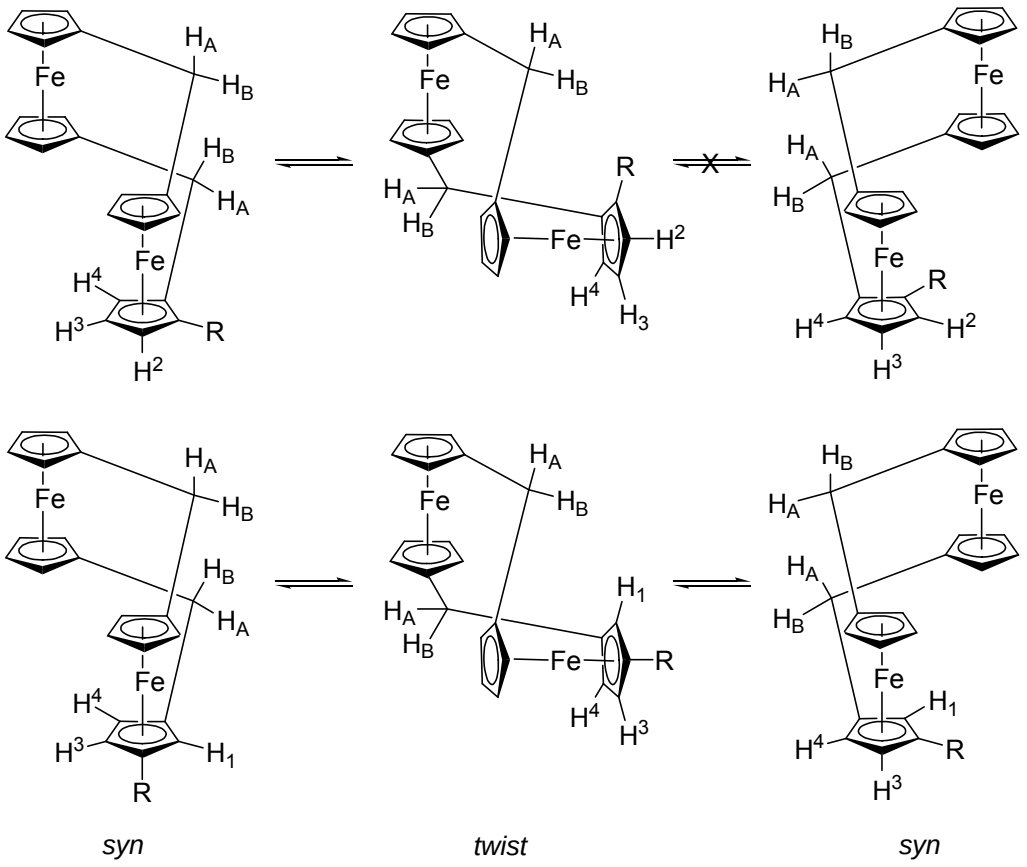

Two derivatives of **11a** were prepared which contained a propyl interannular bridge at either the α or β position of one ferrocene moiety (Figure 1-27).[124] Compounds **11k** and **11l** adopt the *syn* conformation in the solid state. The ^{1}H NMR spectra of **11k** and **11l** differ markedly. Whereas, the peak for the methylene protons in **11l** appear as a sharp singlet, the methylene protons in **11k** produce a single AB quartet. From this difference, one can conclude that **11l** is highly flexible in solution rendering the *endo* and *exo* protons equivalent on the NMR time scale and **11k** is a more rigid molecule in solution. Thus, β-substituted [1.1]FCPs are more

flexible in solution, than α-substituted [1.1]FCPs and a β-substituent does not inhibit a *syn*-to-*syn* isomerization in [1.1]FCP and an α-substituent does inhibit this isomerization.

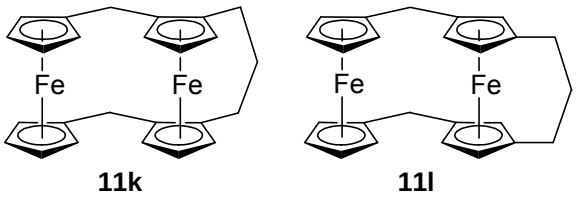

11k **11l**

Figure 1-27. Illustrations of the dicarba[1.1]FCPs **11k** and **11l** with interannular propyl linkers in α- and β-positions.

Metallocene basicity in dicarba[1.1]FCPs has been investigated by several groups. Ling *et al*. demonstrated that addition of one equivalent of trifluoroacetic acid to [1.1]FCP **11a** (ER_x = CH_2) produced one equivalent of a gas, presumed to be hydrogen.[125] The protonation of [1.1]FCPs by acids was later approached theoretically by Waleh *et al*., who determined that hydrogen transfer from an acid to iron is the first step towards hydrogen gas formation.[126] Several other reports examined **11a** as a catalyst for the evolution of hydrogen gas from acidic aqueous media. For example, addition of an aqueous solution of boron trifluoride hydrate, $H[BF_3OH]$, to **11a** results in the evolution of hydrogen gas and the formation of a dicationic derivative of **11a** with two Fe(III) centres.[127] The dicationic derivative could be converted back to **11a** by addition of a reducing agent. Kinetic and electrochemical studies on the reaction of the [1.1]FCPs **11a**, **11k** and **11l** with acids provided experimental evidence that the reaction proceeds through a three-step mechanism: two fast protonation steps followed by a rate determining step of elimination of dihydrogen (Scheme 1-29).[128,129] Experimental evidence for the diprotonated derivative of **11a** with two Fe(III) centres was observed by ^1H NMR spectroscopy (Scheme 1-29).[130] To observe this intermediate, **11a** was protonated with a

superacid comprised of 1 part of FSO_3H and 10 parts of SO_2ClF. The ^1H NMR spectrum of the mixture in CD_2Cl_2 was recorded at –125 °C and based on NOESY experiments, a resonance at δ 1.21 was assigned to the Fe–H groups.

Scheme 1-29. Three-step reaction of dicarba[1.1]FCP with a protic acid generating H_2.

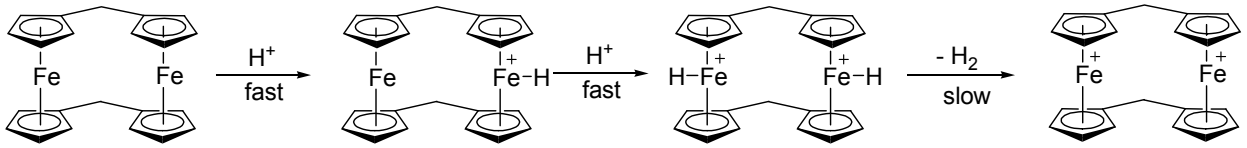

A review in 1986 was published by Mueller-Westerhoff highlighting some of the important structures and properties of carba[1.1]FCPs.[121] For example, [1.1]FCPs should exist as two conformations, *syn* and *anti*, but because the *anti* conformation is rather rigid, the α protons on the Cp rings crowd each other and do not allow for its isolation. Conformational flexibility of the *syn* isomer allows for the two ferrocene moieties to twist away from one another to avoid steric interactions.

The first mention of a dicarba[1.1]FCP *anti* isomer appeared in a publication in 1992. Thioketone-bridged [1.1]ferrocenophanes **11m** and **11n** were prepared from **11d** by treatment with either one or two equivalents of Lawesson's reagent, respectively (Scheme 1-30).[131]

Scheme 1-30. Preparation of dicarba[1.1]FCPs **11m** and **11n** from reaction of **11d** and Lawesson's reagent.

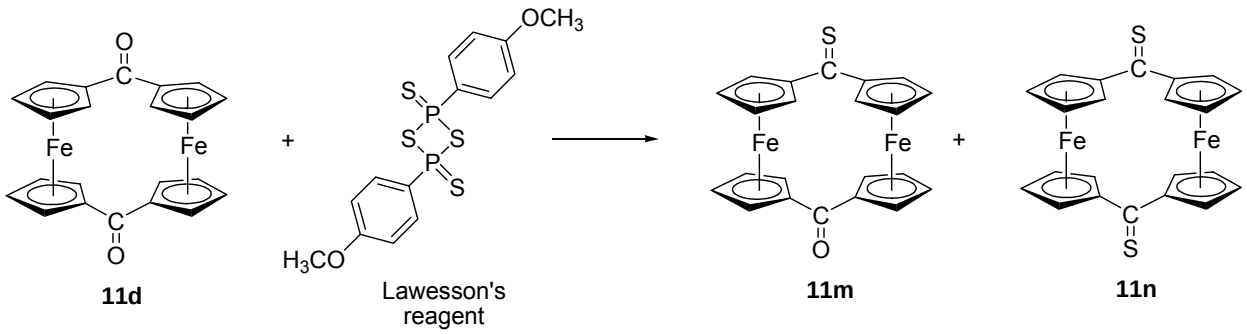

In addition, the preparation of **11o** (ER_x = CH_2, CO) and **11p** (ER_x = CH_2, CS) was reported (Figure 1-28). All compounds were characterized by mass spectrometry and by VT-NMR spectroscopy. Signals in the ^{1}H NMR spectrum of **11o** were broadened at room temperature and became more complex upon cooling, indicative of a dynamic process. The activation energy ($\Delta G^{\ddagger}$) of this dynamic process, a *syn*-to-*syn* interconversion, was calculated to be 64.5 kJ/mol from the coalescence temperature of 315 K (400 MHz). Interestingly, **11d** was also found to be fluxional in solution with the activation energy of 58.7 kJ/mol calculated for the *syn*-to-*syn* interconversion. At 10 ^{o}C, a second set of signals was observed, which the authors tentatively assigned to the *anti* conformer.

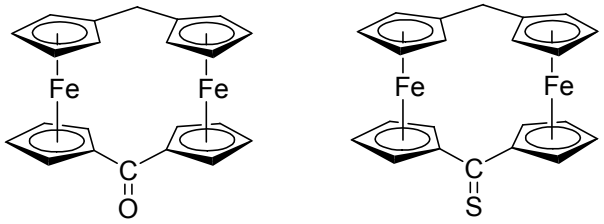

11o **11p**

Figure 1-28. Illustration of dicarba[1.1]FCP **11o** and **11p**.

Shortly thereafter, a serendipitous discovery was made, providing solid-state evidence that dicarba[1.1]FCPs can exist in an *anti* conformation.[132] Earlier, it had been reported that [1.1]FCP **11c** (ER_x = CHMe) crystallized in the *syn* conformation with the methyl groups occupying *exo* positions.[107,114] The *syn* isomer with methyl groups in *exo* and *endo* positions had also been proposed to exist, based on the observation of a second isomer of **11c** by ^{1}H NMR spectroscopy. Löwendahl *et al*. later provided solid-state evidence for this syn isomer with methyl groups in *exo* and *endo* positons.[76] Ahlberg *et al*. were able to separate a different isomer of **11c**. The solid-state structure revealed a molecule that adopted the *anti* conformation with the

methyl groups occupying *exo* positions. This represented the first structurally characterized dicarba[1.1]FCP in an *anti* conformation.[132]

Several groups have examined carbanion derivatives of **11a** where one proton in one of the methylene bridge is removed by a base and the carbanion generated undergoes rapid intramolecular proton transfer through a hydrogen bond between the methylene group and the carbanion (Scheme 1-31).[133,134]

Scheme 1-31. Illustration for proton transfer between the methylene group and the carbanion in dicarba[1.1]FCP **11a**.

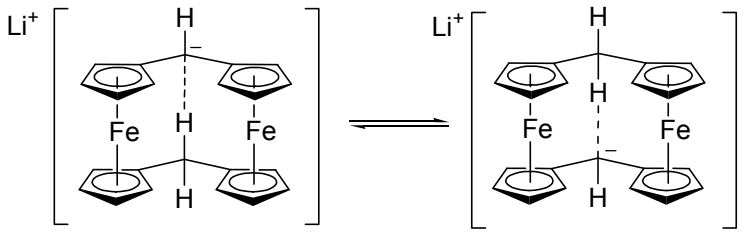

Evidence for lithium coordination to the carbanion have also been obtained through NMR spectroscopy by nuclear spin-spin couplings between ^{6}Li and ^{13}C,[135,136] by VT NMR measurements[137,138] and by X-ray crystallography.[139] The solid-state structure revealed a monomeric molecule in the *syn* conformation with the lithium coordinated to two carbon atoms and two 2,5-dimethyltetrahydrofuran molecules, but no evidence of hydrogen bonding was observed (Figure 1-29).

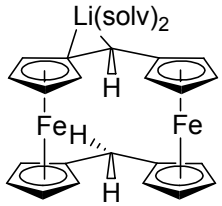

Figure 1-29. Illustration of lithium coordination to the dicarba[1.1]FCP **11a**.

In 1995, two groups independently reported on the synthesis and characterization of the first silicon-bridged [1.1]FCP **11q** (ER_x = $SiMe_2$), surprisingly the bridging moiety in both reports was identical. Chang *et al*. reported that **11q** was obtained in 21% yield from the fly-trap route as a byproduct from the polycondensation reaction of $FeCl_2$ with dilithium salt of dicyclopentadienyldimethylsilane.[88] The ^{1}H NMR spectrum of **11q** (in C_6D_6) revealed two multiplets at δ 4.31 and 4.25 for the Cp protons integrating to four protons each and a singlet at δ 0.39 integrating to six protons, assigned to the $SiMe_2$ groups. The ^{13}C NMR spectrum of **11q** revealed four signals at δ 73.9, 71.5, 70.9 and 2.1. The signal at δ 71.5 was assigned to the *ipso* cyclopentadienyl carbon suggesting the molecule is relatively unstrained. X-ray crystallography revealed that **11q** adopts an *anti* conformation with a tilt angle α of –4.7° for the ferrocene moieties. Manners and co-workers prepared **11q** according to a four-step synthesis with an overall yield of 11% starting from dilithioferrocene (Scheme 1-32).[89] Their early attempts to prepare **11q** from dilithioferrocene and dichlorodimethylsilane always resulted in the formation dimethylsila[1]FCP (**8a**), which is why they devised this four-step synthesis. From the reaction of dilithioferrocene with 2 equiv. of Et_2NSiMe_2Cl, 1,1′-bis(diethylaminodimethylsilyl)ferrocene was isolated in 59% yield. Subsequently, the amino groups were exchanged with chlorides by addition of two equiv. of acetyl chloride, producing 1,1′-bis(chlorodimethylsilyl)ferrocene as a moisture sensitive oil that solidified upon cooling (82% yield). The solid was reacted with 2 equiv. of LiCp producing 1,1′-bis(cyclopentadienyldimethylsilyl)ferrocene in 80% yield. Addition of 2 equiv. of butyllithium produced a dilithium compound as a canary yellow, pyrophoric solid (80% yield) that, when treated with $FeCl_2$, gave **11q** in 35% isolated yield.

Scheme 1-32. Synthetic route to disila[1.1]FCP **11q**.

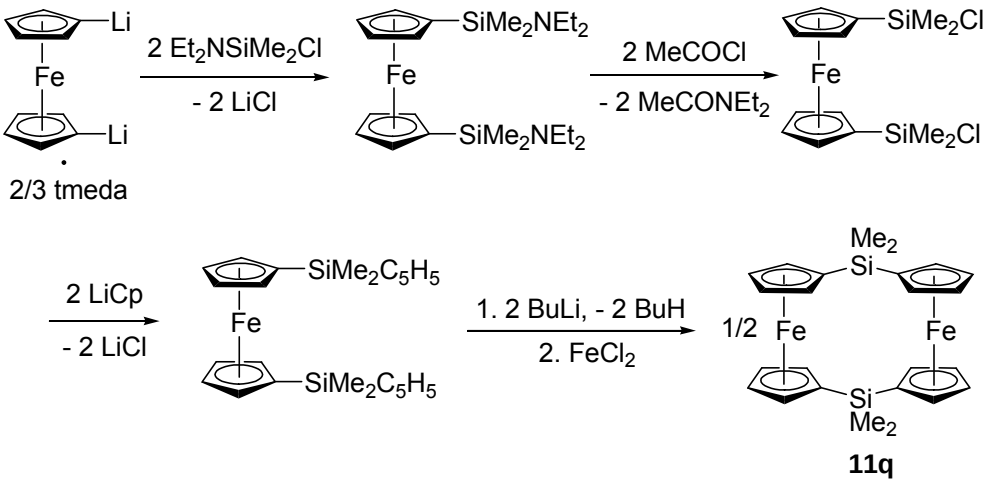

The solid-state structure of **11q** revealed a molecule that adopts an *anti* conformation with the tilt angle α of 4.9(3)° in agreement with the structure reported by Chang within experimental error. Compound **11q** was also investigated as a possible candidate for thermal ROP, however, heating of **11q** to 250 °C did not change its composition. In addition, attempted thermal ring-opening co-polymerizations of **11q** and dimethylsila[1]FCP (**8a**) were unsuccessful leaving **11q** unchanged. Compound **11q** was deemed to be thermally stable and inert towards co-polymerization with **8a**.[89]

Manners *et al*. reported that **11q** was prepared as a isolable byproduct from the transition-metal catalyzed ROP of dimethylsila[1]FCP (**8a**).[64] When [Pd(cod)Cl_2] (0.01 equiv.) was added to **8a** under dilute conditions, poly(ferrocenylsilane) (M_w = 132300) was isolated in 25% yield and **11q** was isolated by column chromatography in 30% yield. In a separate publication, it was reported that **11q** could be isolated in 90% yield by the dimerization of **8a** through a transition-metal catalyzed reaction by [$PdCl_2(PCy_3)_2$] (0.04 equiv.).[90] Complex **11q** along with (polyferrocenyl)silane, cyclic pentamers and hexamers were recently found in the photo-controlled ring-opening reaction of **8a** in presence of 4,4′-dimethylbipyridine.[94]

Cerveau *et al*. isolated a silicon-bridged [1.1]FCP (**11r**, $ER_x = SiCl_2$) in 17% yield as byproduct from the thermal ROP of dichlorosila[1]FCP (**11s**).[91] The ^1H NMR spectrum (in CD_2Cl_2) of **11r** revealed two signals at δ 4.7 and 4.2, assigned to the Cp protons and single-crystal X-ray crystallography revealed that **11r** adopts an *anti* conformation with tilt angle α of – 3.5.

A disila[1.1]FCP **11t** [ER_x = SiMe(CCPh)] was isolated as byproduct in 22% yield from the transition-metal catalyzed ROP of sila[1]FCP **11u** [ER_x = SiMe(CCPh)].[92] By mixing Karstedt's catalyst (0.4 mol%) and **11u** in thf, polyferrocenylsilane (57% yield, $M_w = 2.75 \times 10^5$) and **11t** were generated. The ^1H NMR spectrum of **11t** revealed four multiplets in the Cp region (δ 4.90, 4.47, 4.33 and 4.24) and according to single-crystal X-ray analysis, [1.1]FCP **11t** adopts an *anti* conformation. Interestingly, one of the ferrocene units is significantly tilted (α = –10.3(3)°), whereas the other ferrocene units has cyclopentadienyl rings that are nearly co-planar (α = –1.7(2)°). The cause of the unsymmetrical tilting is not known and no explanation was given.

Hatanka *et al*. reported on the synthesis of a pentacoordinate silicon-bridged [1.1]FCP (**11v**) by controlled dimerization of a strained monomer (**11w**), utilizing an established ring-opening reaction involving a catalytic amount of a Pd(II) source (Scheme 1-33).[93] The only product observed and isolated (62% yield) from the above reaction was **11v**. Surprisingly, in the solid state, the ferrocene moieties of **11v** are rotated with respect to one another by nearly 90°. The authors describe **11v** as an *anti* isomer even though it appeared to have an intermediate conformation between the normally observed *syn* and *anti* conformations. Interestingly, the authors failed to comment on this unusual structure. A more appropriate description of **11v** may be *twist* isomer, like those depicted in Scheme 1-28.

Scheme 1-33. Palladium catalyzed ring-opening dimerization of sila[1]FCP **11w** to yield the disila[1.1]FCP **11v**.

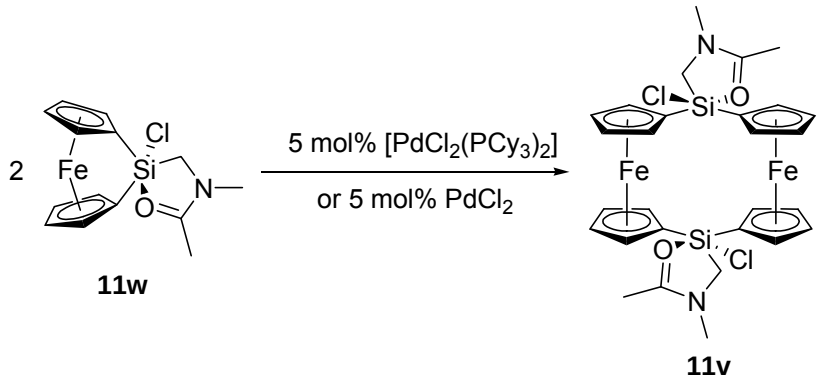

11w **11v**

To date, germanium-bridged [1.1]FCPs have not been reported in the literature.

The first distanna[1.1]FCPs **11x** (ER_x = $SnEt_2$) and **11y** (ER_x = $SnBu_2$) were isolated from equimolar reactions of dilithioferrocene and dialkyltin dichlorides.[56] The authors had hoped to isolate [1]FCPs from the reactions, but instead were only able to isolate polymeric material and a minor component in very low yields (3–6%) from each reaction that were determined to be **11x** and **11y**, respectively. The products were identified based on their NMR and mass spectra. Shortly thereafter, the crystal structure of **11y** was determined revealing that it crystallized as an expected *anti* isomer.[95] Complex **11y** possesses an inversion centre with approximate C_{2h} symmetry in the solid state and the Cp rings are nearly co-planar and eclipsed (dihedral angle of 2.5°). Dong *et al*. published their attempts in preparing cationic derivatives of **11y** with I_3^- counteranions, by addition of iodine to **11y**, but instead were only able to isolate a neutral distanna[1.1]FCP [ER_x = SnBuI (**11z**)].[96] Compound **11z** adopts an *anti* conformation in the solid state with iodine and butyl groups occupying *exo* and *endo* positions, respectively. The Cp rings in each ferrocene moiety are slightly tilted away from the bridging element (α = –3.38°) and nearly eclipsed with an average dihedral angle of 6.5(4)°. The ^{1}H NMR spectrum (in $CDCl_3$) of **11z** revealed two signals at δ 4.16 and 4.39 in the Cp region, instead of the expected four. To

explain the observed equivalence of the α (or β) protons in **11z**, the authors suggest that a fast *anti*-to-*anti* interconversion was occurring in solution.

Distanna[1.1]FCPs **11aa** (ER_x = Sn*t*Bu_2) and **11bb** [ER_x = $SnMes_2$ (Mes = mesitylene)] can be isolated in 32% and 22% yield, respectively, as side products from the thermal ROP reactions of [1]FCPs **11cc** (ER_x = Sn*t*Bu_2) and **11dd** (ER_x = $SnMes_2$), respectively.[97] Solid-state structures of **11aa** and **11bb** reveal molecules in *anti* conformations with small tilt angles α [–5.0(2)° (**11aa**); –3.3(2)° (**11bb**)]. Interestingly, both compounds, as well poly(ferrocenyl)stannane can also be isolated from the ROP of stanna[1]FCPs **11cc** and **11dd** by addition of nucleophiles such as pyridine and 2,6-di-*tert*-butylpyridine.[63,98] This is a special case of a ROP, coined "nucleophilically-assisted ROP", in which a neutral base initiates the polymerization and is comparable to anionic ROP (Chapter 1.3). It differs from anionic ROP by the fact that neutral bases catalyze the ROPs. A second difference is the addition of silicon halides to anionic ROP allows for polymer end-group control (Scheme 1-10), while addition to nucleophilically assisted ROP has no effect on end-group control. Based on this difference, it was suggested that a propagating anion was not generated in the nucleophilically assisted ROPs. Instead, it was proposed that a propagating zwitterionic species was generated according to proposed mechanism illustrated in Scheme 1-34. In this mechanism, a nucleophile first adds to the tin, thereby increasing the nucleophilicity of the Cp carbon bonded to tin without generating a free anion. This increased nucleophilicity allows for attack at the tin of another monomer, thereby proceeding through a transition state with two five coordinate tin centres. Heterolytic Sn–C bond cleavage leads to the propagating zwitterion. Back-biting reactions lead to compounds like **11aa** and **11bb**.

Scheme 1-34. Proposed nucleophilically assisted ROP of stanna[1]FCPs (taken from ref. 98).

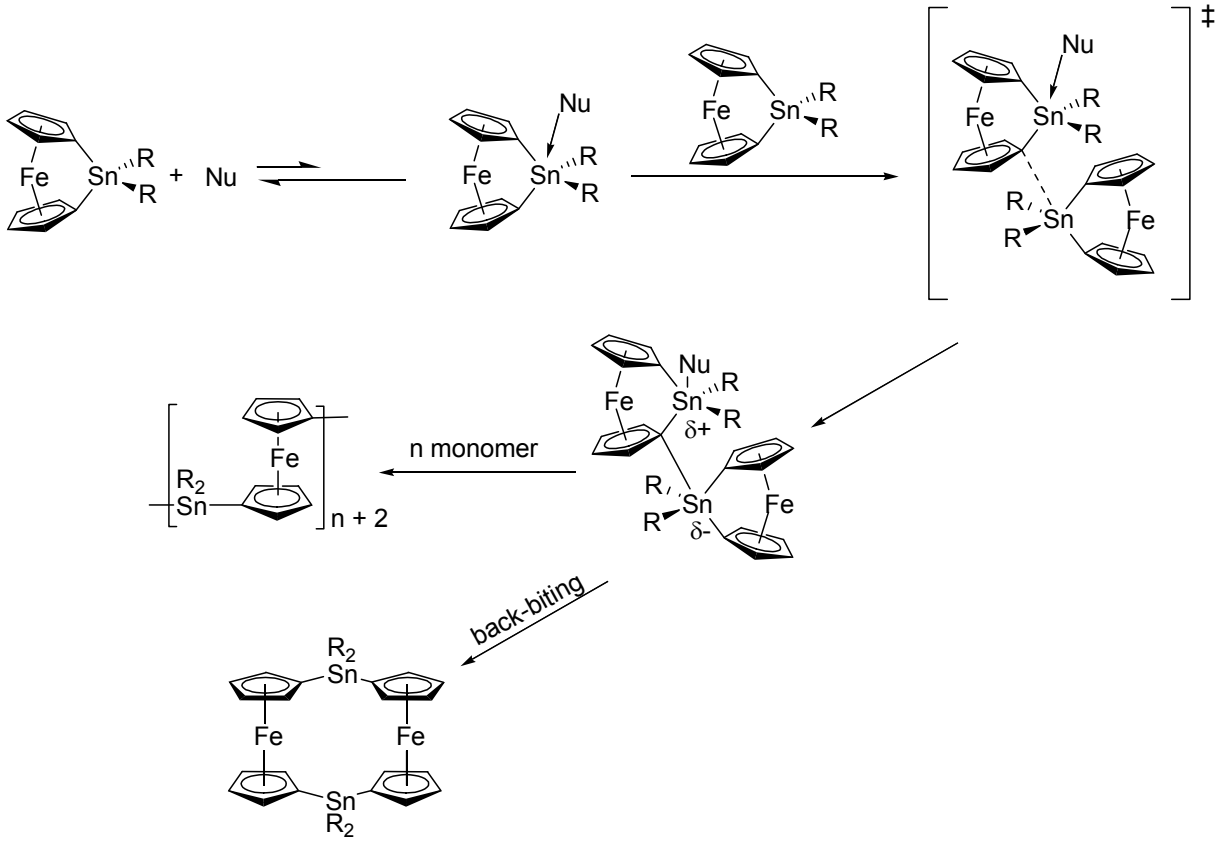

The only lead-bridged [1.1]FCP, **11ee** (ER_x = $PbPh_2$) was isolated (11% yield) by Schwarzhans *et al*. in 1990.[140] It was prepared by addition of dilithioferrocene and monolithioferrocene to a mixture of Ph_2PbCl_2 and Ph_3PbCl (10:1). The monolithioferrocene was reported to be an impurity (6%) of the dilithioferrocene. It is not clear why chlorotriphenyllead was included in this unusual reaction. Compound **11ee** was predicted to adopt the *anti* conformation, based on the fact that all heavier group-14 [1.1]FCP with bulky ligands have adopted the *anti* conformation, even though no solid-state structural evidence was presented. The ^{1}H NMR spectrum obtained for **11ee** did not support a rigid *anti* conformation because only two multiplets were observed in the Cp region, but a fluxional molecule undergoing an *anti*-*anti* interconversion would be consistent with the data. In order to slow down the fluxional behavior

of **11ee,** VT-NMR spectroscopy (^{1}H, 300 MHz) was employed and even at –90 °C only considerable signal broadening was observed. The authors concluded that this broadening was due to a slowing down of the conformational flexibility of the molecule at low temperatures. The authors did not comment on temperature effects in regards to the viscosity of solvent or the solubility of the analyte as possible alternative reasons for the broadening of the signals.

The first published carbon-bridged [1.1]RCP, compound **12c** ($ER_x = CH_2$) was prepared in low yields (12–15%) by Mueller-Westerhoff *et al*. in 1982.[141] Based on an earlier protocol to synthesize dicarba[1.1]FCP **11a** ($ER_x = CH_2$),[116] compound **12c** was prepared by first dilithiating 1,1′-bis(fulvenyl)ruthenocene by treatment with $Li[BHEt_3]$ or $Li[BHBu_3]$, and subsequent treatment with $RuCl_2$·4DMSO. Compound **12c** was isolated as off-white crystals by purification under inert atmosphere, consisting of column chromatography, followed by recrystallization. Crystalline **12c** was rapidly oxidized when introduced to air, producing a dark material, which was not characterized. A ^{1}H NMR spectrum for **12c** (in $CDCl_3$) consisted of two signals in the Cp region at δ 4.60 and 4.41, which both integrate to four protons each and a singlet at δ 3.39, assigned to the two CH_2 groups. This spectrum was very similar to the one observed for fluxional species **11a**. Ten years later, a dication of **12c** was prepared by reaction of **12c** with benzoquinone and BF_3·Et_2O in acetonitrile.[142] According to single-crystal X-ray analysis, the cation in **12c**-$(BF_4)_2$ adopts a *syn* conformation with the ruthenocene moieties significantly twisted relative to one another (twist angle = 33.4°). In addition, the ruthenocene moieties are significantly tilted away from the bridging carbon atoms (α = –28°) and a Ru–Ru bond of 2.953(1) Å was determined. The authors interpreted the twisting of the ruthenocenes relative to one another as a means to relieve the steric crowding of the α protons. An explanation for the large tilt angle was rationalized on the basis of the close proximity of the two ruthenium centres.

That is, for the two ruthenium atoms to approach one another, the Cp rings must deviate from coplanarity. The neutral molecule **12c** also adopts a *syn* conformation.[113]

Izumi *et al*. synthesized dicarba[1.1]RCP [ER_x = CO (**12d**)] in 21% yield by self-condensation of chloroformylruthenocene under Friedel–Craft conditions (Scheme 1-35).[143] By treating **12d** with two equiv. of CH_3MgBr and aqueous ammonium chloride, dicarba[1.1]RCP **12e** [ER_x = $C(CH_3)(OH)$] could be prepared in 94% yield (Scheme 1-35). The ^1H NMR spectrum of **12d** (in $CDCl_3$) displayed two, equally intense signals at δ 4.48 and 4.67, while the spectrum for **12e** displays three signals in the Cp region (δ 4.51, 4.62 and 4.84) in a 4:4:8 integration ratio. The two signals integrating to 4 protons were assigned to the *meta* protons and signal integrating to 8 protons was assigned to all the *ortho* protons. It is important to note that this signal pattern is opposite to what is seen for [1]FCPs and [1]RCPs. The molecular structure of **12d** in a *syn* conformation was reported by Sato *et al*. in 2002.[144]

Scheme 1-35. Preparation of dicarba[1.1]RCPs **12d** and **12e**.

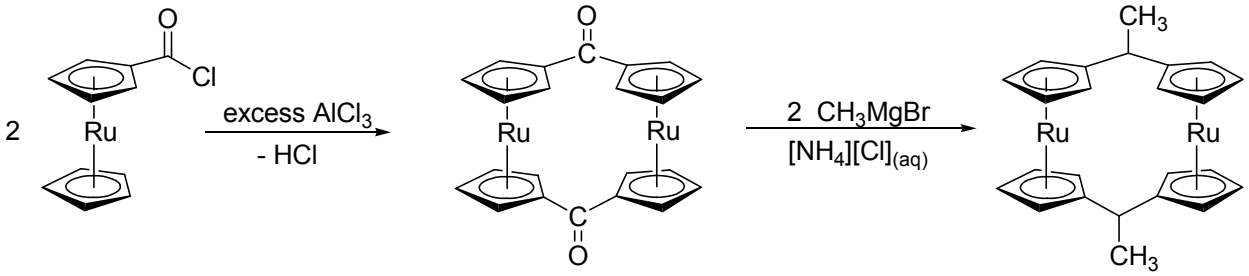

12d **12e**

Herberhold and co-workers reported on a silicon-bridged [1.1]RCP **12e** (ER_x = $SiMe_2$), the only non-carbon-bridged [1.1]RCP known to date.[145] Compound **12e** was prepared through two separate synthetic routes, by reaction of dilithiated ruthenocene with Cl_2SiMe_2 in thf or by reaction of di(lithiocyclopentadienyl)dimethylsilane with $RuCl_2 \cdot 4DMSO$. The ^1H NMR

spectrum of **11c** (in C_6D_6) displayed three resonances (δ 4.63, 4.44 and 0.19) and the *ipso* carbon resonance at 71.4 ppm indicated an unstrained [1.1]RCP was formed.

According to the protocol developed for dicarba[1.1]FCP **11a** and dicarba[1.1]RCP **12c**, dicarba[1.1]RFCP **13a** (ER_x = CH_2) was prepared in low yields (20–25%) by Mueller-Westerhoff *et al*. in 1982. Compound **13a** was prepared by treating bis(fulvenyl)ruthenocene with $Li[BHEt_3]$ or $Li[BHBu_3]$, resulting in formation of a dilithium salt, which was reacted with $RuCl_2$·4DMSO. Compound **13a** adopts a *syn* conformation in the solid state with coplanar Cp groups in the ferrocene and ruthenocene moieties.[113] Watanabe *et al*. have thoroughly investigated the controlled oxidation reactions of **13a**.[146-148]

A second known carbon-bridged [1.1]RFCP [ER_x = CO **(13b)**] was prepared through the Friedel-Crafts reaction involving $AlCl_3$, 1,1′-bis(chloroformyl)ferrocene and ruthenocene, similar to the reaction shown in Scheme 1-35.[149] Single-crystal X-ray analysis reveals compound **13b** as a s*yn* isomer in the solid state.[150]

1.4.4 Group-15-Bridged [1.1]Metallocenophanes

In 2000, the first diphospha[1.1]FCP **14a** [ER_x = P(-)Men, Men = menthyl] was isolated by Brunner *et al*. in 2000 from an equimolar reaction of dilithioferrocene·2/3 tmeda and the chiral phoshine compound Cl_2P(-)Men at low temperature (Scheme 1-36).[100] Though it was not clear why they chose this particular phosphine, it had been previously shown that chlorodiphenylphosphine reacts with dilithioferrocene to give phenylphospha[1]FCP (**14b**).[151] Based on this result, they were probably attempting to synthesize a [1]FCP but were only able to prepare the [1.1]FCP **14a**. In addition to the dimer **14a**, trimers, tetramers and pentamers comprised of ferrocene moities bridged by P(-)Men groups were found in the reaction mixture

by field desorption mass spectrometry. These oligomers were not isolated and no other experimental data were reported for these species. According to single-crystal X-ray analysis, **14a** adopts an *anti* conformation with tilt angles α of –2.12° and –6.11° determined for the ferrocene moieties. As mentioned before, the negative values indicate that the Cp rings tilt away from the bridging element.

Scheme 1-36. Illustration of a chiral diphospha[1.1]FCP **14a**.

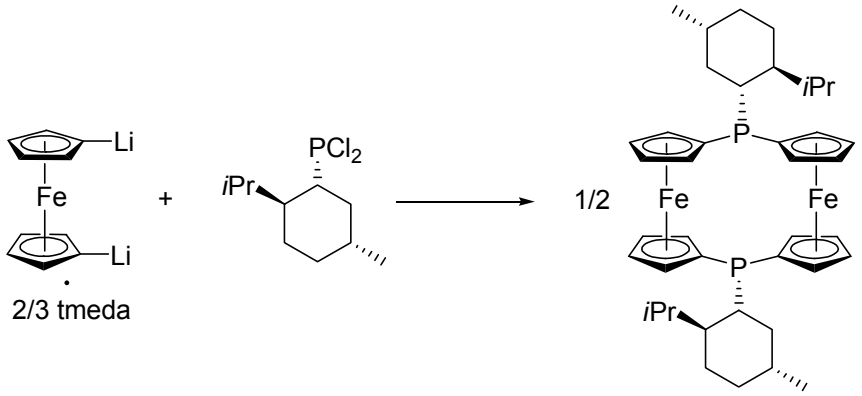

14a

Miyoshi *et al*. reported on the isolation of a diphospha[1.1]FCP [ER_x = P(S)(Ph) (**14c**)] as a side product from the photo-controlled ROP of phenylphospha[1]FCP (**14b**) after treatment with elemental sulfur.[72] In 2005, Miyoshi and co-workers published solid-state structural details of **14c** and, remarkably, both the *anti* and *syn* isomers were isolated.[101] The *syn* isomer of **14c** could be desulfurized by treatment with Si_2Cl_6 in refluxing benzene producing the *syn* isomer phenylphospha[1.1]FCP [ER_x = PPh (**14d**)]. Treatment of the *anti* isomer of **14c** with Si_2Cl_6 in refluxing benzene produced exclusively the *syn* isomer **14d** meaning that an *anti*-to-*syn* isomerization takes place during the desulfurization.

Miyoshi *et al*. also reported on the synthesis of several other diphospha[1.1]FCPs [ER_x = $P(NEt_2)$ (**14e**), PCl **(14f**), $P(CH_2SiMe_3)$ (**14g**), P(*p*-Tol) (**14h**)].[102] The *syn* and *anti*

conformations of **14e** were prepared in 5:4 ratio by treating 1,1′-bis(chlorodiethylaminophosphyl)ferrocene in succession with 2 equivalents of NaCp and two equivalents of butyllithium, followed by addition of $FeCl_2$. By treating the *syn* and *anti* isomers of **14e** with two equivalents of HCl, the *syn* isomer of **14f** was exclusively prepared indicating that an *anti*-to-*syn* conversion takes place during the reaction. The *syn* isomer **14f** can be converted to the *syn* isomers of **14e**, **14g**, **14h** and **14h** by treatment with diethylamine or with an appropriate lithium alkyl or lithium aryl reagent.

The synthesis of a diarsa[1.1]FCP [ER_x = AsCl (**14h**)] was published by Roesky *et al*. in 1989.[103] Compound **14h** was isolated from a low temperature (–78 °C) synthesis involving dilithioferrocene·2/3 tmeda and $AsCl_3$ in dimethyoxyethane. The identity of **14h** was confirmed through mass spectrometry and NMR spectroscopy. The peak of the molecular ion in the mass spectrum of **14h** supported its characterization as a [1.1]FCP.

To date, group-15-bridged [1.1]RCPs and [1.1]RFCPs have not been reported in the literature.

1.4.5 Group-16-Bridged [1.1]Metallocenophanes

A group-16-bridged [1.1]FCP [ER_x = S **(15a)**] containing sulfur as a bridging element was published very recently.[152] Complex **15a** was prepared in 38% yield by the photoinduced ring-opening reaction of thia[1]FCP **15b** (ER_x = S) in thf. The solid-state structure of **15a** revealed that the molecule adopts a *syn* conformation and the authors noted that the distinct pair of pseudo-triplets in the Cp region of the ^{1}H NMR spectrum suggest that only one isomer is present in solution at 22 °C, assuming a fast *syn*-to-*syn* interconversion.

1.5 Electrochemistry of [1.1]Metallocenophanes

As mentioned earlier, [1.1]metallocenophanes can be considered to be model compounds for investigating metal-metal interactions. Cyclic voltammetry can be used to investigate the through-space or through bridging-element-mediated interactions of [1.1]metallocenophanes because they have at least two redox active sites in close proximity. Any information that is obtained from cyclic voltammetry on these metal-metal interactions can be applied to polymers with similar compositions. It is important to note that [1.1]metallocenophanes investigated by cyclic voltammetry to date have contained identical bridging moieties ER_x. [1.1]Metallocenophanes that have been investigated by electrochemical measurements include [1.1]FCPs, [1.1]RCPs and [1.1]RFCPs. As mentioned earlier, before this Ph.D. project was undertaken, [1.1]metallarenophanes were unknown in the literature.

The oxidation of ferrocene to the ferrocenium ion is a reversible one-electron step, whereas the oxidation of ruthenocene is an irreversible two-electron step. As a result, the electrochemistry of [1.1]FCPs, [1.1]RCPS and [1.1]RFCPs are considerably different from one another. When two redox centres are in close proximity, the electronic communication between the redox centres can be investigated. A classification system devised by Robin and Day can be used to describe molecules that contain atoms of the same element in different formal oxidation states.[104] To classify mixed-valence species, the Robin and Day classification system is broken down into three classes. Class I compounds display no charge delocalization at all, because the redox active centres are insulated from one another, thereby inhibiting electron transfer between the redox active centres. In Class I compounds, both redox active centres are oxidized (reduced)

at the same potential. Class II compounds exhibit charge delocalization, but the redox centres that are in different oxidation states are distinguishable because an electron that is transferred does not spend equal amounts of time on both centres. The end result is the two metal centres are oxidized at slightly different potentials. Class III compounds show complete delocalization in the mixed-valent state, with the mixed-valent sites being indistinguishable from each other, that is, the electron transferred between the redox centres spends equal time on both redox centres. Müller *et al*. reported on the only known example of Class I [1.1]FCP recently, the aluminum-bridged [1.1]FCP **10d**.[84] Class II metallocenophanes are known for [1.1]FCPs bridged by boron,[81] gallium,[84] indium,[84] carbon,[153-155] silicon,[89,91,94] and tin.[96,97] No Class III [1.1]FCPs are known; it is expected that the redox centres would be oxidized (reduced) at substantially different potentials compared to one another.

As mentioned earlier, the electrochemistry of [1.1]RCPs and [1.1]RFCPs is considerably different from [1.1]FCPs. Surprisingly, the carbon-bridged [1.1]RCP **12c** ($ER_x = CH_2$) can be reversibly oxidized in a two-electron step, generating a dicationic ruthenocene linked to a neutral ruthenocene.[142,153] This is in stark contrast to the parent ruthenocene, which is irreversibly oxidized in a two-electron step. It was suggested that a Ru–Ru bond forms in the dication **12c**, which acts to stabilize the dication. In fact, solid-state evidence supports this claim. The dication of **12c**-$(BF_4)_2$ possesses a Ru–Ru bond of 2.953(1) Å.[142] [1.1]RFCP **13a** ($ER_x = CH_2$) shows the presence of two independent metallocenes, the ferrocene moiety can be reversibly oxidized in a one-electron step and the ruthenocene moiety can be irreversibly oxidized in a two-electron step.[146,149,153]

The electrochemistry of [1.1]CAPs, [1.1]VAPs and [1.1]MAPs should be similar to that observed for [1.1]FCPs based on the fact that ferrocene is oxidized in a reversible one-electron

step and bis(benzene)chromium, bis(benzene)vanadium and bis(benzene)molybdenum are oxidized in quasi-reversible one-electron steps.

1.6 Research Objectives

The primary objectives of this Ph.D. project were to synthesize heavier group-13-bridged [1]metallarenophanes (E = Al, Ga, In), and to explore their potential application as monomers for ROP (Chapter 1.3). As mentioned in the introduction, before this Ph.D. project was undertaken, these compounds were unknown in the literature (Chapter 1.1). Organometallic polymers are attractive targets because of their unique properties. For example, polyferrocenylsilane, the most widely investigated organometallic polymer, has been shown to possess electrochromic behaviour and electronic communication between metal centres due to metal-metal interactions.[51] These metal-metal interactions could potentially be tuned so that conducting polymers could be prepared.

To date, [1]metallarenophanes have been only prepared by the dilithiation route (Scheme 1-1). For this reason, compounds of the type REX_2 are required for the synthesis of these strained sandwich compounds. Because heavier group-13 compounds of the type ER_3 and EX_3 are Lewis acids, they tend to be oligomeric and less reactive than their monomeric counterparts. It is therefore desirable to have monomeric, well-defined starting materials that will react in an expected way. Consequently, to achieve the set goal, the preparation of heavier group-13-bridged [1]metallarenophanes, the required starting compounds REX_2 (E = Al, Ga, In; X = halogen atoms) needed to be synthesized first, which raised the question what should the ligand R be. In order to get monomeric, well-defined starting compounds REX_2, the ligand R must either be sterically demanding or equipped with a Lewis-donor group; the latter can intramolecularly satisfy the electronic needs of the element E through acid-base adduct

formation. For example, Mes*$AlCl_2$ (Mes* = 2,4,6-*t*BuC_6H_2) is a solvent-free monomer in the solid state,[158] whereas the less sterically protected $PhAlCl_2$ is a dimer in non-coordinating solvents.[159] Based on the background of the Müller's group experience with intramolecularly stabilized group-13 species,[160,161] it was decided to use the same concept for the required starting compounds REX_2. From the numerous known intramolecularly stabilizing ligands R, *trisyl*-based species[162] [*trisyl* = tris(trimethylsilyl)methyl] looked promising because they combine steric protection and intramolecular donation. In addition, the $SiMe_3$ groups are not just sterically demanding, but they have electron-donating properties through the ß-silyl effect.

A third objective arose as a direct result of my colleague's work. Jörg Schachner synthesized and characterized aluminum-, gallium- and indium-bridged [1.1]FCPs equipped with intramolecularly stabilizing ligands (Chapter 1.4.2; Figures 1-24 and 1-25).[84] Based on these results, I wanted to explore whether [1.1]metallarenophanes, bridged by heavier group-13 elements equipped with similar ligands, could be synthesized. As mentioned earlier, before this Ph.D. project was undertaken, despite the large number of known [1.1]metallocenophanes, not a single example of a [1.1]metallarenophane was known in the literature (see Chapter 1.4). Even though [1.1]metallarenophanes were expected to be unstrained and, therefore, unsuitable for ROP, they are interesting compounds for investigating metal-metal interactions in solution by cyclic voltammetry (Chapter 1.5). Any information obtained from metal-metal interactions in [1.1]metallarenophanes could be applicable to polymers with similar compositions; in other words, [1.1]metallarenophanes serve as models for their respective polymers.

Chapters 2–9 of this Ph.D. thesis are verbatim copies of journal articles published in the literature. Before each publication, there is a short summary of the work and preamble addressing each author's contributions. In addition, connecting text describing how each paper

relates to the stated objectives of this thesis has been included. In short, chapters 2–5 primarily focus on synthesis and characterization of monomeric group-13 compounds that are equipped with *trisyl*-based ligands with nitrogen-donor functionalities. These compounds provided the groundwork for the preparation of aluminum cations[156] and [1]FCPs[82,105,157]. Chapters 6 and 7 address the primary objective and describe the synthesis and characterization of the first aluminum- and gallium-bridged [1]CAPs, [1]VAPs and [1]MAPs equipped with donor-stabilizing ligands. It is important to note that before this Ph.D. project began, the bora[1]CAPs **9d–9f**[14] (Chapter 1.1.2) were the only known group-13-bridged [1]metallarenophanes published in the literature and not a single [1]MAP had been published in the literature. Chapter 8 addresses the third objective of this Ph.D. thesis and describes how the first [1.1]CAPs and [1.1]MAPs were obtained. Chapter 9 describes the synthesis and characterization of an indium-bridged [1.1]FCP, a surprising result that provided very important insight into the chemistry of group-13-bridged metallacyclophanes.

1.7 References

(1) Elschenbroich, C.; Koch, J. *J. Organomet. Chem.* **1982**, *229*, 139-158.
(2) Hultzsch, K. C.; Nelson, J. M.; Lough, A. J.; Manners, I. *Organometallics* **1995**, *14*, 5496-5502.
(3) Elschenbroich, C.; Schmidt, E.; Gondrum, R.; Metz, B.; Burghaus, O.; Massa, W.; Wocadlo, S. *Organometallics* **1997**, *16*, 4589-4596.
(4) Butler, I. R.; Cullen, W. R.; Ni, J.; Rettig, S. J. *Organometallics* **1985**, *4*, 2196-2201.
(5) Elschenbroich, C. *J. Organomet. Chem.* **1968**, *14*, 157-163.
(6) Elschenbroich, C.; Hurley, J.; Metz, B.; Massa, W.; Baum, G. *Organometallics* **1990**, *9*, 889-897.
(7) Braunschweig, H.; Buggisch, N.; Englert, U.; Homberger, M.; Kupfer, T.; Leusser, D.; Lutz, M.; Radacki, K. *J. Am. Chem. Soc.* **2007**, *129*, 4840-4846.
(8) Foucher, D. A.; Tang, B. Z.; Manners, I. *J. Am. Chem. Soc.* **1992**, *114*, 6246-6248.
(9) Herbert, D. E.; Mayer, U. F. J.; Manners, I. *Angew. Chem., Int. Ed. Engl.* **2007**, *46*, 5060-5081.
(10) Bellas, V.; Rehahn, M. *Angew. Chem., Int. Ed. Engl.* **2007**, *46*, 5082-5104.
(11) Elschenbroich, C.; Schmidt, E.; Metz, B.; Harms, K. *Organometallics* **1995**, *14*, 4043-4045.
(12) Broussier, R.; Da Rold, A.; Gautheron, B.; Dromzee, Y.; Jeannin, Y. *Inorg. Chem.* **1990**, *29*, 1817-1822.
(13) Broussier, R.; Da Rold, A.; Gautheron, B. *J. Organomet. Chem.* **1992**, *427*, 231-244.
(14) Braunschweig, H.; Homberger, M.; Hu, C.; Zheng, X.; Gullo, E.; Clentsmith, G.; Lutz, M. *Organometallics* **2004**, *23*, 1968-1970.
(15) Braunschweig, H.; Adams, C. J.; Kupfer, T.; Manners, I.; Richardson, R. M.; Whittell, G. R. *Angew. Chem., Int. Ed. Engl.* **2008**, *47*, 3826-3829.
(16) Holleman-Wiberg *In Inorganic Chemistry*, 1st English ed.; Wiberg, N., Ed.; Academic Press: San Diego, 2001, 1756-1759.
(17) Rulkens, R.; Lough, A. J.; Manners, I. *Angew. Chem., Int. Ed. Engl.* **1996**, *35*, 1805-1807.
(18) Elschenbroich, C.; Bretschneider-Hurley, A.; Hurley, J.; Behrendt, A.; Massa, W.; Wocadlo, S.; Reijerse, E. *Inorg. Chem.* **1995**, *34*, 743-745.
(19) Berenbaum, A.; Manners, I. *J. Chem. Soc., Dalton Trans.* **2004**, 2057-2058.
(20) Elschenbroich, C.; Bretschneider-Hurley, A.; Hurley, J.; Massa, W.; Wocadlo, S.; Pebler, J.; Reijerse, E. *Inorg. Chem.* **1993**, *32*, 5421-5424.
(21) Jellinek, F. *J. Organomet. Chem.* **1963**, *1*, 43-50.
(22) Fischer, E. O.; Frit, H. P.; Maneho, J.; Priebe, E.; Schneider, R. *Chem. Ber.* **1963**, *96*, 1418-1423.
(23) Green, M. L. H.; Treurnicht, I.; Bandy, J. A.; Gourdon, A.; Prout, K. *J. Organomet. Chem.* **1986**, *306*, 145-165.
(24) Braunschweig, H.; Kupfer, T. *Organometallics* **2007**, *26*, 4634-4638.
(25) Ishiyama, T.; Miyaura, N. *J. Organomet. Chem.* **2000**, *611*, 392-402.

(26) Braunschweig, H.; Kupfer, T.; Lutz, M.; Radacki, K.; Seeler, F.; Sigritz, R. *Angew. Chem., Int. Ed. Engl.* **2006**, *45*, 8048-8051.
(27) Elschenbroich, C.; Sebbach, J.; Metz, B. *Helv. Chim. Acta* **1991**, *74*, 1718-1724.
(28) Braunschweig, H.; Kupfer, T. *J. Am. Chem. Soc.* **2008**, *130*, 4242-4243.
(29) Nesmeyanov, A. N.; Zaitseva, N. N.; Domrachev, G. A.; Zinov'ev, V. D.; Yur'eva, L. P.; Tverdokhlebova, L. I. *J. Organomet. Chem.* **1976**, *121*, C52-C54.
(30) Nesmeyanov, A. N.; Yur'eva, L. P.; Zaitseva, N. N.; Domrachev, G. A.; Zinov'ev, V. D. *J. Organomet. Chem.* **1978**, *153*, 181-186.
(31) Van Oven, H. O.; de Liefde Meijer, H. J. *J. Organomet. Chem.* **1970**, *23*, 159-163.
(32) Zeinstra, J. D.; De Boer, J. L. *J. Organomet. Chem.* **1973**, *54*, 207-211.
(33) King, R. B.; Stone, F. G. A. *J. Am. Chem. Soc.* **1959**, *81*, 5263-5264.
(34) Engebretson, G.; Rundle, R. E. *J. Am. Chem. Soc.* **1963**, *85*, 481-482.
(35) Fischer, E. O.; Breitschaft, S. *Angew. Chem., Int. Ed. Engl.* **1963**, *2*, 44.
(36) Lyssenko, K. A.; Antipin, M. Y.; Ketkov, S. Y. *Russ. Chem. Bull.* **2001**, *50*, 130-141.
(37) Ogasa, M.; Rausch, M. D.; Rogers, R. D. *J. Organomet. Chem.* **1991**, *403*, 279-291.
(38) Elschenbroich, C.; Paganelli, F.; Nowotny, M.; Neumüller, B.; Burghaus, O. *Z. Anorg. Allg. Chem.* **2004**, *630*, 1599-1606.
(39) Braunschweig, H.; Lutz, M.; Radacki, K. *Angew. Chem., Int. Ed. Engl.* **2005**, *44*, 5647-5651.
(40) Tamm, M.; Kunst, A.; Bannenberg, T.; Herdtweck, E.; Sirsch, P.; Elsevier, C. J.; Ernsting, J. M. *Angew. Chem., Int. Ed. Engl.* **2004**, *43*, 5530-5534.
(41) Braunschweig, H.; Kupfer, T.; Lutz, M.; Radacki, K. *J. Am. Chem. Soc.* **2007**, *129*, 8893-8906.
(42) Fischer, E. O.; Breitschaft, S. *Chem. Ber.* **1966**, *99*, 2213-2226.
(43) Herberhold, M.; Hofmann, T.; Milius, W.; Wrackmeyer, B. *J. Organomet. Chem.* **1994**, *472*, 175-183.
(44) Braunschweig, H.; Kupfer, T.; Radacki, K. *Angew. Chem., Int. Ed. Engl.* **2007**, *46*, 1630-1633.
(45) Braunschweig, H.; Lutz, M.; Radacki, K.; Schaumlöffel, A.; Seeler, F.; Unkelbach, C. *Organometallics* **2006**, *25*, 4433-4435.
(46) Tamm, M.; Kunst, A.; Bannenberg, T.; Randoll, S.; Jones, P. G. *Organometallics* **2007**, *26*, 417-424.
(47) Bartole-Scott, A.; Braunschweig, H.; Kupfer, T.; Lutz, M.; Manners, I.; Nguyen, T. L.; Radacki, K.; Seeler, F. *Chem.—Eur. J.* **2006**, *12*, 1266-1273.
(48) Tamm, M.; Kunst, A.; Herdtweck, E. *Chem. Commun.* **2005**, 1729-1731.
(49) Thomas, R. L.; Souza, F. E. S.; Marder, T. B. *J. Chem. Soc., Dalton Trans.* **2001**, 1650-1656.
(50) Finckh, W.; Tang, B. Z.; Lough, A.; Manners, I. *Organometallics* **1992**, *11*, 2904-2911.
(51) Manners, I. *Polyhedron* **1996**, *15*, 4311-4329.
(52) Tanabe, M.; Vandermeulen, G. W. M.; Chan, W. Y.; Cyr, P. W.; Vanderark, L.; Rider, D. A.; Manners, I. *Nature Materials* **2006**, *5*, 467-470, and references therein.
(53) Rosenberg, H.; Rausch, M. D. U.S. Patent 3060215, 1962.
(54) Rosenberg, H. U.S. Patent 3426053, 1969.
(55) Pudelski, J. K.; Manners, I. *J. Am. Chem. Soc.* **1995**, *117*, 7265-7266.
(56) Seyferth, D.; Withers, H. P. *Organometallics* **1982**, *1*, 1275-1282.

(57) Withers, H. P.; Seyferth, D.; Fellmann, J. D.; Garrou, P. E.; Martin, S. *Organometallics* **1982**, *1*, 1283-1288.
(58) Honeyman, C. H.; Peckham, T. J.; Massey, J. A.; Manners, I. *Chem. Commun.* **1996**, 2589-2590.
(59) Rulkens, R.; Lough, A. J.; Manners, I. *J. Am. Chem. Soc.* **1994**, *116*, 797-798.
(60) Rulkens, R.; Ni, Y.; Manners, I. *J. Am. Chem. Soc.* **1994**, *116*, 12121-12122.
(61) Resendes, R.; Nguyen, P.; Lough, A. J.; Manners, I. *Chem. Commun.* **1998**, 1001-1002.
(62) Resendes, R.; Nelson, J. M.; Fischer, A.; Jäkle, F.; Bartole, A.; Lough, A. J.; Manners, I. *J. Am. Chem. Soc.* **2001**, *123*, 2116-2126.
(63) Baumgartner, T.; Jäkle, F.; Rulkens, R.; Zech, G.; Lough, A. J.; Manners, I. *J. Am. Chem. Soc.* **2002**, *124*, 10062-10070.
(64) Ni, Y.; Rulkens, R.; Pudelski, J. K.; Manners, I. *Macromol. Rapid Commun.* **1995**, *16*, 637-641.
(65) Cundy, C. S.; Eaborn, C.; Lappert, M. F. *J. Organomet. Chem.* **1972**, *44*, 291-297.
(66) Reddy, N. P.; Yamashita, H.; Tanaka, M. *Chem. Commun.* **1995**, 2263-2264.
(67) Sheridan, J. B.; Lough, A. J.; Manners, I. *Organometallics* **1996**, *15*, 2195-2197.
(68) Sheridan, J. B.; Temple, K.; Lough, A. J.; Manners, I. *J. Chem. Soc., Dalton Trans.* **1997**, 711-713.
(69) Temple, K.; Jäkle, F.; Sheridan, J. B.; Manners, I. *J. Am. Chem. Soc.* **2001**, *123*, 1355-1364.
(70) Gómez-Elipe, P.; Resendes, R.; Macdonald, P. M.; Manners, I. *J. Am. Chem. Soc.* **1998**, *120*, 8348-8356.
(71) Young, R. J.; Grushin, V. V. *Organometallics* **1999**, *18*, 294-296.
(72) Mizuta, T.; Onishi, M.; Miyoshi, K. *Organometallics* **2000**, *19*, 5005-5009.
(73) Mizuta, T.; Imamura, Y.; Miyoshi, K. *J. Am. Chem. Soc.* **2003**, *125*, 2068-2069.
(74) Tanabe, M.; Bourke, S. C.; Herbert, D. E.; Lough, A. L.; Manners, I. *Angew. Chem., Int. Ed. Engl.* **2005**, *44*, 5886-5890.
(75) Tanabe, M.; Manners, I. *J. Am. Chem. Soc.* **2004**, *126*, 11434-11435.
(76) Löwendahl, M.; Håkansson, M. *Organometallics* **1995**, *14*, 4736-4741.
(77) Nesmeyanov, A. N.; Kritskaya, I. I. *Bull. Acad. Sci. USSR Div. Chem. Sci. (Engl. Transl.)* **1956**, 243-244.
(78) Kuz'mina, L. G.; Struchkov, Y. T.; Lemenovskii, D. A.; Urazovskii, I. F.; Nifant'ev, I. E.; Perevalova, E. G. *Koord. Khim.* **1983**, *9*, 1212-1219.
(79) Lemenovskii, D. A.; Urazowski, I. F.; Baukova, T. V.; Arkhipov, I. L.; Stukan, R. A.; Perevalova, E. G. *J. Organomet. Chem.* **1984**, *264*, 283-288.
(80) Kuz'mina, L. G.; Struchkov, Y. T.; Lemenovsky, D. A.; Urazowsky, I. F. *J. Organomet. Chem.* **1984**, *277*, 147-151.
(81) Scheibitz, M.; Winter, R. F.; Bolte, M.; Lerner, H. W.; Wagner, M. *Angew. Chem., Int. Ed. Engl.* **2003**, *42*, 924.
(82) Schachner, J. A.; Lund, C. L.; Quail, J. W.; Müller, J. *Acta Crystallogr., Sect. E: Struct. Rep. Online* **2005**, *61*, M682-M684.
(83) Braunschweig, H.; Burschka, C.; Clentsmith, G. K. B.; Kupfer, T.; Radacki, K. *Inorg. Chem.* **2005**, *44*, 4906-4908.
(84) Schachner, J. A.; Orlowski, G. A.; Quail, J. W.; Kraatz, H.-B.; Müller, J. *Inorg. Chem.* **2006**, *45*, 454-459.

(85) Uhl, W.; Hahn, I.; Jantschak, A.; Spies, T. *J. Organomet. Chem.* **2001**, *637*, 300-303.
(86) Jutzi, P.; Lenze, N.; Neumann, B.; Stammler, H. G. *Angew. Chem., Int. Ed. Engl.* **2001**, *40*, 1423-1427.
(87) Althoff, A.; Jutzi, P.; Lenze, N.; Neumann, B.; Stammler, A.; Stammler, H. G. *Organometallics* **2003**, *22*, 2766-2774.
(88) Park, J.; Seo, Y.; Cho, S.; Whang, D.; Kim, K.; Chang, T. *J. Organomet. Chem.* **1995**, *489*, 23-25.
(89) Zechel, D. L.; Foucher, D. A.; Pudelski, J. K.; Yap, G. P. A.; Rheingold, A. L.; Manners, I. *J. Chem. Soc., Dalton Trans.* **1995**, 1893-1899.
(90) Reddy, N. P.; Choi, N.; Shimada, S.; Tanaka, M. *Chem. Lett.* **1996**, 649-650.
(91) Calleja, G.; Carré, F.; Cerveau, G. *Organometallics* **2001**, *20*, 4211-4215.
(92) Berenbaum, A.; Lough, A. J.; Manners, I. *Organometallics* **2002**, *21*, 4415-4424.
(93) Bao, M.; Hatanaka, Y.; Shimada, S. *Chem. Lett.* **2004**, *33*, 520-521.
(94) Chan, W. Y.; Lough, A. J.; Manners, I. *Angew. Chem., Int. Ed. Engl.* **2007**, *46*, 9069-9072.
(95) Clearfield, A.; Simmons, C. J.; Withers Jr., H. P.; Seyferth, D. *Inorg. Chim. Acta* **1983**, *75*, 139-144.
(96) Dong, T. Y.; Hwang, M. Y.; Wen, Y. S.; Hwang, W. S. *J. Organomet. Chem.* **1990**, *391*, 377-385.
(97) Jäkle, F.; Rulkens, R.; Zech, G.; Foucher, D. A.; Lough, A. J.; Manners, I. *Chem.—Eur. J.* **1998**, *4*, 2117-2128.
(98) Jäkle, F.; Rulkens, R.; Zech, G.; Massey, J. A.; Manners, I. *J. Am. Chem. Soc.* **2000**, *122*, 4231-4232.
(99) Utri, G.; Schwarzhans, K. E.; Allmaier, G. M. *Z. Naturforsch., B: Chem. Sci.* **1990**, *45*, 755-762.
(100) Brunner, H.; Klankermayer, J.; Zabel, M. *J. Organomet. Chem.* **2000**, *601*, 211-219.
(101) Mizuta, T.; Imamura, Y.; Miyoshi, K.; Yorimitsu, H.; Oshima, K. *Organometallics* **2005**, *24*, 990-996.
(102) Imamura, Y.; Mizuta, T.; Miyoshi, K. *Organometallics* **2006**, *25*, 882-886.
(103) Spang, C.; Edelmann, F. T.; Noltemeyer, M.; Roesky, H. W. *Chem. Ber.* **1989**, *122*, 1247-1254.
(104) Robin, M. B.; Day, P. *Adv. Inorg. Chem. Radiochem.* **1967**, *10*, 247-422.
(105) Schachner, J. A.; Lund, C. L.; Quail, J. W.; Müller, J. *Organometallics* **2005**, *24*, 785-787.
(106) Watts, W. E. *J. Am. Chem. Soc.* **1966**, *88*, 855-856.
(107) McKechnie, J. S.; Bersted, B.; Paul, I. C.; Watts, W. E. *J. Organomet. Chem.* **1967**, *8*, P29-P31.
(108) Watts, W. E. *J. Organomet. Chem.* **1967**, *10*, 191-192.
(109) Nesmeyanov, A. N.; Reutov, O. A. *Dokl. Akad. Nauk.* **1958**, *120*, 1267-1270.
(110) Kasahara, A.; Izumi, T.; Ohnishi, S. *Bull. Chem. Soc. Jpn.* **1972**, *45*, 951-952.
(111) Salazar, D. C. O.; Cowan, D. O. *J. Organomet. Chem.* **1991**, *408*, 219-225.
(112) Barr, T. H.; Lentzner, H. L.; Watts, W. E. *Tetrahedron* **1969**, *25*, 6001-6013.
(113) Rheingold, A. L.; Mueller-Westerhoff, U. T.; Swiegers, G. F.; Haas, T. J. *Organometallics* **1992**, *11*, 3411-3417.

(114) McKechnie, J. S.; Maier, C. A.; Bersted, B.; Paul, I. C. *J. Chem. Soc., Perkin Trans. 2* **1973**, 138-143.
(115) Katz, T. J.; Acton, N.; Martin, G. *J. Am. Chem. Soc.* **1969**, *91*, 2804-2805.
(116) Mueller-Westerhoff, U. T.; Nazzal, A.; Prössdorf, W. *J. Organomet. Chem.* **1981**, *205*, C21-C23.
(117) Cassens, A.; Eilbracht, P.; Nazzal, A.; Prössdorf, W.; Mueller-Westerhoff, U. T. *J. Am. Chem. Soc.* **1981**, *103*, 6367-6372.
(118) Mueller-Westerhoff, U. T.; Nazzal, A.; Prössdorf, W.; Mayerle, J. J.; Collins, R. L. *Angew. Chem., Int. Ed. Engl.* **1982**, *21*, 686-695.
(119) Moore, M. F.; Wilson, S. R.; Hendrickson, D. N.; Mueller-Westerhoff, U. T. *Inorg. Chem.* **1984**, *23*, 2918-2920.
(120) Kansal, V. K.; Watts, W. E.; Mueller-Westerhoff, U. T.; Nazzal, A. *J. Organomet. Chem.* **1983**, *243*, 443-449.
(121) Mueller-Westerhoff, U. T. *Angew. Chem., Int. Ed. Engl.* **1986**, *25*, 702-717.
(122) Löwendahl, M.; Davidson, Ö.; Ahlberg, P. *J. Chem. Res., Synop.* **1993**, 40-41.
(123) Rudziński, J. M.; Ōsawa, E. *J. Phys. Org. Chem.* **1993**, *6*, 107-112.
(124) Singletary, N. J.; Hillman, M.; Dauplaise, H.; Kvick, A.; Kerber, R. C. *Organometallics* **1984**, *3*, 1427-1434.
(125) Bitterwolf, T. E.; Ling, A. C. *J. Organomet. Chem.* **1973**, *57*, C15-C18.
(126) Waleh, A.; Loew, G. H.; Mueller-Westerhoff, U. T. *Inorg. Chem.* **1984**, *23*, 2859-2863.
(127) Mueller-Westerhoff, U. T.; Nazzal, A. *J. Am. Chem. Soc.* **1984**, *106*, 5381-5382.
(128) Hillman, M.; Michaile, S.; Feldberg, S. W.; Eisch, J. J. *Organometallics* **1985**, *4*, 1258-1263.
(129) Michalle, S.; Hillman, M.; Eisch, J. J. *Organometallics* **1988**, *7*, 1059-1065.
(130) Karlsson, A.; Hilmersson, G.; Ahlberg, P. *J. Phys. Org. Chem.* **1997**, *10*, 590-592.
(131) Sato, M.; Asai, M. *J. Organomet. Chem.* **1992**, *430*, 105-110.
(132) Löwendahl, M.; Davidsson, Ö.; Ahlberg, P.; Håkansson, M. *Organometallics* **1993**, *12*, 2417-2419.
(133) Ahlberg, P.; Davidson, Ö. *Chem. Commun.* **1987**, *8*, 623-624.
(134) Mueller-Westerhoff, U. T.; Nazzal, A.; Prössdorf, W. *J. Am. Chem. Soc.* **1981**, *103*, 7678-7681.
(135) Ahlberg, P.; Davidson, Ö.; Johnsson, B.; Ewen, I. M.; Rönnqvist, M. *Bull. Soc. Chim. Fr.* **1988**, *2*, 177-186.
(136) Davidson, Ö.; Löwendahl, M.; Ahlberg, P. *Chem. Commun.* **1992**, *14*, 1004-1005.
(137) Ahlberg, P.; Davidsson, Ö.; Löwendahl, M.; Hilmersson, G.; Karlsson, A.; Håkansson, M. *J. Am. Chem. Soc.* **1997**, *119*, 1745-1750.
(138) Ahlberg, P.; Karlsson, A.; Davidsson, Ö.; Hilmersson, G.; Löwendahl, M. *J. Am. Chem. Soc.* **1997**, *119*, 1751-1757.
(139) Ahlberg, P.; Davidson, Ö.; Hilmersson, G.; Löwendahl, M.; Håkansson, M. *Chem. Commun.* **1994**, 1573-1574.
(140) Utri, G.; Schwarzhans, K.-E.; Allmaier, G. M. *Z. Naturforsch., B: Chem. Sci.* **1990**, *45*, 755-762.
(141) Mueller-Westerhoff, U. T.; Nazzal, A.; Tanner, M. *J. Organomet. Chem.* **1982**, *236*, C41-C44.

(142) Mueller-Westerhoff, U. T.; Rheingold, A. L.; Swiegers, G. F. *Angew. Chem., Int. Ed. Engl.* **1992**, *31*, 1352-1354.
(143) Izumi, T.; Asakura, K.; Kasahara, A. *Bull. Yamagata Univ.(Eng.)* **1988**, *20*, 95-100.
(144) Sato, M.; Suzuki, M.; Okoshi, M.; Kurasina, M.; Watanabe, M. *J. Organomet. Chem.* **2002**, *648*, 72-80.
(145) Herberhold, M.; Baertl, T. *Z. Naturforsch., B: Chem. Sci.* **1995**, *50*, 1692-1698.
(146) Watanabe, M.; Sano, H. *Hyperfine Interact.* **1990**, *53*, 425-430.
(147) Watanabe, M.; Motoyama, I.; Takayama, T.; Shimoi, M.; Sano, H. *J. Organomet. Chem.* **1995**, *496*, 87-92.
(148) Watanabe, M.; Motoyama, I.; Sano, H. *J. Organomet. Chem.* **1996**, *510*, 243-253.
(149) Watanabe, M.; Sano, H. *Chem. Lett.* **1988**, *17*, 1457-1460.
(150) Watanabe, M.; Sato, M.; Nagasawa, A.; Motoyama, I.; Takayama, T. *Bull. Chem. Soc. Jpn.* **1998**, *71*, 2127-2136.
(151) Seyferth, D.; Withers, H. P. *J. Organomet. Chem.* **1980**, *185*, C1-C5.
(152) Ieong, N. S.; Chan, W. Y.; Lough, A. J.; Haddow, M. F.; Manners, I. *Chem.—Eur. J.* **2008**, *14*, 1253-1263.
(153) Diaz, A. F.; Mueller-Westerhoff, U. T.; Nazzal, A.; Tanner, M. *J. Organomet. Chem.* **1982**, *236*, C45-C48.
(154) Chen, J.; Too, C. O.; Wallace, G. G.; Swiegers, G. F. *Electrochim. Acta* **2004**, *49*, 691-702.
(155) Rulkens, R.; Lough, A. J.; Manners, I.; Lovelace, S. R.; Grant, C.; Geiger, W. E. *J. Am. Chem. Soc.* **1996**, *118*, 12683-12695.
(156) Stanga, O.; Lund, C. L.; Liang, H.; Quail, J. W.; Müller, J. *Organometallics* **2005**, *24*, 6120-6125.
(157) Schachner, J. A.; Lund, C. L.; Quail, J. W.; Müller, J. *Organometallics* **2005**, *24*, 4483-4488.
(158) Wehmschulte, R. J.; Power, P. P. *Inorg. Chem.* **1996**, *35*, 3262-3267.
(159) Mole, T. *Aust. J. Chem.* **1963**, *16*, 794-800.
(160) Müller, J.; Englert, U. *Chem. Ber.* **1995**, *128*, 493-497.
(161) Müller, J.; Scröder, R.; Wang, R. *Eur. J. Inorg. Chem.* **2000**, 153-157.
(162) Eaborn, C.; Smith, J. D. *J. Chem. Soc., Dalton Trans.* **2001**, 1541-1552.

CHAPTER 2
PUBLICATION 1

Description

The following chapter is a verbatim copy of an article which was published in *Organometallics*[*] in November 2005[†] and describes the synthesis and structural characterization of neutral and cationic aluminum compounds equipped with the Pytsi ligand [Pytsi = $-C(SiMe_3)_2SiMe_2(2\text{-}C_6H_4N)$]. The compounds $(Pytsi)AlMe_2$ (**1**), $(Pytsi)AlEt_2$ (**2**), $[(Pytsi)AlMe]^+[MeB(C_6F_5)_3]^-$ (**3**), and $[(Pytsi)AlMe(thf)]^+[MeB(C_6F_5)_3]^-$ (**3**·thf) have been synthesized and characterized by standard methods, and the molecular structures of **1**, **2**, and **3** have been determined by single-crystal X-ray analysis.

Author Contributions

My contribution to this publication was the synthesis and characterization of $(Pytsi)AlMe_2$ (**1**). The coauthors on this paper are Olimpiu Stanga, who synthesized and characterized the aluminum diethyl compound $(Pytsi)AlEt_2$ (**2**) and the cationic aluminum compounds $[(Pytsi)AlMe]^+[MeB(C_6F_5)_3]^-$ (**3**) and $[(Pytsi)AlMe(thf)]^+[MeB(C_6F_5)_3]^-$ (**3**·thf), Huan Liang, who repeated the synthesis of **3** and characterized it by VT-NMR spectroscopy, J. Wilson Quail, who performed all single-crystal X-ray analyses, and my supervisor Jens Müller.

[*] Reproduced with permission from Organometallics. © 2005 American Chemical Society
[†] Stanga, O.; Lund, C. L.; Liang, H.; Quail, J. W.; Müller, J. *Organometallics* **2005**, *24*, 6120-6125.

Written permission was obtained from all contributing authors to include material within this thesis.

Relation of Publication 1 to the Objectives of this Project

As mentioned in the introduction, the first objective of this Ph.D. project was to synthesize [1]metallarenophanes bridged by heavier group-13 elements (Chapter 1.6). To achieve this goal, I proposed to prepare compounds of the type REX_2, where R is a *trisyl*-based species, to be used in salt-metathesis reactions with dilithiobis(benzene) compounds. In particular, the known Pytsi ligand was targeted,[‡] which combines the bulkiness of the *trisyl* ligand with a pyridyl donor. As a stepping stone towards the primary objective, I first prepared the dimethyl alane **1**, instead of the targeted dihalogen species, because methyl groups attached to aluminum can be identified by ^{1}H NMR spectroscopy. These groups produce diagnostic peaks for determining indirectly whether a compound contains aluminum or not. A second motivation for preparing **1**, independent from the targeted [1]metallarenophanes, is the fact that methyl aluminum species can be used to prepare aluminum cations. In fact, compound **1** was utilized by my colleague Olimpiu Stanga to prepare the aluminum cations **3** and **3**·thf by using the well-known methyl abstraction agent, $B(C_6F_5)_3$.

Even though **1** could not be used directly to synthesize [1]metallarenophanes, its isolation provided a foundation to begin preparing aluminum and gallium dihalides equipped with the Pytsi ligand which are described later in this Ph.D. thesis.

[‡] Al-Juaid, S. S.; Eaborn, C.; Hitchcock, P. B.; Hill, M. S.; Smith, J. D. *Organometallics* **2000**, *19*, 3224-3231.

2. Synthesis and Characterization of Neutral and Cationic Intramolecularly Coordinated Aluminum Compounds. Structural Determination of $[(Pytsi)AlMe]^+[MeB(C_6F_5)_3]^-$ (Pytsi = $C(SiMe_3)_2SiMe_2(2\text{-}C_5H_4N)$)

Olimpiu Stanga,[‡§] Clinton L. Lund,[‡] Huan Liang,[‡] J. Wilson Quail,[§] Jens Müller[‡*]

[‡]*Department of Chemistry, University of Saskatchewan, 110 Science Place, Saskatoon, Saskatchewan, Canada, S7N 5C9,* [§]current address: *Akzo Nobel Polymer Chemicals bv, Stationsstraat 77, 3811 MH Amersfoort, The Netherlands,* [§]*Saskatchewan Structural Sciences Centre, University of Saskatchewan, 110 Science Place, Saskatoon, Saskatchewan, Canada, S7N 5C9*

Received May 27, 2005

2.1 Abstract

The synthesis and structure of neutral and cationic aluminum compounds equipped with the intramolecular donating $C(SiMe_3)_2SiMe_2(2\text{-}C_5H_4N)$ ligand denoted by Pytsi is described. The compounds $(Pytsi)AlMe_2$ (**1**), $(Pytsi)AlEt_2$ (**2**), $[(Pytsi)AlMe]^+[MeB(C_6F_5)_3]^-$ (**3**), and $[(Pytsi)AlMe(thf)]^+[MeB(C_6F_5)_3]^-$ (**3** · thf) have been synthesized and characterized by standard methods and the molecular structures of **1**, **2**, and **3** have been determined by single-crystal X-ray analyses. Compound **3** was obtained by an addition of one equivalent of $B(C_6F_5)_3$ to the dimethyl species **1**. The salt-like title compound **3** shows a methyl group in a bridging position between Al and B atoms consisting of a long Al–C distance of 2.380(2) Å and a B–C bond length of 1.681(3) Å.

2.2 Introduction

Cationic aluminum species with coordination numbers from 2 to 7 are known.[1] Those with low-coordinated Al centres are strong Lewis acids and are potentially useful as transition-metal-free olefin polymerization catalysts or initiators. Bochmann *et al.* reported in 1996 that the aluminocenium cation in $[Cp_2Al]^+[MeB(C_6F_5)_3]^-$ initiates polymerization of isobutene and isobutene-isoprene mixtures.[2] Three years earlier, the decamethyl derivative $Cp^*_2Al^+$ was already characterized by Schnöckel *et al*.[3] From a formal viewpoint, aluminum in the aluminocenium cation is 2-fold coordinated, however, because of the pentahapto coordinated Cp rings the coordination number in $[Cp_2Al]^+$ is not well defined. Reed *et al.* reported the synthesis of $[Et_2Al]^+[CB_{11}H_6X_6]^-$ (X = Cl, Br).[4] On the basis of the X-ray structural analyses, the Et_2Al^+ moiety is weakly coordinated to two halogen atoms of the carborane unit with C–Al–C angles of 130º (X = Br) and 137º (X = Cl). The salt-like species $[Et_2Al]^+[CB_{11}H_6X_6]^-$ has been shown to be an extremely efficient catalyst for polymerization of cyclohexene oxide.[4] Recently, a quasi-two-coordinated diorganoaluminum cation had been described by Wehmschulte *et al.*[5] The Al atom in $[(2,6\text{-}Mes_2C_6H_3)_2Al]^+[B(C_6F_5)_4]^-$ is shielded by very bulky m-terphenyl substituents with C–Al–C angles of 159º and 157º found in two different polymorphs. Jordan *et al*. reported in 1997 that three- and four-coordinated aluminum cations equipped with N,N′-dialkylamidinate ligands $RC(NR')_2^-$ can be used for ethylene polymerization under mild conditions.[6] Comparable monoanionic N,N-bidentate ligands,[7–19] O,N-bidentate ligands,[20–25] and C,N-bidentate ligands,[26] had been used to stabilize cationic Al centres with low coordination numbers.

Eaborn and Smith and others have shown that the sterically demanding *trisyl* ligand (*trisyl* = tris(trimethylsilyl)methyl, $C(SiMe_3)_3$; commonly denoted as Tsi) can be used to stabilize compounds with unusual low coordination numbers.[27] In addition to the bulkiness of the *trisyl*

ligand, β-silyl effects contribute to a stabilization of an attached metal centre. Several *trisyl* derivatives in which one or more methyl groups are replaced by substituents with Lewis-base donor capabilities are known, among which the pytrisyl ligand, $C(SiMe_3)_2SiMe_2(2\text{-}C_5H_4N)$, is the most studied example.[28–33] Recently, we took advantage of the unique properties of the bulky and intramolecularly stabilizing pytrisyl ligand and synthesized the [1]ferrocenophanes with aluminum[34] and gallium[35] in bridging positions.

Within this report we describe the synthesis and structural characterization of neutral and cationic pytrisyl alanes.

2.3 Results and Discussion

The dimethyl alane **1** is readily accessible by metathesis starting with the known Li(thf)(Pytsi)[28] and chlorodimethylalane (equation 2-1).

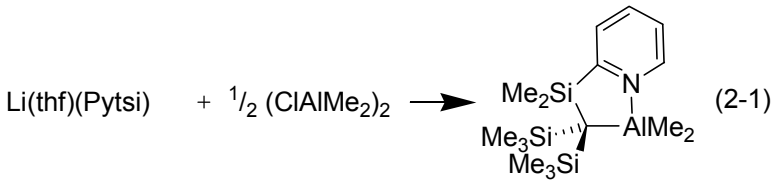

1

Compound **1** had been described in a very recent publication by Hill and Smith.[33] The authors mentioned a disorder of **1** in the crystal lattice; however, the molecular structure of **1** was not described. We also found disordered molecules **1** in the crystal lattice, but could successfully model it. The structure of compound **1** is disordered about a plane of symmetry, bisecting the ring along the Si_2C plane in the $(Me_3Si)_2C$ moiety. One half of the molecule reflects almost on top of the other half of molecule. Both halves of the compound **1**, one with a $SiMe_2$ group and the other with a Me_2Al group, have similar shapes and sizes, and a disorder as found for **1** is not

unexpected. The diethyl alane **2**, which we synthesized similarly to compound **1**, does not exhibit two similar shaped molecular halves and, consequently, is not disordered in the crystal lattice (Figure 2-1, Table 2-1). In order to model the disorder in **1**, we used the structure of compound **2**. The terminal methyl groups on the two ethyl groups were replaced by H atoms, giving the same formula as **1**. A rigid model of the so modified molecule **2**, with occupancies set at 0.50 was used to refine into the data for compound **1** resulting in an R value of 7.9% with all atoms isotropic.

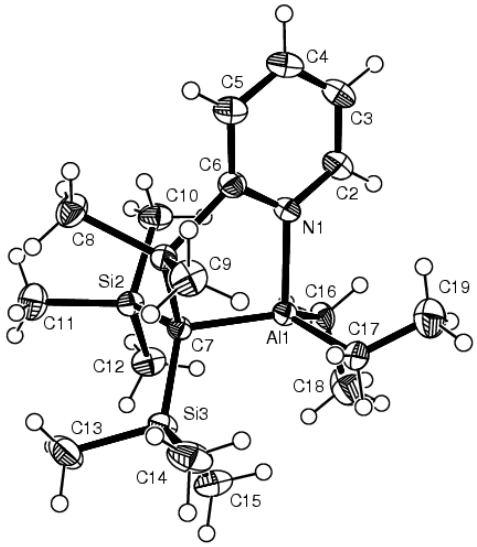

Figure 2-1. Molecular structure of $(Pytsi)AlEt_2$ (**2**) with thermal ellipsoids drawn at a 50% probability level. Selected bond lengths [Å] and angles [°]: Al1–N1 = 2.0034(18), Al1–C16 = 2.017(2), Al1–C17 = 1.994(2), Al1–C7 = 2.043(2), C7–Si1 = 1.865(2), C7–Si2 = 1.889(2), C7–Si3 = 1.884(2), N1–Al1–C7 = 96.02(8), N1–Al1–C16 = 103.66(9), N1–Al1–C17 = 102.73(9), C16–Al1–C7 = 123.29(10), C17–Al1–C7 = 116.10(10), C17–Al1–C16 = 110.47(10), Al1–C7–Si1 = 100.15(10), C7–Si1–C6 = 103.11(9), Si1–C6–N1 = 114.61(15), C6–N1–Al1 = 114.84(14).

Table 2-1. Crystal and structural refinement data for compounds (Pytsi)$AlMe_2$ (**1**), (Pytsi)$AlEt_2$ (**2**), and $[(Pytsi)AlMe]^+[MeB(C_6F_5)_3]^-$ (**3**).

cryst params	**1**	**2**	**3**·0.5 toluene
empirical formula	$C_{16}H_{34}AlNSi_3$	$C_{18}H_{38}AlNSi_3$	$C_{37.50}H_{38}AlBF_{15}NSi_3$
formula weight	351.69	379.74	909.75
wavelength, Å	0.71073	0.71073	0.71073
crystal system	orthorhombic	triclinic	monoclinic
space group (No.)	*Pnma* (62)	$P\bar{1}$ (2)	*C*2/*c* (15)
Z	4	2	8
a, Å	12.7464(4)	8.8068(2)	21.4717(3)
b, Å	14.1803(4)	8.9623(2)	16.2706(2)
c, Å	12.1479(3)	17.2181(4)	25.7972(4)
α, deg	90	85.4238(8)	90
β, deg	90	75.5482(9)	113.1518(7)
γ, deg	90	62.6172(8)	90
vol, $Å^3$	2195.71(11)	1167.59(5)	8286.6(2)
d (calc), mg/m^3	1.064	1.080	1.458
temp, K	173(2)	173(2)	173(2)
abs coefficient, mm^{-1}	0.252	0.241	0.233
theta range, deg	3.20 – 22.0	3.17 – 27.48	3.34 – 26.37
refl collected	2557	10231	13405
indep refl	1418	5339 [R(int) = 0.0458]	8451 [R(int) = 0.0329]
abs correction	none	none	none
ref method		full-matrix least-squares on F^2	
data / restr / params	1418 / 0 / 38	5339 / 0 / 218	8451 / 57 / 563
goodness-of-fit on F^2	1.260	1.024	1.046
final R indices [I>2sigma(I)]	R1 = 0.0790, wR2 = 0.2044	R1 = 0.0472, wR2 = 0.1044	R1 = 0.0453, wR2 = 0.1043
R indices (all data)	R1 = 0.1105, wR2 = 0.2890	R1 = 0.0773, wR2 = 0.1173	R1 = 0.0704, wR2 = 0.1170
largest diff. peak and hole, $e.Å^{-3}$	0.702 and –0.946	0.389 and –0.302	0.474 and –0.409

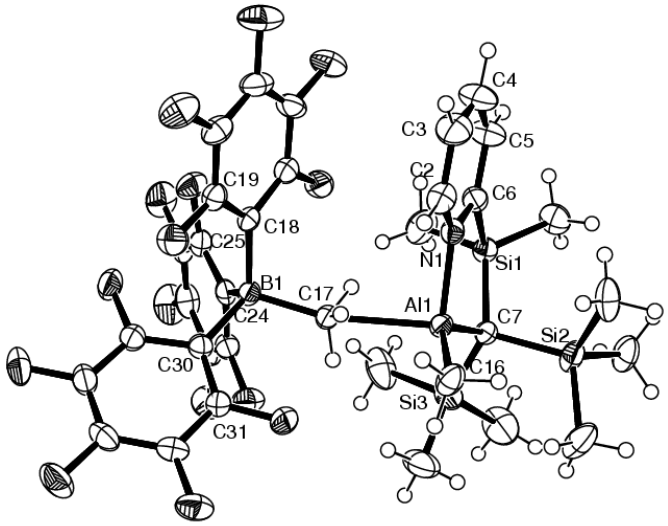

Figure 2-2. Molecular structure of $[(Pytsi)AlMe]^+[MeB(C_6F_5)_3]^-$ (**3**) with thermal ellipsoids drawn at a 50% probability level. Solvent molecules are omitted for clarity. Selected bond lengths [Å] and angles [°]: Al1–N1 = 1.9485(18), Al1–C16 = 1.943(3), Al1–C17 = 2.380(2), Al1–C7 = 1.975(2), C7–Si1 = 1.875(2), C7–Si2 = 1.912(2), C7–Si3 = 1.893(2), B1–C17 = 1.681(3), N1–Al1–C7 = 100.58(9), N1–Al1–C16 = 111.49(10), N1–Al1–C17 = 93.91(8), C16–Al1–C7 = 129.77(10), C17–Al1–C7 = 112.38(10), C17–Al1–C16 = 103.11(10), Al1–C7–Si1 = 101.83(10), C7–Si1–C6 = 102.42(10), Si1–C6–N1 = 115.93(15), C6–N1–Al1 = 113.66(15).

One methyl substituent of **1** can be abstracted by the perfluorinated borane $B(C_6F_5)_3$ resulting in the salt-like compound $[(Pytsi)AlMe]^+[MeB(C_6F_5)_3]^-$ (**3**). Compound **3** crystallizes in the monoclinic space group *C*2/*c* with half a molecule of toluene in the asymmetric unit (Figure 2-2, Table 2-1). The most interesting part of the molecular structure of **3** is displayed by the Me group bridging the Al and B atoms. The positions of the hydrogen atoms of the bridging Me group were located in ΔF maps and refined. The nearly linear bridge [Al1–C17–B1 = 163.76(17)°] consists of a long Al1–C17 distance of 2.380(2) Å and a B1–C17 bond length of 1.681(3) Å. To the best of our knowledge, structures of salt-like compounds with a cationic Al centre and methyl group bridging to a $B(C_6F_5)_3$ moiety are not described in the literature. However, the structural motif $L_nM\text{---}H_3C\text{–}B(C_6F_5)_3$ is known for transition metal species such as Ti,[36–38] Zr,[39–44] and Hf[45] compounds. A textbook example is $[Cp_2ZrMe]^+[MeB(C_6F_5)_3]^-$ with an

Zr–μMe distance being 0.30 Å longer than the Zr–Me_{term} distance of 2.251(3) Å; the B–Me bond length is 1.667(3) Å.[42] In comparison, the Al1–C17 distance of 2.380(2) Å in **3** is 0.44 Å longer than that of the Al–Me_{term} bond [Al1–C16 = 1.943(3) Å]. This is a significant difference and the Al1–C17 distance is far too long to be a covalent bond. Aluminum is 3-fold coordinated by the bidentate pytrisyl ligand and the remaining Me group plus weakly coordinated by the bridging Me group. This intermediate coordination is also reflected in the sum (342°) over the three angles between the C7, N1, and C16 and the central Al atom. This value is in between the sum over the three corresponding angles in compound **2** with four-fold coordination (323°) and the sum over three angles in an idealized trigonal planar arrangement (360°).

We intended to characterize compound **3** in solution by NMR spectroscopy. The reaction batch that we used to obtain single crystals showed the typical pattern of a pytrisyl ligand exhibiting a mirror plane on time average in the ^{1}H NMR spectrum. Unfortunately, we could not measure a proton NMR spectrum of **3** free of byproducts. However, if in an NMR tube containing a 1:1 mixture of the solid starting materials **1** and $B(C_6F_5)_3$, cooled to –78 °C, is dissolved in pre-cooled toluene-d_8 (–78 °C), low-temperature ^{1}H, ^{11}B, ^{19}F, and ^{13}C NMR spectra of compound **3**, nearly free of byproducts can be obtained (see Experimental Section and Supporting Information). For example, the ^{1}H NMR spectra show one singlet for each of the AlMe, $SiMe_2$, $C(SiMe_3)_2$, and BMe moieties, and four singlets for the pyridyl group. The chemical shift of the Me group of the anion is temperature dependent. It changes from δ 1.47 at –78 °C to δ 1.35 at –18 °C and is broadened at higher temperatures before it disappears in the baseline at 12 °C. For the AlMe group, only insignificant changes of the chemical shift can be observed in the range of –78 to –18 °C, but at higher temperatures, it behaves similar to the BMe group and is also hidden in the baseline at 12 °C. At temperatures above –8 °C new ^{1}H NMR

peaks appeared and prolonged exposure of the flame-sealed NMR tube to ambient temperatures resulted in ^{1}H NMR spectra with numerous signals; we could neither identify a byproduct nor could we isolate one. This temperature sensitivity prevented a complete uncovering of the dynamic behaviour of **3** in solution. Similar dynamic behaviour had been observed for other salt-like species, e.g. $[\{HC(CMeNAr)_2\}AlMe][MeB(C_6F_5)_3]$[11] and it was proposed that an exchange of the Me groups occur in solution as illustrated in equation 2-2. We assume that such equilibrium also exists for compound **3**.

$$LAlMe_2 + B(C_5F_6)_3 \rightleftharpoons [LAlMe]^+ + [MeB(C_5F_6)_3]^- \quad (2\text{-}2)$$

L = chelating ligand

The chemical shift of the Me group of $[MeB(C_6F_5)_3]^-$ for **3** is significantly downfield from those of salts of the type $A[MeB(C_6F_5)_3]$ with A^+ being an "innocent" cation. Jordan *et al*. chose $[NBu_3Bz][MeB(C_6F_5)_3]$ (δ 1.09; toluene-d_8)[11] as a reference compound. We found a chemical shift of δ 0.99 (toluene-d_8) for the thf adduct of compound **3**, $[(Pytsi)AlMe(thf)][MeB(C_6F_5)_3]$, which is discussed below. The downfield shift is indicative of ion-pairing in solution and shows that compound **3**, dissolved in toluene, exhibits a molecular structure with an Al–Me–B moiety, similar as that found in the crystal lattice.

If the synthesis of compound **3** is performed in the presence of 1 equivalent of thf, a new compound $[(Pytsi)AlMe(thf)][MeB(C_6F_5)_3]$ (**3**·thf) is formed. The ^{1}H NMR spectrum reveals an asymmetric pytrisyl ligand: two singlets for the $C(SiMe_3)_2$ moiety and two singlets for the $SiMe_2$ group. These NMR data are consistent with the formation of the expected cation shown in chart 2-1a.

Chart 2-1. a) Cation of [(Pytsi)AlMe(thf)]$^+$[MeB(C_6F_5)$_3$]$^-$ (**3**·thf) b) NMR time-averaged molecular symmetry of the cation of [(Pytsi)AlMe(thf)]$^+$[MeB(C_6F_5)$_3$]$^-$ (**3**·thf).

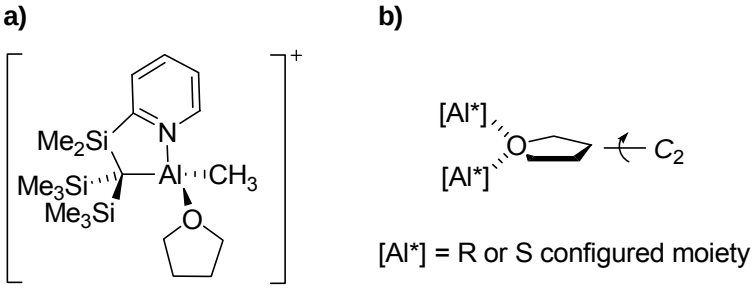

The cation of the salt **3**·thf exhibits C_1 point group symmetry. Therefore, all H and C atoms of the coordinated thf molecule are nonequivalent and, in principle, should give one resonance each. The coordinated thf moiety, however, shows only two ^{13}C NMR peaks at δ 24.75 and 74.69 and three multiplets in the ^{1}H NMR spectrum at δ 1.35 (4H), 3.08 (2H), and 3.34 (2H). This result can be interpreted as being due to the well-known inversion of the envelope conformation of thf, resulting in a time-averaged C_2 symmetry of the cation (Chart 2-1b).

The NMR data show that the thf molecule does not dissociate and re-associate rapidly on the NMR time scale; a process like this would be accompanied by an inversion at the Al atom. However, if two equivalents of thf-d_8 are added to a NMR sample of **3**·thf in toluene-d_8, two new multiplets appear, unequivocally indicating non-coordinated thf. In addition, the relative intensity of the sets of signals of coordinated thf decreased respectively, revealing that added thf-d_8 replaces coordinated thf in **3**·thf. At ambient temperature the free thf resonates at δ 1.48 and 3.48, which is down-field with respect to those of the coordinated thf at δ 1.35 (4H), 3.08 (2H), and 3.34 (2H). By increasing the temperature the chemical shifts of the coordinated thf move closer to those of the non-coordinated thf, so that at 100 °C (500 MHz) the signals at higher field

coalesced to one signal at δ 1.53 ($C\underline{H_2}CH_2O$) and that at lower field still appeared as two but broad signals (δ 3.54 and 3.34). Coalescence phenomena can be observed for the two sets of singlets for the diastereotopic methyl group in $SiMe_2$ and $C(SiMe_3)_2$, respectively, which broaden with increasing temperature, and at 100 °C only two very broad singlets are present. These NMR results show that a fast exchange of the coordinated thf and non-coordinated thf occurs resulting in an inversion of the Al atom.

2.4 Conclusions

We have shown that one methyl group of the dimethylalane **1** can be abstracted by the perfluorinated borane $B(C_6F_5)_3$ resulting in the salt-like compound $[(Pytsi)AlMe]^+[MeB(C_6F_5)_3]^-$ (**3**). The molecular structure of **3** in the solid state shows a methyl group in a bridging position between aluminum and boron with a long Al–C distance of 2.380(2) Å. Compound **3** is not stable in solution at ambient temperature, however, a stable thf adduct can be obtained. These initial results show that the pytrisyl ligand is capable of stabilizing an aluminum cation with a low coordination number. We started to change compound **3** systematically by using different weakly coordinating anions, by exchanging the remaining methyl group at aluminum by a sterically more demanding group, and by increasing the steric bulk of the pytrisyl ligand by introducing sterically demanding groups in position 6 of the pyridine ring. By fine tuning compound **3**, we hope to control the reactivity of cationic pytrisyl alanes and make use of them in catalytic processes like olefin polymerization.

2.5 Experimental Section

General Procedures. All manipulations were carried out using standard Schlenk techniques. Solvents were dried using a MBraun Solvent Purification System and stored under nitrogen over 4 Å molecular sieves. All solvents for NMR spectroscopy were degassed prior to use and stored under nitrogen over 4 Å molecular sieves. Li(thf)(Pytsi)[28] [Pytsi = $C(SiMe_3)_2SiMe_2(2\text{-}C_5H_4N)$] and $B(C_6F_5)_3$[46] were synthesized as described in the literature. Me_2AlCl and Et_2AlCl were purchased from Aldrich and used as received. ^1H, ^{13}C, ^{11}B, ^{27}Al, and ^{19}F NMR spectra were recorded on a Bruker 500 MHz Avance. ^1H (500 MHz) and ^{13}C (125.8 MHz) chemical shifts were referenced to the residual protons of the deuterated solvents. In the case of toluene-d_8, the peak of the Me group of was used as a reference (^1H NMR: δ 2.09; ^{13}C NMR δ 20.40). Other nuclei were referenced to an external standards dissolved in C_6D_6: ^{27}Al NMR (130.3 MHz; $[Al(acac)_3]$), ^{11}B NMR (165.5 MHz, $BF_3\text{-}OEt_2$), ^{19}F NMR (470.5 MHz, $CFCl_3$). Samples were dissolved in C_6D_6 and NMR spectra were obtained at ambient temperature unless noted differently. We could not detect the ^{13}C NMR signal of the pytrisyl C atom directly bound to Al for compound **1**, **2**, and **4**. Mass spectra were measured on a VG 70SE and signals of the most abundant ions are listed. Elemental analyses were performed on a Perkin Elmer 2400 CHN Elemental Analyzer using V_2O_5 to promote complete combustion.

$(Pytsi)AlMe_2$ (**1**). A solution of Me_2AlCl (4.9 mL, 1 M in hexanes) was added dropwise to a stirred solution of Li(thf)(Pytsi) (1.828 g, 4.9 mmol) in hexane (20 mL) at –78 °C. The resulting solution was stirred for 20 min at –78 °C, and then allowed to warm to ambient temperature. After the reaction mixture was stirred for 16 h, the solid was filtered off and washed with hexane (3 x 5 mL). Removal of the solvent left a light yellow solid that was sublimed at 90 ºC and high vacuum to give the colorless crude product. Crystallization from hexane (10 mL) at

–30 °C resulted in colorless crystals, suitable for single-crystal X-ray structural determination (1.184 g, 69%). Compound **1** was first described in reference 33. Our spectroscopic data were identical to those given earlier but we consider that amendments are required to assignments of ^1H and ^{13}C resonances from the pyridine moiety. Our assignments were confirmed by ^1H-^1H COSY and HMQC experiments. ^1H NMR: δ –0.21 (s, 6H, $AlMe_2$), 0.27 (s, 18H, $SiMe_3$), 0.40 (s, 6H, $SiMe_2$), 6.34 (pst, 1H, 5-H), 6.79 (pst, 1H, 4-H), 6.92 (d, 1H, 3-H), 7.93 (d, 1H, 6-H). $^{13}C\{^1H\}$ NMR: δ –3.16 (br, $AlMe_2$), 4.35 ($SiMe_2$), 6.57 ($SiMe_3$), 124.39 (5-C), 129.22 (3-C), 138.37 (4-C), 145.88 (6-C), 174.05 (*ipso*-C). ^{27}Al NMR: δ 176 ($w_{1/2}$ = 2850 Hz). MS: m/z 336 (100, $M–Me^+$), 264 (52, $C_{12}H_{22}NSi_3^+$), 248 (20, $C_{11}H_{18}NSi_3^+$). Anal. calcd for $C_{16}H_{34}NAlSi_3$ (351.691): C, 54.64; H, 9.74; N, 3.98. Found: C, 54.67; H, 10.11; N, 3.75.

(Pytsi)$AlEt_2$ (**2**). Li(thf)(Pytsi) (3.206 g, 8.6 mmol) was dissolved in hexane (40 mL) at ambient temperature and cooled with an acetone-dry ice bath. Et_2AlCl (8.6 mL, 1M in hexane) was added over a period of 10 min using a syringe and a septum, and the resulting solution was stirred for another 20 min, before the dry ice bath was removed. The reaction mixture was stirred overnight at ambient temperature. The solution was filtered and the solid was washed with hexane (3 x 10 mL). After the solvent was removed from the filtrate in high vacuum, pale-yellow crystals were obtained by sublimation at 140 ºC in high vacuum. The sublimed compound was dissolved in hexane (25 mL) and crystallization at ca. –20 °C resulted in colorless compound **2** (2.281 g, 70%). ^1H NMR: δ 0.26 (s, 18H, $SiMe_3$), 0.31 (d/q, 2H, $^2J_{HH}$ = 14.3 Hz, $^3J_{HH}$ = 8.1 Hz, $AlCH_2$), 0.39 (s, 6H, $SiMe_2$), 0.50 (d/q, 2H, $^2J_{HH}$ = 14.3 Hz, $^3J_{HH}$ = 8.1 Hz, $AlCH_2$), 1.37 (d/d, 6H, $^3J_{HH}$ = 8.1 Hz, $AlCH_2C\underline{H}_3$), 6.34 (pst, 1H, 5-H), 6.78 (pst, 1H, 4-H), 6.92 (d, 1H, 3-H), 8.10 (d, 1H, 6-H). $^{13}C\{^1H\}$ NMR: δ 4.09 ($SiMe_2$), 4.19 (br, $AlCH_2$), 6.32 ($SiMe_3$), 10.49 ($AlCH_2\underline{C}H_3$), 123.61 (5-C), 129.15 (3-C), 138.09 (4-C), 146.09 (6-C), 173.83 (*ipso*-C). ^{27}Al

NMR: δ 173 ($w_{1/2}$ = 2400 Hz). MS (70 eV) m/z (%) 364 (7, M–Me^+), 350 (100, M–$C_2H_5^+$), 295 (12 $PytsiH^+$), 280 (36, $C_{13}H_{26}NSi_3^+$), 264 (18, $C_{12}H_{22}NSi_3^+$), 248 (8, $C_{11}H_{18}NSi_3^+$). Anal. calcd for $C_{18}H_{38}AlNSi_3$ (379.745): C, 56.93; H, 10.09; N, 3.69. Found: C, 56.37; H, 9.47; N, 3.12.

(Pytsi)$AlMe^+$[$MeB(C_6F_5)_3$]$^-$ (**3**). A NMR tube, charged with **1** (0.0176 g, 0.0500 mmol) and $B(C_6F_5)_3$ (0.0256g, 0.0500 mmol), was cooled to –78 °C, pre-cooled toluene-d_8 (1 mL, –78 °C) was added with a syringe, and the tube was carefully shaken in such a way that a significant increase of the temperature was avoided. The NMR tube containing a clear and colorless solution was inserted into a cooled NMR probe head (see Supporting Information for NMR spectra). ^{1}H NMR (225 K, toluene-d_8): δ –0.12 (s, 18H, $SiMe_3$), –0.09 (s, 3H, AlMe), 0.04 (s, 6H, $SiMe_2$), 1.40 (s, 3H, BMe), 6.40 (m, br, 1H, 4-H or 5-H), 6.51 (d, 1H, 3-H), 6.83 (m, 1H, 5-H or 4-H), 7.58 (d, 1H, 6-H). ^{13}C{^{1}H} NMR: δ –4.98 (AlMe), 1.16 (C($SiMe_3$)$_2$), 2.57 ($SiMe_2$), 4.63 ($SiMe_3$), 12.1 (br, BMe), 125.65 (4-C or 5-C), 130.46 (3-C), 136.94 (d/m, $^1J_{CF}$ = 241 Hz, m-C_6F_5), 141.36 (5-C or 4-C), 144.69 (6-C), 148.30 (d/m, $^1J_{CF}$ = 241 Hz, o-C_6F_5), 171.96 (*ipso*-C_5H_4N); peaks for *ipso*-C_6F_5 and p-C_6F_5 are hidden by the solvent signals. ^{11}B NMR: δ –14.80 (s). ^{19}F NMR: δ –133.55 (d, 6F, o-F), –159.95 (m, 3F, p-F), –164.34 (m, 6F, m-F); small amounts of $B(C_6F_5)_3$ were detected at δ –128.66 (d, 6F, o-F), –140.43 (m, 3F, p-F), –159.75 (m, 6F, m-F) (see reference 11).

Single crystals of **3** were obtained as follows (see Results and Discussion). $B(C_6F_5)_3$ (0.716 g dissolved in 10 mL of toluene, 1.4 mmol) was added via a cannula to a solution of **1** (0.492 g, 1.4 mmol) in toluene (10 mL), and the resulting reaction mixture was stirred for 1 h. The solvent was removed in high vacuum from the clear, colorless solution, resulting in a formation of a white wax. Trituration with hexane (2 x 20 mL) gave **3** as a white solid (0.938 g, 78%). Toluene (10 mL) was added and the flask was placed in the freezer (ca. –20 °C) resulting

in the formation of two liquid layers and some colorless crystals. The two liquid layers were syringed off and all remaining volatiles were removed in high vacuum. X-ray analysis of the crystals revealed the desired compound.

(Pytsi)AlMe(thf)$^+$[MeB(C_6F_5)$_3$]$^-$ (**3**·thf). B(C_6F_5)$_3$ (0.472 g dissolved in 10 mL of toluene, 0.921 mmol) was added via a cannula to a stirred solution of **1** (0.324 g, 0.921 mmol) and thf (0.08 mL, ~0.921 mmol) in toluene (10 mL). The reaction mixture was stirred for 30 min, resulting in the formation of two layers. All volatiles were removed in high vacuum. Trituration with hexane (2 x 20 mL) did not result in the formation of a solid, but gave a colorless sticky foam after the remaining solvent was removed in high vacuum (0.789 g, 92%). ^{1}H NMR (toluene-d_8): δ –0.50 (s, 3H, AlMe), –0.17 (s, 9H, $SiMe_3$), 0.00 (s, 9H, $SiMe_3$), 0.10 (s, 3H, SiMe), 0.29 (s, 3H, SiMe), 0.99 (s, 3H, BMe), 1.35 (m, 4H, C$H_2$$CH_2O$), 3.08 (m, 2H, CH_2O), 3.34 (m, 2H, CH_2O), 7.00 (pst, 1 H, 5-H), 7.24 (d, 1H, 3-H), 7.38 (pst, 1H, 4-H), 7.80 (d, 1H, 6-H). ^{13}C{^{1}H} NMR (toluene-d_8): δ –7.89 (AlMe), 2.04 (SiMe), 4.01 (SiMe), 5.15 ($SiMe_3$), 5.59 ($SiMe_3$), 11.3 (br, BMe), 24.75 (C$H_2$$CH_2O$), 74.69 ($CH_2O$), 126.53 (5-C), 130.1 (br, *ipso*-C_6F_5), 131.27 (3-C), 137.1 (d/m, $^1J_{CF}$ = 245 Hz, m-C_6F_5), 138.1 (d/m, $^1J_{CF}$ = 245 Hz, p-C_6F_5), 142.22 (4-C), 145.46 (6-C), 149.21 (d/m, $^1J_{CF}$ = 239 Hz, o-C_6F_5), 173.69 (*ipso*-C_5H_4N). ^{11}B NMR ($CDCl_3$): δ –15.1 (s, br). ^{19}F NMR ($CDCl_3$): δ –137.29 (d, 6 F, o-F), –168.90 (m, 3 F, p-F), –171.61 (m, 6 F, m-F).

X-ray structural analysis. For all three structures **1**, **2**, and **3**, data were collected at –100 °C on a Nonius Kappa CCD diffractometer, using the COLLECT program.[47] Cell refinement and data reductions used the programs DENZO and SCALEPACK.[48] SIR97[49] was used to solve the structure and SHELXL97[50] was used to refine the structure. Except for the bridge methyl protons in **3**, H atoms were placed in calculated positions with U_{iso} constrained to

be 1.2 times U_{eq} of the carrier atom for aromatic protons and 1.5 times U_{eq} of the carrier atoms for methyl and methylene hydrogen atoms.

Because of the disorder of compound **1**, the structure of compound **2** was used as a model for compound **1** (see Results and Discussion). A rigid model of the modified molecule **2**, with occupancies set at 0.50 was used to refine into the data for compound **1**. Since the reflected half of **1** has atoms very close to the other half of **1**, it was not possible to allow the positions to refine independently and it was also not possible to refine the atoms anisotropically, because strong correlations result in meaningless thermal ellipsoids. The crystal only diffracted to 22 degrees. Only 38 parameters (6 to define the position and orientation of the rigid molecule, temp. factor on 21 non-H atoms and rotation of the 10 methyl groups plus scale) were refined against 1418 reflections (1138 observed). For further information see supporting information.

ACKNOWLEDGMENT. The authors thank the Natural Sciences and Engineering Research Council of Canada (NSERC Discovery Grant, JM), the Department of Chemistry, and the University of Saskatchewan for their generous support. We thank the Canada Foundation for Innovation (CFI) and the government of Saskatchewan for funding of the X-ray and NMR facilities in the Saskatchewan Structural Sciences Centre (SSSC). We thank Keith Brown for his support to conduct NMR experiments.

SUPPORTING INFORMATION PARAGRAPH. Crystallographic data for **1**, **2**, and **3** in CIF file format. This material is available free of charge via the internet at http://pubs.acs.org.

2.6 References

(1) Atwood, D. A. *Coord. Chem. Rev.* **1998**, *176*, 407-430.
(2) Bochmann, M.; Dawson, D. M. *Angew. Chem., Int. Ed.* **1996**, *35*, 2226-2228.
(3) Dohmeier, C.; Schnöckel, H.; Robl, C.; Schneider, U.; Ahlrichs, R. *Angew. Chem., Int. Ed.* **1993**, *32*, 1655-1657.
(4) Kim, K. C.; Reed, C. A.; Long, G. S.; Sen, A. *J. Am. Chem. Soc.* **2002**, *124*, 7662-7663.
(5) Young, J. D.; Khan, M. A.; Wehmschulte, R. J. *Organometallics* **2004**, *23*, 1965 - 1967.
(6) Coles, M. P.; Jordan, R. F. *J. Am. Chem. Soc.* **1997**, *119*, 8125-8126.
(7) Ihara, E.; Young, V. G.; Jordan, R. F. *J. Am. Chem. Soc.* **1998**, *120*, 8277-8278.
(8) Cosledan, F.; Hitchcock, P. B.; Lappert, M. F. *Chem. Commun.* **1999**, 705-706.
(9) Korolev, A. V.; Guzei, I. A.; Jordan, R. F. *J. Am. Chem. Soc.* **1999**, *121*, 11605-11606.
(10) Ong, C. M.; McKarns, P.; Stephan, D. W. *Organometallics* **1999**, *18*, 4197-4204.
(11) Radzewich, C. E.; Guzei, I. A.; Jordan, R. F. *J. Am. Chem. Soc.* **1999**, *121*, 8673-8674.
(12) Dagorne, S.; Guzei, I. A.; Coles, M. P.; Jordan, R. F. *J. Am. Chem. Soc.* **2000**, *122*, 274-289.
(13) Korolev, A. V.; Ihara, E.; Guzei, I. A.; Young, V. G.; Jordan, R. F. *J. Am. Chem. Soc.* **2001**, *123*, 8291-8309.
(14) Pappalardo, D.; Tedesco, C.; Pellecchia, C. *Eur. J. Inorg. Chem.* **2002**, 621-628.
(15) Schmidt, J. A. R.; Arnold, J. *Organometallics* **2002**, *21*, 2306-2313.
(16) Baugh, L. S.; Sissano, J. A. *J. Polym. Sci., Part A: Polym. Chem.* **2002**, *40*, 1633-1651.
(17) Dagorne, S.; Bellemin-Laponnaz, S.; Welter, R. *Organometallics* **2004**, *23*, 3053-3061.
(18) Masuda, J. D.; Walsh, D. M.; Wei, P. R.; Stephan, D. W. *Organometallics* **2004**, *23*, 1819-1824.
(19) Welch, G. C.; Piers, W. E.; Parvez, M.; McDonald, R. *Organometallics* **2004**, *23*, 1811-1818.
(20) Cameron, P. A.; Gibson, V. C.; Redshaw, C.; Segal, J. A.; Bruce, M. D.; White, A. J. P.; Williams, D. J. *Chem. Commun.* **1999**, 1883-1884.
(21) Cameron, P. A.; Gibson, V. C.; Redshaw, C.; Segal, J. A.; Solan, G. A.; White, A. J. P.; Williams, D. J. *J. Chem. Soc., Dalton Trans.* **2001**, 1472-1476.
(22) Cameron, P. A.; Gibson, V. C.; Redshaw, C.; Segal, J. A.; White, A. J. P.; Williams, D. J. *J. Chem. Soc., Dalton Trans.* **2002**, 415-422.
(23) Dagorne, S.; Lavanant, L.; Welter, R.; Chassenieux, C.; Haquette, P.; Jaouen, G. *Organometallics* **2003**, *22*, 3732-3741.
(24) Dagorne, S.; Janowska, I.; Welter, R.; Zakrzewski, J.; Jaouen, G. *Organometallics* **2004**, *23*, 4706-4710.
(25) Pappalardo, D.; Mazzeo, M.; Montefusco, P.; Tedesco, C.; Pellecchia, C. *Eur. J. Inorg. Chem.* **2004**, 1292-1298.
(26) Engelhardt, L. M.; Kynast, U.; Raston, C. L.; White, A. H. *Angew. Chem., Int. Ed.* **1987**, *26*, 681-682.
(27) Eaborn, C.; Smith, J. D. *J. Chem. Soc., Dalton Trans.* **2001**, 1541-1552.
(28) Al-Juaid, S. S.; Eaborn, C.; Hitchcock, P. B.; Hill, M. S.; Smith, J. D. *Organometallics* **2000**, *19*, 3224-3231.
(29) Eaborn, C.; Hill, M. S.; Hitchcock, P. B.; Smith, J. D. *Chem. Commun.* **2000**, 691-692.
(30) Al-Juaid, S. S.; Avent, A. G.; Eaborn, C.; El-Hamruni, S. M.; Hawkes, S. A.; Hill, M. S.; Hopman, M.; Hitchcock, P. B.; Smith, J. D. *J. Organomet. Chem.* **2001**, *631*, 76-86.

(31) Al-Juaid, S. S.; Avent, A. G.; Eaborn, C.; Hill, M. S.; Hitchcock, P. B.; Patel, D. J.; Smith, J. D. *Organometallics* **2001**, *20*, 1223-1229.
(32) Eaborn, C.; Hill, M. S.; Hitchcock, P. B.; Smith, J. D. *J. Chem. Soc., Dalton Trans.* **2002**, 2467-2472.
(33) Howson, J.; Eaborn, C.; Hitchcock, P. B.; Hill, M. S.; Smith, D. J. *J. Organomet. Chem.* **2005**, *690*, 69-75.
(34) Schachner, J. A.; Lund, C. L.; Quail, J. W.; Müller, J. *Organometallics* **2005**, *24*, 785-787.
(35) Schachner, J. A.; Lund, C. L.; Quail, J. W.; Müller, J. *Organometallics* **2005**, *24*, 4483-4488.
(36) Guerin, F.; Stephan, D. W. *Angew. Chem., Int. Ed.* **2000**, *39*, 1298-1300.
(37) Guerin, F.; Stewart, J. C.; Beddie, C.; Stephan, D. W. *Organometallics* **2000**, *19*, 2994-3000.
(38) Shafir, A.; Arnold, J. *J. Am. Chem. Soc.* **2001**, *123*, 9212-9213.
(39) Yang, X. M.; Stern, C. L.; Marks, T. J. *J. Am. Chem. Soc.* **1994**, *116*, 10015-10031.
(40) Baumann, R.; Davis, W. M.; Schrock, R. R. *J. Am. Chem. Soc.* **1997**, *119*, 3830-3831.
(41) Bazan, G. C.; Cotter, W. D.; Komon, Z. J. A.; Lee, R. A.; Lachicotte, R. J. *J. Am. Chem. Soc.* **2000**, *122*, 1371-1380.
(42) Guzei, I. A.; Stockland, R. A.; Jordan, R. F. *Acta Crystallographica Section C-Crystal Structure Communications* **2000**, *56*, 635-636.
(43) Beck, S.; Lieber, S.; Schaper, F.; Geyer, A.; Brintzinger, H. H. *J. Am. Chem. Soc.* **2001**, *123*, 1483-1489.
(44) Choukroun, R.; Wolff, F.; Lorber, C.; Donnadieu, B. *Organometallics* **2003**, *22*, 2245-2248.
(45) Sadow, A. D.; Tilley, T. D. *J. Am. Chem. Soc.* **2003**, *125*, 9462-9475.
(46) Lancaster, S. *SyntheticPage* **2003**, 215.
(47) *COLLECT*; Nonius BV: Delft, The Netherlands, 1998.
(48) Otwinowski, Z.; Minor, W. In *Macromolecular Crystallography, Part A*; Carter, C. W., Sweet, R. M., Eds.; Academic Press: London, 1997; Vol. 276, pp 307-326.
(49) Altomare, A.; Burla, M. C.; Camalli, M.; Cascarano, G.; Giacovazzo, C.; Guagliardi, A.; Moliterni, A. G. G.; Polidori, G.; Spagna, R. *J. Appl. Crystallogr.* **1999**, *32*, 115-119.
(50) Sheldrick, G. M. *SHELXL97*; University of Göttingen: Germany, 1997.

2.7 Supporting Information

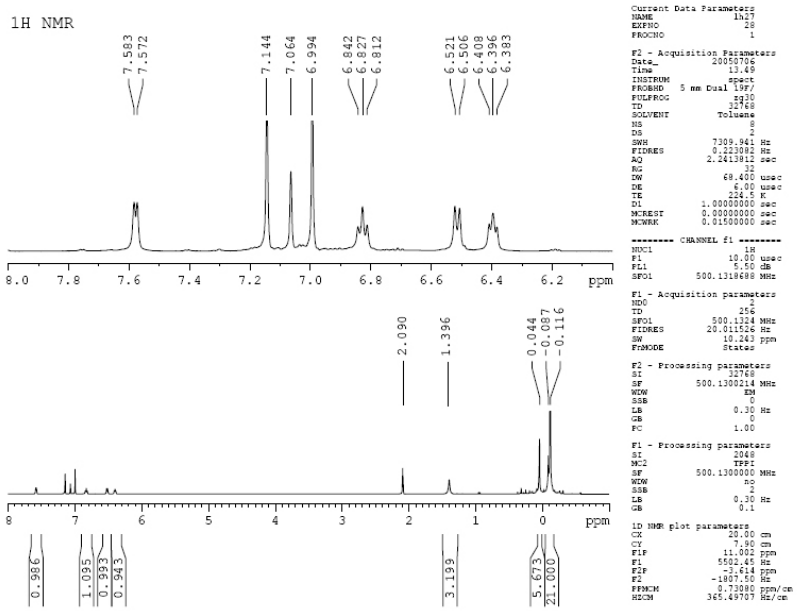

Figure 2-S1. ^{1}H NMR spectrum of $[(Pytsi)AlMe]^+[MeB(C_6F_5)_3]^-$ (**3**) in C_7D_8 at 225 K.

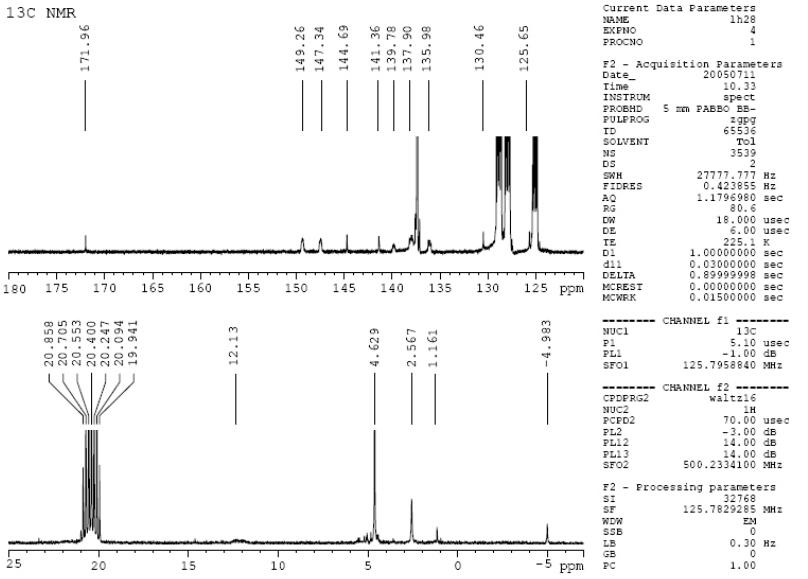

Figure 2-S2. ^{13}C NMR spectrum of $[(Pytsi)AlMe]^+[MeB(C_6F_5)_3]^-$ (**3**) in C_7D_8 at 225 K.

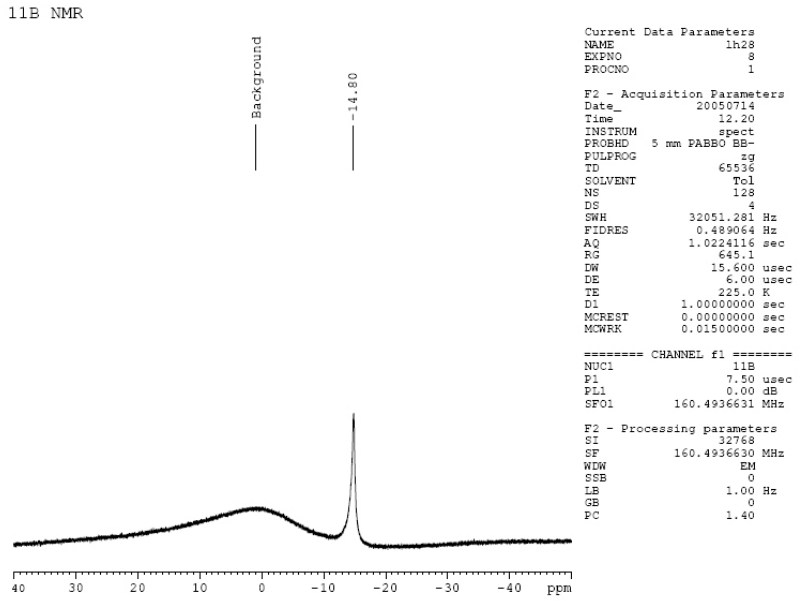

Figure 2-S3. ^{27}Al NMR spectrum of $[(Pytsi)AlMe]^+[MeB(C_6F_5)_3]^-$ (**3**) in C_7D_8 at 225 K.

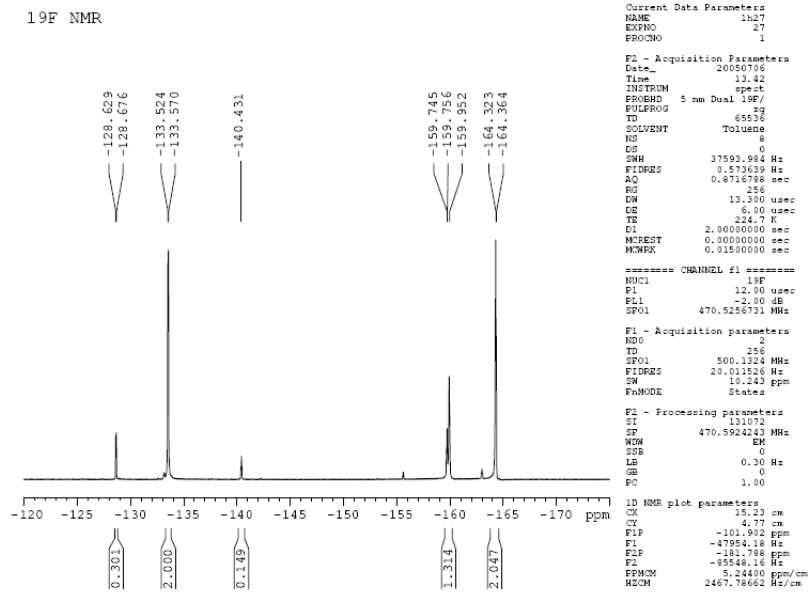

Figure 2-S4. ^{19}F NMR spectrum of $[(Pytsi)AlMe]^+[MeB(C_6F_5)_3]^-$ (**3**) in C_7D_8 at 225 K.

CHAPTER 3
PUBLICATION 2

Description

The following chapter is a verbatim copy of an article which was published in the *Canadian Journal of Chemistry*[*] in July 2007[†] and describes the synthesis of five new intramolecularly coordinated aluminum species. The two compounds (Pytsi)AlMeCl (**1**) and (Pytsi)Al*t*BuCl (**2**) make use of the underivatized Pytsi ligand. The other three compounds are derivatives of (Pytsi)$AlMe_2$ with additional groups in the ortho position of the pyridyl group: (6-MePysti)$AlMe_2$ (**3**), (6-PhPytsi)$AlMe_2$ (**4**) and (6-DippPytsi)$AlMe_2$ (**5**) (Dipp = 2,6-diisopropylphenyl).

Author Contributions

My contributions to this publication were the synthesis and characterization of compounds **1** and **3**–**5**. The coauthors on this paper are Olimpiu Stanga, who synthesized and characterized compound **2**, J. Wilson Quail, who performed all single-crystal X-ray analyses, and my supervisor Jens Müller. Written permission was obtained from all contributing authors to include material within this thesis.

[*] Reproduced with permission from the Canadian Journal of Chemistry. © 2007 NRC Canada
[†] Lund, C. L.; Stanga, O.; Quail, J. W.; Müller, J. *Can. J. Chem.* **2007**, *85*, 483-490.

Relation of Publication 2 to the Objectives of this Project

By building on the results from publication 1, novel compounds featuring aluminum methyl bonds were prepared. Specifically, this paper focused on making alterations to (Pytsi)$AlMe_2$, by introducing additional steric protection to the aluminum centre. To shield the Al centre more effectively, derivatives of (Pytsi)$AlMe_2$ in which the ortho position of the pyridine ring carries a Me (**3**), Ph (**4**) or Dipp group (**5**) were prepared. These derivatives could potentially be used to produce reactive cationic aluminum species through alkyl abstraction reactions like those described in Chapter 2.

It is also important to point out that all attempts to prepare dichloro species from the new Pytsi-type ligands directly or to convert the dimethyl species **3**, **4** and **5** to dichloro compounds using published procedures[‡] for similar $AlMe_2$ compounds were not successful.

[‡] Schnitter, C.; Klimek, K.; Roesky, H. W.; Albers, T.; Schmidt, H.; Röpken, C.; Parisini, E. *Organometallics* **1998**, *17*, 2249-2257.

3. Synthesis and Characterization of Intramolecularly Coordinated Alanes with New Sterically Demanding *Trisyl*-Based Ligands

Clinton L. Lund,[‡] Olimpiu Stanga,[‡§] J. Wilson Quail,[§] Jens Müller[‡*]

[‡]*Department of Chemistry, University of Saskatchewan, 110 Science Place, Saskatoon, Saskatchewan, Canada, S7N 5C9,* [§]current address: *Akzo Nobel Polymer Chemicals bv, Stationsstraat 77, 3811 MH Amersfoort, The Netherlands,* [§]*Saskatchewan Structural Sciences Centre, University of Saskatchewan, 110 Science Place, Saskatoon, Saskatchewan, Canada, S7N 5C9*

Received March 21, 2007

3.1 Abstract

Five new intramolecularly coordinated aluminum species, whose molecular structures have been elucidated in solution by NMR spectroscopy and in the solid state by single-crystal X-ray analysis, are described. All species are equipped with a *trisyl*-based ligand with a pyridyl donor group [Pytsi stands for $-C(SiMe_3)_2SiMe_2(2\text{-}C_5H_4N)$]. While the compound (Pytsi)AlMeCl was accessible either from Li(thf)(Pytsi) and $MeAlCl_2$ or from (Pytsi)$AlCl_2$ and LiMe, the *tert*-butyl derivative (Pytsi)Al*t*BuCl could only be obtained from Li(thf)(Pytsi) and *t*Bu$AlCl_2$. Attempted synthesis of (Pytsi)Al*t*BuCl from (Pytsi)$AlCl_2$ and Li*t*Bu or from (Pytsi)$AlCl_2$ and *t*BuMgCl failed. Three other compounds (**3**–**5**) were synthesized and can be described as derivatives of (Pytsi)$AlMe_2$ with additional groups in the ortho-position of the pyridyl group. Compound **3** carried a Me group in the ortho-position, while compound **4** and **5** were equipped with Ph and 2,6-diisopropylphenyl moieties, respectively.

3.2 Introduction

Group-13 element compounds EX_3 are the text book examples of Lewis acids. Usually, the electronic needs of the heavier group members Al, Ga, and In cannot be satisfied intramolecularly through π bonds and, hence, oligomers are found throughout their structural chemistry. By employing ligands that are equipped with donor groups, Lewis acid-base adducts are formed intramolecularly and oligomers can be prevented. One of the most commonly used intramolecularly coordinating ligands is the 'one-armed' phenyl ligand (Ar′, Figure 3-1). For example, employing the Ar′ ligand gives access to well-defined, monomeric aluminium halides.[1] Azides of the heavier group-13 elements are usually oligomers[2], however, the application of Ar′ and Pr′ (Figure 3-1), respectively, allowed for the preparation of the first monomeric aluminum azides[3–5]. The use of the Pr′ ligand usually results in species of higher volatility than those equipped with Ar′ ligands and respective Al, Ga, and In azides had been employed as single-source precursors for chemical vapor deposition (CVD) of nitrides.[2, 6]

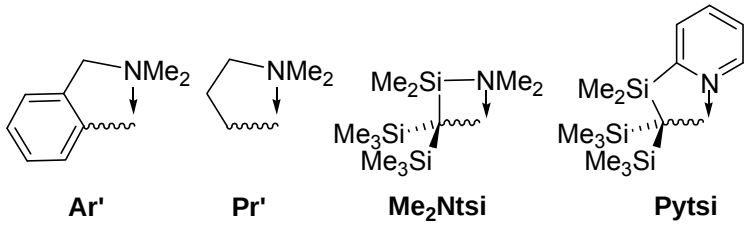

Figure 3-1. Intramolecularly coordinating ligands.

The tris(trimethylsilyl)methyl ligand, commonly referred to as the *trisyl* ligand, is a widely used sterically demanding ligand with electron donor properties provided by three silyl groups (β-silyl effect).[7] Eaborn and co-workers[8] developed a series of *trisyl*-based ligands in which one of the methyl groups is formally replaced by a substituent with σ donor abilities. Modifications included ligands of the type $–C(SiMe_3)_2(SiMe_2R)$ with R being MeO[7], Ph_2P[7],

CH_2PPh_2[7], Me_2N (Figure 3-1)[7], and 2-C_5H_4N (Pytsi, Figure 3-1)[8]. Recently, we had shown that Pytsi and Me_2Ntsi (Figure 3-1) stabilized alanes and gallanes can be used for the preparation of [1]metallacyclophanes, like [1]ferrocenophanes[9–11], [1]chromarenophanes[11], and [1]vanadarenophanes[11]. The type of intramolecularly coordinating ligand is of crucial importance for getting strained organometallic species: a change from the sterically demanding Pytsi and Me_2Ntsi, respectively, to the slimmer Ar′ ligand (Figure 3-1) resulted in unstrained [1.1]ferrocenophanes.[12, 13]

Because of the bulkiness and the β-silyl effect, *trisyl*-type ligands might be ideal to stabilize low-coordinated, Lewis-acidic metal complexes. Starting with this working hypothesis, we set out to explore cationic aluminum species equipped with the Pytsi ligand. Cationic low-coordinated aluminum compounds are potential catalysts or initiator for olefin polymerizations.[14–19] Recently, we described the synthesis of salt-like compound [(Pytsi)AlMe][$MeB(C_6F_5)_3$].[19] This species was obtained by a methyl abstraction reaction from (Pytsi)$AlMe_2$ with the perfluorinated borane $B(C_6F_5)_3$, however, the salt-like compound slowly decomposed in toluene at ambient temperature. We planned to increase its stability by shielding the Al centre more effectively with sterically demanding groups, either attached to aluminum directly or attached to the backbone of the chelating ligand.

In this paper we describe the synthesis and characterization of new alanes equipped with *trisyl*-based intramolecularly coordinating ligands.

3.3 Results and Discussion

Cations are commonly synthesized through halide abstraction reactions from suitable halogen containing precursors. Often, silver salts of weakly coordinating anions are employed.[20]

Against this background, we intended to prepare precursor species of the type (Pytsi)AlClR. First, we prepared (Pytsi)AlClMe (**1**) from Li(thf)(Pytsi) and $MeAlCl_2$ (equation 3-1). A similar route had been employed for Ar′AlClMe.[1] Compound **1** can also be synthesized by a substitution reaction from (Pytsi)$AlCl_2$ and LiMe. Both routes to species **1** work comparably well (see Experimental Section). In accordance with the known synthesis of Ar′AlCl*t*Bu (1), we attempted the synthesis of (Pytsi)AlCl*t*Bu (**2**) from (Pytsi)$AlCl_2$[21] and Li*t*Bu in Et_2O or with *t*BuMgCl in Et_2O. Both reactions proved unsuccessful. In the case Li*t*Bu, a very rich ^1H NMR spectrum hinted at complex reactions and showed that the target compound **2b** had not been formed. In the case of the Grignard reaction, no reaction happened at all. However, the target molecule **2** was accessible in a moderate isolated yield of 54% by reacting Li(thf)(Pytsi) with *t*Bu$AlCl_2$ (equation 3-1).

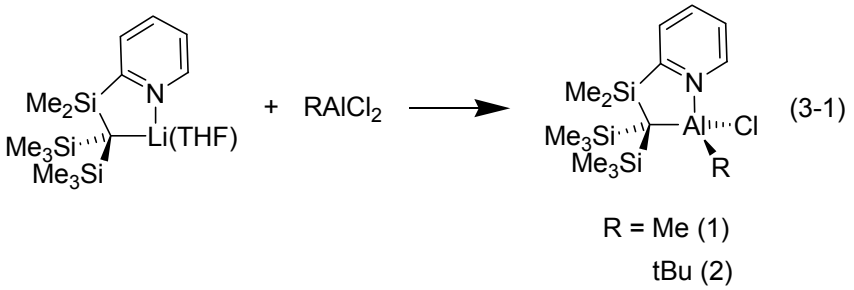

(3-1)

Compounds **1** and **2** are asymmetric species as being revealed by NMR spectroscopy. For example, for both compounds the $SiMe_2$ and the two $SiMe_3$ moieties give rise to two singlets each in ^1H NMR- as well as in $^{13}C\{^1H\}$ NMR spectra.Compounds **1** and **2**, respectively, crystallize in the monoclinic space group $P2_1/c$. Figures 3-2 and 3-3 depict their molecular structures, and Table 3-1 shows their structural parameters.

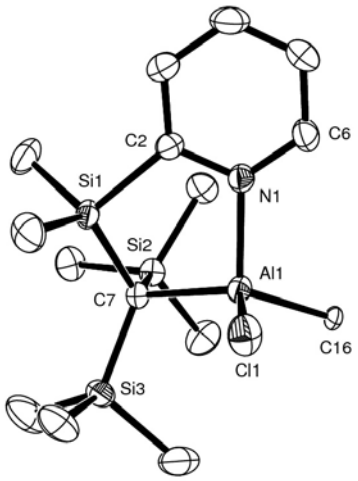

Figure 3-2. Molecular structure of (Pytsi)AlClMe (**1**) with thermal ellipsoids at the 50% probability level. H atoms are omitted for clarity. Selected bond length (Å) and angles (º): Al1–N1 = 1.962(2), Al–Cl1 = 2.1813(9), Al1–C7 = 2.008(2), Al1–C16 = 1.978(2), N1–Al1–Cl1 = 98.98(7), N1–Al1–C16 = 109.28(9), N1–Al1–C7 = 98.34(9), C7–Al1–Cl1 = 113.42(7), C7–Al1–C16 = 125.37(10), Cl1–Al1–C16 = 107.68(7).

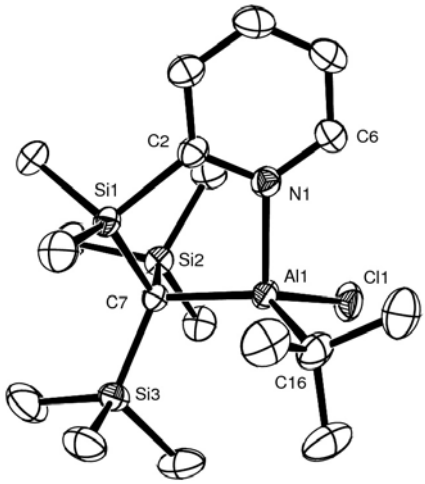

Figure 3-3. Molecular structure of (Pytsi)Al*t*BuCl (**2**) with thermal ellipsoids at the 50% probability level. H atoms are omitted for clarity. Selected bond length (Å) and angles (º): Al1–N1 = 1.9765(14), Al–Cl1 = 2.1787(6), Al1–C7 = 2.0340(15), Al1–C16 = 2.0077(18), N1–Al1–Cl1 = 103.92(4), N1–Al1–C16 = 103.92(7), N1–Al1–C7 = 96.43(6), C7–Al1–Cl1 = 115.31(5), C7–Al1–C16 = 127.95(7), Cl1–Al1–C16 = 105.48(6).

Table 3-1. Crystal and structural refinement data for aluminum dimethyl compounds equipped with Pytsi-like ligands **1**–**5**.

cryst params	**1**	**2**	**3**	**4**	**5**
empirical formula	$C_{15}H_{31}AlClNSi_3$	$C_{18}H_{37}AlClNSi_3$	$C_{17}H_{36}AlNSi_3$	$C_{22}H_{38}AlNSi_3$	$C_{28}H_{50}AlNSi_3$
formula weight	372.11	414.19	365.72	427.78	511.94
wavelength, Å	0.71073	0.71073	0.71073	0.71073	0.71073
crystal system	monoclinic	monoclinic	monoclinic	monoclinic	triclinic
space group (No.)	$P2_1/c$	$P2_1/c$	$P2_1/c$	$P2_1/c$	$P\bar{1}$
Z	4	4	4	4	2
a, Å	9.04630(10)	9.0520(2)	17.1251(3)	13.8716(4)	8.5860(2)
b, Å	9.31560(10)	16.7560(4)	9.1309(2)	9.7136(3)	12.0067(4)
c, Å	25.5316(4)	18.2311(3)	15.5683(3)	18.6390(8)	16.6488(6)
α, deg	90	90	90	90	71.2665(15)
β, deg	94.8075(5)	118.6060(10)	111.7240(10)	90.394(2)	80.8750(18)
γ, deg	90	90	90	90	75.5988(17)
vol, $Å^3$	2144.02(5)	2427.67(9)	2261.48(8)	2511.42(15)	1568.51(9)
d (calc), mg/m^3	1.153	1.133	1.074	1.131	1.084
temp, K	173(2)	173(2)	173(2)	173(2)	173(2)
abs coeff., mm^{-1}	0.382	0.344	0.247	0.232	0.195
theta range, deg	2.26 to 27.55	2.55 to 30.00	2.57 to 28.20	2.78 to 27.48	2.74 to 27.48
refl collected	17648	13876	42198	10258	13539
indep refl	4921 [R(int) = 0.0631]	7071 [R(int) = 0.0298]	5491 [R(int) = 0.0799]	5732 [R(int) = 0.0457]	7178 [R(int) = 0.0238]
abs correction	Semi-empirical from equivalents				
ref method	Full-matrix least-squares on F^2				
data / restr / params	4922 / 0 / 199	7071 / 0 / 228	5491 / 0 / 242	5732 / 0 /254	7178 / 0 / 312
goodness-of-fit on F^2	1.043	1.058	1.042	1.024	1.001
final R indices [I>2sigma(I)]	R1 = 0.0454, wR2 = 0.1053	R1 = 0.0418, wR2 = 0.0956	R1 = 0.0442, wR2 = 0.0943	R1 = 0.0477, wR2 = 0.1027	R1 = 0.0448, wR2 = 0.1096
R indices (all data)	R1 = 0.0749, wR2 = 0.1242	R1 = 0.0634, wR2 = 0.1050	R1 = 0.0637, wR2 = 0.1020	R1 = 0.0843, wR2 = 0.1205	R1 = 0.0604, wR2 = 0.1191
largest diff. peak and hole, $e.Å^{-3}$	0.635 and –0.462	0.417 and –0.275	0.369 and –0.291	0.310 and –0.355	0.503 and –0.384

Expectedly, both molecular structures are very similar. The Al atoms are four-fold coordinated by two C atoms, one Cl- and one N atom with nearly identical bond lengths (Figure 3-2 and 3-3). The major difference between **1** and **2** is due to a different folding of the five-membered ring. For both compounds, the five-membered ring adopts an envelope conformation with C7 being the tip of the envelope. However, because of the stereogenic Al centre two different folding directions of C7 are possible. While in compound **1** C7 is folded away from the Cl atom, in compound **2** C7 is folded towards the Cl atom. The conformer found for **2** places the

*t*Bu group in an axial position and allows a maximum distance towards the two neighbouring $SiMe_3$ groups, indicating that steric factors play the mayor role for finding a particular isomer.

As mentioned in the introduction, we attempted to shield the Al centre more effectively with sterically demanding groups. Therefore, we synthesized derivatives of (Pytsi)$AlMe_2$[19, 21] in which the ortho position of the pyridine ring carries a Me (**3**), Ph (**4**) or Dipp group (**5**) (Dipp = 2,6-diisopropylphenyl). As illustrated in Scheme 3-1, compounds **3**–**5** have been prepared similarly as the known (Pytsi)$AlMe_2$.[19, 21] Of course, the methyl group in the 6 position of the pyridine ring is too small to sterically protect the aluminum atom. However, compound **3** was the first test case to find out, if a small change to the pyridyl group has an influence on the synthesis of the respective dimethyl alane.

The preparation of **3**–**5** differs mainly in the way we synthesized the ortho-lithiated pyridine (Scheme 3-1). In all cases the ortho-lithiated pyridine derivative was prepared *in situ*. However, for compound **3** and **4**, we generated it from a respective bromopyridine and LiBu. For compound **5**, we first used a nickel-catalyst cross-coupling of a Grignard reagent[22, 23] followed by a selective deprotonation in the ortho-position, a method that had been applied to other phenylpyridine derivatives before [24] (Scheme 3-2).

The dimethylalanes **3**–**5** were isolated in moderate to good yields of 51 to 86% as crystalline, colorless solids. All three compounds reveal pattern in their ^{1}H- and ^{13}C NMR spectra that are consistent with time-averaged C_s symmetrical species. The most noteworthy feature in all the spectra is the appearance of the two isopropyl groups of the Dipp ligand of compound **5**. They show two doublets for the Me groups (δ 0.82 and 1.34) and one multiplet for the CH group (δ 2.40) in the ^{1}H NMR spectrum and two singlets for the Me groups and one singlet for the CH groups in the $^{13}C\{^1H\}$ NMR spectrum. This shows that both isopropyl groups

are chemical equivalent, but the methyl groups are nonequivalent for each isopropyl group. As already mentioned above, the NMR spectra can be rationalized by assuming compound **5** is a time-averaged C_s symmetrical species; e.g., the $SiMe_3$ and the $AlMe_2$ moieties each give rise to one singlet. All facts combined prove that the Dipp ligand is oriented perpendicular to the pyridiyl moiety and is not rotating fast on the NMR time scale.

Scheme 3-1. Synthesis of aluminum dimethyl compounds equipped with Pytsi-like ligands **3**–**5**.

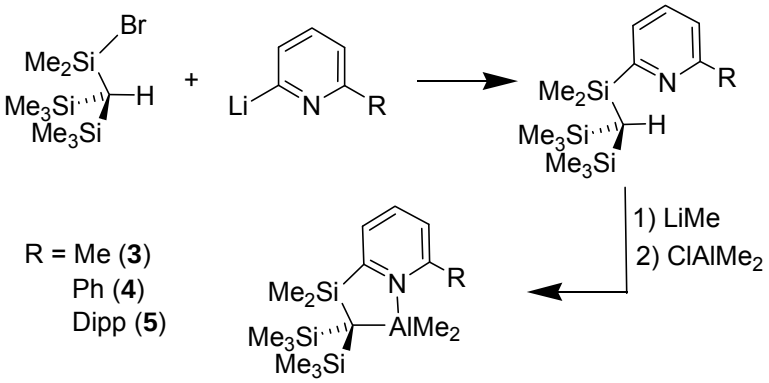

Scheme 3-2. Synthesis of the lithiopyridine for {{[6-(2,6-diisopropylphenyl)pyrid-2yl]dimethylsilyl}bis(trimethylsilyl)methyl}-dimethylaluminum (**5**).

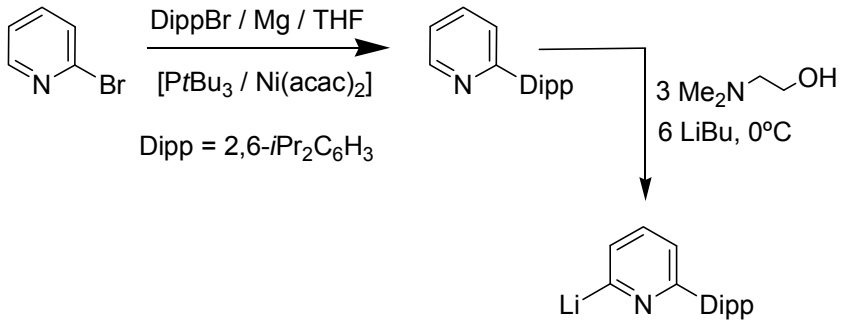

The molecular structures of compounds **3**–**5** were determined with single-crystal X-ray analysis (Figures 3-4, 3-5 and 3-6 and Table 3-1). All species exhibit an envelope conformation of the five-membered heterocycle with C7 being the tip of the envelope. In all compounds, aluminum is tetrahedrally surrounded by a set of three C atoms and one N atom with very similar bond lengths and angles (Figures 3-4, 3-5 and 3-6). For example, the Al–N bond lengths are

found in the narrow range between 2.0393(16) and 2.0587(15) Å, even though these donor bonds are expected to be the most flexible bonds in the molecules. A similar but slightly shorter Al–N bond was found for (Pytsi)$AlEt_2$ (Al–N = 2.0034(18) Å)[19]. Reliable bond lengths and angles are not available for the closely related dimethylalane (Pytsi)$AlMe_2$, because it is disordered about a plane of symmetry, which bisects the molecule along the Si_2C plane in the $C(SiMe_3)_2$ group.[19] In both halves of the molecule the Me_2Al- and the Me_2Si moieties on one side and the two halves of the pyridine ring on the other side, have similar sizes and shapes, which makes the disordering understandable.[19] Both halves of (Pytsi)$AlMe_2$ can be made dissimilar by either changing the alkyl groups at aluminum or adding a substituent to the pyridyl moiety; neither (Pytsi)$AlEt_2$ [19] nor compound **3** are disordered in the crystal lattice.

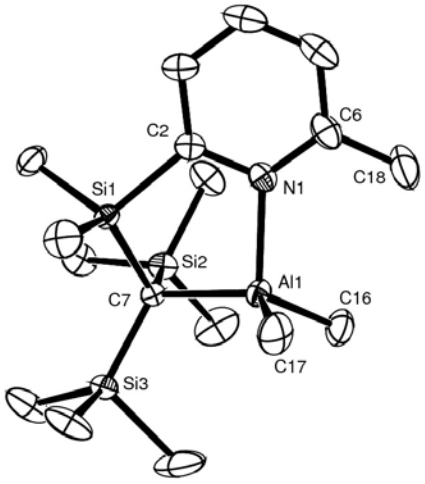

Figure 3-4. Molecular structure of {[dimethyl(6-methylpyrid-2-yl)silyl]bis(trimethylsilyl)methyl}dimethylaluminum (**3**) with thermal ellipsoids at the 50% probability level. H atoms are omitted for clarity. Selected bond length (Å) and angles (º): Al1–N1 = 2.0393(16), Al1–C7 = 2.0416(17), Al1–C16 = 1.976(2), Al1–C17 = 1.980(2), C16–Al1–C17 = 110.30(10), C7–Al1–C16 = 116.94(8), C7–Al1–C17 = 118.49(8), N1–Al1–C16 = 112.74(8), N1–Al1–C17 = 99.94(8), N1–Al1–C7 = 96.01(6).

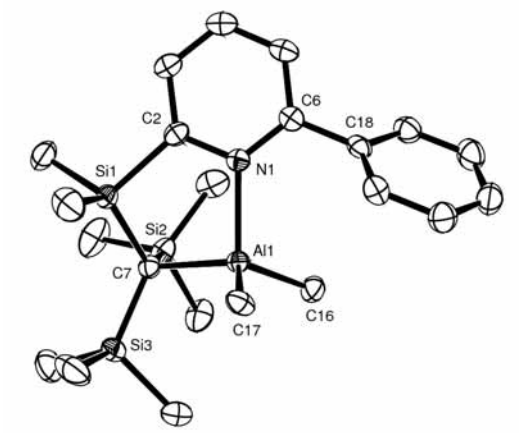

Figure 3-5. Molecular structure of {[dimethyl(6-phenylpyrid-2-yl)silyl]bis(trimethylsilyl)methyl}dimethylaluminum (**4**) with thermal ellipsoids at the 50% probability level. H atoms are omitted for clarity. Selected bond length (Å) and angles (º): Al1–N1 = 2.0537(19), Al1–C7 = 2.054(2), Al1–C16 = 1.983(2), Al1–C17 = 2.002(2), C16–Al1–C17 = 111.50(11), C7–Al1–C16 = 117.62(9), C7–Al1–C17 = 113.27(9), N1–Al1–C16 = 110.26(9), N1–Al1–C17 = 106.83(9), N1–Al1–C7 = 95.71(8).

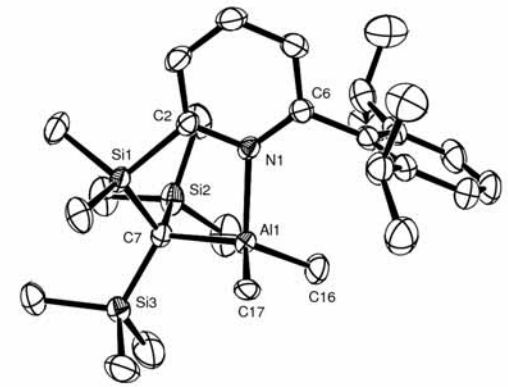

Figure 3-6. Molecular structure of {{[6-(2,6-diisopropylphenyl)pyrid-2yl]dimethylsilyl}bis(trimethylsilyl)methyl}-dimethylaluminum (**5**) with thermal ellipsoids at the 50% probability level. H atoms are omitted for clarity. Selected bond length (Å) and angles (º): Al1–N1 = 2.0587(15), Al1–C7 = 2.0595(17), Al1–C16 = 1.965(2), Al1–C17 = 2.0390(19), C16–Al1–C17 = 109.25(9), C7–Al1–C16 = 118.47(9), C7–Al1–C17 = 117.17(7), N1–Al1–C16 = 114.48(8), N1–Al1–C17 = 99.89(7), N1–Al1–C7 = 95.32(6).

3.4 Conclusion

We synthesized five new intramolecularly coordinated aluminum species, whose molecular structures have been elucidated in solution by NMR spectroscopy and in the solid

state by single-crystal X-ray analysis. All species **1**–**5** are equipped with a *trisyl*-based ligand with a pyridyl donor group (Figure 3-1, Pytsi). While the mono-methyl compound (Pytsi)AlMeCl (**1**) is accessible either from Li(thf)(Pytsi) and $MeAlCl_2$ (equation 3-1) or from (Pytsi)$AlCl_2$ and LiMe, the *tert*-butyl derivative (Pytsi)Al*t*BuCl (**2**) could only be obtained from Li(thf)(Pytsi) and *t*$BuAlCl_2$ (equation 3-1). The latter result is in contrast to the synthesis of the related species Ar′AltBuCl (Figure 3-1, Ar′), which was synthesized from Ar′$AlCl_2$ and Li*t*Bu.[1] The different substitution behavior of (Pytsi)$AlCl_2$ and Ar′$AlCl_2$ towards Li*t*Bu can be interpreted as being due to the higher steric demand of Pytsi compared to Ar′ (Figure 3-1).

Compounds **3**–**5** can all be described as derivatives of (Pytsi)$AlMe_2$ with additional groups in the ortho-position of the pyridyl group. From the molecular structures of the Ph substituted compound **4** (Figure 3-5) and the 2,6-diisopropylphenyl derivative **5** (Figure 3-6) one gets the impression that the aromatic group in the ortho position of the pyridyl ring might serve as a shield to help protect the Al atom and, consequently, we intend to employ these species as precursors for cationic aluminum compounds.

3.5 Experimental

General Procedures. All manipulations were carried out using standard Schlenk techniques. Solvents were dried using a MBraun Solvent Purification System and stored under nitrogen over 4 Å molecular sieves. All solvents for NMR spectroscopy were degassed prior to use and stored under nitrogen over 4 Å molecular sieves. $HC(SiMe_3)_2(SiMe_2Br)$[8], Li(thf)(Pytsi) [Pytsi = $C(SiMe_2)(SiMe_3)_2C_5H_4N$)][8], (Pytsi)$AlCl_2$[21], 2-bromo-6-methylpyridine[25], 2-bromo-6-phenylpyridine[24], and bromo-2,6-diisopropylbenzene[26] were synthesized as described in the literature. *t*$BuAlCl_2$ was synthesized similar to *t*$BuAlBr_2$.[27] 2-(2,6-Diisopropylphenyl)pyridine was synthesized similar to 2-(2,6-diisopropylphenyl)-6-methylpyridine.[22] Me_2AlCl and $MeAlCl_2$

were purchased from Sigma–Aldrich and used as received. LiMe (Sigma–Aldrich) and LiBu (VWR) were titrated with 2,6-di-*tert*-butylphenol/fluorine before usage.[28] Silica Gel 60 (particle size 0.040 – 0.063 mm) was purchased from EMD Chemicals. ^{1}H, ^{13}C, and ^{27}Al NMR spectra were recorded on a Bruker 500 MHz Avance at 25 ºC in C_6D_6 unless noted differently. ^{1}H chemical shifts were referenced to the residual protons of the deuterated solvents (C_6D_6 at δ 7.15; $CDCl_3$ at δ 7.26), ^{13}C chemical shifts were referenced to the deuterated solvent (C_6D_6 signal at δ 128.0; $CDCl_3$ signal at δ 77.0), and ^{27}Al NMR spectra were referenced to [Al(acac)$_3$] dissolved in C_6D_6. Mass spectra were measured on a VG 70SE (*m*/*z* > 10% are listed for signals of the most abundant ions). Elemental analyses were performed on a Perkin Elmer 2400 CHN Elemental Analyzer using V_2O_5 to promote complete combustion.

Chloro{[dimethyl(pyrid-2-yl)silyl]bis(trimethylsilyl)methyl}methylaluminum (1).

Route 1: A solution of $MeAlCl_2$ (4.2 mL, 1.0 M in hexane, 4.2 mmol) was added to a solution of Li(thf)(Pytsi) (1.577 g, 4.220 mmol) in hexane at –78 ºC. After stirring for 20 min, the reaction mixture was allowed to warm to ambient temperature and stirred for 16 h. The solid was filtered off, extracted with Et_2O (3 × 10 mL), the combined organic extracts were reduced in volume to 10 mL, and crystallization at ca. –30 ºC resulted in colorless crystals of **1** (1.395 g, 88%).

Route 2: MeLi (4.4 mL, 0.93 M, 4.1 mmol) was added to (Pytsi)$AlCl_2$ (1.625 g, 4.140 mmol) in Et_2O (50 mL) at –78 ºC. The slurry was stirred for 30 min at –78 ºC, allowed to warm to ambient temperature and stirred for 16 h. The white solid was filtered off and the product extracted with Et_2O (3 × 10 mL). The combined extracts were reduced in volume to 20 mL and kept at –30 ºC to give colorless crystals of 1 (1.257 g, 82%).

^{1}H NMR (500 MHz): δ 0.01 (s, 3H, AlMe), 0.15 (s, 9H, $SiMe_3$), 0.33 (s, 3H, $SiMe_2$), 0.44 (s, 9H, $SiMe_3$), 0.49 (s, 3H, $SiMe_2$), 6.31 (pst, 1H, H-5), 6.77 (pst, 1H, H-4), 6.88 (d, 1H, H-3),

8.06 (d, 1H, H-6). ^{13}C NMR (125.8 MHz): δ 3.2 (SiMe), 4.2 (SiMe), 5.8 ($SiMe_3$), 6.2 ($SiMe_3$), 124.4 (C-5), 129.0 (C-3), 138.9 (C-4), 145.8 (C-6), 173.1 (*ipso*-C). ^{27}Al NMR (130.3 MHz): 157 ($w_{1/2}$ = 2000 Hz). MS (70 eV): *m*/*z* (%): 356 (61) [M^+–CH_3], 295 (13) [MH^+–Al–Cl–CH_3], 280 (37) [MH^+–Al–Cl–2 CH_3], 264 (100) [$C_{12}H_{22}NSi_3^+$], 73 (11) [$SiMe_3^+$]. Anal. cacld. for $C_{15}H_{31}AlClNSi_3$ (372.104): C, 54.64; H, 9.74; N, 3.98. Found: C, 54.67; H, 10.11; N, 3.75.

***tert*-Butylchloro{[dimethyl(pyrid-2-yl)silyl]bis(trimethylsilyl)methyl}aluminum (2)**. Li(thf)(Pytsi) (2.200 g, 5.887 mmol) was dissolved in hexane (40 mL) and cooled to –78 ºC. A solution of *t*$BuAlCl_2$ (0.913 g, 5.890 mmol) in hexane (30 mL) was filled into a dropping funnel and added to the cooled solution of Li(thf)(Pytsi) over a period of 5 min. This resulted in the formation of a slightly yellow solution with a white precipitate. After stirring the reaction mixture for 30 min, the cooling bath was removed and the solution was stirred for another 2 h. The formed dark brown solution was filtered and all volatiles were removed in high vacuum. Sublimation at 150 ºC in high vacuum produced a yellow-orange solid. The sublimed solid was dissolved in hexane (35 mL) and crystallization at ca. –30 ºC resulted in pale yellow crystals of **2** (1.322 g, 54%). ^{1}H NMR (500 MHz): δ 0.30 (s, 9H, $SiMe_3$), 0.36 (s, 9H, $SiMe_3$), 0.40 (s, 3H, $SiMe_2$), 0.44 (s, 3H, $SiMe_2$), 1.25 (s, 9H, $C(CH_3)_3$), 6.37 (pst, 1H, H-5), 6.81 (d, 1H, H-3), 6.92 (pst, 1H, H-4), 8.45 (d, 1H, H-6). ^{13}C{^{1}H} NMR (125.8 MHz): δ 1.15 [br, $C(SiMe_3)_2$], 4.41 ($SiMe_2$), 4.61 ($SiMe_2$), 6.94 ($SiMe_3$), 7.10 ($SiMe_3$), 17.1 [$C(CH_3)_3$], 31.2 [$C(CH_3)_3$], 124.1 (C-5), 129.5 (C-3), 139.1 (C-4), 146.9 (C-6), 172.61 (*ipso*-C). ^{27}Al (130.3 MHz): δ 150 ($w_{1/2}$ = 4300 Hz). MS (70 eV) *m*/*z* (%) 398 (6) [M^+–CH_3], 356 (72) [M^+–tBu], 336 (16) [$C_{15}H_{31}AlNSi_3^+$], 264 (100) [$C_{12}H_{22}NSi_3^+$]. Anal. calcd for $C_{18}H_{37}AlClNSi_3$ (414.184): C, 52.20; H, 9.00; N, 3.38; Found: C, 52.88; H, 8.96; N, 3.18.

[Dimethyl(6-methylpyrid-2-yl)silyl]bis(trimethylsilyl)methane. LiBu (15.0 mL, 2.7 M in hexane, 40.5 mmol) was added dropwise to a solution of 2-bromo-6-methylpyridine (8.796 g, 37.12 mmol) in Et_2O (30 mL) at –78 °C to give a dark red solution. The solution was stirred for 20 min before being added to a cold solution (–78 °C) of $HC(SiMe_3)_2(SiMe_2Br)$ (11.751 g, 39.505 mmol) in Et_2O (100 mL), which gave a brown solution. The cold bath was removed and the reaction mixture was stirred for 16 h. After the solvent was removed in vacuum, a dark-brown oil remained, which was transferred onto a dry silica column. The product was eluted with ethyl acetate and a subsequent flask-to-flask condensation under inert gas atmosphere yielded a light yellow oil (bp 82–84 °C, 10^{-3} mbar, 8.920 g, 77%). ^{1}H NMR (500 MHz): δ 0.10 (s, 18H, $SiMe_3$), 0.46 (s, 6H, $SiMe_2$), 2.43 (s, 3H, o-Me), 6.64 (d, 1H, H-5), 7.06 (pst, 1H, H-4), 7.11 (d, 1H, H-3). ^{13}C NMR (125.8 MHz): δ 1.5 ($SiMe_2$), 3.4 ($SiMe_3$), 24.8 (CH_3), 121.8 (C-5), 125.7 (C-3), 134.0 (C-4), 158.0 (*ipso*-C-6), 169.2 (*ipso*-C-2).

{[Dimethyl(6-methylpyrid-2-yl)silyl]bis(trimethylsilyl)methyl}dimethylaluminum (3). LiMe (6.6 mL, 1.0 M in thf/cumene, 6.6 mmol) was added dropwise to [dimethyl(6-methylpyrid-2-yl)silyl]bis(trimethylsilyl)methane (1.866 g, 6.026 mmol) in thf (30 mL) at ambient temperature to give a red solution. Gas was given off immediately. After 1 h of stirring, the solvent was removed in vacuum to leave an oily residue behind, which was dissolved in hexane (20 mL). The solution was cooled to –78 ºC and Me_2AlCl (6.6 mL, 1.0 M in hexane, 6.6 mmol) was added dropwise over 10 min. The cold bath was removed and the reaction mixture stirred for 16 h at ambient temperature. Removal of all volatiles from the solution in high vacuum gave a white solid, which was extracted with hexane (3 × 15 mL). The combined organic fractions were separated from the solid remains by filtration. The organic phase was concentrated to 20 mL and kept at –30 ºC to give light yellow crystalline plates of **3** (1.132 g,

51%). ^{1}H NMR (500 MHz): δ –0.17 (s, 6H, $AlMe_2$), 0.29 (s, 18H, $SiMe_3$), 0.42 (s, 6H, $SiMe_2$), 2.26 (s, 3H, Me), 6.22 (d, 1H, H-5), 6.78 (pst, 1H, H-4), 6.88 (d, 1H, H-3). ^{13}C NMR (125.8 MHz): δ –1.9 ($AlMe_2$), 4.5 ($SiMe_2$), 6.4 ($SiMe_3$), 23.0 (CH_3), 125.3 (C-5), 126.3 (C-3), 138.1 (C-4), 157.4 (*ipso*-C-6), 173.8 (*ipso*-C-2). ^{27}Al NMR (130.3 MHz): δ 174.3 ($w_{1/2}$ = 2750 Hz). MS (70 eV): *m*/*z* (%) 350 (100) [M^+–CH_3], 278 (37) [M^+–Al–4 CH_3], 262 (15) [$C_{12}H_{20}NSi_3^+$]. Anal. calcd. for $C_{17}H_{36}AlNSi_3$ (365.713): C, 55.83; H, 9.92; N, 3.83. Found: C, 55.16; H, 10.57; N, 3.63.

[Dimethyl(6-phenylpyrid-2-yl)silyl]bis(trimethylsilyl)methane. LiBu (2.2 mL, 2.8 M in hexane, 6.2 mmol) was added dropwise to a stirring solution of 2-bromo-6-phenylpyridine (1.321 g, 5.643 mmol) in Et_2O (15 mL) at –78 °C. The resulting red solution was stirred for 20 min before a cold solution (–78 °C) of $CH(Me_3Si)_2(SiMe_2Br)$ (1.712g, 5.755 mmol) in Et_2O (15 mL) was added. The cold bath was removed and the reaction mixture stirred overnight. The red-brown liquid phase was separated from the solids by filtration. Removal of all volatiles at ambient temperature in high vacuum from the liquid phase gave a red oil. The product was collected as a golden yellow oil by a flask-to-flask condensation (b.p. 145–150 °C, 10^{-3} mbar, 1.339 g, 64%). The fraction collected at 65–95 °C was discarded. ^{1}H NMR (500 MHz): δ 0.11 (s, 18H, $SiMe_3$), 0.17 (s, 1H, CH), 0.52 (s, 6H, $SiMe_2$), 7.17(m, 2H, Py H-4, Ph H-5), 7.21 (d, 1H, Py, H-3 or H-5), 7.27 (t, 2H, Ph, H-3, H-4), 7.30 (d, 1H, Py, H-5 or H-3) 8.17 (d, 2H, Ph, H-2, H-6). ^{13}C NMR (125.8 MHz): δ 1.4 ($SiMe_2$), 1.7 (CH), 3.3 ($SiMe_3$), 119.1 (Py, C-3 or C-5), 127.1 (Py, C-3 or C-5), 127.2 (Ph, C-2, C-6), 128.8 (Ph, C-3, C-5), 129.0 (Py, C-4), 134.6 (Ph, C-4), 140.3 (Ph, *ipso*-C), 156.7 (Py, *ipso*-C-6), 169.8 (Py, *ipso*-C-2).

{[Dimethyl(6-phenylpyrid-2-yl)silyl]bis(trimethylsilyl)methyl}dimethylaluminum (4). MeLi (4.0 mL, 1.0 M in thf–cumene, 4.0 mmol) was added dropwise to a stirring solution of

[dimethyl(6-phenylpyrid-2-yl)silyl]bis(trimethylsilyl)methane (1.339 g, 3.602 mmol) in thf (30 mL) at ambient temperature resulting in the formation of gas and a red solution. After 1 h of stirring at ambient temperature, the red solution was cooled to 0 °C and Me_2AlCl (5.0 mL, 1.0 M in hexane, 5.0 mmol) was added dropwise to give a clear brown solution that was stirred for 16 h at ambient temperature. Removal of all volatiles in high vacuum at ambient temperature yielded a light brown solid. The solid was extracted with ether (3 × 20 mL), and the solvent was removed to give a light brown solid, which was subsequently sublimed (140 °C, 10^{-3} mbar) to give a white solid (1.171 g, 76%). Crystallization from diethyl ether at –30 °C yielded colorless crystals of **4** (1.095 g, 71%). ^{1}H NMR (500 MHz): δ –0.58 (s, 6H, $AlMe_2$), 0.26 (s, 18H, $SiMe_3$), 0.51 (s, 6H, $SiMe_2$), 6.62 (d, 1H, H-5), 6.90 (pst, 1H, H-4), 7.05 (d, 1H, H-3), 7.10–7.11 (m, 3H, Ph), 7.20–7.22 (m, 2H, Ph). ^{13}C NMR (125.8 MHz): δ –2.3 ($AlMe_2$, br), 4.7 ($SiMe_2$), 6.3 ($SiMe_3$), 125.7, (C-5), 127.7 (C-3), 128.4 (Ph), 129.1 (Ph) 129.7 (Ph, *ipso*-C), 138.0 (C-4), 160.3 (*ipso*-C-6), 174.8 (*ipso*-C-2). ^{27}Al NMR (130.3 MHz): δ 182 ($w_{1/2}$ = 4500 Hz). MS (70 eV): *m*/*z* (%) 412 (100) [M^+–CH_3], 340 (24) [M^+–Al–4 CH_3], 217 (16). Anal. calcd. for $C_{22}H_{38}AlNSi_3$ (422.804): C, 61.77; H, 8.95; N, 3.27; found: C, 61.09; H, 8.88; N, 3.18.

2-(2,6-Diisopropylphenyl)pyridine. Bromo-2,6-diisopropylbenzene (6.115 g, 25.36 mmol) in thf (10 mL) was added to Mg turnings (0.740 g, 30.45 mmol) in thf (20 mL) in a flask equipped with reflux condenser. Heat was used to start the Grignard reaction. The mixture was refluxed for 24 h before being added to a mixture of P*t*Bu_3 (0.1472 g, 0.7376 mmol), $Ni(acac)_2$ (0.1684 g, 0.6555 mmol), and 2-bromopyridine (3.388 g, 21.44 mmol) in thf (100 mL) cooled to 0 °C, which resulted in a brown solution. The solution refluxed for 24 h and subsequently was poured into dilute HCl (200 mL; 0 °C). The organic phase was discarded and the aqueous phase was extracted with Et_2O (2 × 50 mL) and the Et_2O phase was discarded. K_2CO_3 was added to the

aqueous phase until the evolution of CO_2 ceased during which the color of the solution went from brown to yellow. The aqueous phase was extracted with dichloromethane (3 × 150 mL) followed by removal of volatiles in high vacuum from the combined organic phases to leave a brown oil behind. Flask-to-flask condensation under high vacuum at 120–125 ºC yielded a viscous yellow oil (2.467 g, 48%). ^{1}H NMR (500 MHz, $CDCl_3$): δ 1.06 (6 H, d, $HC(CH_3)CH_3$), 1.10 (d, 6 H, $HC(CH_3)CH_3$), 2.46 (m, 2H, $HC(CH_3)CH_3$), 7.19 (d, 1H, Ph), 7.25 (m, 2H, Py H-4, H-3), 7.33 (pst, 1H, Ph), 7.71 (pst, 1H, Py H-5), 8.70 (d, 1H, Py H-6). ^{13}C NMR (125.8 MHz, $CDCl_3$): δ 23.9 ($HC(CH_3)CH_3$), 24.2 ($HC(CH_3)CH_3$), 30.3 (2 $HC(CH_3)CH_3$), 121.5 (Py, C-3 or C-4), 122.6 (Ph, C-3, C-5), 124.9 (Py, C-4 or C-3), 128.5 (Ph, C-4), 135.6 (Py, C-5), 138.6 (Ph, C-1), 146.4 (Py, *ipso*-C-6), 149.3 (Ph, C-2, C-6), 160.0 (Py, *ipso*-C-2).

{[6-(2,6-Diisopropylphenyl)pyrid-2yl]dimethylsilyl}bis(trimethylsilyl)methane. LiBu (22.0 mL, 2.87 M in hexane, 63.1 mmol) was added dropwise to a solution of 2-dimethylaminoethanol (2.802 g, 31.43 mmol) in hexane (30 mL) cooled to 0 ºC and the resulting yellow solution was stirred for an additional 30 min. 2-(2,6-Diisopropylphenyl)pyridine (2.499 g, 10.44 mmol) in hexane (30 mL) was added and the color of the reaction mixture changed immediately to red. After 1 h of stirring at 0 ºC, the mixture was cooled to –78 ºC and $HC(SiMe_3)_2(SiMe_2Br)$ (11.355 g, 38.17 mmol) in hexane (30 mL) was added dropwise. The mixture was kept at –78 ºC for 1 h before the cold bath was removed and stirring was continued for 16 h at ambient temperature. Deionized H_2O (100 mL) was added, and the aqueous phase was extracted with Et_2O (3 × 100 mL). The combined extracts were dried over $MgSO_4$, filtered, and the volatiles from the organic phase were subsequently removed in vacuum. Flask-to-flask condensation of the orange oil at high vacuum gave two fractions. The fraction at 85–125 ºC was discarded. The product was received as an oil (bp 135–140 °C, 10^{-3} mbar, 3.214 g, 68%) which

turned into a light yellow solid upon cooling to ambient temperature. ^{1}H NMR (500 MHz): δ 0.10 (s, 18H, $SiMe_3$), 0.21 (s, 1H, CH), 0.47 (s, 6H, $SiMe_2$), 1.12 (d, 6H, $CH(CH_3)CH_3$), 1.23 (d, 6H, $CH(CH_3)CH_3$), 2.72 (m, 2H, $CH(CH_3)CH_3$), 6.92 (d, 1H, Py, H-3 or H-5), 7.12 (pst, 1H, Ph, H-4), 7.20 (m, 3H, Ph H-3, H-5, Py H-3 or H-5), 7.30 (pst, 1H, Py H-4). ^{13}C NMR (125.8 MHz): δ 0.8 (CH), 1.3 ($SiMe_2$), 3.3 (2 $SiMe_3$), 23.9 ($HC(CH_3)CH_3$), 25.0 ($HC(CH_3)CH_3$), 30.7 ($HC(CH_3)CH_3$), 122.9 (Ph, 3-C, 5-C), 123.6 (Py, C-3 or C-5), 126.2 (Py, C-5 or C-3), 128.8 (Ph, C-4), 133.6 (Py, C-4), 140.2 (Ph, *ipso*-C-1), 146.7 (Ph, *ipso*-C-2, *ipso*-C-6), 160.3 (Py, *ipso*-C-6), 169.9 (Py, *ipso*-C-2).

{{[6-(2,6-Diisopropylphenyl)pyrid-2yl]dimethylsilyl}bis(trimethylsilyl)methyl}-dimethylaluminum (5). LiMe (2.6 mL, 1.0 M in thf–cumene) was added dropwise to {[6-(2,6-diisopropylphenyl)pyrid-2yl]dimethylsilyl}bis(trimethylsilyl)methane (0.984 g, 2.158 mmol) in thf (20 mL). The solution was stirred for 4 h during which the solution turned brown and gas evolved. Subsequently, the flask was cooled to –78 ºC and Me_2AlCl (2.6 mL, 1.0 M in hexanes) was added dropwise. The cold bath was removed and the reaction mixture stirred overnight. After removal of volatiles from the clear yellow solution a yellow solid remained, which was extracted with ether (10 mL), the extract was filtered and volatiles were removed in vacuum from the filtrate to give a light yellow solid. The solid was dissolved in warm hexane (10 mL) and kept at –30 ºC to give colorless crystals of **5** (0.953 g, 86%). ^{1}H NMR (500 MHz): δ –0.62 (s, 6H, $AlMe_2$), 0.31 (s, 18H, $SiMe_3$), 0.50 (s, 6H, $SiMe_2$), 0.82 (d, 6H, $HC(CH_3)CH_3$), 1.34 (d, 6H, $HC(CH_3)CH_3$), 2.40 (m, 2H, $HC(CH_3)CH_3$), 6.91 (t, 1H, Py, H-4,), 6.96 (d, 1H, Py, H-3 or H-5), 7.08 (d, H, Py, H-5 or H-3), 7.11 (d, 2H, Ph, H-3, H-5), 7.26 (pst, 1H, Ph, H-4). ^{13}C NMR (125.8 MHz): δ –2.5 ($AlMe_2$), 4.7 ($SiMe_2$), 6.5 (2 $SiMe_3$), 22.2 ($HC(CH_3)CH_3$), 26.4 ($HC(CH_3)CH_3$), 30.9 ($HC(CH_3)CH_3$), 123.1 (Ph, C-3, C-5), 127.8 (Py, C-3 or C-5), 128.3 (Py,

C-5 or C-3), 130.7 (Ph, C-4), 134.9 (Ph, C-1), 136.7 (Py, C-4), 147.3 (Ph, C-2, C-6), 159.5 (Py, C-6), 175.5 (Py, C-2). ^{27}Al NMR: δ 179 ($w_{1/2}$ = 4300 Hz). MS (70 eV): *m*/*z* (%) 496 (10) [M^+–CH_3], 455 (100) [MH^+–Al–2 CH_3], 440 (35) [MH^+–Al–3 CH_3], 73 (13) [$SiMe_3^+$]. Anal. calcd. for $C_{28}H_{50}AlNSi_3$ (511.94): C, 65.69; H, 9.84; N, 2.74; found: C,64.89; H, 9.42; N, 2.38.

X-ray structural analysis for 1–5. Data was collected at –100 °C on a Nonius Kappa CCD diffractometer, using the COLLECT program[29]. Cell refinement and data reductions used the programs DENZO and SCALEPACK[30]. The program SIR97[31] was used to solve the structure and SHELXL97[32] was used to refine the structure. ORTEP-3 for *Windows*[33] was used for molecular graphics and PLATON[34] was used to prepare material for publication. H atoms were placed in calculated positions with U_{iso} constrained to be 1.5 times U_{eq} of the carrier atom for all methyl H atoms and 1.2 times U_{iso} for all other H atoms.

The three methyl groups on Si_3 (compound **3**) are disordered and were modeled with occupancies of 0.72 and 0.28 for the two components. Only one position for the methyl groups is shown in Figure 3-4.

Acknowledgement. We thank the Natural Sciences and Engineering Research Council of Canada (JM, NSERC Discovery Grant), the Department of Chemistry, the Saskatchewan Structural Sciences Centre, and the University of Saskatchewan for their generous support. We thank the Canada Foundation for Innovation (CFI) and the government of Saskatchewan for funding of the X-ray and NMR facilities in the Saskatchewan Structural Sciences Centre (SSSC).

Supporting Information Available. CCDC 641212–641216 contains the supplementary crystallographic data for this paper. These data can be obtained, free of charge, via www.ccdc.cam.ac.uk/conts/retrieving.html or from the Cambridge Crystallographic Data Centre, 12 Union Road, Cambridge CB2 1EZ, U.K. (Fax: 44-1223-336033 or e-mail: deposit@ccdc.cam.ac.uk).

3.6 References

(1) Müller, J.; Englert, U. *Chem. Ber.* **1995**, *128*, 493-497.
(2) Müller, J. *Coord. Chem. Rev.* **2002**, *235*, 105-119.
(3) Fischer, R. A.; Miehr, A.; Sussek, H.; Pritzkow, H.; Herdtweck, E.; Müller, J.; Ambacher, O.; Metzger, T. *Chem. Commun.* **1996**, 2685-2686.
(4) Müller, J.; Fischer, R. A.; Sussek, H.; Pilgram, P.; Wang, R.; Pritzkow, H.; Herdtweck, E. *Organometallics* **1998**, *17*, 161-166.
(5) Müller, J.; Boese, R. *J. Mol. Struct.* **2000**, *520*, 215-219.
(6) Devi, A.; Schmid, R.; Müller, J.; Fischer, R. A. *Topics in Organometallic Chemistry*; Fischer, R. A., Ed. Heidelberg, Germany, 2005; Vol. 9, 49.
(7) Eaborn, C.; Smith, J. D. *J. Chem. Soc., Dalton Trans.* **2001**, 1541-1552.
(8) Al-Juaid, S. S.; Eaborn, C.; Hitchcock, P. B.; Hill, M. S.; Smith, J. D. *Organometallics* **2000**, *19*, 3224-3231.
(9) Schachner, J. A.; Lund, C. L.; Quail, J. W.; Müller, J. *Organometallics* **2005**, *24*, 785-787.
(10) Schachner, J. A.; Lund, C. L.; Quail, J. W.; Müller, J. *Organometallics* **2005**, *24*, 4483-4488.
(11) Lund, C. L.; Schachner, J. A.; Quail, J. W.; Müller, J. *Organometallics* **2006**, *25*, 5817-5823.
(12) Braunschweig, H.; Burschka, C.; Clentsmith, G. K. B.; Kupfer, T.; Radacki, K. *Inorg. Chem.* **2005**, *44*, 4906-4908.
(13) Schachner, J. A.; Orlowski, G. A.; Quail, J. W.; Kraatz, H.-B.; Müller, J. *Inorg. Chem.* **2006**, *45*, 454-459.
(14) Bochmann, M.; Dawson, D. M. *Angew. Chem., Int. Ed. Engl.* **1996**, *35*, 2226-2228.
(15) Coles, M. P.; Jordan, R. F. *J. Am. Chem. Soc.* **1997**, *119*, 8125-8126.
(16) Bruce, M.; Gibson, V. C.; Redshaw, C.; Solan, A.; White, J. P.; Williams, D. J. *Chem. Commun.* **1998**, 2523-2524.
(17) Atwood, D. A. *Coord. Chem. Rev.* **1998**, *176*, 407-430.
(18) Kim, K. C.; Reed, C. A.; Long, G. S.; Sen, A. *J. Am. Chem. Soc.* **2002**, *124*, 7662-7663.
(19) Stanga, O.; Lund, C. L.; Liang, H.; Quail, J. W.; Müller, J. *Organometallics* **2005**, *24*, 6120-6125.
(20) Krossing, I.; Raabe, I. *Angew. Chem., Int. Ed. Engl.* **2004**, *43*, 2066-2090.
(21) Howson, J.; Eaborn, C.; Hitchcock, P. B.; Hill, M. S.; Smith, J. D. *J. Organomet. Chem.* **2005**, *690*, 69-75.
(22) Speiser, F.; Braunstein, P.; Saussine, L. *Organometallics* **2004**, *23*, 2633-2640.
(23) Volker, P. W.; Böhm, T.; Weskamp, C.; Gstöttmayr, W. K.; Herrmann, W. A. *Angew. Chem., Int. Ed. Engl.* **2000**, *39*, 1602-1604.
(24) Gros, P.; Fort, Y. *J. Org. Chem.* **2003**, *68*, 2028-2029.
(25) Schubert, U. S.; Eschbaumer, C.; Heller, M. *Org. Lett.* **2000**, *2*, 3373-3376.
(26) Schrock, R. R.; Wesolek, M.; Liu, A. H.; Wallace, K. C.; Dewan, J. C. *Inorg. Chem.* **1988**, *27*, 2050-2054.
(27) Uhl, W.; Schnepf, J. E. O. *Z. Anorg. Allg. Chem.* **1991**, *595*, 225-238.
(28) Brown, C. A. *Synthesis* **1974**, *427*.
(29) *Nonius*; Nonius BV Delft, The Netherlands,1998.

(30) Otwinowski, Z.; Minor, W. *Macromolecular Crystallography, Part A*; Academic Press: New York, 1997; Vol. 276, 307-326.
(31) Altomare, A.; Burla, M. C.; Camalli, M.; Cascarano, G. L.; Giacovazzo, C.; Guagliardi, A.; Moliterni, A. G. G.; Polidori, G.; Spagna, R. *J. Appl. Crystallogr.* **1999**, *32*, 115-119.
(32) Sheldrick, G. M. *SHELXL-97*; University of Göttingen: Göttingen, Germany,1997.
(33) Farrugia, L. J. *J. Appl. Crystallogr.* **1997**, *30*, 565.
(34) Spek, A. L.; University of Utrecht: The Netherlands,2001.

CHAPTER 4
PUBLICATION 3

Description

The following chapter is a verbatim copy of an article which was published in *Organometallics*[*] in August 2005[†] and describes the synthesis of two gallium and two indium species equipped with the Pytsi ligand. The compounds (Pytsi)$GaCl_2$ (**1**), (Pytsi)Ga[1]FCP (**2**), (Pytsi)$InCl_2$ (**3**) and an unusual ferrocenophane (**4**), containing an In–(μ-Cl)$_2$–In group in the bridging position, were synthesized.

Author Contributions

My contributions to this publication were the synthesis and characterization of the monomeric gallium compound **1** and the indium compound **3**, which are equipped with the intramolecularly donating Pytsi ligand. The coauthors on this paper are Jörg A. Schachner, who synthesized the [1]FCP **2** and the compound **4**, J. Wilson Quail, who performed all single-crystal X-ray analyses, and my supervisor Jens Müller. Written permission was obtained from all contributing authors to include material within this thesis.

[*] Reproduced with permission from Organometallics. © 2005 American Chemical Society
[†] Schachner, J. A.; Lund, C. L.; Quail, J. W.; Müller, J. *Organometallics* **2005**, *24*, 4483-4488.

Relation of Publication 3 relates to the Objectives of this Project

This paper describes the synthesis and characterization of a gallium- and indium dihalide equipped with Pytsi ligands. Because compounds **1** and **3** were used to prepare ferrocenophanes, it was envisioned that these compounds could also be used to prepare the targeted [1]metallarenophanes. Even though it was later determined that these compounds could not be used to prepare metallarenophanes, the results described in publication 3 had shown that *trisyl*-based ligands are in principle suitable to stabilize strained, heavier group-13-bridged sandwich compounds.

4. Synthesis and Characterization of Heavier Group-13 Element Ferrocenophanes: The First Gallium-Bridged [1]Ferrocenophane and an Unusual Indium Species

Jörg A. Schachner,[‡] Clinton L. Lund,[‡] J. Wilson Quail,[§] and Jens Müller[‡*]

[‡]*Department of Chemistry, University of Saskatchewan, 110 Science Place, Saskatoon, Saskatchewan, Canada, S7N 5C9,* [§]*Saskatchewan Structural Sciences Centre, University of Saskatchewan, 110 Science Place, Saskatoon, Saskatchewan, Canada, S7N 5C9*

Received May 17, 2005

4.1 Abstract

On the basis of our previous results with aluminum, we herein report the synthesis of the first gallium-bridged ferrocenophane. The attempt to synthesize the respective indium compound resulted in an unusual ferrocenophane containing an In-(μ-Cl)$_2$-In group in the bridging position. All compounds have been characterized by NMR spectroscopy and single-crystal X-ray structural determination.

4.2 Introduction

Since their discovery in 1975 by Osborne and Whiteley,[1] strained [1]ferrocenophanes containing metals in the bridging position (Figure 4-1) have sparked much interest throughout the scientific community. Manners *et al.* showed that strained ferrocenophanes can serve as monomers for polymetallocenes via ring-opening polymerization (ROP).[2] Until recently, strained [1]ferrocenophanes containing a bridging group-13 element were only known for boron (ER_x = $BN(SiMe_3)_2$, $BN(SiMe_3)t$Bu, $BNiPr_2$).[3] Very recently, we successfully synthesized the first ferrocenophane containing the heavier group-13 element aluminum. The

[1]aluminaferrocenophane (Al-FCP), equipped with the stabilizing "pytrisyl" ligand [ER_x = Al(Pytsi) with Pytsi = $C(SiMe_3)_2SiMe_2(2\text{-}C_5H_4N)$], was characterized by a single-crystal X-ray analysis.[4] The pytrisyl ligand, derived from the parent *trisyl* ligand $C(SiMe_3)_3$ by a formal substitution of one methyl group with a pyridyl ring, provides intramolecular coordination via the N atom of the pyridine ring and steric shielding through the trimethylsilyl groups. The pytrisyl ligand was introduced in 2000[5] and has mainly been used for transition metal chemistry.[6]

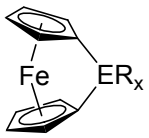

Figure 4-1. ER_x-bridged ferrocenophane.

Unstrained [1.1]ferrocenophanes, formal dimers of ferrocenophanes, where two ferrocene moieties are bridged by two metals, are investigated for their redox properties as model compounds for electronic interactions of iron centres.[7] So far, [1.1]ferrocenophanes containing group-13 elements have been known for boron[7] and gallium.[8] Very recently, we characterized the first aluminum-containing [1.1]ferrocenophane by single-crystal X-ray analysis.[9] Within this publication we report on our results to synthesize gallium- and indium-bridged [1]ferrocenophanes.

4.2 Results and Discussion

The successful synthesis of the first [1]Al-FCP was achieved by reaction of dilithioferrocene with $(Pytsi)AlCl_2$.[4] To apply the same method to gallium and indium, the respective starting compounds $(Pytsi)ECl_2$ [E = Ga (**1**), In (**3**)] were needed. The aluminum

compound (Pytsi)$AlCl_2$ was described in 2005,[10] and the same publication described the attempted synthesis of the dihalides (Pytsi)$GaBr_2$ and (Pytsi)$InCl_2$ (**3**). However, only partly hydrolyzed compounds of the type (Pytsi)$EX_x(OH)_y$ could be isolated, and the authors speculated that this was due to partly hydrolyzed starting materials.[10] We encountered no problems in isolating analytically pure **1** and **3** in good yields by using readily available $GaCl_3$ and $InCl_3$ (see Experimental Section for details).

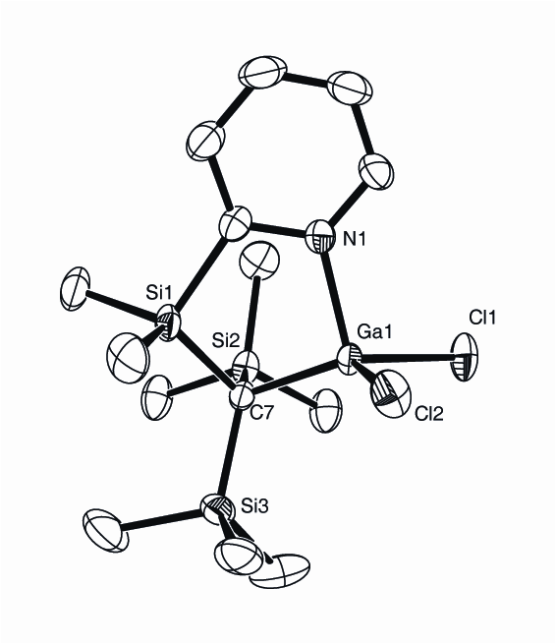

Figure 4-2. Molecular structure of (Pytsi)$GaCl_2$ (**1**) with thermal ellipsoids at the 50% probability level. H atoms are omitted for clarity. Selected bond length (Å) and angles (º): Ga1–N1 = 2.004(2), Ga1–C7 = 1.988(2), Ga1–Cl1 = 2.1816(7), Ga1–Cl2 = 2.2016(7), N1–Ga1–C7 = 98.03(9), N1–Ga1–Cl1 = 104.91(7), N1–Ga1–Cl2 = 98.95(7), Cl1–Ga1–Cl2 = 103.73(3), Cl2–Ga1–C7 = 121.49(8), C7–Ga1–Cl1 = 124.77(8).

As expected, the starting gallane **1** is a monomeric species in the solid state (Figure 4-2, Table 4-1). The Ga–N bond length of 2.004(2) Å is slightly shorter than that of 2.047(5) Å found in the (Pytsi)GaBr(OH),[10] with a similar difference found for the Ga–C bond lengths [1.988(2) Å for **1** and 2.008(5) Å for (Pytsi)GaBr(OH)]. As expected, the M–N bond of the respective dichloro alane (Pytsi)$AlCl_2$, at 1.9383(16) Å, significantly shorter,[10] exemplifying the well-

known fact that a $GaCl_2$ moiety is the weaker Lewis acceptor for a hard Lewis donor compared to an $AlCl_2$ group.

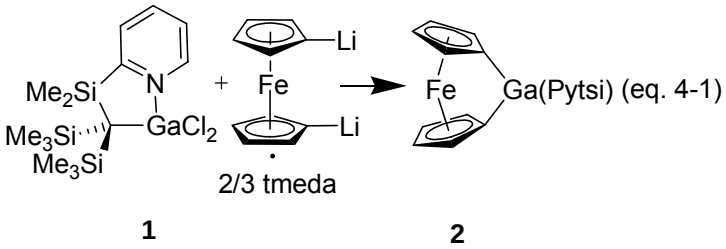

1 **2**

A slurry of dilithioferrocene·2/3 tmeda in toluene was slowly added to a cooled solution of **1** in toluene to give the gallium-bridged [1]ferrocenophane **2** (equation 4-1). Compound **2** was isolated as deep red crystal from hexane in a yield of 59%. Compound **2** is a gallium-bridged [1]ferrocenophane, which is clearly revealed by its NMR data. It shows similar signal pattern and shifts in the ^{1}H- and ^{13}C NMR spectra similar to those of the [1]Al-FCP;[4] both ferrocenophanes are time-averaged C_s symmetrical species in solution.

Table 4-1. Crystal and structural refinement data for compounds (Pytsi)$GaCl_2$ (**1**), (Pytsi)$InCl_2$ (**3**), and indium-bridged ferrocenophane (**4**).

	1	**3**	**4** · 2.5 toluene
empirical formula	$C_{14}H_{28}Cl_2GaNSi_3$	$C_{28}H_{56}Cl_4In_2N_2Si_6$	$C_{55.50}H_{84}Cl_2FeIn_2N_2Si_6$
formula weight	435.26	960.7318	1304.18
wavelength, Å	0.71073	0.71073	0.71073
crystal system	triclinic	monoclinic	triclinic
space group (No.)	$P\bar{1}$ (2)	$P2_1/c$ (14)	$P\bar{1}$ (2)
Z	2	2	2
a, Å	9.0460(2)	9.2181(2)	14.1309(9)
b, Å	10.0441(2)	24.3893(5)	14.7231(11)
c, Å	11.8243(3)	12.5633(3)	16.135(2)
α, deg	84.7182(10)	90	72.624(4)
β, deg	89.2236(10)	131.6290(10)	77.960(6)
γ, deg	87.5315(10)	90	87.868(4)
vol, $Å^3$	1068.74(4)	2111.22(9)	3132.1(5)
d (calc), mg/m^3	1.353	1.511	1.383
temp, K	173(2)	173(2)	173(2)
abs coefficient, mm^{-1}	1.700	1.537	1.194
theta range, deg	2.04 to 27.65	2.32 – 27.47	2.90 – 25.03
refl collected	9350	8767	40880
indep refl	4911	4810	11048
abs correction	none	semi-empirical from equivalents	
ref method		full-matrix least-squares on F^2	
data / restr / params	4911 / 0 / 198	4810 / 0 / 198	11048 / 242 / 638
goodness-of-fit on F^2	1.030	1.061	1.102
final R indices [I>2σ(I)]	R1 = 0.0373, wR2 = 0.0793	R1 = 0.0334, wR2 = 0.0653	R1 = 0.0595, wR2 = 0.1030
R indices (all data)	R1 = 0.0587, wR2 = 0.0888	R1 = 0.0481, wR2 = 0.0709	R1 = 0.0882, wR2 = 0.1114
largest diff. peak and hole, $e.Å^{-3}$	0.382 and –0.467	0.493 and –0.688	0.988 and –0.793

So far, several attempts to solve the structure of **2** by single-crystal X-ray analysis ended in partially solved structures (Figure 4-3; see Experimental Section for details). The best solution shows four molecules in the asymmetric unit ($P2_1$) with an *R* value of 14.3%. The crystals of **2** diffracted very poorly, and the data does not give a complete crystal structure of **2** with accurate bond lengths and bond angles, but shows with certainty the presence of the targeted [1]Ga-FCP (Figure 4-3). A set of tilt angles is commonly used to describe strained [1]ferrocenophanes (Figure 4-4).[11] The asymmetric unit of compound **2** exhibits four molecules with tilt angles α of

13.6(2.1), 15.0(1.6), 15.4(1.9), and 18.8(1.8)º, resulting in an average of 15.7º. This is a very reasonable value if compared with α = 14.9(3)º found for the [1]Al-FCP.[4]

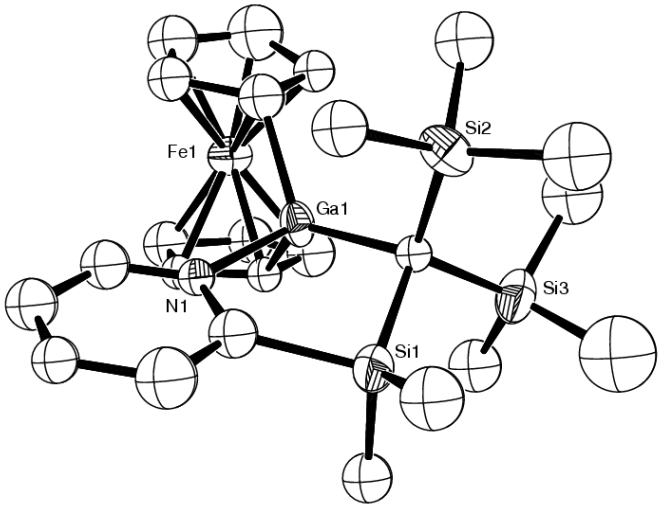

Figure 4-3. Molecular framework structure of (Pytsi)Ga[1]FCP (**2**). One of four independent molecules is shown (see experimental part for details).

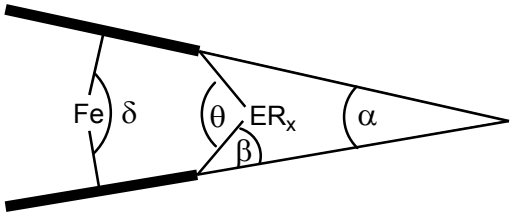

Figure 4-4. Common set of tilt angles to describe [1]ferrocenophanes.

It is common practice to deduce the amount of ring strain present in [1]ferrocenophanes from two NMR parameters: the difference in the splitting of the Cp protons (denoted as $\Delta\delta$) and the upfield shift of the two *ipso*-C atoms of each Cp ring in the ^{13}C NMR spectra. The ^{1}H NMR spectra of **2** shows four pseudotriplets at δ = 4.08, 4.45, 4.61, and 4.65, corresponding to a $\Delta\delta$ = 0.57, and the resonance of the *ipso*-C is found at δ = 47.24. The respective values for the [1]Al-

FCP are 0.77 (Δδ) and 52.92 (*ipso*-C). For comparison, the highly strained sulfur-bridged [1]ferrocenophane (ER_x = S), with the large tilt angle of α = 31.05(10)°, shows a splitting of the two pseudotriplets of Δδ = 0.65 and the *ipso*-C resonates at δ = 14.6.[12] From first glance, the comparable large Δδ of the less strained compound **2** and [1]Al-FCP, respectively, might indicate highly strained molecules. However, most of the [1]ferrocenophanes are C_{2v} symmetrical species resulting in two pseudotriplets. Consequently, the Δδ value expresses the splitting between the two Cp protons adjacent to the bridge and the two Cp protons away from the bridge. To obtain a more realistic splitting value Δδ, we assigned all four pseudotriplets to Cp protons in compound **2** using NOE experiments (Figure 4-5). The difference between average chemical shifts of Cp protons adjacent to gallium (H_a and $H_{a'}$) and away from gallium (H_b and $H_{b'}$) amounts to Δδ = 0.37; a similar procedure gives a Δδ of 0.49 ppm for the [1]Al-FCP.[4] Still, compared with other [1]ferrocenophanes such as [1]Si-FCP (ER_x = $SiMe_2$; α = 20.8(5)º; Δδ = 0.40),[13] [1]Ge-FCP (ER_x = $GeMe_2$; α = 19.0(9)º; Δδ = 0.26),[13] [1]Sn-FCP (ER_x = Sn*t*Bu_2; α = 14.1(2)º; Δδ = 0.22; ER_x = $SnMes_2$; α = 15.2(2)º; Δδ = 0.13),[13] and [1]B-FCP (ER_x = $BN(SiMe_3)_2$; α = 32.4(2)º; Δδ = 0.50; ER_x = BN*i*Pr_2; α = 31.0(2) and 31.4(2)º; Δδ = 0.39)[3] the splitting in **2** and [1]Al-FCP, respectively, are large and do not correlate nicely with the small ring tilt.

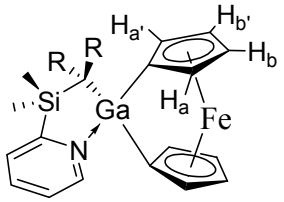

Figure 4-5. Assignment of the Cp protons via NOE experiment (R = $SiMe_3$): δ = 4.08 (H_a), 4.45 ($H_{a'}$), 4.61 (H_b), 4.65 ($H_{b'}$).

As an indication for ring strain, the *ipso*-C shift seems more reliable, because it is not dependent on the overall symmetry of the [1]ferrocenophane. The values for the *ipso*-C atoms in **2** (δ = 47.24) and [1]Al-FCP (δ = 52.92) are significantly upfield shifted with respect to parent ferrocene (δ = 68). However, they are only slightly downfield from the value of the known [1]B-FCP (δ = 44–45), which does not correlate with the tremendous difference in the ring tilt.[3b] The boron-bridged compounds exhibit the highest known ring tilt in ferrocenophanes, but their *ipso*-C resonances are compared with the similar strained [1]S-FCP (δ = 14.6) appearing at unexpected low field.[3b] Braunschweig and Manners suggested that this is a result of the electropositive nature of the bridging boron atom.[3b] Silicon is more electropositive than boron, but the *ipso*-C atoms of less-strained [1]Si-FCP are found at higher fields (ER_x = $SiMe_2$; δ = 33.1).[13] In summary, one can say that an upfield shift of the *ipso*-C atom resonances compared to the parent ferrocene indicates tilted Cp rings, but a simple correlation for all known [1]ferrocenophanes seems not to be existing.

In a similar manner to that described for the gallane **2**, we attempted to synthesize an indium-bridged [1]ferrocenophane. We synthesized the required starting complex (Pytsi)$InCl_2$ (**3**) from $InCl_3$ and Li(thf)(Pytsi)[5] (see Experimental Section for details). As revealed by a single-crystal X-ray analysis, compound **3** forms dimers in the solid state (Figure 4-6; Table 4-1). This is not surprising, because indium prefers higher coordination numbers than 4.

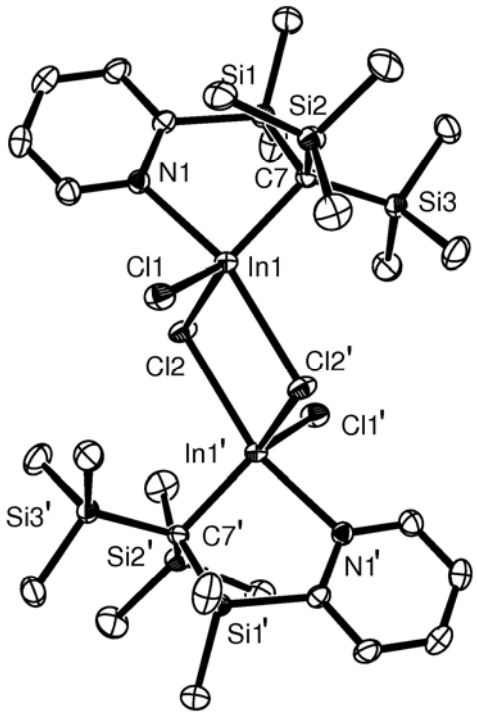

Figure 4-6. Molecular structure of (Pytsi)$InCl_2$ (**3**) with thermal ellipsoids at the 50% probability level. H atoms are omitted for clarity. Primed atoms are generated by –x, –y, –z operation. Selected bond length (Å) and angles (°): In1–Cl1 = 2.3845(7), In1–Cl2 = 2.4812(7), In1–Cl2′ = 2.7706(7), In1–C7 = 2.195(3), In1–N1 = 2.307(2), Cl1–In1–C7 = 124.01(8), Cl2–In1–C7 = 126.80(8), Cl1–In1–Cl2 = 109.10(3), N1–In1–Cl2′ = 162.50(6), N1–In1–C7 = 90.07(9), N1–In1–Cl1 = 90.25(6), N1–In1–Cl2 = 86.53(6), Cl2′–In1–C7 = 105.89(7), Cl2′–In1–Cl1 = 86.73(3), Cl2′–In1–Cl2 = 78.21(2).

Each indium atom is 5-fold coordinated, with two chlorine atoms bridging the two metal centres and two terminal chlorine ligands, which are *trans* to each other (Figure 4-6). Both indium atoms are in a centre of a distorted trigonal bipyramid with both polyhedra sharing the Cl2–Cl2′ edge to form a centrosymmetric dimer. For example, In1 is coordinated by Cl1, Cl2, and C7 in the equatorial position (angle sum = 359.9°) and by N1 and Cl2′ in the axial position (N1–In1–Cl2′ = 162.50(6)°) (Figure 4-6). Both chlorine bridges are asymmetric, e.g., with a long In1–Cl2′ bond of 2.7706(7) Å and a short In1–Cl2 bond of 2.4812(7) Å.

The dimer **3** (C_i point group symmetry) is very flexible in solution. The ^{1}H and ^{13}C NMR spectra show only one type of pytrisyl ligand, which is C_s symmetrical in solution, e. g., only one singlet for $SiMe_2$ and one singlet for the $SiMe_3$ groups. These NMR data could be interpreted in several ways, and one can speculate that a fast monomer-dimer equilibrium occurs in solution.

Similar to the synthesis of compound **2** (equation 4-1), a synthesis of an [1]In-FCP was attempted. The only isolable product from this batch was the unexpected ferrocenophane **4**, and consequently, we changed the In to Fe ration to 2:1 to optimize the synthesis of the novel compound **4** (equation 4-2).

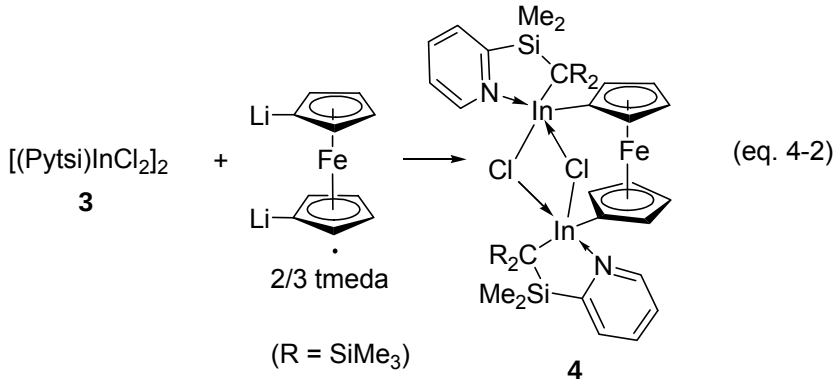

Dropwise addition of the poorly soluble complex **3** in toluene to a cooled slurry of dilithioferrocene·2/3 tmeda[16] in toluene and subsequent filtration yielded an orange solution, which was concentrated, resulting in a crystallization of **4** at –10 °C (see Experimental Section for details). Suitable crystals for X-ray diffraction were taken directly out of the toluene solution (Figure 4-7; Table 4-1).

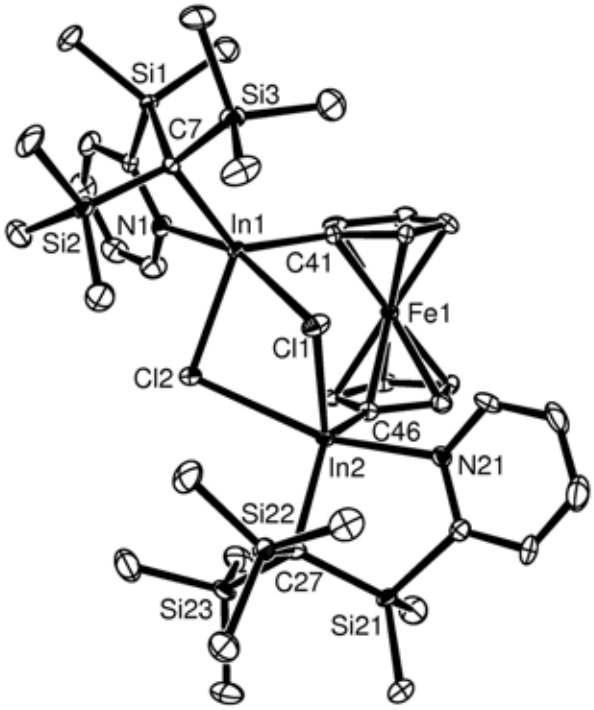

Figure 4-7. Molecular structure of indium-bridged ferrocenophane (**4**) with thermal ellipsoids at the 50% probability level. H atoms and solvent molecules are omitted for clarity. Selected bond length (Å) and angles (º): In1–Cl1 = 2.8322(15), In2–Cl2 = 2.8655(15), In1–Cl2 = 2.5087(14), In2–Cl1 = 2.5072(15), In1–C7 = 2.236(5), In2–C27 = 2.227(5), In1–N1 = 2.364(5), In2–N21 = 2.358(4), In1–C41 = 2.155(6), In2–C46 = 2.136(6), Cl2–In1–C7 = 120.58(14), Cl1–In2–C27 = 120.61(15), C7–In1–C41 = 128.1(2), C27–In2–C46 = 128.2(2), C41–In1–Cl2 = 111.30(15), C46–In2–Cl1 = 111.12(15), N1–In1–Cl1 = 162.37(11), N21–In2–Cl2 = 161.86(12), N1–In1–C7 = 87.29(18), N21–In2–C27 = 86.72(18), N1–In1–Cl2 = 84.69(12), N21–In2–Cl1 = 84.83(12), N1–In1–C41 = 95.17(19), N21–In2–C46 = 95.22(19), Cl1–In1–C7 = 102.66(14), Cl2–In2–C27 = 103.95(14), Cl1–In1–Cl2 = 77.73(5), Cl1–In2–Cl2 = 77.12(5), Cl1–In1–C41 = 90.09(15), Cl2–In2–C46 = 89.66(15).

The isolated ferrocene **4** contains a similar In–$(\mu$-Cl$)_2$–In unit as the starting indane **3**, but in contrast to compound **3**, there is not a 2-fold symmetry element that renders the two molecular halves of **4** identical. However, the molecular geometry of compound **4** is very close to C_2 point group symmetry. Each indium atom is trigonal bipyramidally surrounded. In each case, a set of two C atoms and one Cl atom define the equatorial plane (angle sum = 359.9º for In1 and In2,

respectively); N and Cl atoms are coordinated at the axial positions (N1–In1–Cl1 = 162.37(11) and N21–In2–Cl2 = 161.86(12)°; Figure 4-7). As for **3**, the In–(μ-Cl)$_2$–In moiety shows a short [In1–Cl2 = 2.5087(14) and In2–Cl1 = 2.5072(15) Å] and a long [In1–Cl1 = 2.8322(15) and In2–Cl2 = 2.8655(15) Å] indium chlorine bond. These distances are slightly longer than those found in **3** [In1–Cl2 = 2.4812(7) Å, and In1–Cl2′ = 2.7706(7) Å; Figure 4-6], which might reflect the weaker Lewis-acidity of indium in **4**, caused by fewer chloride substituents. Compound **4** is unstrained, as revealed by a tilt angle α = 2.10(45)°; the Cp rings are staggered at an average angle of 29.12(38)° to each other. It seems that the rotational flexibility of the Cp ligands in ferrocene allows for an ideal adjustment to fit in an In–(μ-Cl)$_2$–In unit.

The NMR spectra of **4** can be interpreted as being caused by C_2 symmetrical molecules with a chlorine-bridged structure similar to that revealed in the crystal lattice: one set of signals for asymmetric pytrisyl ligands and one set of signals for asymmetric Cp groups. These C_2 symmetrical species must be a racemic mixture of molecules with the same relative configuration at each In atom, the *rac* isomers. There are no signs of the presence of diastereomers with opposite configurations at each In atom, the *meso* isomers. The molecular structure of **4** in the crystal lattice gives the impression that a respective *meso* isomer with an In–(μ-Cl)$_2$–In moiety is impossible for steric reasons. If the two molecular halves are *not* linked through Cl bridges, a mixture of *rac* and *meso* isomers should be present. The fact that this is not the case supports the interpretation of the NMR data as being caused by compound **4** with a similar structure similar to that in the crystal lattice. Interestingly the four pseudotriplets of the Cp groups resonate at δ of 3.44, 4.18, 4.43, and 5.18 resulting in a very large splitting of Δδ = 1.74 ppm. However, the ^{13}C NMR spectrum displays the *ipso*-C at δ 67.71, clearly indicating an unstrained ferrocenophane. In the course of assigning ^{1}H NMR peaks to protons in **4** by NOESY

experiments we found that compound **4** fluctuates in solution (Figure 4-8; see Experimental Section for details). If one methyl of the $SiMe_2$ group, the methyl groups of a $SiMe_3$ moiety, or one CH proton is irradiated, one can observe, in addition to nuclear Overhauser effects, magnetization transfer to respective diastereotopic protons (Figure 4-8; Me_a to $Me_{a'}$, R to R′, H_a to $H_{a'}$, H_b to $H_{b'}$ and vice versa). This clearly indicates that the two enantiomers of the *rac* isomer form an equilibrium.

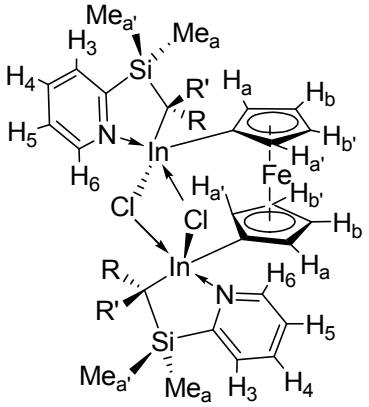

Figure 4-8. Assignment of the ^{1}H NMR peaks for indium-bridged ferrocenophane (**4**) (R and R′ = $SiMe_3$; none-primed groups R and Me_a are on the same side of the ferrocene moiety; primed groups R′ and $Me_{a'}$ are on the opposite side of the ferrocene moiety (see experimental for details).

The equilibration between the R/R isomer and the S/S isomer is slow at ambient temperature, and signals do not coalesce in a ^{1}H NMR spectrum (500 MHz). In the temperature range of 25 to 80 °C coalescence between the primed and none-primed atoms and groups, respectively, is observed, indicating a time-averaged C_{2v} symmetrical molecule. Besides exhibiting dynamic behavior, compound **4** is temperature sensitive. After one series of variable-temperature experiments, new signals appeared in the ^{1}H NMR spectrum remeasured at ambient temperature, indicating unidentified thermolysis products. We have no experimental evidence on how the equilibration takes place. It is known for 4- and 5-fold coordinated indium species that

the donor bond between In atoms and the dimethylamino group from the chelating "one-arm" phenyl ligand 2-$Me_2NCH(Z)C_6H_4$ (Z = H, Me)[14] breakes and re-forms in solution. We assume that a similar process takes place with the pyridine donor groups in compound **4**, and it is feasible that both pyridine ligands are lifted off the In atoms, followed by rotations of the pytrisyl ligand around the In–C bonds, and are reattached which results in inversions of both metal centres. A process like this could explain the observed equilibration.

4.4 Conclusions

Like the aluminum-bridged [1]ferrocenophane, the pytrisyl ligand provides the right combination of steric bulkiness and intramolecular coordination to allow the synthesis of the first example of a gallium-bridged [1]ferrocenophane (**2**). For the heavier homologue indium, we isolated the first example of a ferrocene molecule bridged by an indium-containing moiety (**4**). Interestingly, the synthesis is diastereoselective and the resulting product fluctuates in solution. It is evident from solution NMR experiments that the two Cp ligands in compound **4** are bridged by a In–$(\mu\text{-Cl})_2$–In unit; the molecular structure of **4** in solution is similar to that found in the solid state. IUPAC defines ferrocenophanes as "compounds in which the two ring components of ferrocene are linked by one or more bridging chains".[15] Because of the linkage between the Cp ligands, compound **4** is clearly a ferrocenophane. However, the bridging In–$(\mu\text{-Cl})_2$–In unit is not a simple chain, and therefore, an IUPAC name for species **4** as a ferrocenophane is not defined.

The bridging In–$(\mu\text{-Cl})_2$–In unit of the starting indane **3** is preserved in the product **4**, which suggests that a monomerization of the starting indium dihalide might open the door to the targeted [1]In-FCP. We are currently increasing the bulkiness of the pytrisyl ligand by

introducing sterically demanding groups in position 6 of the pyridine ring. This might prevent dimerization and, therefore, change the course of the reaction with dilithioferrocene. We hope to report on the outcome shortly.

4.5 Experimental Section

General Procedures. All manipulations were carried out using standard Schlenk techniques, if not noted differently. Solvents were dried using a MBraun Solvent Purification System and stored under Argon over a 4 Å molecular sieve. C_6D_6 and C_7D_8 were degassed prior to use and stored under argon over a 4 Å molecular sieve. $GaCl_3$ and $InCl_3$ were purchased from VWR and used as received. ^1H and ^{13}C NMR spectra were recorded on a Bruker 500 MHz Avance spectrometer; chemical shifts were referenced to the residual protons of the deuterated solvent. All NMR spectra were recorded in C_6D_6 at 25 °C, unless noted differently. Mass spectra were measured on a VG 70SE and were reported in the form M (%I) [F], where M is the mass observed, %I is the intensity of the peak relative to the most intense peak in the spectrum and F is the molecular ion or fragment. Only ions with intensities higher than 10% are listed. Elemental analysis was performed on a Perkin–Elmer 2400 CHN Elemental Analyzer; samples were prepared in a glovebox, and V_2O_5 was added to promote combustion.

Synthesis of 1. Li(thf)(Pytsi) (1.939 g, 5.19 mmol)[5] dissolved in Et_2O (30 mL) was cooled to –80 ºC and added to a stirring solution of $GaCl_3$ (0.920 g, 5.22 mmol) in Et_2O (40 mL; –80 ºC). The reaction mixture was stirred at –80 ºC for 20 min before being warmed to ambient temperature with stirring continued for 16 h to give a yellow solution. Subsequently, the solvent was removed from the filtered solution. The remaining white solid was then sublimed at 130 ºC at high vacuum to yield **1** as a white crystalline solid (1.672 g, 74%). ^1H NMR (500 MHz): δ =

0.29 (s, 18H, $SiMe_3$), 0.36 (s, 6H, $SiMe_2$), 6.37 (pst, 1H, 5-H), 6.82–6.84 (m, 2H, 3-H, 4-H), 8.42 (d, 1H, 6-H). ^{13}C NMR (125.8 MHz): δ = 3.25 ($SiMe_2$), 5.84 ($SiMe_3$), 125.64 (5-C), 129.37 (3-C), 139.93 (4-C), 146.29 (6-C), 169.27 (*ipso*-C, C_5H_4N). Carbon attached to gallium was obscured in baseline. MS (70 eV, EI+): *m/z* (%): 420 (27) [M^+–Me], 264 (100) [$Pytsi^+$–2 Me]. Anal. Calcd for $C_{14}H_{28}Cl_2GaNSi_3$ (435.264): C, 38.63; H, 6.48; N, 3.22. Found: C, 38.74; H, 6.49; N, 3.07.

Synthesis of 2. (Pytsi)$GaCl_2$ (**1**) (0.621 g, 1.42 mmol) was dissolved in toluene (15 mL) and chilled to –10 °C. A suspension of dilithioferrocene·2/3 tmeda (0.506 g, 1.83 mmol)[16] in toluene (15 mL) was added dropwise via tubing. After stirring for 16 h, the color of the solution changed to red. After filtration, the solvent was removed at high vacuum (25 °C/0.01 mbar) to yield red, viscous oil. The residue was extracted with hexane (2 × 10 mL). After concentration, product **2** (0.460 g, 59%) was obtained as red crystals at ambient temperature. ^1H NMR (500 MHz): δ = 0.38 (s, 18H, $SiMe_3$), 0.43 (s, 6H, $SiMe_2$), 4.08 (H_a), 4.45 ($H_{a'}$), 4.61 (H_b), 4.65 ($H_{b'}$) (pst, 8H, Cp, see Figure 4-5), 6.46 (pst, 1H, 4-H or 5-H), 6.85 (pst, 1H, 4-H or 5-H), 6.96 (d, 1H, 3-H), 8.73 (d, 1H, 6-H). ^{13}C NMR (125.8 MHz): δ = 1.27 (Si–C($SiMe_3$)$_2$–Ga), 3.22 ($SiMe_2$), 5.94 ($SiMe_3$), 47.24 (*ipso*-C, Cp), 75.39, 75.53, 76.71, 77.19 (Cp), 124.22 (5-C), 129.40 (3-C), 138.21 (4-C), 147.87 (6-C), 172.74 (*ipso*-C, C_5H_4N). MS (70 eV, EI+): *m/z* (%): 547 (100) [M^+], 532 (69) [M^+–Me], 293 (91) [$Pytsi^+$–H], 278 (69) [$Pytsi^+$–H–Me], 264 (42) [$Pytsi^+$–2 Me], 73 (10) [$SiMe_3^+$]. Anal. Calcd for $C_{24}H_{36}GaFeNSi_3$ (548.379): C, 52.57; H, 6.62; N, 2.55. Found: C, 53.22; H, 6.80; N, 2.31.

Synthesis of 3. Li(thf)(Pytsi) (1.901 g, 5.09 mmol) was dissolved in thf (20 mL, –80 ºC) and added to a solution of $InCl_3$ (1.125 g, 5.09 mmol) in thf (40 mL; –80 ºC). The reaction mixture was stirred at –80 ºC for 20 min before slowly being warmed to ambient temperature

with stirring continued for 16 h to give a green solution initially, and finally a yellow solution. Subsequently, the solvent was removed, and the residue washed with hexane (2 x 30 mL) and filtered. Upon removal of all volatiles at ambient temperature, a white solid remained, which was then sublimed at 135 ºC at high vacuum (0.01 mbar) to yield **3** as a white crystalline solid (1.634 g, 67%). ^{1}H NMR (500 MHz): δ = 0.20 (s, 18H, $SiMe_3$), 0.32 (s, 6H, $SiMe_2$), 6.30 (pst, 1H, 5-H), 6.74 (pst, 1H, 4-H), 6.81 (d, 1H, 3-H), 8.30 (d, 1H, 6-H). ^{13}C NMR (125.8 MHz): δ = 3.13 ($SiMe_2$), 6.31 ($SiMe_3$), 125.46 (5-C), 129.54 (3-C), 139.16 (4-C), 148.40 (6-C), 170.14 (*ipso*-C, C_5H_4N). Carbon attached to indium was obscured in baseline. MS (70 eV, EI+): *m/z* (%): 464 (15) [M^+–Me], 444 (16) [M^+–Cl], 264 (100) [$Pytsi^+$–2 Me]. Anal. Calcd for $C_{14}H_{28}Cl_2InNSi_3$ (480.364): C, 35.01; H, 5.88; N, 2.92 Found: C, 35.62; H, 5.97; N, 2.31.

Synthesis of 4. A suspension of **3** (1.562 g, 1.62 mmol) in toluene (50 mL) and was added dropwise via tubing to a suspension of dilithioferrocene·2/3 tmeda (0.448 g, 1.62 mmol)[16] in toluene (20 mL) that was chilled to –10 °C. After stirring for 16 h, the color of the solution had changed to orange. After filtration and concentration at high vacuum (25 °C/0.01 mbar), crystallization occurred at –10 °C (0.990 g, 57.0%). Single-crystal X-ray analysis was performed on a toluene wet crystal. ^{1}H NMR (500 MHz; see Figure 4-8 for assignments): δ = 0.22 (s, 3H, Me_a of $SiMe_2$), 0.34 (s, 9H, R′ = $SiMe_3$), 0.48 (s, 3H, $Me_{a'}$ of $SiMe_2$), 0.59 (s, 9H, R = $SiMe_3$), 3.44 (H_a), 4.18 (H_b), 4.43 ($H_{b'}$), 5.18 ($H_{a'}$) (pst, 4H, Cp), 6.62 (pst, 1H, 5-H), 6.92 (pst, 1H, 4-H), 7.03 (d, 1H, 3-H), 9.25 (d, 1H, 6-H). ^{13}C NMR (125 MHz): δ = 0.57, 3.01 ($SiMe_2$), 4.60, 4.96 ($SiMe_3$), 5.32 (Si–C($SiMe_3$)$_2$–In, –40 °C, C_7D_8), 67.71 (*ipso*-C, Cp), 69.61, 70.21, 74.26, 75.76 (Cp), 122.73, 127.84, 136.09, 147.47, 169.48 (aromatic, C_5H_4N). MS (70 eV, EI+): *m/z* (%): 629 (22) [MH^+ – (Pytsi)In(Cl)], 444 (32) [(Pytsi)$InCl^+$], 264 (100) [$Pytsi^+$–2 Me], 115 (11) [In^+].

Anal. Calcd for $C_{38}H_{64}Cl_2FeIn_2N_2Si_6$ (1073.843): C, 42.50; H, 6.01; N, 2.61; Found: C, 43.61; H, 6.12; N, 2.59.

X-ray structural analysis for 1, 2, 3, and 4. Data were collected at –100 °C on a Nonius Kappa CCD diffractometer, using the COLLECT program.[17] Cell refinement and data reductions used the programs DENZO and SCALEPACK.[18] The program SIR97[19] was used to solve the structure and SHELXL97[20] was used to refine the structure. All H atoms were placed in calculated positions, with C–H distances in the range 0.95–0.99 Å, and included in a riding model approximation. For compound **1**, U_{iso}(H) was constrained to be 1.2 U_{eq}(C) for all protons. For **3** and **4**, U_{iso}(H) was constrained to be 1.2 U_{eq}(C) for all aromatic protons and 1.5 U_{eq}(C) for all methyl protons.

The crystals of **2** diffracted very poorly, and data could be obtained only to a maximum diffraction angle of 22º using Mo radiation. The unit cell had three angles near 90º with cell edges of 14.342, 18.200 and 20.442 Å. Systematic absences suggested $P2_12_12_1$ or $P2_12_12$, but neither SIR97[19] nor SHELXS97[20] could find a solution in either of these space groups. The data were processed as triclinic and solved with SIR97[19] to give an eight molecule solution, and refined using SHELXL97[20] using rigid models of the Al analolgue of **2**[4] to complete the molecules. The eight molecules were examined using Platon[21] and conversion to $P2_1$ was suggested. In $P2_1$ the asymmetric unit had four molecules. All atoms were refined isotropically with no constraints, and the structures of the four molecules were maintained. The Ga, Fe, and Si atoms were then refined anisotropically. The number of data did not allow all atoms to be refined anisotropically, but H atoms were placed in calculated positions with U_{iso} constrained to be 1.2 times U_{eq} of the carrier atom for aromatic protons and 1.5 times U_{eq} of the carrier atoms for methyl hydrogen atoms. The R value refined to 0.143. All four molecules maintained their

geometry. No further symmetry elements could be identified. The angles between the cyclopentadienyl rings for the four molecules are 13.6(2.1), 15.0(1.6), 15.4(1.9), and 18.8(1.8)º for an average of 15.7º. An ORTEP diagram of one of the molecules is shown in Figure 4-3. The data does not give a complete crystal structure of **2** with accurate bond lengths and bond angles, but they do determine the arrangement of the atoms of **2**.

Acknowledgement. We thank the Natural Sciences and Engineering Research Council of Canada (NSERC Discovery Grant, J.M.), the Department of Chemistry, the Saskatchewan Structural Sciences Centre, and the University of Saskatchewan for their generous support.

Supporting Information Available. Crystallographic data for **1**, **3**, and **4** in CIF file format. This material is available free of charge via the Internet at http://pubs.acs.org.

4.6 References

(1) Osborne, A. G.; Whiteley, R. H. *J. Organomet. Chem*. **1975**, *101*, C27-C28.
(2) Nguyen, P.; Gómez-Elipe, P.; Manners, I. *Chem. Rev.* **1999**, *99*, 1515-1548.
(3) (a) Braunschweig, H.; Dirk, R.; Müller, M.; Nguyen, P.; Resendes, R.; Gates, D. P.; Manners, I. *Angew. Chem., Int. Ed. Engl.* **1997**, *36*, 2338-2340. (b) Berenbaum, A.; Braunschweig, H.; Dirk, R.; Englert, U.; Green, J. C.; Jäkle, F.; Lough, A. J.; Manners, I. *J. Am. Chem. Soc. 2000*, 122, 5765-5774.
(4) Schachner, J. A.; Lund, C. L.; Quail, J. W.; Müller, J. *Organometallics* **2005**, *24*, 785-787.
(5) Al-Juaid, S. S.; Eaborn, C.; Hitchcock, P. B.; Hill, M. S.; Smith, J. D. *Organometallics* **2000**, *19*, 3224-3231.
(6) (a) Eaborn, C.; Hill M. S.; Hitchcock P. B.; Smith J. D. *J. Chem. Soc., Chem. Commun.* **2000**, 691-692. (b) Al-Juaid, S. S.; Avent A. G.; Eaborn, C.; El-Hamruni, S. M.; Hawkes, S. A.; Hill, M. S.; Hitchcock, P. B.; Smith, J. D. *J. Organomet. Chem.* **2001**, *631*, 76-86. (c) Al-Juaid, S. S.; Avent A. G.; Eaborn, C.; Hill, M. S.; Hitchcock, P. B.; Patel, D. J.; Smith, J. D. *Organometallics* **2001**, *20*, 1223-1229. (d) Eaborn, C.; Hill, M. S.; Hitchcock, P. B.; Smith, J. D. *J. Chem. Soc., Dalton Trans.* **2002**, 2467-2472.
(7) Scheibitz, M.; Winter, R. F.; Bolte, M.; Lerner, H-W.; Wagner, M. *Angew. Chem., Int. Ed. Engl.* **2003**, *42*, 924-927.
(8) (a) Uhl, W.; Hahn, I.; Jantschak, A.; Spies, T. *J. Organomet. Chem.* **2001**, *637*, 300-303. (b) Althoff, A.; Jutzi, P.; Lenze, N.; Neumann, B.; Stammler, A.; Stammler, H-G. *Organometallics* **2002**, *21*, 3018-3022. (c) Jutzi, P.; Lenze, N.; Neumann, B.; Stammler, H-G.

Angew. Chem., Int. Ed. Engl. **2001**, *40*, 1424-1427. (d) , A.; Jutzi, P.; Lenze, N.; Neumann, B.; Stammler, A.; Stammler, H-G. *Organometallics* **2003**, *22*, 2766-2774.
(9) Schachner, J. A.; Lund, C. L.; Quail, J. W.; Müller, *J. Acta Crystallogr.* **2005**, *E61*, m682-m684.
(10) Howson, J.; Eaborn, C.; Hitchcock, P. B.; Hill, M. S.; Smith, J. D. *J. Organomet. Chem*. **2005**, *690*, 69-75.
(11) Rulkens, R.; Gates, D. P.; Balaishis, D.; Pudelski, J. K.; McIntosh, D. F.; Lough, A. J.; Manners, I. *J. Am. Chem. Soc.* **1997**, *119*, 10976-10986.
(12) Pudelski, J. K.; Gates, D. P.; Rulkens, R.; Lough, A. J.; Manners, I. *Angew. Chem., Int. Ed. Engl.* **1995**, *43*, 1506-1508.
(13) Jäkle, F.; Rulkens, R.; Zech, G.; Foucher, D. A.; Lough, A. J.; Manners, I. *Chem., Eur. J.* **1998**, *4*, 2117-2128, and references therein.
(14) Jastrzebski, J. T. B. H.; van Koten, G.; Tuck, D. G.; Meinema, H. A.; Noltes, J. G. *Organometallics* **1982**, *1*, 1492-1495.
(15) online version of the IUPAC Compendium of Chemical Terminology (www.iupac.org/publications/compendium/)
(16) Butler, I. R.; Cullen, W. R.; Ni, J.; Rettig, S. J. *Organometallics* **1985**, *4*, 2196-2201.
(17) Nonius; Nonius BV, Delft, The Netherlands, **1998**.
(18) Otwinowski, Z.; Minor, W. In *Macromolecular Crystallography, Part A*; Carter, C. W., Sweet, R. M., Eds.; Academic Press: London, **1997**; Vol. 276, pp 307-326.
(19) Altomare, A.; Burla, M. C.; Camalli, M.; Cascarano, G.; Giacovazzo, C.; Guagliardi, A.; Moliterni, A. G. G.; Polidori, G.; Spagna, R. *J. Appl. Crystallogr.* **1999**, *32*, 115-119.
(20) Sheldrick, G. M.; *SHELXS97 and SHELXL97*, University of Göttingen, Germany, 1997.
(21) Spek, A. L.; *PLATON, A Multipurpose Crystallographic Tool*, University of Utrecht, The Netherlands, 2003.

CHAPTER 5
PUBLICATION 4

Description

The following chapter is a verbatim copy of an electronic communication which was published in *Acta Crystallographica Section E*[*] in September 2005[†] and describes the synthesis and characterization of the monomeric compound (Pytsi)InI_2 (**2**).

Author Contributions

My contribution to this publication was the synthesis and characterization of the title compound. The coauthors on this paper are Jörg A. Schachner, who helped with the synthesis of starting materials and made the suggestion to synthesize the title compound, J. Wilson Quail, who performed the single-crystal X-ray analysis, and my supervisor Jens Müller. Written permission was obtained from all contributing authors to include material within this thesis.

Relation of Publication 4 to the Objectives of this Project

As described in publication 3 (Chapter 4), (Pytsi)$InCl_2$ is a dimer in the solid state and it seemed that in reactions with dilithioferrocene the dimeric nature was preserved. Based on these results it was believed that a monomeric starting compound of the type (Pytsi)EX_2 might open an alley toward the targeted strained [1]FCPs. As expected, the diiodide **2** is a monomer, but,

[*] Reproduced with permission of the International Union of Crystallography © 2005, http://journals.iucr.org/
[†] Lund, C. L.; Schachner, J. A.; Quail, J. W.; Müller, J. *Acta Crystallogr., Sect. E: Struct. Rep. Online* **2005**, *61*, m2063-m2065.

unexpectedly, it could not be used to produce [1]metallacyclophanes under various experimental conditions.

5. A Monomeric Four-fold Coordinated Indium Dihalide with an Unusual Coordination Geometry

Clinton L. Lund,[‡] Jörg A. Schachner,[‡] J. Wilson Quail,[§] and Jens Müller[‡*]

[‡]*Department of Chemistry, University of Saskatchewan, 110 Science Place, Saskatoon, Saskatchewan, Canada, S7N 5C9,* [§]*Saskatchewan Structural Sciences Centre, University of Saskatchewan, 110 Science Place, Saskatoon, Saskatchewan, Canada, S7N 5C9*

Received July 22, 2005

The single-crystal X-ray analysis of the title compound,{[dimethyl(2-pyridyl)silyl]bis(trimethylsilyl)methyl}diiodoindium(III), $[In(C_{14}H_{28}NSi_3)I_2]$, revealed monomeric molecules containing tetracoordinated In with an unusual trigonal–pyramidal geometry.

5.1 Comment

We recently synthesized the first [1]alumina- and [1]gallaferrocenophanes (Scheme 5-1).[1,2] We intended to use a similar procedure to prepare a hitherto unknown [1]indaferrocenophane and synthesized the starting material, (Pytsi)$InCl_2$, (I) [Pytsi = $C(SiMe_3)_2SiMe_2(C_5H_4N\text{-}2)$].[2] In contrast with the respective dichlorides of aluminium and gallium (Scheme 5-1), indane (I) is a chloro-bridged dimer in the solid state (Scheme 5-2). Compound (I) reacted with dilithioferrocene, but did not give the targeted [1]ferrocenophane. Instead, an unusual ferrocene derivative could be isolated, in which the two Cp ligands were bridged by an $In(\mu\text{-}Cl)_2In$ group (Scheme 5-2). This result might suggest that a monomeric indium dihalide is needed for the synthesis of the target [1]indaferrocenophane.

Scheme 5-1. Synthesis of (Pytsi)Al[1]FCP and (Pytsi)Ga[1]FCP.

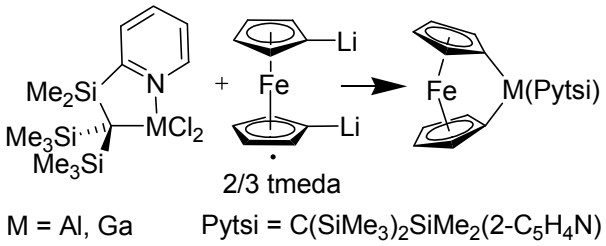

Scheme 5-2. Synthesis of an indium-bridged ferrocenophane.

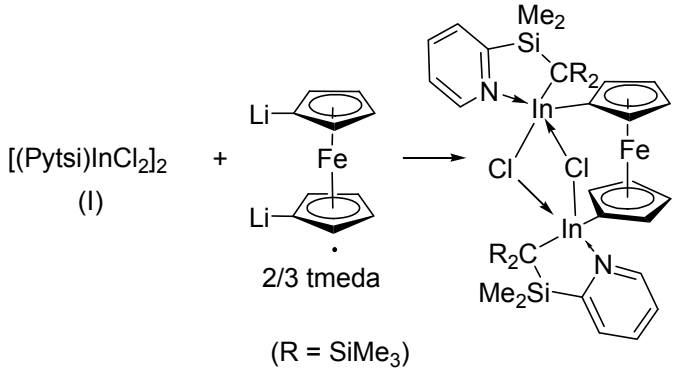

Reaction of InI_3 with Li(thf)(Pytsi) (thf is tetrahydrofuran) in a 1:1 ratio resulted in (Pytsi)InI_2, (II), in a moderate isolated yield of 56%. In contrast with the dichloride, (I), the title compound, (II), crystallizes as a monomer (Figure 5-1).

The In atom in compound (II) is four-fold coordinated by atoms I1, I2, C7 and N1. The In1/I1/I2/C7 subset can be described as a trigonal pyramid, with atom In1 at the centre of the trigonal base and atom N1 at the apex. The sum of the three angles I1–In1–I2, C7–In1–I1 and C7–In1–I2 is 356.4°, which is only a few degrees away from an idealized planar coordination. At first glance, the coordination of the In centre looks like that of a trigonal–bipyramid with one apical position unoccupied. A close inspection of the packing of the molecules shows an I atom at a distance of 4.3421 (4) Å, approximately along the axis of the trigonal pyramid, with the N1–

In1–I1^{i} angle being 165.79 (11)° [symmetry code: (i) – x,1 – y, –z]. The In1–I1^{i} distance is ~ 0.4 Å greater than the sum of the usually accepted van derWaals radii, which are 1.93 and 1.96 Å, respectively.[3]

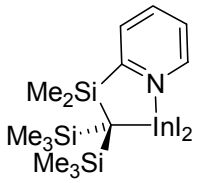

(II)

Compound (II) is an example of a structurally characterized indium dihalide species with only four-fold coordinated In atoms in monomeric molecules. A search of the Cambridge Structural Database[4] for indium dihalides with at least one In–C or one In–N bond revealed that several species with four-fold coordination[5-22] and one species with three-fold coordination are known[23, 24]. However, all known species with tetracoordination exhibit In in a tetrahedral environment. From the study of Lewis acid–base adducts, it is known that the pyramidalization of the Lewis acid moiety becomes more pronounced with increasing donor bond strength.[25, 26] If this effect were to be of importance in species (II), then the nearly planar I_2InC group would suggest a very weak In–N donor interaction. The weakness of the bond should be evident in an unusually long In–N bond. However, the known indium dichloride (η^1-$Me_4C_5CH_2CH_2NMe_2$)$InCl_2$, in which the In atom shows a similar set of coordinated atoms to those in compound (II), exhibits tetrahedrally surrounded In atoms, with an In–N bond length of 2.265(5) Å.[11]. Within the standard uncertainty, the In–N distance in compound (II) is the same (Table 5-1).

We can only speculate that the unusual coordination geometry of In in compound (II) results mainly from steric crowding in the vicinity of In. It may be that the large I atoms and two

bulky $SiMe_3$ groups do not allow for a pyramidalization of the Lewis acid moiety. To the best of our knowledge, compound (II) is the first indium dihalide with such an unusual coordination polyhedron (Figure 1).

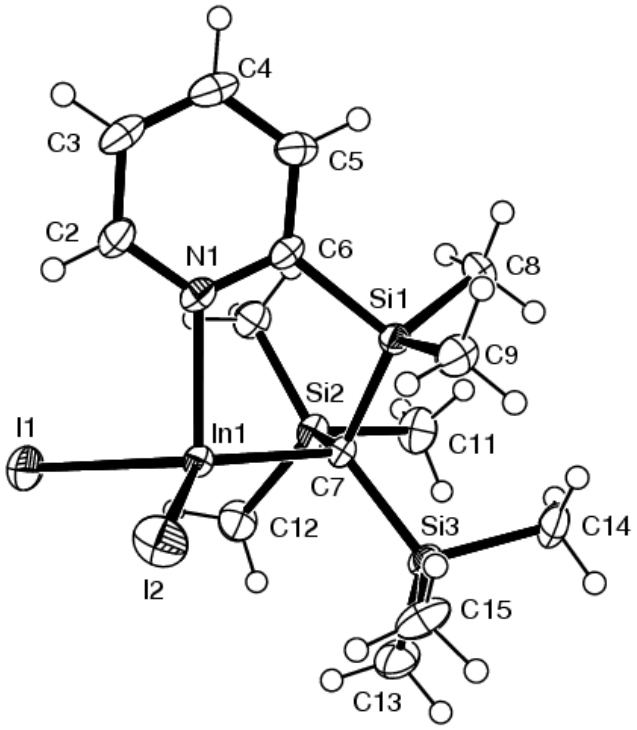

Figure 5-1. A view of the molecule of (Pytsi)InI_2 (**II**), with displacement ellipsoids drawn at the 50% probability level.

5.2 Experimental

InI_3 (1.642 g, 3.31 mmol) in tetrahydrofuran (thf; 25 mL) at 195 K was added to Li(thf)(Pytsi)[27] in thf (10 mL) at 195 K, resulting in a green solution. The solution was stirred for 1 h at 195 K before being allowed to warm to room temperature. After the mixture had been stirred for an additional 16 h, all volatiles were removed in vacuo and a green solid was left behind. This crude product was washed with diethyl ether (3 × 15 mL) and the washings were

combined and filtered. Subsequently, the solvent was removed in vacuo and the remaining solid was heated to 373 K under vacuum to remove unreacted starting materials by a flask-to-flask condensation. Diethyl ether (10 mL) was added to the remaining solid, and the resulting solution was filtered and finally kept at 248 K to afford (II) (1.237 g, 56%). Spectroscopic analysis: ^{1}H NMR (500 MHz, C_6D_6, 298 K, δ, p.p.m.): 0.26 (18H, s,$SiMe_3$), 0.36 (6H, s, $SiMe_2$), 6.32 (1H, pst, 5-H), 6.72 (1H, pst, 4-H), 6.79 (1H, d, J = 7.6 Hz, 3-H), 8.46 (1H, d, J = 5.4 Hz, 6-H); ^{13}C NMR: 3.97 ($SiMe_2$), 6.55 ($SiMe_3$), 125.50 (5-C), 129.48 (3-C), 138.83 (4-C), 147.81 (6-C), 169.32 (*ipso*-C); MS: m/z = 536 (100) $[C_{14}H_{28}IInNSi_3]^+$, 264 (85) $[C_{12}H_{22}NSi_3]^+$. Anal. Calcd for $C_{14}H_{28}NSi_3InI_2$ (663.272): C, 25.35; H, 4.26; N, 2.11. Found: C, 25.19; H, 4.51; N, 2.06.

Crystal data	
$[In(C_{14}H_{28}NSi_3)I_2]$	$D_x = 1.929$ mg m^{-3}
$M_r = 663.26$	Mo *K*α radiation
Monoclinic $P2_1/c$	Cell parameters from 8085
a = 9.9492 (1) Å	reflections
b = 13.6254 (2) Å	θ = 1.0–32.0°
c = 18.9012 (3) Å	μ = 3.89 mm^{-1}
β = 116.972 (1)°	T = 173 (2) K
V = 2283.58 (6) Å^3	Block, colourless
Z = 4	0.20 × 0.20 × 0.12 mm

Data collection	
Nonius KappaCCD diffractometer	6166 reflections with I >2σ(I)
	$R_{int} = 0.031$,
φ scans, and ω scans with κ offsets	$\theta_{max} = 32.0$
Absorption correction: none	h = –14 → 14
14706 measured reflections	k = –18 → 20
7936 independent reflections	l = –28 → 28

Refinement	
Refinement on F^2	$w = 1/[\sigma^2 (F_0^2) + (0.0364P)^2 + 7.7352P]$
$R[F^2 > 2\sigma(F^2)] = 0.041$	where $P = (F_0^2 + 2F_c^2)/3$
$wR(F^2) = 0.104$	$(\Delta/\sigma)_{max} < 0.001$
$S = 1.06$	$\Delta\rho_{max} = 1.75$ e Å^{-3}
7936 reflections	$\Delta\rho_{min} = -2.16$ e Å^{-3}
198 parameters	
H-atom parameters constrained	

Table 5-1. Selected geometric parameters for (Pytsi)InI_2 (**II**) (Å,°).

In1–I1	2.712 (4)	In1–C7	2.207 (3)
In1–I2	2.6891 (4)	In1–I1^{i}	4.3421 (4)
In1–N1	2.270 (3)	I1–In1–I2	103.958 (14)
N1–In1–C7	91.00 (12)	C7–In1–I1	127.91 (9)
N1–In1–I2	102.26 (8)	C7–In1–I2	124.57 (9)
N1–In1–I1	96.56 (9)		
N1–In1–I1^{i}	165.79 (11)		

Symmetry code: (i) –x, –y + 1, –z

H atoms were placed in calculated positions, with C–H distances ranging from 0.95 to 0.99 Å, and included in the refinement in the riding-model approximation, with U_{iso}(H) values constrained to be 1.2 U_{eq}(C) for all aromatic H atoms and 1.5U_{eq}(C) for all methyl H atoms. The highest peak was located 0.40 Å from In1 and the deepest hole 0.57 Å from In.

Data collection: COLLECT[28]; cell refinement: SCALEPACK[29]; data reduction: SCALEPACK and DENZO[29]; program(s) used to solve structure: SIR97[30]; program(s) used to refine structure: SHELXL97[31]; molecular graphics: ORTEP-3 for Windows[32]; software used to prepare material for publication: PLATON[33].

We thank the Natural Sciences and Engineering Research Council of Canada (NSERC Discovery Grant for JM), the Department of Chemistry and the University of Saskatchewan for their generous support. The authors also thank the Canadian Foundation for Innovation and the

Government of Saskatchewan for funding of the X-ray laboratory of the Saskatchewan Structural Sciences Centre.

5.3 References

(1) Schachner, J. A.; Lund, C. L.; Quail, J. W.; Müller, J. *Organometallics* **2005**, *24*, 785-787.
(2) Schachner, J. A.; Lund, C. L.; Quail, J. W.; Müller, J. *Organometallics* **2005**, *24*, 4483-4488.
(3) Bondi, A. *J. Phys. Chem.* **1964**, *68*, 441-451.
(4) Allen, F. H. *Acta Cryst. B* **2002**, *58*, 380-388.
(5) Veith, M.; Recktenwald, O. *J. Organomet. Chem.* **1984**, *264*, 19-27.
(6) Veith, M.; Goffing, F.; Becker, S.; Huch, V. *J. Organomet. Chem.* **1991**, *406*, 105-118.
(7) Annan, T. A.; Tuck, D. G.; Khan, M. A.; Peppe, C. *Organometallics* **1991**, *10*, 2159-2166.
(8) de Souza, A. C.; Peppe, C.; Tian, Z. G.; Tuck, D. G. *Organometallics* **1993**, *12*, 3354-3357.
(9) Cowley, A. H.; King, C. S.; Decken, A. *Organometallics* **1995**, *14*, 20-23.
(10) Fischer, R. A.; Nlate, S.; Hoffman, H.; Herdtweck, E.; Blumel, J. *Organometallics* **1996**, *15*, 5746-5752.
(11) Jutzi, P.; Dahlhaus, J.; Neumann, B.; Stammler, H.-G. *Organometallics* **1996**, *15*, 747-752.
(12) Black, S. J.; Hibbs, D. E.; Hursthouse, M. B.; Jones, C.; Kloth, M. *J. Chem. Soc., Dalton Trans.* **1997**, 4313-4319.
(13) Delpech, F.; Guzei, I. A.; Jordan, R. F. *Organometallics* **2002**, *21*, 1167-1176.
(14) Kuhner, S.; Hausen, H. D.; Weidlein, J. *Z. Anorg. Allg. Chem.* **1998**, *624*, 13-14.
(15) Abernethy, C. D.; Cole, M. L.; Jones, C. *Organometallics* **2000**, *19*, 4852-4857.
(16) Felix, L. D.; de Oliveira, C. A. F.; Kross, R. K.; Peppe, C.; Brown, M. A.; Tuck, D. G.; Hernandes, M. Z.; Longo, E.; Sensato, F. R. *J. Organomet. Chem.* **2000**, *603*, 203-212.
(17) Stender, M.; Eichler, B. E.; Hardman, N. J.; Power, P. P.; Prust, J.; Noltemeyer, M.; Roesky, H. W. *Inorg. Chem.* **2001**, *40*, 2794-2799.
(18) Peppe, C.; Nobrega, J. A.; Hernandes, M. Z.; Longo, R. L.; Tuck, D. G. *J. Organomet. Chem.* **2001**, *626*, 68.
(19) Cheng, Q. M.; Stark, O.; Merz, K.; Winter, M.; Fischer, R. A. *J. Chem. Soc., Dalton Trans.* **2002**, 2933-2936.
(20) Baker, R. J.; Davies, A. J.; Jones, C.; Kloth, M. *J. Organomet. Chem.* **2002**, *656*, 203-210.
(21) Schulte, M.; Gabbai, F. P. *Chem.—Eur. J.* **2002**, *8*, 3802-3807.
(22) Bock, B.; Braun, U.; Habereder, T.; Mayer, P.; Nöth, H. *Z. Naturforsch. Teil. B.* **2004**, *59*, 681-684.
(23) Schulz, S.; Pusch, S.; Pohl, E.; Dielkus, S.; Herbstirmer, R.; Meller, A.; Roesky, H. W. *Inorg. Chem.* **1993**, *32*, 3343-3346.

(24) Petrie, M. A.; Power, P. P.; Dias, H. V. R.; Ruhlandt-Senge, K.; Waggoner, K. M.; Wehmschulte, R. J. *Organometallics* **1993**, *12*, 1086-1093.
(25) Jiao, H.; von Ragué Schleyer, P. *J. Am. Chem. Soc.* **1994**, *116*, 7429-7430.
(26) Jonas, V.; Frenking, G.; Reetz, M. T. *J. Am. Chem. Soc.* **1994**, *116*, 8741.
(27) Al-Juaid, S. S.; Eaborn, C.; Hitchcock, P. B.; Hill, M. S.; Smith, J. D. *Organometallics* **2000**, *19*, 3224-3231.
(28) *Nonius*; Nonius BV Delft, The Netherlands,1998.
(29) Otwinowski, Z.; Minor, W. *Macromolecular Crystallography, Part A*; Academic Press: New York, 1997; Vol. 276, 307-326.
(30) Altomare, A.; Burla, M. C.; Camalli, M.; Cascarano, G. L.; Giacovazzo, C.; Guagliardi, A.; Moliterni, A. G. G.; Polidori, G.; Spagna, R. *J. Appl. Crystallogr.* **1999**, *32*, 115-119.
(31) Sheldrick, G. M. *SHELXL-97*; University of Göttingen: Göttingen, Germany,1997.
(32) Farrugia, L. J. *J. Appl. Crystallogr.* **1997**, *30*, 565.
(33) Spek, A. L. *J. Appl. Crystallogr.* **2003**, *36*, 7-13.

CHAPTER 6
PUBLICATION 5

Description

The following chapter is a verbatim copy of an article which was published in *Organometallics*[*] in August 2006[†] and describes the synthesis of the first aluminum- and gallium-bridged [1]CAPs (**5a**, **5b**) and [1]VAPs (**6a**, **6b**) and an improved synthesis of [1]ferrocenophanes; all compounds are equipped with the Me_2Ntsi ligand [Me_2Ntsi = $C(SiMe_3)_2(SiMe_2NMe_2)$]. In addition, the aluminum dichloride compound (**2a**) that incorporates the new *trisyl*-based ligand Me_2NCH_2tsi [Me_2NCH_2tsi = $–C(SiMe_3)_2(SiMe_2CH_2NMe_2)$] was synthesized.

Author Contributions

My contributions to this publication were the synthesis and characterization of the first aluminum- and gallium-bridged [1]CAPs (**5a**, **5b**) and [1]VAPs (**6a**, **6b**) and the preparation of a new dichloro aluminum compound (Me_2NCH_2tsi)$AlCl_2$ (**2a**). The coauthors on this paper are Jörg A. Schachner, who synthesized the aluminum- and gallium-bridged [1]ferrocenophanes, J. Wilson Quail, who performed all single-crystal X-ray analyses, and my supervisor Jens Müller. Written permission was obtained from all contributing authors to include material within this thesis.

[*] Reproduced with permission from Organometallics © 2006 American Chemical Society
[†] Lund, C. L.; Schachner, J. A.; Quail, J. W.; Müller, J. *Organometallics* **2006**, *25*, 5817-5823.

Relation of Publication 5 to the Objectives of this Project

After months of preparing compounds of the type (Pytsi)EX_2, and employing these species in salt metathesis reactions with dilithiobis(benzene)chromium unsuccessfully, I turned my attention to Me_2Ntsi ligand. This ligand required the same starting material, $HC(SiMe_3)_2(SiMe_2Br)$, that was used in the synthesis of the Pytsi ligand, but overall required fewer synthetic steps. In addition, the compounds (Me_2Ntsi)$AlCl_2$ (**3a**) and (Me_2Ntsi)$GaCl_2$ (**3b**) were known in the literature,[‡] which made their preparation straightforward.

Through salt-metathesis reactions of **3a** or **3b** with $[M(C_6H_5Li)_2]$·tmeda (M = Cr, V), I was able to prepare and isolate the first aluminum- and gallium-bridged [1]CAPs (**5a**, **5b**) and [1]VAPs (**6a**, **6b**). Thus, the stated primary objective of this thesis had been satisfied (Chapter 1.6).

Also, included in this chapter is the synthesis and characterization of compound (Me_2NCH_2tsi)$AlCl_2$ (**2a**). This compound was targeted because it possesses a five-membered heterocycle, similar to five-membered heterocycle in the Pytsi ligand, and the dimethylamino donor like in the Me_2Ntsi ligand. It was envisioned that this compound could be used to produce [1]metallacyclophanes. Surprisingly though, **2a** does not react with dilithium sandwich complexes, for unknown reasons. The results in publication 5 show that 'ligand fine-tuning' is of utmost importance; however, the tuning is often based on trial-and-error.

[‡] Al-Juaid, S. S.; Eaborn, C.; El-Hamruni, S. M.; Hitchcock, P. B.; Smith, J. D. *Organometallics* **1999**, *18*, 45-52.

6. [1]Ferrocenophanes, [1]Chromarenophanes, and [1]Vanadarenophanes with Aluminium and Gallium in Bridging Positions

Clinton L. Lund,[‡] Jörg A. Schachner,[‡] J. Wilson Quail,[§] Jens Müller[‡*]

[‡]*Department of Chemistry, University of Saskatchewan, 110 Science Place, Saskatoon, Saskatchewan, Canada, S7N 5C9,* [§]*Saskatchewan Structural Sciences Centre, University of Saskatchewan, 110 Science Place, Saskatoon, Saskatchewan, Canada, S7N 5C9*

Received August 14, 2006

6.1 Abstract

Aluminium- and gallium-bridged [1]ferrocenophanes (**4a**, **4b**), [1]chromarenophanes (**5a**, **5b**), and [1]vanadarenophanes (**6a**, **6b**) were synthesized from the respective dilithiated sandwich compounds with element dichlorides $(Me_2Ntsi)ECl_2$ [E = Al, Ga; Me_2Ntsi = $C(SiMe_3)_2(SiMe_2NMe_2)$] in moderate to high isolated yields (54–97%). The new intramolecularly stabilized aluminum compound $(Me_2NCH_2tsi)AlCl_2$ (**2a**) was synthesized, but was proven to be unreactive with respect to $[Fe(LiC_5H_4)_2]\cdot 2/3$ tmeda. The diamagnetic species **2a**, **4a**, **4b**, **5a**, and **5b** were characterized by NMR spectroscopy (^1H, ^{13}C, ^{27}Al), CHN elemental analysis, and mass spectrometry, whereas the paramagnetic compounds **6a** and **6b** were characterized by IR spectroscopy, CHN elemental analysis, and mass spectrometry. In addition, the molecular structures of compounds **2a**, **4a**, **4b**, **5a**, **5b**, **6a**, and **6b** were determined by single-crystal X-ray analysis. All [1]cyclophanes are strained species as revealed by the following tilt angles α [°]: 14.33(14) (**4a**), 15.83(19) (**4b**), 11.81(9) (**5a**), 13.24(13) (**5b**), 14.65(14) (**6a**), and 15.63(14) (**6b**).

6.2 Introduction

Since their discovery in 1975 by Osborne and Whiteley,[1] strained [1]ferrocenophanes containing main-group elements in the bridging position have sparked a lot of interest throughout the scientific community. Manners *et al*. showed that [1]ferrocenophanes ([1]FCPs) produce high molecular weight polyferrocenes via ring-opening polymerization (ROP).[2] Because of the incorporation of metals into the backbone of the polymer chain, these materials show interesting new properties (e.g., redox, magnetic, electrical, and chemical).[3–5] Over the last two decades, new [1]ferrocenophanes with bridging elements ranging from group-13 to 16 were synthesized and their use for polymer synthesis was explored.[6] However, group-13 [1]ferrocenophane chemistry was restricted to boron.[7–9]

Recently, by reactions of intramolecularly coordinated element dichlorides (Pytsi)ECl_2 [E = Al, Ga; Pytsi = $C(SiMe_3)_2SiMe_2(2\text{-}C_5H_4N)$] with dilithioferrocene, we isolated the first alumina[1]ferrocenophane (Al[1]FCP)[10] and the first galla[1]ferrocenophane (Ga[1]FCP)[11] (Figure 6-1).

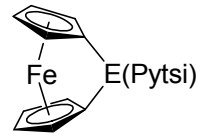

E = Al (**1a**), Ga (**1b**)

Figure 6-1. Al- and Ga[1]FCP [Pytsi = $C(SiMe_3)_2SiMe_2(2\text{-}C_5H_4N)$].

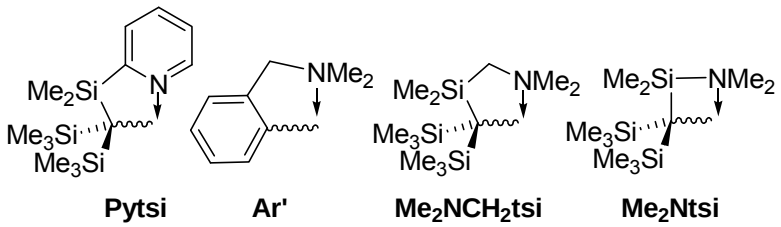

Figure 6-2. Intramolecularly coordinating ligands.

The Pytsi ligand, derived from the well-known *trisyl* ligand $C(SiMe_3)_3$ by a formal substitution of one methyl group with a pyridyl ring, provides intramolecular coordination via the pyridyl moiety and steric shielding through the trimethylsilyl groups (Figure 6-2).[12]

In order to use strained [1]FCP as monomers for ROP, ideally, they should be accessible in high yields and high purities. In light of these requirements, the preparations of the Al[1]FCP **1a** and the Ga[1]FCP **1b** were unsatisfactory (Figure 6-1); yields were low to moderate and significant amounts of ferrocene were always produced during the synthesis. The aluminum compound **1a** (Figure 6-1) even crystallized with half of a molecule of $FeCp_2$ in the asymmetric unit.[10] Consequently, we focused our attention on improving the synthesis of Al- and Ga[1]FCPs by altering the ligand that remains attached at the bridging element. Furthermore, we started to explore the possibilities of using intramolecularly coordinated alanes and gallanes for the synthesis of strained [1]metallarenophanes. Our first results are described in this paper.

6.3 Results and Discussion

If the popular "one-armed phenyl" ligand (Ar′ , Figure 6-2) is applied instead of the Pytsi ligand, [1.1]FCPs are produced exclusively (E = Al,[13,14] Ga,[14] In[14]). In our first attempt to improve the synthesis of an Al[1]FCP, we formally replaced the pyridyl donor of the Pytsi ligand by the saturated CH_2NMe_2 "arm" of the Ar′ ligand (Figure 6-2). By adapting known procedures, we synthesized the aluminum compound $(Me_2NCH_2tsi)AlCl_2$ (**2a**) (see Experimental Section for details). As expected, the molecular structure of compound **2a** reveals no surprises (Figure 6-3).

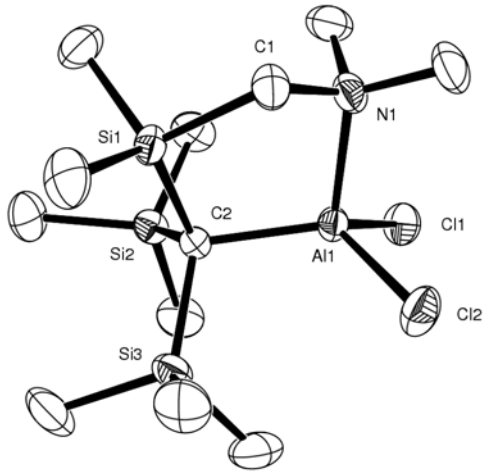

Figure 6-3. Molecular structure of $(Me_2NCH_2tsi)AlCl_2$ (**2a**) with thermal ellipsoids at the 50% probability level. H atoms are omitted for clarity. Selected bond lengths [Å] and angles [°]: Al1–N1 = 1.9783(12), Al1–C2 = 1.9805(13), Al1–Cl1 = 2.1501(5), Al1–Cl2 = 2.1661(5), N1–Al1–C2 = 103.80(5), N1–Al1–Cl1 = 106.42(4), N1–Al1–Cl2 = 100.24(4), C2–Al1–Cl1 = 119.03(4), C2–Al1–Cl2 = 117.37(4).

The Al atom in **2a** is similarly coordinated to that in the known compound $(Pytsi)AlCl_2$.[15] For both species, the central metal atom is surrounded by C-, N-, and two Cl atoms with bond lengths of 1.9783(12) Å (Al–N), 1.9805(13) Å (Al–C), 2.1501(5) Å (Al–Cl), and 2.1661(5) Å (Al–Cl) for compound **2a** (Figure 6-3) compared with 1.9383(16) Å (Al–N), 1.9784(19) Å (Al–C), 2.1295(8) Å (Al–Cl), and 2.1529(8) Å (Al–Cl) for $(Pytsi)AlCl_2$.[15] For both species, the set of four atoms around the Al atom form a similarly distorted tetrahedron. On the basis of this comparison, we expected a similar reactivity of **2a** relative to $(Pytsi)AlCl_2$. However, reaction of **2a** with dilithioferrocene, under similar conditions to those we applied for the syntheses of the [1]FCPs **1a** and **1b**,[10,11] revealed that the dichloride **2a** was significantly less reactive than $(Pytsi)AlCl_2$. ^1H NMR spectra taken from the reaction mixtures showed only small peaks in the typical range for Cp groups, indicating the presence of substituted ferrocenes; ca. 90% of the

dichloride **2a** was still present in solution. None of the ^{1}H NMR signals indicated the presence of the targeted Al[1]FCP.

A drastic change in reactivity can be observed if, instead of Me_2NCH_2tsi ligand, the shorter Me_2Ntsi is employed (Figure 6-2). Alanes and gallanes of the type $(Me_2Ntsi)ECl_2$ were already synthesized by Eaborn and Smith *et al.*[16] Reaction of $(Me_2Ntsi)AlCl_2$ (**3a**) with dilithioferrocene gave the new Al[1]FCP **4a** in an isolated yield of 97% (Scheme 6-1). Similarly, we synthesized the Ga[1]FCP **4b**. Encouraged by these results, we were able to synthesize the first aluminum- and gallium-bridged [1]chromarenophanes (**5a,b**) and the respective vanadium compounds (**6a,b**; Scheme 6-1).

Scheme 6-1. Synthesis of aluminum- and gallium-bridged [1]metallacyclophanes.

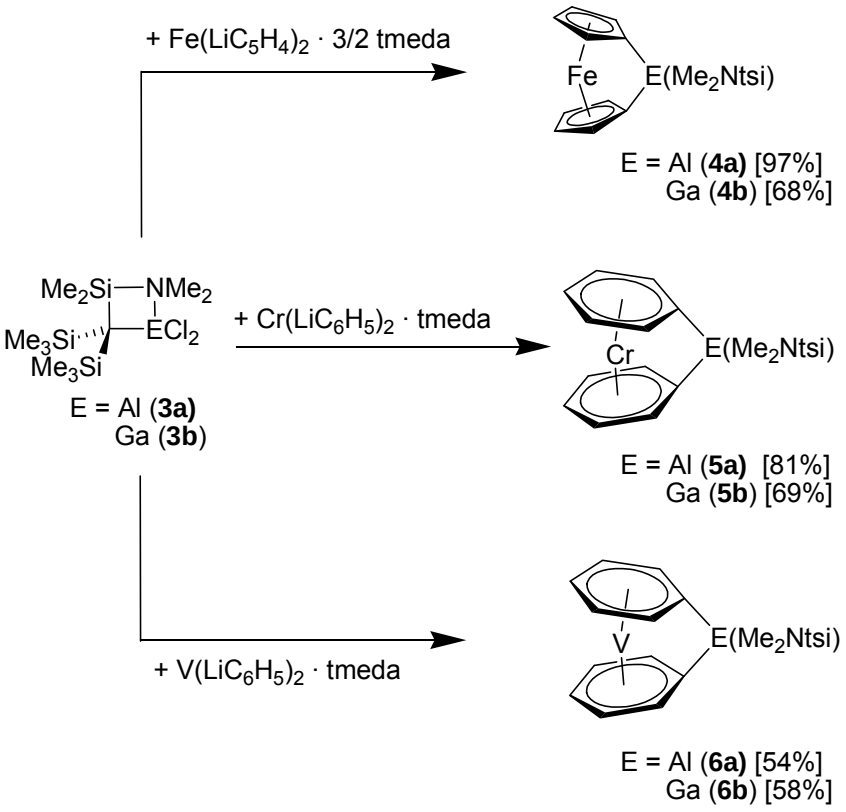

6.3.1 [1]Ferrocenophanes.

Compounds **4a** and **4b** both show signal patterns in the ^{1}H- and ^{13}C NMR spectra that can be interpreted as being caused by [1]FCPs with time-averaged C_s symmetry. For example, the ^{1}H NMR spectrum of **4a** shows three pseudo triplets for the C_5H_4 rings with a 1:1:2 intensity ratio at δ 3.76 (α-H), 4.24 (α-H), and 4.58 (β-H). This signal pattern is similar to that of the Pytsi species **1a**,[10] except for the fact that the splitting of the β-protons in **4a** is so small that their signals overlap. The most indicative spectroscopic data to prove that indeed strained [1]FCPs were formed comes from ^{13}C NMR spectroscopy. The signal of the *ipso*-C atoms of the cyclopentadienyl ligands should be shifted upfield with respect to that of the $FeCp_2$ (δ 68). The detected shifts for **4a** (δ 53.0) and **4b** (δ 47.3) match very well with those of the [1]FCPs **1a** (δ = 52.9)[10] and **1b** (δ 47.2).[11]

The new [1]FCPs **4a** and **4b** are isostructural and crystallized with half of a molecule of C_6H_6 in the asymmetric unit (Table 6-1); the molecular structure of the aluminum species **4a** is depicted in Figure 6-4 (ORTEP plot of **4b** see Supporting Information).

In both cases, the bridging element is part of a planar, four-membered ring [rms deviations from planarity [Å] are: 0.0074 (**4a**), 0.0068 (**4b**)] and surrounded by one N atom and three C atoms. As expected, the E–C bonds are very similar for both species [Al1–C1 2.000(2), Al1–C6 1.988(2), Al1–C11 2.0301(19) Å, for **4a**; Ga1–C1 2.008(3), Ga1–C6 2.017(3), Ga1–C11 2.048(3) Å for **4b**] and the E–N bonds are significantly different [Al1–N1 2.0123(17) and Ga1–N1 2.105(2) Å]. The extent of strain present in [1]FCPs can be expressed by a set of angles, among which the tilt angle α is the most common one (Figure 6-5).[17]

Table 6-1. Crystal and structural refinement data for compounds ($Me_2NCH_2tsi)AlCl_2$ (**2a**), ($Me_2Ntsi)Al[1]FCP$ (**4a**), and ($Me_2Ntsi)Ga[1]FCP$ (**4b**).

	2a	**4a** · ½ C_6H_6	**4b** · ½ C_6H_6
empirical formula	$C_{12}H_{32}AlCl_2NSi_3$	$C_{24}H_{41}AlFeNSi_3$	$C_{24}H_{41}FeGaNSi_3$
formula weight	372.54	510.68	553.42
wavelength, Å	0.71073	0.71073	0.71073
crystal system	monoclinic	triclinic	triclinic
space group (No.)	$P2_1/c$ (14)	$P\bar{1}$ (2)	$P\bar{1}$ (2)
Z	4	2	2
a, Å	14.5558(2)	9.0703(2)	9.0689(3)
b, Å	10.5318(2)	9.1867(2)	9.1768(3)
c, Å	14.0477(2)	18.8627(3)	18.9466(6)
α, deg	90	79.4549(12)	79.2406(18
β, deg	101.3318(12)	85.2343(11)	85.294(2)
γ, deg	90	61.3777(10)	61.6414(16)
vol, $Å^3$	2111.51(6)	1356.36(5)	1363.14(8)
d (calc), mg/m^3	1.172	1.250	1.348
temp, K	173(2)	173(2)	173(2)
abs coeff., mm^{-1}	0.510	0.733	1.664
theta range, deg	2.43 to 30.04	2.56 to 30.51	2.69 to 27.60
refl collected	12031	35005	18573
indep refl	6185 [R(int) = 0.0187]	8264 [R(int) = 0.0615]	6232 [R(int) = 0.0538]
abs correction	none	psi-scan	psi-scan
ref method		Full-matrix least-squares on F^2	
data / restr / params	6185 / 0 / 182	8264 / 0 / 281	6232 / 0 / 281
goodness-of-fit on F^2	1.024	1.025	1.040
final R indices [I>2sigma(I)]	R1 = 0.0340, wR2 = 0.0829	R1 = 0.0449, wR2 = 0.0942	R1 = 0.0403, wR2 = 0.0805
R indices (all data)	R1 = 0.0452, wR2 = 0.0886	R1 = 0.0739, wR2 = 0.1070	R1 = 0.0623, wR2 = 0.0900
max diff. peak-hole, $e.Å^{-3}$	0.340 and –0.353	0.333 and –0.534	0.371 and –0.541

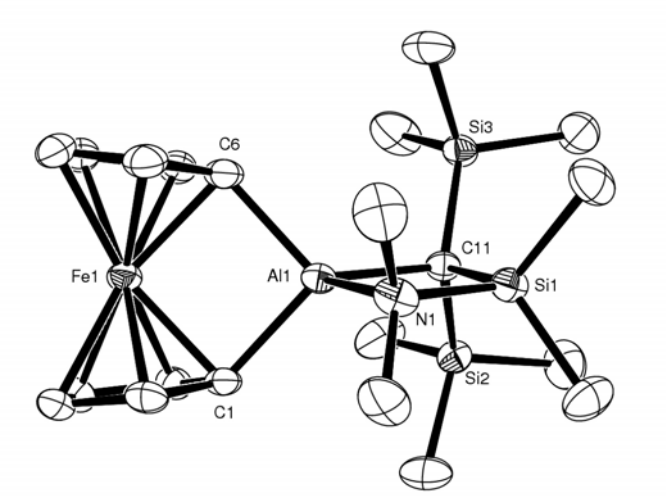

Figure 6-4. Molecular structure of (Me_2Ntsi)Al[1]FCP (**4a**) with thermal ellipsoids at the 50% probability level. H atoms and ½ benzene are omitted for clarity. Selected atom-atom distances [Å] and bond angles [º] for **4a**: Al1–N1 2.0123(17), Al1–C1 2.000(2), Al1–C6 1.988(2), Al1–C11 2.0301(19), Al1–Fe1 2.7708(6), C1–Al1–C6 94.51(8), N1–Al1–C11 86.71(7).

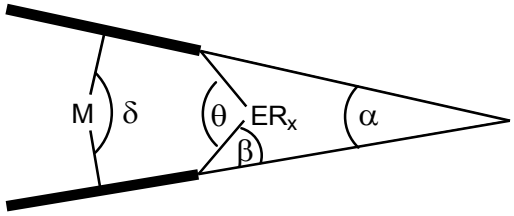

Figure 6-5. Set of angles to describe deformations in [1]metallocenophanes and [1]metallarenophanes.

We determined tilt angles α of 14.33(14)° for **4a** and 15.83(19)° for **4b**. The value for **4a** is very close to that of 14.9(3)° determined for the Pytsi containing Al[1]FCP **1a** (Figure 6-1).[10] Compound **4b** is the first fully characterized Ga[1]FCP; the structural analysis of its Pytsi-containing counterpart **1b**[11] (Figure 6-1) did not allow the extraction of structural details like bond lengths and angles. The tilt angles α for **4a** and **4b** are similar as those determined for Sn[1]FCP [$SntBu_2$ α = 14.1(2)°,[18] $SnMes_2$ α = 15.2(2)°[19]] and significantly smaller than those found for B[1]FCP, with the latter holding the record with 32.4(2)° for the largest known tilt

angle in [1]FCP.[8] Even though the difference in the tilt of **4a** and **4b** is small, it is significant within three estimated standard deviations.

6.3.2 [1]Chromarenophanes and [1]Vanadarenophanes.

Compared to [1]FCPs, only a few examples of [1]chromarenophanes ([1]CAPs) and the [1]vanadarenophanes ([1]VAPs) are known in the literature. The first [1]CAPs and the first [1]VAPs were published in 1990 by Elschenbroich *et al*. ($SiPh_2$ moieties in bridging positions).[20] Since then, [1]CAPs had been described with silicon,[21–23] germanium,[24] zirconium,[25] and boron[26] in bridging positions.[27] Strained [1]VAPs are known with the bridging elements silicon,[20–22] germanium,[24] and zirconium[25]. Very recently, highly strained cyclophanes of cycloheptrienyl-cyclopentadienyl sandwich compounds, isoelectronic species to bis(benzene) complexes, had been characterized.[28–32]

We have synthesized the first aluminum- and gallium-bridged [1]chromarenophanes ([1]CAPs) and [1]vanadarenophanes ([1]VAPs) in isolated yields of 54–81% from slurries of dilithiated metalloarenes and the dihalogen species **3a** and **3b**, respectively (Scheme 6-1). Usually, we apply ^{1}H NMR spectroscopy to check on the progress of a new reaction. However, the vanadium compounds are paramagnetic and inaccessible for NMR spectroscopy, and, consequently, we started with the syntheses of the chromium compounds. The optimized synthetic procedures for **5a** and **5b** were then adapted for the syntheses of the vanadium compounds **6a** and **6b**.

The [1]CAPs **5a** and **5b** show the expected signal pattern for time-averaged C_s symmetrical species in the ^{1}H and ^{13}C NMR spectra. For example, the aluminum compound **5a** exhibits five signals for the benzene rings [δ 3.74 and 4.35 (*o*-H), 4.53 and 4.60 (*m*-H), and 4.87

(*p*-H)] whereas in the case of the gallium counterpart **5b** a coincidental equivalency of the meta- and para protons results in just three signals [δ 3.69 and 4.18 (*o*-H), 4.74 (*m*-H and *p*-H)]. All these proton signals are relatively broad, and their width depends on how often a particular compound had been manipulated. ^{1}H NMR spectra with the smallest peak width and best resolved structure of the aromatic protons were obtained from freshly synthesized samples. Elschenbroich *et al*. described a similar phenomenon for $[(Ph_3SiC_6H_5)_2Cr]$. It was proposed that the presence of the paramagnetic chromium(I) species $[(Ph_3SiC_6H_5)_2Cr]^+$ leads to a fast electron transfer with the neutral species $[(Ph_3SiC_6H_5)_2Cr]$, resulting in line broadening.[20] Electron exchange reactions of this type had been investigated before.[33] On the basis of these results, and in the absence of direct experimental evidence, we can only speculate that small amounts of the paramagnetic chromium(I) species $\mathbf{5a}^+$ and $\mathbf{5b}^+$, respectively, are responsible for the observed line broadening. The ^{13}C NMR spectra clearly reveal that both products **5a** and **5b** are strained [1]CAP. The resonances of the *ipso*-C atoms at δ 62.1 (**5a**) and 56.6 (**5b**) are significantly upfield shifted with respect to the parent bis(benzene)chromium (δ 74.8).[34] More pronounced upfield shifts are exhibited by the known [1]CAPs with $SiMe_2$ (δ 39.5),[23] $GeMe_2$ (δ 37.5),[24] $GePh_2$ (δ 36.4),[24] and $Zr(t\text{Bu}C_5H_4)_2$ (δ 30.7).[25]

The [1]CAPs **5a** and **5b** and the [1]VAPs **6a** and **6b** all crystallized with half of a molecule of benzene in the asymmetric unit; all four compounds are isomorphous. Table 6-2 compiles crystal and structural refinement data and Figures 6-6 and 6-7 depict their molecular structures of the aluminum species (ORTEP plots of the gallium compounds **5b** and **6b** see Supporting Information).

Table 6-2. Crystal and structural refinement data for [1]CAPs **5a**–**b** and [1]VAPs **6a**–**b**.

	5a·½ C_6H_6	**5b**·½ C_6H_6	**6a**·½ C_6H_6	**6b**·½ C_6H_6
	$C_{26}H_{43}AlCrNSi_3$	$C_{26}H_{43}CrGaNSi_3$	$C_{26}H_{43}AlNSi_3V$	$C_{26}H_{43}GaNSi_3V$
M_r	532.86	575.60	531.80	574.54
wavelength, Å	0.71073			
crystal system	triclinic			
space group (No.)	$P\bar{1}$ (2)			
Z	2	2	2	2
a, Å	8.96730(10)	8.9883(2)	8.9681(3)	8.9868(3)
b, Å	9.16420(10)	9.1772(2)	9.1579(3)	9.1721(3)
c, Å	19.6077(3)	19.6458(4)	19.6320(5)	19.6692(5)
α, deg	81.9412(11)	81.3833(14)	82.0285(18)	81.577(2)
β, deg	89.5973(11)	89.3431(14)	89.204(2)	89.047(2)
γ, deg	63.0923(11)	63.0831(11)	63.2623(17)	63.324(2)
vol, $Å^3$	1419.78(3)	1425.74(6)	1423.90(8)	1430.88(8)
d (calc), mg/m^3	1.246	1.341	1.240	1.334
temp, K	173(2)	173(2)	173(2)	173(2)
abs coeff., mm^{-1}	0.575	1.467	0.520	1.408
theta range, deg	2.52 to 30.50	2.52 to 30.51	2.52 to 27.58	2.52 to 27.54
refl collected	36806	39640	20973	21117
indep refl	8649 [R(int) = 0.0563]	8694 [R(int) = 0.0741]	6521 [R(int) = 0.0766]	6560 [R(int) = 0.0602]
abs correction	Psi-scan			
ref method	Full-matrix least-squares on F^2			
data / restr / params	8649 / 0 / 299	8694 / 0 / 299	6521 / 0 / 299	6560 / 0 / 299
goodness-of-fit on F^2	1.026	1.036	1.027	1.034
final R indices [I>2sigma(I)]	R1 = 0.0425, wR2 = 0.0984	R1 = 0.0469, wR2 = 0.0932	R1 = 0.0510, wR2 = 0.1034	R1 = 0.0403, wR2 = 0.0820
R indices (all data)	R1 = 0.0608, wR2 = 0.1089	R1 = 0.0776, wR2 = 0.1067	R1 = 0.0874, wR2 = 0.1205	R1 = 0.0610, wR2 = 0.0918
largest diff. peak and hole, $e.Å^{-3}$	0.384 and –0.609	0.564 and –0.722	0.333 and –0.455	0.362 and –0.537

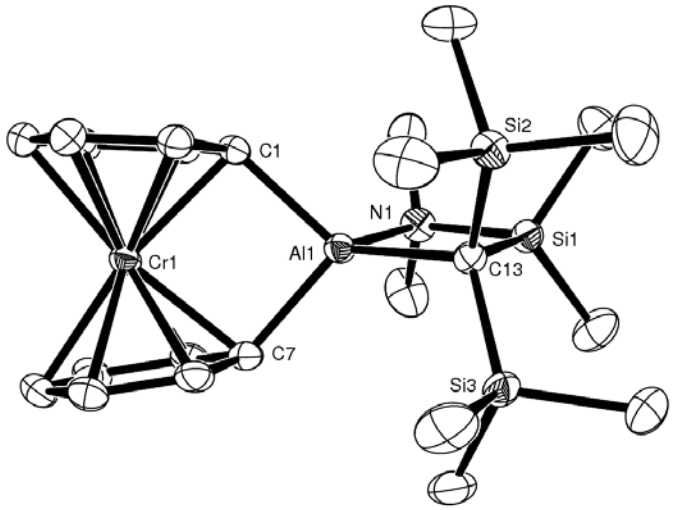

Figure 6-6. Molecular structure of (Me_2Ntsi)Al[1]CAP (**5a**) with thermal ellipsoids drawn at 50% probability level. H atoms and ½ benzene are omitted for clarity. Selected atom–atom distances [Å] and bond angles [º] for **5a**: Al1–N1 = 2.0257(15), Al–C1 = 1.9979(17), Al1–C7 = 1.9940(17), Al1–C13 = 2.0412(16), Al1–Cr1 = 2.9740(5), C7–Al–C1 = 91.93(7), C7–Al1–N1 = 118.15(7), C1–Al1–N1 = 110.54(7), C7–Al1–C13 = 122.40(7), C1–Al–C13 = 129.30(7), N1–Al1–C13 = 86.47(6).

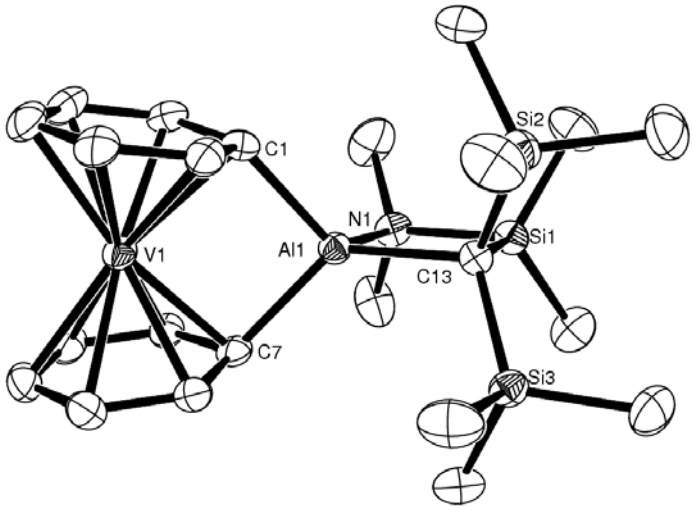

Figure 6-7. Molecular structure of (Me_2Ntsi)Al[1]VAP (**6a**) with thermal ellipsoids drawn at 50% probability level. H atoms and ½ benzene are omitted for clarity. Selected atom-atom distances [Å] and bond angles [º] for **6a**: Al1–N1 = 2.020(2), Al–C1 = 1.985(3), Al1–C7 = 1.995(3), Al1–C13 = 2.039(3), Al1–V1 = 2.9805(9), C7–Al–C1 = 93.78(11), C7–Al1–N1 = 110.27(11), C1–Al1–N1 = 117.52(11), C7–Al1–C13 = 128.51(11), C1–Al–C13 = 121.77(11), N1–Al1–C13 = 86.50(10).

As in the case of the [1]FCPs **4a** and **4b** described before, the [1]CAPs and [1]VAPs show planar heterocycles containing the bridging elements aluminum and gallium, respectively [rms deviations from planarity [Å] are: 0.0082 (**5a**), 0.0042 (**5b**), 0.0050 (**6a**), 0.0042 (**6b**)]. The bridging elements are distorted tetrahedrally surrounded by three C- and one N atom. Al–C distances are slightly shorter than respective Ga–C distances; respective E–C bond lengths are similar for the chromium and the vanadium species (Figure 6-6 and 6-7). Expectedly, E–N donor bonds are significantly shorter for aluminum than for gallium [Al1–N1 = 2.0257(15) (**5a**), Ga1–N1 = 2.121(2) (**5b**), Al1–N1 = 2.020(2) (**6a**), Ga1–N1 = 2.122(2) (**6b**)], which exemplifies that the lighter group-13 element is the stronger Lewis acid with respect to the NMe_2 donor group.

The alumina- and galla[1]metallarenophanes **5** and **6** are strained species. Table 6-3 shows the set of common deformation angles α, θ, and δ (Figure 6-5) for the four species.

Table 6-3. Deformation angles α, θ, and δ [°] of [1]CAP **5** and [1]VAP **6** (see Figure 6-5).

	5a [**5b**]	**6a** [**6b**]
α	11.81(9) [13.24(13)]	14.65(14) [15.63(14)]
θ	91.93(7) [89.77(10)]	93.78(11) [92.37(10)]
δ[a]	170.63(7) [169.43(11)]	168.43(11) [167.30(11)]

[a] It was assumed that the δ angle have similar esd's as found for respective C–M–C angles (M = Cr, V; C: aromatic C atoms). The largest esd of C–M–C angles was taken for δ.

For the chromium and the vanadium compounds, respectively, the benzene rings are more tilted for the gallium-bridged species than for the aluminum-bridged species. The differences between the angles α for the [1]CAPs **5a** and **5b** of 1.4°, and for the [1]VAPs **6a** and **6b** of 1.0° are small but significant. A similar trend was observed for the [1]FCPs **4a** and **4b** discussed before (1.5°). The α angles of known [1]CAPs are 14.4° ($SiPh_2$),[20] 16.6(3)° ($SiMe_2$),[23]

14.4(2)° ($GePh_2$),[24] and 26.6(3)° [26]; those of [1]VAPs are 20.8° [21] 19.9° [$Si(CH_2)_3$],[22] and 8° [$Zr(t BuC_5H_4)_2$].[25]

6.4 Conclusions

Six new strained organometallic species were synthesized and structurally characterized. For all six species, the bridging Al- and Ga atom, respectively, are equipped with the same *trisyl* based ligand Me_2Ntsi (Figure 6-2). Hence, within the pairs of compounds **4a**,**b**, **5a**,**b**, and **6a**,**b**, respectively, only the bridging element differs and this close relation reveals the influence of aluminum versus gallium as a bridging element. Commonly, the tilt angle α is taken as a measure of the extent of strain in cyclophanes (Figure 6-5). One major factor that governs α is the size of the bridging element. On the basis of covalent radii of 1.25 Å for aluminum and of 1.26 Å for gallium alone (singly bonded, 3-fold coordinated elements),[35] a similar or a slightly higher tilt angle for the aluminum-bridged species **4a**, **5a**, and **6a** in comparison with the respective gallium-bridged species would be expected; surprisingly, just the opposite is the case. However, a glance at the neighboring group-14 elements Si and Ge reveals a similar situation, if only those molecules are compared that are equipped with the same set of ligands at the bridging element. On the basis of covalent radii of 1.17 Å for Si and of 1.22 Å for Ge alone (singly bonded tetracoordinated elements),[35] smaller angles of α are expected for germanium-bridged species. However, for [1]CAPs with $SiPh_2$ and $GePh_2$ in bridging positions, respectively, the same value of α was detected [14.4(2)°].[24] Similarly, for [1]FCPs with $SiMe_2$ [α = 20.8(5)°][36] and $GeMe_2$ [α = 19.0(9)°][37] bridging moieties, the tilt angles α are the same within three estimated standard deviations. Causes for these small structural differences are unknown today.

With the synthesis of the new strained molecules **4**–**6** on hand, we started to explore their chemistry, in particular, with respect to polymerizations. Initial DSC measurements for **4a** and **4b**, respectively, showed exothermic peaks above 210 °C, a typical indication that ROP occurred.

6.5 Experimental Section

General Procedures. All manipulations were carried out using standard Schlenk techniques. Solvents were dried using a MBraun Solvent Purification System and stored under nitrogen over 4 Å molecular sieves. All solvents for NMR spectroscopy were degassed prior to use and stored under nitrogen over 4 Å molecular sieves. $[Fe(LiC_5H_4)_2]\cdot 2/3$ tmeda,[38] $[Cr(C_6H_6)_2]$,[39] $[V(C_6H_6)_2]$,[40] $AlCl_2[C(SiMe_3)(SiMe_2NMe_2)]$ (**3a**),[16] and $GaCl_2[C(SiMe_3)(SiMe_2NMe_2)]$ (**3b**)[16] were synthesized as described in the literature. ^1H, ^{13}C, and ^{27}Al NMR spectra were recorded on a Bruker 500 MHz Avance at 25 °C, unless noted differently. ^1H chemical shifts were referenced to the residual protons of the deuterated solvents (C_6D_6 at δ 7.15); ^{13}C chemical shifts were referenced to the C_6D_6 signal at δ 128.0; ^{27}Al NMR spectra were referenced to $[Al(acac)_3]$ dissolved in the C_6D_6. Mass spectra were measured on a VG 70SE (*m*/*z* > 10% are listed for signals of the most abundant ions). Elemental analyses were performed on a Perkin-Elmer 2400 CHN Elemental Analyzer using V_2O_5 to promote complete combustion.

$HC(SiMe_3)_2SiMe_2CH_2NMe_2$ (Me_2NCH_2tsiH). $HC(SiMe_3)_2Si(Me_2)Br$[41] (3.697 g, 12.4 mmol) in diethyl ether (30 mL) was added to $LiCH_2NMe_2$[42] (0.800 g, 12.3 mmol) in diethyl ether (20 mL) at –78 °C. The dry ice bath was removed and the solution stirred for 1 h to give a yellow solution. Volatiles were removed in vacuum, and the product was extracted with hexane (3 x 10

mL). After removal of hexane in vacuum, a yellow oil of $HC(SiMe_3)_2SiMe_2CH_2NMe_2$ was left behind (3.41 g, 99%). ^{1}H NMR (500 MHz): δ –0.56 (s, 1H, CH), 0.17 (s, 18H, $SiMe_3$), 0.23 (s, 6H, $SiMe_2$), 1.83 (s, 2H, CH_2), 2.15 (s, 6H, NMe_2).

$(Me_2NCH_2tsi)AlCl_2$ (2a). Due to an unsuccessful usage of **2a** as a starting material for [1]FCPs, the following procedure was not optimized. MeLi (11.5 mL, 1.0 M in thf, 11.5 mmol) was added to $HC(SiMe_3)_2SiMe_2CH_2NMe_2$ (2.87 g, 10.4 mmol) in thf (15 mL) at ambient temperature. After stirring for 1 h all volatiles were removed in vacuum to give an orange solid. Diethyl ether (20 mL) was added and $AlCl_3$ (1.42 g, 10.6 mmol) in diethyl ether (30 mL) was added at –78 °C. The mixture was stirred for 16 h at ambient temperature and filtered, and the solids were washed with 20 mL of diethyl ether. The combined filtrates were concentrated to 20 mL, and crystallization at ca. –30 °C gave yellow cubes of **2a** (1.41 g, 36%). ^{1}H NMR (500 MHz): δ 0.10 (s, 6H, $SiMe_2$), 0.44 (s, 18 H, $SiMe_3$), 1.48 (s, 2H, CH_2), 1.99 (s, 6H, NMe_2). ^{13}C NMR: δ 4.1 ($SiMe_2$), 5.8 (CSi_3), 7.4 ($SiMe_3$), 49.9 (NMe_2), 54.6 (CH_2). ^{27}Al NMR (130.3 MHz): δ 131 ($h_{½}$ = 800 Hz). MS (70 eV): m/z (%) = 356 (100) [M^+–Me], 244 (62) [$C_{10}H_{26}NSi_3^+$], 73 (50) [SiMe3$^+$]. Anal. Calcd. for $C_{12}H_{32}AlCl_2NSi_3$ (372.536): C, 38.69; H, 8.66; N, 3.76. Found: C, 38.45; H, 8.93; N, 3.11.

Al[1]FCP (4a). A suspension of dilithioferrocene·2/3 tmeda (0.874 g, 3.17 mmol)[38] in toluene (15 mL) was added dropwise via tubing to a solution of **3a** (1.04 g, 2.90 mmol)[16] in toluene (15 mL; –20 °C). After stirring for 16 h at ambient temperature, the red solution was filtered and all volatiles were removed at high vacuum (25 °C/0.01 mbar), upon which crystallization of pure **4a** occurred (1.33 g, 2.82 mmol, 97%). Single crystals of **4a**·½ C_6H_6 for X-ray analysis were grown from benzene solutions at ca. 8 °C. ^{1}H NMR (500 MHz): δ 0.18 (s, 6H, $SiMe_2$), 0.45 (s, 18H, $SiMe_3$), 2.11 (s, 6H, NMe_2), 3.76, 4.24 (pst, 4H, C_5H_4), 4.58 (pst, 4H,

C_5H_4). ^{13}C NMR (125.8 MHz): δ 2.9 ($SiMe_2$), 7.7 ($SiMe_3$), 40.9 (NMe_2), 53.0 (*ipso*-C, C_5H_4, –40 °C, C_7D_8), 75.4, 75.6, 75.9, 76.1 (C_5H_4); signal of $C(SiMe_3)_2$ not detected. ^{27}Al NMR (130.3 MHz): δ 154 ($h_{1/2}$ = 4300 Hz). MS (70 eV): *m*/*z* (%) = 471 (100) [M^+], 456 (27) [M^+–Me], 186 (12) [$FeCp_2^+$], 73 (10) [$SiMe_3^+$]. Anal. Calcd for $C_{21}H_{38}AlFeNSi_3$ (471.62): C, 53.48; H, 8.12; N, 2.97. Found: C, 53.65; H, 8.35; N, 2.70.

Ga[1]FCP (4b). As described for **4a**, dilithioferrocene·2/3 tmeda (1.17 g, 4.25 mmol)[38] in toluene (20 mL) and **3b** (1.70 g, 4.24 mmol)[16]16 in toluene (20 mL; –20 °C) resulted in a crude product of **4b**. Re-crystallization from toluene yielded red, needle shaped crystals of **4b** (1.48 g, 2.88 mmol, 68%). Single crystals of **4b**·½ C_6H_6 for X-ray analysis were grown from benzene solutions at ca. 8 °C. ^{1}H NMR (500 MHz): δ 0.19 (s, 6H, $SiMe_2$), 0.42 (s, 18H, $SiMe_3$), 2.15 (s, 6H, NMe_2), 3.90, 4.24 (pst, 4H, C_5H_4), 4.54 (pst, 4H, C_5H_4). ^{13}C NMR (125.8 MHz): δ 3.0 ($SiMe_2$), 6.7 ($SiMe_3$), 41.9 (NMe_2), 47.2 (*ipso*-C, C_5H_4), 75.3, 76.2, 76.5 (C_5H_4); signal of $C(SiMe_3)_2$ not detected. MS (70 eV): *m*/*z* (%) = 513 (10) [M^+], 186 (100) [$FeCp_2^+$], 121 (22) [$FeCp^+$], 73 (6) [$SiMe_3^+$], 58 (16) [Fe^+]. Anal. Calcd for $C_{21}H_{38}GaFeNSi_3$ (514.361): C, 49.04; H, 7.45; N, 2.72. Found: C, 49.93; H, 7.70; N, 2.42.

Al[1]CAP (5a). *n*BuLi (3.2 mL, 2.6 M in hexanes, 8.3 mmol) was added dropwise to a refluxing solution of [$Cr(C_6H_6)_2$] (0.638 g, 3.06 mmol) and tmeda (1.217 g, 10.47 mmol) in cyclohexane (30 mL).[20] After refluxing for 1 h, the red reaction mixture was cooled to 0 °C, the liquid phase was removed via syringe, and the residual solid was dried on high vacuum (0.646 g, 1.92 mmol). A slurry of this solid in diethyl ether (30 mL, –20 °C) was added to a solution of **3a** (0.690 g, 1.92 mmol) in diethyl ether (10 mL, –20 °C). The reaction mixture was stirred for 16 h at ambient temperature and filtered, and additional product was extracted with diethyl ether (2 × 10 mL) from the filter cake. From the combined organic phases, all volatiles were removed in

vacuum resulting in a crude solid, which was washed with hexane (3 × 15 mL) to give **5a** as a red-brown solid (0.490 g). Concentration of the washings to 10 mL gave an additional 0.272 g of **5a** (overall yield 0.762 g, 81%). Single crystals of **5a**·½ C_6H_6 for X-ray analysis were grown from benzene solutions at ca. 8 °C. ^{1}H NMR (500 MHz, C_6D_6): δ 0.20 (s, 6H, $SiMe_2$), 0.49 (s, 18 H, 2 $SiMe_3$), 2.14 (s, 6H, NMe_2), 3.74 (d, 2H, *o*-H), 4.35 (d, 2H, *o*-H), 4.53 (pst, 2H, *m*-H), 4.60 (pst, 2H, *m*-H), 4.87 (pst, 2H, *p*-H). ^{13}C NMR: δ 3.0 ($SiMe_2$), 7.9 (2 $SiMe_3$), 9.2 ($AlCSiMe_3$) 40.6 (NMe_2), 62.1 (*ipso*-C), 77.6 (*p*-C), 77.9 (*o*-C), 78.4 (*o*-C), 80.7 (*m*-C), 81.2 (*m*-C). ^{27}Al NMR: δ 154 ($h_{1/2}$ = 3400 Hz); MS (70 eV): *m*/*z* (%) 493 (100) $[C_{23}H_{40}CrAlNSi_3]^+$, 450 (18) $[C_{21}H_{35}AlCrSi_3]^+$, 364 (95) $[C_{17}H_{35}AlNSi_3]^+$, 319 (16) $[C_{15}H_{28}AlSi_3]^+$, 287 (32) $[C_{11}H_{30}AlNSi_3]^+$, 247 (18), 230 (39) $[C_9H_{24}NSi_3]^+$, 201 (20) $[C_8H_{21}Si_3]^+$, 187 (18) $[C_7H_{19}Si_3]^+$, 175 (25), 129 (16) $[C_5H_{13}Si_2]^+$, 78 (32) $[C_6H_6]^+$, 73 (39) $[C_3H_9Si]^+$, 69 (49), 59 (13). Anal. Calcd for $C_{23}H_{40}AlCrNSi_3$ (493.810): C, 55.94; H, 8.16; N, 2.84. Found: C, 54.80; H, 8.58; N, 2.82.

Ga[1]CAP (5b). As described for **5a**, *n*BuLi (3.8 mL, 2.6 M in hexanes, 9.8 mmol), $[Cr(C_6H_6)_2]$ (0.8112 g, 3.89 mmol), tmeda (1.339 g, 8.64 mmol), and cyclohexane (25 mL)[20] resulted in a solid (0.923 g, 2.74 mmol). A slurry of this solid in benzene (30 mL, 0 °C) and **3b** (1.063 g, 2.65 mmol) in benzene (10 mL, 0 °C) resulted in red-brown crystals of **5b**·½ C_6H_6 (1.076 g, 69%) after crystallization from benzene. ^{1}H NMR (500 MHz, C_6D_6, 298 K): δ 0.21 (s, 6H, $SiMe_2$), 0.47 (s, 18 H, 2 $SiMe_3$), 2.16 (s, 6H, NMe_2), 3.69 (br. s, 2H, *o*-H), 4.18 (br. s, 2H, *o*-H), 4.74 (br. s, 6H, *m*-H, *p*-H). ^{13}C NMR: δ 3.1 ($SiMe_2$), 7.3 ($SiMe_3$), 12.4 ($GaCSi_3$) 41.8 (NMe_2), 56.6 (br, *ipso*-C), 78.0 (*p*-C), 78.4 (br, *o*-C) 82.4 (br, *m*-C). MS (70 eV): *m*/*z* (%) 535 (42) $[C_{23}H_{40}CrGaNSi_3]^+$, 406 (27) $[C_{17}H_{35}GaNSi_3]^+$, 290 (22), 230 (61) $[C_9H_{24}NSi_3]^+$, 187 (52) $[C_7H_{19}Si_3]^+$, 175 (32), 129 (41) $[C_5H_{13}Si_2]^+$, 73 (100) $[C_3H_9Si]^+$. Anal. Calcd for $C_{26}H_{43}CrGaNSi_3$ (575.605): C, 54.25; H, 7.53; N, 2.43. Found: C, 54.05; H, 8.07; N, 2.28.

Al[1]VAP (6a). As described for **5a**, *n*BuLi (2.8 mL, 2.6 M in hexanes, 7.3 mmol), $[V(C_6H_6)_2]$ (0.6019 g, 2.905 mmol), tmeda (1.127 g, 9.70 mmol), and cyclohexane (25 mL) resulted in a solid (0.797 g, 2.38 mmol).[20] A slurry of this solid in diethyl ether (30 mL, –20 °C) and **3a** (0.863 g, 2.41 mmol) in diethyl ether (10 mL, –20 °C) resulted in dark-red crystals of **6a**·½ C_6H_6 (0.678 g, 54%) after crystallization from benzene. IR (KBr; selected value are given): 846 (s), 1012 (w), 1251 (m), 2898 (w), 2953 (w). MS (70 eV): *m*/*z* (%) 492 (100) $[C_{23}H_{40}CrGaNSi_3]^+$, 449 (26) $[C_{21}H_{35}AlSi_3V]^+$, 364 (39) $[C_{17}H_{35}AlNSi_3]^+$, 302 (26) $[C_{12}H_{33}AlNSi_3]^+$, 246 (34), 230 (26) $[C_9H_{24}NSi_3]^+$, 219 (40), 217 (17) $[C_8H_{24}AlNSi_2]^+$, 207 (11) $[C_{12}H_{12}V]^+$, 203 (21), 129 (24) $[C_4H_{12}AlNSi]^+$, 102 (19) $[C_4H_{12}NSi]^+$, 78 (52) $[C_6H_6]^+$, 73 (40) $[C_3H_9Si]^+$. Anal. Calcd for $C_{23}H_{40}AlNSi_3V$ (531.812): C, 58.72; H, 8.15; N, 2.63. Found: C, 58.73; H, 8.60; N, 2.43;

Ga[1]VAP (6b). As described for **5a**, *n*BuLi (3.0 mL, 2.6 M in hexanes, 7.8 mmol), $[V(C_6H_6)_2]$ (0.6508 g, 3.141 mmol), tmeda (1.362 g, 11.7 mmol), and cyclohexane (25 mL) resulted in a solid (0.839 g, 2.50 mmol).[20] A slurry of this solid in diethyl ether (30 mL, –20 °C) and **3b** (1.011 g, 2.51 mmol) in diethyl ether (10 mL, –20 °C) resulted in dark-red crystals of **6b**·½ C_6H_6 (0.830 g, 58%) after crystallization from benzene. IR (KBr; selected value are given): 676 (w) 845 (s), 997 (w), 1249 (m), 1458 (w), 2896 (w), 2953 (w). MS (70 eV): *m*/*z* (%) 534 (80) $[C_{23}H_{40}GaNSi_3V]^+$, 390 (25) $[C_{16}H_{31}GaNSi_3]^+$, 344 (25), 247 (21), 230 (14) $[C_9H_{24}NSi_3]^+$, 102 (13) $[C_4H_{12}NSi]^+$, 78 (100) $[C_6H_6]^+$, 73 (21) $[C_3H_9Si]^+$, 59 (13). Anal. Calcd for $C_{26}H_{43}GaNSi_3V$ (574.550): C, 54.35; H, 7.54; N, 2.44. Found: C, 54.82; H, 7.78; N, 2.41. \

X-ray structural analysis for 2a, 4a, 4b, 5a, 5b, 6a, and 6b. Data was collected at –100 °C on a Nonius Kappa CCD diffractometer, using the COLLECT program.[43] Cell refinement and data reductions used the programs DENZO and SCALEPACK.[44] The program SIR97[45] was used

to solve the structure and SHELXL97[46] was used to refine the structure. ORTEP-3 for Windows[47] was used for molecular graphics, and PLATON[48] was used to prepare material for publication. H atoms were placed in calculated positions with U_{iso} constrained to be 1.2 times U_{eq} of the carrier atom for the methylene protons and 1.5 times U_{eq} of the carrier atom for methyl hydrogen atoms.

Acknowledgement. We thank the Natural Sciences and Engineering Research Council of Canada (NSERC Discovery Grant, J.M.), the Department of Chemistry, the Saskatchewan Structural Sciences Centre, and the University of Saskatchewan for their generous support. We thank the Canada Foundation for Innovation (CFI) and the government of Saskatchewan for funding of the X-ray and NMR facilities in the Saskatchewan Structural Sciences Centre. We thank Alan J. Lough (University of Toronto) for a helpful discussion about tilt angles.

Supporting Information Available. Crystallographic data for **2a**, **4a**, **4b**, **5a**, **5b**, **6a**, and **6b** in CIF file format. ORTEP plots for compounds **4b**, **5b**, and **6b**. This material is available free of charge via the Internet at http://pubs.acs.org.

6.6 References

(1) Osborne, A. G.; Whiteley, R. H. *J. Organomet. Chem.* **1975**, *101*, C27-C28.
(2) Foucher, D. A.; Tang, B. Z.; Manners, I. *J. Am. Chem. Soc.* **1992**, *114*, 6246-6248.
(3) Manners, I. *Chem. Commun.* **1999**, *10*, 857-944.
(4) Manners, I. *Science* **2001**, *294*, 1664-1666.
(5) Nguyen, P.; Gomez-Elipe, P.; Manners, I. *Chem. Rev.* **1999**, *99*, 1515-1548.
(6) Tanabe, M.; Vandermeulen, G. W. M.; Chan, W. Y.; Cyr, P. W.; Vanderark, L.; Rider, D. A.; Manners, I. *Nature Materials* **2006**, *5*, 467-470 and references therein.
(7) Berenbaum, A.; Braunschweig, H.; Dirk, R.; Englert, U.; Green, J. C.; Jäkle, F.; Lough, A. J.; Manners, I. *J. Am. Chem. Soc.* **2000**, *122*, 5765-5774.
(8) Braunschweig, H.; Dirk, R.; Müller, M.; Nguyen, P.; Resendes, R.; Gates, D. P.; Manners, I. *Angew. Chem., Int. Ed.* **1997**, *36*, 2338-2340.
(9) Braunschweig, H.; Breitling, F. M.; Gullo, E.; Kraft, M. *J. Organomet. Chem.* **2003**, *680*, 31-42.

(10) Schachner, J. A.; Lund, C. L.; Quail, J. W.; Müller, J. *Organometallics* **2005**, *24*, 785-787.
(11) Schachner, J. A.; Lund, C. L.; Quail, J. W.; Müller, J. *Organometallics* **2005**, *24*, 4483-4488.
(12) Eaborn, C.; Smith, J. D. *J. Chem. Soc., Dalton Trans.* **2001**, 1541-1552.
(13) Braunschweig, H.; Burschka, C.; Clentsmith, G. K. B.; Kupfer, T.; Radacki, K. *Inorg. Chem.* **2005**, *44*, 4906-4908.
(14) Schachner, J. A.; Orlowski, G. A.; Quail, J. W.; Kraatz, H.-B.; Müller, J. *Inorg. Chem.* **2006**, *45*, 454-459.
(15) Howson, J.; Eaborn, C.; Hitchcock, P. B.; Hill, M. S.; Smith, D. J. *J. Organomet. Chem.* **2005**, *690*, 69-75.
(16) Al-Juaid, S. S.; Eaborn, C.; El-Hamruni, S. M.; Hitchcock, P. B.; Smith, J. D. *Organometallics* **1999**, *18*, 45-52.
(17) See for example: Herberhold, M. *Angew. Chem., Int. Ed.* **1995**, *34*, 1837-1839.
(18) Rulkens, R.; Lough, A. J.; Manners, I. *Angew. Chem., Int. Ed.* **1996**, *35*, 1805-1807.
(19) Jäkle, F.; Rulkens, R.; Zech, G.; Foucher, D. A.; Lough, A. J.; Manners, I. *Chem. Eur. J.* **1998**, *4*, 2117-2128.
(20) Elschenbroich, C.; Hurley, J.; Metz, B.; Massa, W.; Baum, G. *Organometallics* **1990**, *9*, 889-897.
(21) Elschenbroich, C.; Bretschneider-Hurley, A.; Hurley, J.; Massa, W.; Wocadlo, S.; Pebler, J.; Reijerse, E. *Inorg. Chem.* **1993**, *32*, 5421-5424.
(22) Elschenbroich, C.; Bretschneider-Hurley, A.; Hurley, J.; Behrendt, A.; Massa, W.; Wocadlo, S.; Reijerse, E. *Inorg. Chem.* **1995**, *34*, 743-745.
(23) Hultzsch, K. C.; Nelson, J. M.; Lough, A. J.; Manners, I. *Organometallics* **1995**, *14*, 5496-5502.
(24) Elschenbroich, C.; Schmidt, E.; Gondrum, R.; Metz, B.; Burghaus, O.; Massa, W.; Wocadlo, S. *Organometallics* **1997**, *16*, 4589-4596.
(25) Elschenbroich, C.; Schmidt, E.; Metz, B.; Harms, K. *Organometallics* **1995**, *14*, 4043-4045.
(26) Braunschweig, H.; Homberger, M.; Hu, C. H.; Zheng, X. L.; Gullo, E.; Clentsmith, G.; Lutz, M. *Organometallics* **2004**, *23*, 1968-1970.
(27) For an historical overview and leading references about bis(benzene)chromium chemistry see: Seyferth, D. *Organometallics* **2002**, *21*, 1520-1530.
(28) Elschenbroich, C.; Paganelli, F.; Nowotny, M.; Neumüller, B.; Burghaus, O. *Z. Anorg. Allg. Chem.* **2004**, *630*, 1599-1606.
(29) Tamm, M.; Kunst, A.; Bannenberg, T.; Herdtweck, E.; Sirsch, P.; Elsevier, C. J.; Ernsting, J. M. *Angew. Chem., Int. Ed.* **2004**, *41*, 5530-5534.
(30) Braunschweig, H.; Lutz, M.; Radacki, K. *Angew. Chem., Int. Ed.* **2005**, *44*, 5647-5651.
(31) Bartole-Scott, A.; Braunschweig, H.; Kupfer, T.; Lutz, M.; Manners, I.; Nguyen, T.-l.; Radacki, K.; Seeler, F. *Chem. Eur. J.* **2006**, *12*, 1266-1273.
(32) Braunschweig, H.; Lutz, M.; Radacki, K.; Schaumlöffel, A.; Seeler, F.; Unkelbach, C. *Organometallics* **2006**, *25*, 4433-4435.
(33) Elschenbroich, C.; Zenneck, U. *J. Organomet. Chem.* **1978**, *160*, 125-137.
(34) Elschenbroich, C.; Koch, J. *J. Organomet. Chem.* **1982**, *229*, 139-158.
(35) Holleman-Wiberg *Inorganic Chemistry*; 1st English ed.; Academic Press: San Diego, London, 2001, p 1756.

(36) Finckh, W.; Tang, B. Z.; Foucher, D. A.; Zamble, D. B.; Ziembinski, R.; Lough, A.; Manners, I. *Organometallics* **1993**, *12*, 823-829.
(37) Foucher, D. A.; Edwards, M.; Burrow, R. A.; Lough, A. J.; Manners, I. *Organometallics* **1994**, *13*, 4959-4966.
(38) Butler, I. R.; Cullen, W. R.; Ni, J.; Rettig, S. J. *Organometallics* **1985**, *4*, 2196-2201.
(39) *Synthetic methods of organometallic and inorganic chemistry* Herrmann, W. A., Ed.; Georg Thieme Verlag Stuttgart: New York, 1997; Vol. 8.
(40) Fischer, E. O.; Reckziegel, A. *Chem. Ber.* **1961**, *94*, 2204-2208.
(41) Al-Juaid, S. S.; Eaborn, C.; Hitchcock, P. B.; Hill, M. S.; Smith, J. D. *Organometallics* **2000**, *19*, 3224-3231.
(42) Steinborn, D.; Becke, F.; Boese, R. *Inorg. Chem.* **1995**, *34*, 2625-2628.
(43) Nonius; Nonius BV, Delft, The Netherlands: 1998.
(44) Otwinowski, Z.; Minor, W. In *Macromolecular Crystallography, Part A*; Carter, C. W., Sweet, R. M., Eds.; Academic Press: London, 1997; Vol. 276, p 307-326.
(45) Altomare, A.; Burla, M. C.; Camalli, M.; Cascarano, G.; Giacovazzo, C.; Guagliardi, A.; Moliterni, A. G. G.; Polidori, G.; Spagna, R. *J. Appl. Crystallogr.* **1999**, *32*, 115-119.
(46) Sheldrick, G. M.; University of Göttingen, Germany: 1997.
(47) Farrugia, L. J. *J. Appl. Crystallogr.* **1997**, *30*, 565.
(48) Spek, A. L.; University of Utrecht, The Netherlands: 2001.

6.7 Supporting Information

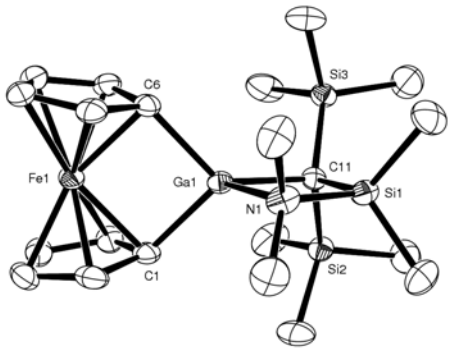

Figure 6-S1. Molecular structure of (Me_2Ntsi)Ga[1]FCP (**4b**) with thermal ellipsoids at the 50% probability level. H atoms and ½ benzene are omitted for clarity. Selected atom-atom distances [Å] and bond angles [º] for **4b**: Ga1–N1 2.105(2), Ga1–C1 2.008(3), Ga1–C6 2.017(3), Ga1–C11 2.048(3), Ga1–Fe1 2.8184(5), C1–Ga1–C6 92.75(11), N1–Ga1–C11 84.98(10).

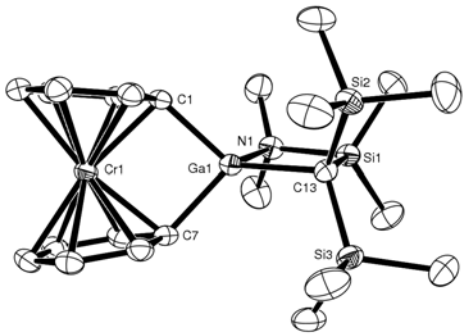

Figure 6-S2. Molecular structure of (Me_2Ntsi)Ga[1]CAP (**5b**) with thermal ellipsoids drawn at 50% probability level. H atoms and ½ benzene are omitted for clarity. Selected bond lengths (Å), atom-atom distances [Å], and angles [º] for **5b**: Ga1–N1 = 2.121(2), Ga–C1 = 2.017(2), Ga1–C7 = 2.012(3), Ga1–C13 = 2.055(2), Ga1–Cr1 = 3.0256(5), C7–Ga–C1 = 89.77(10), C7–Ga1–N1 = 117.79(9), C1–Ga1–N1 = 109.85(9), C7–Ga1–C13 = 124.90(10), C1–Ga1–C13 = 131.70(10), N1–Ga1–C13 = 86.50(9).

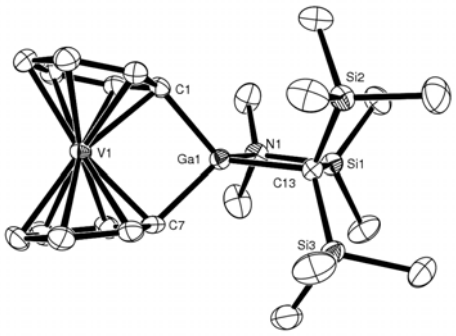

Figure 6-S3. Molecular structure of (Me_2Ntsi)Ga[1]VAP (**6b**) with thermal ellipsoids drawn at 50% probability level. H atoms and ½ benzene are omitted for clarity. Selected atom-atom distances [Å] and bond angles [º] for 6b: Ga1–N1 = 2.122(2), Ga–C1 = 2.017(3), Ga1–C7 = 2.007(3), Ga1–C13 = 2.053(2), Ga1–V1 = 3.0212(5), C7–Ga–C1 = 92.37(10), C7–Ga1–N1 = 117.21(11), C1–Ga1–N1 = 109.29(10), C7–Ga1–C13 = 124.15(10), C1–Ga1–C13 = 130.34(11), N1–Ga1–C13 = 84.53(9).

CHAPTER 7
PUBLICATION 6

Description

The following chapter is a verbatim copy of an article which was published in the *Journal of the American Chemical Society*[*] in August 2007[†] and describes the synthesis and characterization of the first [1]MAPs bridged by aluminum (**2a)**, and gallium (**2b**), which are equipped with Me_2Ntsi ligands. In addition, the synthesis of the first silicon-bridged [1]MAP [ER_x = $SiPh_2$ (**2c**)] and the unexpected ring-opening reaction catalyzed by donor molecules to produce [(η^6-C_6H_6)Mo{η^6-C_6H_5[GaPh(Me_2Ntsi)]} (**3b**)] from **2b** are described.

Author Contributions

My contributions to this publication were the synthesis and characterization of all [1]MAPs reported, as well as the work on the ring-opening reactions. The coauthors on this paper are Jörg A. Schachner, who prepared the compound [Pt$(cod)_2$], J. Wilson Quail, who performed all single-crystal X-ray analyses, and my supervisor Jens Müller. Written permission was obtained from all contributing authors to include material within this thesis.

[*] Reproduced with permission from the Journal of the American Chemical Society. © 2007 American Chemical Society
[†] Lund, C. L.; Schachner, J. A.; Quail, J. W.; Müller, J. *J. Am. Chem. Soc.* **2007**, *129*, 9313-9320.

Relation of Publication 6 to the Objectives of this Project

After synthesizing and characterizing [1]CAPs and [1]VAPs, reported in Publication 5, a logical step was to target the heavy congener of chromium, in the synthesis of [1]MAPs. Not only were [1]MAPs unknown in the literature, it had been speculated they were thermally labile, making their isolation highly improbable (Chapter 1.1.4). A strategy that was used to prepare aluminum- and gallium-bridged [1]CAPs and [1]VAPs could be successfully transferred to the synthesis of the first [1]MAPs **2a** and **2b**. Surprisingly, both compounds turned out to be thermally robust. In addition, a silicon-bridged[1]MAP (**2c**) was synthesized. In addition to the synthesis and characterization of these new strained sandwich species, their reactivity was explored, in particular, towards transition-metal catalyzed ROP which lead to the discovery of an unprecedented ring-opening reaction. Even though I was able to satisfy the stated primary objective, the group-13-bridged [1]MAPs did not exhibit transition-metal catalyzed ROP.

7. [1]Molybdarenophanes: Strained Metallarenophanes with Aluminum, Gallium and Silicon in Bridging Positions

Clinton L. Lund,[‡] Jörg A. Schachner,[‡] J. Wilson Quail,[§] and Jens Müller[‡*]

[‡]*Department of Chemistry, University of Saskatchewan, 110 Science Place, Saskatoon, Saskatchewan, Canada, S7N 5C9,* [§]*Saskatchewan Structural Sciences Centre, University of Saskatchewan, 110 Science Place, Saskatoon, Saskatchewan, Canada, S7N 5C9*

Received April 19, 2007.

7.1 Abstract

The first [1]molybdarenophanes were synthesized and structurally characterized. The aluminum and gallium compounds [$(Me_2Ntsi)Al(\eta^6\text{-}C_6H_5)_2Mo$] (**2a**) and [$(Me_2Ntsi)Ga(\eta^6\text{-}C_6H_5)_2Mo$] (**2b**) [$Me_2Ntsi = C(SiMe_3)_2(SiMe_2NMe_2)$] were obtained from $[Mo(LiC_6H_5)_2]\cdot$tmeda and $(Me_2Ntsi)ECl_2$ [E = Al, Ga;] in analytical pure form with isolated yields of 74% (**2a**) and 52% (**2b**). The silicon-bridged species [$Ph_2Si(\eta^6\text{-}C_6H_5)_2Mo$] (**2c**) was synthesized from $[Mo(LiC_6H_5)_2]\cdot$tmeda and Ph_2SiCl_2. Compound **2c** was isolated as a crystalline material in an approximately 90% overall purity, from which a single crystal was used for X-ray analysis. The molecular structures of all three [1]molybdarenophanes **2a–c** were determined by single-crystal X-ray analysis. The ring-tilt angle α was found to be 18.28(17), 21.24(10), and 20.23(29)° for **2a**, **2b**, and **2c**, respectively. Variable temperature NMR measurements of **2a** and **2b** (–80 to 80 ºC; 500 MHz) showed a dynamic behavior of the gallium species **2b** but not of compound **2a**. The dynamic behavior of **2b** was rationalized by assuming that the Ga–N donor bond breaks, inversion at the nitrogen atom occurs, a rotation of the Me_2Ntsi ligand takes place followed by a re-formation of the Ga–N bond on the other side of the gallium atom. The analysis of the signals

of meta and ortho protons of **2b** gave approximate values of $\Delta G^{\neq}$ of 59.6 and 59.1 kJ mol^{-1}, respectively. Compound **2b** reacted with $[Pt(PEt_3)_3]$ to give the ring-open product $[(\eta^6\text{-}C_6H_6)Mo\{\eta^6\text{-}C_6H_5[GaPh(Me_2Ntsi)]\}]$ (**3b**). The molecular structure of **3b** was deduced from a single-crystal X-ray determination. The formation of the unexpected platinum-free product **3b** can be rationalized by assuming that benzene reacted with the **2b** in a 1:1 ratio. Through a series of ^1H NMR experiments with **2b** it was shown that small amounts of donor molecules (e.g. thf) in benzene are needed in order to form **3b**; in the absence of a donor molecule, **2b** is thermally stable.

7.2 Introduction

Since the discovery that ring-opening polymerization (ROP) of sila[1]ferrocenophanes yield high molecular weight polymers, many new strained [1]metallacyclophanes have been described in the literature (Figure 7-1).[1,2] Very recently, this area of organometallic chemistry has witnessed important contributions from several research groups. For example, a new class of strained species derived from cycloheptatrienyl–cyclopentadienyl sandwich compounds, $[(\eta^5\text{-}C_7H_7)(\eta^5\text{-}C_5H_5)M]$ (M = Ti, Zr, Cr, V), had been prepared during the last 3 years (Figure 7-1).[3-8] Braunschweig et al. reported on the synthesis of the first strained manganese sandwich, a derivative of the parent compound $[(\eta^6\text{-}C_6H_6)(\eta^5\text{-}C_5H_5)Mn]$.[9] The first [1]metallacyclophanes with aluminum and gallium in bridging positions were made accessible by our efforts using *trisyl*-type ligands with donor abilities at the group-13 element [*trisyl* stands for tris(trimethylsilyl)methyl, $(Me_3Si)_3C$]. To date, we have characterized [1]ferrocenophanes,[10-12] [1]chromarenophanes,[12] and [1]vanadarenophanes.[12]

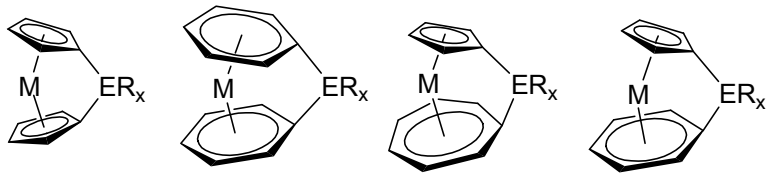

Figure 7-1. [1]Metallacyclophanes.

The chemistry of strained [1]metallacyclophanes has essentially been restricted to compounds that contain 3d transition metals in the sandwich moiety. Besides the zirconium compound mentioned above,[5] [1]ruthenocenophanes are the only strained 4d metal sandwich compounds known today.[13] Surprisingly, even though numerous examples of [1]chromarenophanes are known, not a single [1]molybdarenophane is described in the literature. Bis(benzene)molybdenum was first synthesized by E.O. Fischer *et al*.[14] Its dilithiation and subsequent reactions with silicon dihalides resulted in sparingly characterized polymeric materials.[15] In the course of the preparation of this manuscript, Braunschweig *et al*. reported on the dilithiation of $[Mo(C_6H_6)_2]$ and a structural determination of $[Mo(LiC_6H_5)_2(thf)_6]$. However, attempted syntheses of bora[1]- and sila[1]molybdarenophanes were not successful.[16]

Herein, we report on the first successful syntheses of [1]molybdarenophanes, strained organometallic compounds with aluminum, gallium, and silicon in bridging positions.

7.3 Results and Discussions

A reaction of freshly prepared $[Mo(LiC_6H_5)_2]\cdot$tmeda with an intramolecularly coordinated alane or gallane $(Me_2Ntsi)ECl_2$ [$Me_2Ntsi = C(SiMe_3)_2(SiMe_2NMe_2)$] resulted in [1]molybdarenophanes in moderate isolated yields (Scheme 7-1).

Scheme 7-1. Synthesis of aluminum- and gallium-bridged [1]MAPs.

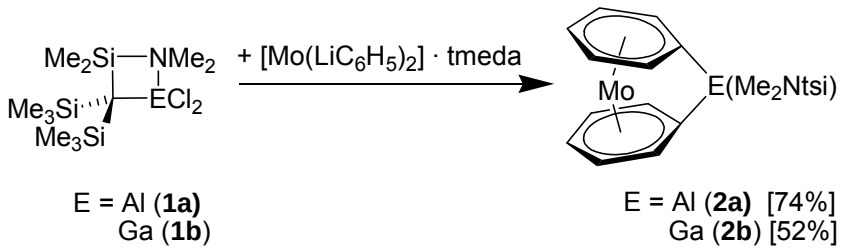

Both [1]molybdarenophanes **2a** and **2b** show the expected signal pattern for time-averaged C_s symmetric species in their ^{1}H and ^{13}C NMR spectra. The ^{1}H NMR spectrum of the alane **2a**, for example, displays two doublets at δ 3.75 and 4.43 (*o*-H) and three pseudo triplets at δ 5.08, 5.16 and 5.57 (*m*-H, *p*-H) with equal signal intensities (25 ºC in C_6D_6). At similar conditions, compound **2b** (25 ºC in C_7D_8) shows only four instead of the expected five signals: three broad signals at δ 3.52 (*o*-H), 4.05 (*o*-H) and 5.24 (*m*-H), and one well resolved pseudo triplet at δ 5.52 (*p*-H) (Figure 7-2). A similar sequence of signals for ortho, meta, and para protons was found for the alumina and galla[1]chromarenophanes.[12] A definite proof that the isolated products **2a** and **2b** are indeed strained [1]metallarenophanes comes from their ^{13}C NMR data. The aromatic *ipso*-C atoms resonate at δ 54.4 (**2a**) and 44.5 (**2b**) which is a significant upfield shift compared to that of the unstrained parent bis(benzene)molybdenum (δ 75.7). These shifts are larger than those observed for alumina and galla[1]chromarenophanes equipped with the same stabilizing *trisyl*-type ligand [δ 62.1 (Al) and 56.6 (Ga) relative to δ 74.8 for $Cr(C_6H_6)_2$].[12] The larger shift is expected as [1]molybdarenophanes should be more highly strained than their chromium analogues.

As mentioned above, the peaks in the proton NMR spectrum of **2b** are broader and not as well resolved as those of **2a** (Figure 7-2). However, the signals of the gallane **2b** sharpen at lower temperature so that at –10 ºC its pattern is similar to that of **2a** (Figure 7-2). We performed

variable temperature NMR measurements of **2a** and **2b** (–80 to 80 ºC; 500 MHz). While the alane **2a** does not show coalescences, the signals of meta and ortho protons of **2b** coalescence at 19.0 and 40.1 ºC, respectively, resulting in approximate values of $\Delta G^{\neq}$ of 59.6 and 59.1 kJ mol^{-1}.[17] The dynamic behavior can be rationalized by assuming that the E–N donor bond breaks, inversion at the nitrogen atom occurs, rotation of the Me_2Ntsi ligand takes place followed by a re-formation of the E–N bond on the other side of the bridging atom. This process is fast enough in the case of the gallane **2b** resulting in a time-averaged C_{2v} species at higher temperatures. The fact that compound **2a** does not show coalescence within the accessible temperature range matches the expectation that Al–N donor bonds are stronger than Ga–N donor bonds.

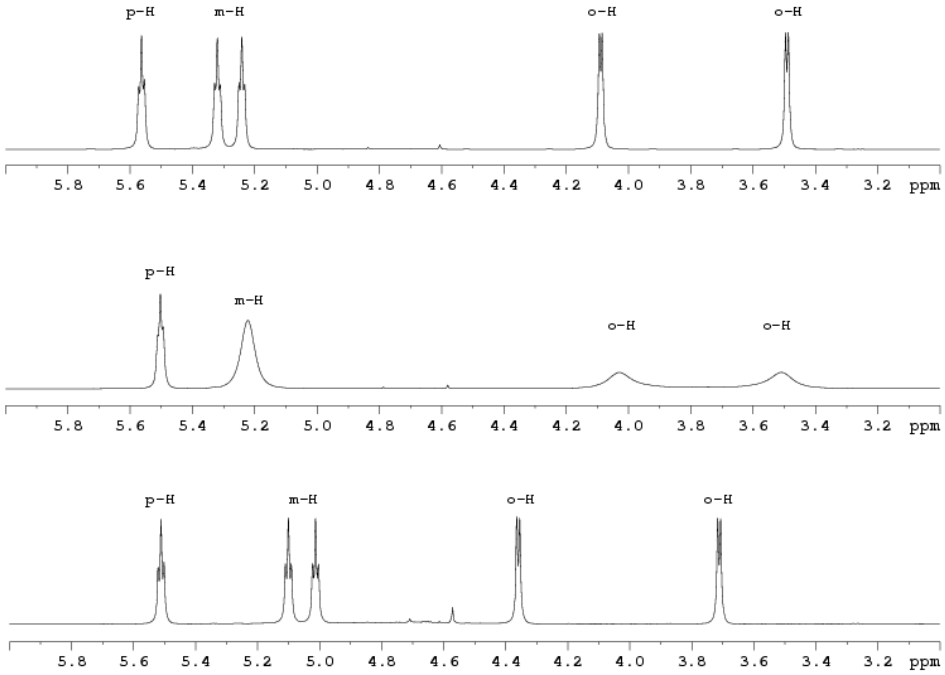

Figure 7-2. ^{1}H NMR spectra in the region of the arene protons of (Me_2Ntsi)Al[1]MAP (**2a**) at 25 ºC (bottom), of (Me_2Ntsi)Ga[1]MAP (**2b**) at 25 ºC (middle), and (Me_2Ntsi)Ga[1]MAP (**2b**) at –10 ºC (top) taken in C_7D_8 (small singlet at δ 4.58 (r.t) and 4.61 (–10 ºC) is due to [Mo(C_6H_6)$_2$]).

Suitable crystals for X-ray structural determinations of both [1]molybdarenophanes were obtained by crystallizations from aromatic solvents. The alane was obtained as **2a**·½ $C_6H_5CH_3$ and the gallane as **2b**·C_6H_6 (Table 7-1 and Figure 7-3 and 7-4). The group-13 element is situated in a spiro position and part of a four-membered ring that deviates only slightly from planarity (rms deviations from planarity are 0.0387 Å (**2a**) and 0.0330 Å (**2b**)). Aluminum and gallium, respectively, are distorted tetrahedrally coordinated by one N and three C atoms. Whereas Al–C bonds are slightly shorter than the respective Ga–C bonds, the Al–N bond of 2.021(4) Å is significantly shorter than the Ga–N bond of 2.120(3) Å (Figure 7-3 and 7-4). Similar sets of bond lengths had been determined for the [1]chromarenophanes and [1]vanadarenophanes.[12] The difference of ca. 0.10 Å between the two E–N bond lengths renders the Ga–N bond much weaker than the Al–N bond, a fact that fits to the observed fluctuating behavior of **2b** in solution.

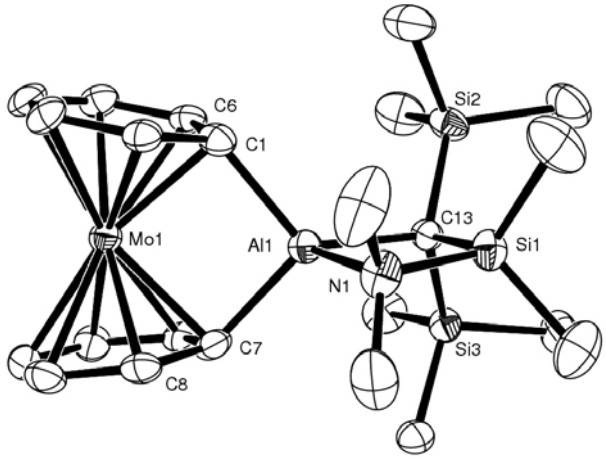

Figure 7-3. Molecular structure of (Me_2Ntsi)Al[1]MAP (**2a**) with thermal ellipsoids at the 50% probability level. H atoms and ½ a molecule of toluene are omitted for clarity. Selected bond lengths [Å] and angles [º]: Al1–N1 = 2.021(4), Al1–C1 = 2.005(5), Al1–C7 = 2.012(5), Al1–C13 = 2.048(5), C1–Al1–C7 = 98.2(2), C7–Al1–C13 = 125.10(19), C1–Al1–C13 = 122.0(2), C7–Al1–N1 = 111.7(2), C1–Al1–N1 = 113.90(19), C13–Al1–N1 = 86.16(19).

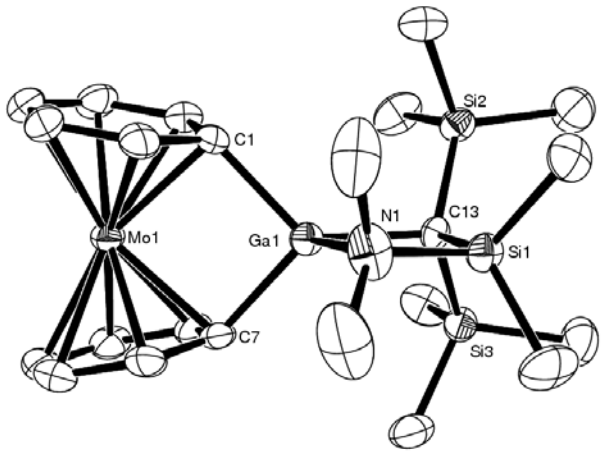

Figure 7-4. Molecular structure of (Me_2Ntsi)Ga[1]MAP (**2b**) with thermal ellipsoids at the 50% probability level. H atoms and one benzene are omitted for clarity. Selected bond lengths [Å] and angles [º]: Ga1–N1 = 2.120(3), Ga1–C1 = 2.029(4), Ga1–C7 = 2.023(4), Ga1–C13 = 2.054(3), C1–Ga1–C7 = 93.74(14), C7–Ga1–C13 = 125.85(14), C1–Ga1–C13 = 128.35(14), C7–Ga1–N1 = 114.54(15), C1–Ga1–N1 = 109.96(16), C13–Ga1–N1 = 84.50(14).

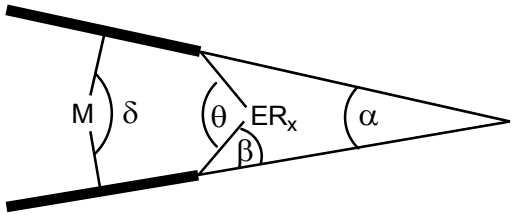

Figure 7-5. Common angles to describe [1]metallacylophanes. Values for **2a** [**2b**] in [deg]: α = 18.28(17) [21.24(10)], θ = 98.2(2) [93.74(14)], and δ = 167.31(20) [164.20(17)].

Table 7-1. Crystal and structural refinement data for compounds (Me_2Ntsi)Al[1]MAP (**2a**), (Me_2Ntsi)Ga[1]MAP (**2b**), Ph_2Si[1]MAP (**2c**), and [(η^6-C_6H_6)Mo{η^6-C_6H_5[GaPh(Me_2Ntsi)]}(**3b**).

	(**2a**·½ toluene)$_2$	**2b**·benzene	**2c**	**3b**
empirical formula	$C_{53}H_{88}Al_2Mo_2N_2Si_6$	$C_{29}H_{46}GaMoNSi_3$	$C_{24}H_{20}MoSi$	$C_{29}H_{46}GaMoNSi_3$
formula weight	1167.63	658.60	432.43	658.60
wavelength, Å		0.71073		
crystal system	triclinic	triclinic	monoclinic	triclinic
space group (No.)	$P\bar{1}$	$P\bar{1}$	$P2_1/c$	$P\bar{1}$
Z	1	2	4	2
a, Å	9.0050(4)	9.2069(3)	7.8790(5)	9.2936(5)
b, Å	9.7930(5)	13.3959(4)	18.5687(13)	9.7991(5)
c, Å	17.0803(8)	13.5754(3)	14.5051(9)	17.2637(10)
α, deg	98.873(3)	110.073(2)	90	90.071(4)
β, deg	97.435(2)	90.698(2)	120.590(4)	102.786(3)
γ, deg	96.174(3)	96.944(2)	90	92.141(4)
vol, Å^3	1463.15(12)	1558.49(8)	1826.8(2)	1532.06(14)
d (calcd), mg/m^3	1.325	1.403	1.572	1.428
temp, K	173(2)	173(2)	173(2)	173(2)
abs coeff., mm^{-1}	0.617	1.400	0.788	1.424
theta range, deg	2.26 to 26.02	2.58 to 27.54	2.81 to 23.25	3.12 to 24.41
refl collected	17573	22845	9175	15565
indep refl	5736 [*R*(int) = 0.0959]	7144 [*R*(int) = 0.0607]	2624 [*R*(int) = 0.1586]	5028 [*R*(int) = 0.1303]
abs correction	ψ-scan	ψ-scan	none	ψ-scan
ref method		full-matrix		
data/ restraints/params	5736/99/321	7144/38/296	2624/0/235	5028/0/327
GOF on F^2	1.072	1.041	1.056	1.065
final *R* indices	*R*1 = 0.0540	*R*1 = 0.0441	*R*1 = 0.0633	*R*1 = 0.0690
[I > 2σ(I)]	w*R*2 = 0.1220	w*R*2 = 0.0986	w*R*2 = 0.1002	w*R*2 = 0.1584
R indices (all data)	*R*1 = 0.0935	*R*1 = 0.0655	*R*1 = 0.1169	*R*1 = 0.1053
	w*R*2 = 0.1459	w*R*2 = 0.1107	w*R*2 = 0.1167	w*R*2 = 0.1785
largest diff. peak and hole, e.Å^{-3}	0.717 and –0.819	0.826 and –0.628	0.480 and –0.563	1.317 and –0.943

The extent of strain in metallacyclophanes is usually illustrated by a set of angles (Figure 7-5). The tilt angles α, which is a measure of the deviation of the two phenyl rings from co-planarity, is the most commonly used parameter to compare different [1]metallacyclophanes. Compounds **2a** and **2b** with tilt angles α of 18.28(17) and 21.24(10)º are expectedly higher tilted than their chromium counterparts [α = 11.81(9) (Al) and 13.24(13)º (Ga)].[12] Dimethylsila[1]ferrocenophane, the most thoroughly investigated [1]metallacyclophane, shows with α = 20.8(5)º[18] a similar distortion as **2a** and **2b**.

For most new [1]metallacyclophanes, silicon-bridged species were the first ones which were explored. On the basis of the promising results we obtained with the synthesis of **2a** and **2b**, we performed initial experiments targeted at silicon-bridged [1]molybdarenophanes. As already mentioned in the introduction, independent from our efforts, Braunschweig and coworker's targeted these species, but their attempted synthesis of sila[1]molybdarenophanes failed and 1,1′-disubstituted bis(benzene)molybdenum compounds were isolated instead.[16] The authors speculated that the targeted [1]molybdarenophanes were thermally instable, which prevented their isolation; no direct evidence for the formation of these ansa species were found. Following the procedure for the synthesis of **2a–b**, we reacted $[Mo(LiC_6H_5)_2]\cdot$tmeda with Ph_2SiCl_2. According to the ^{1}H NMR spectrum of the reaction mixture the targeted diphenylsila[1]molybdarenophane (**2c**) was unequivocally formed among other products. On the basis of the published NMR data for 1,1′-disubstituted bis(benzene)molybdenum compounds,[16] compound **2c** is formed in an approximate 1:1 mixture with $[Mo\{C_6H_5(SiPh_2Cl)\}_2]$. The separation of pure **2c** from this mixture proved to be very difficult. To date, we have successfully crystallized **2c** from benzene, resulting in single crystals suitable for X-ray structural analysis. However, the overall purity of isolated **2c** was estimated to be >90% (see Experimental Section). This first silicon-bridged [1]molybdarenophane (**2c**) was unequivocally identified by ^{1}H and ^{13}C NMR spectroscopy. For example, a large splitting between the resonances of ortho, meta, and para protons at δ 4.04 (d), 4.98 (pst) and 5.46 (pst) (Figure 7-6), respectively, clearly shows that a strained C_{2v} symmetrical [1]molybdarenophane had been formed.

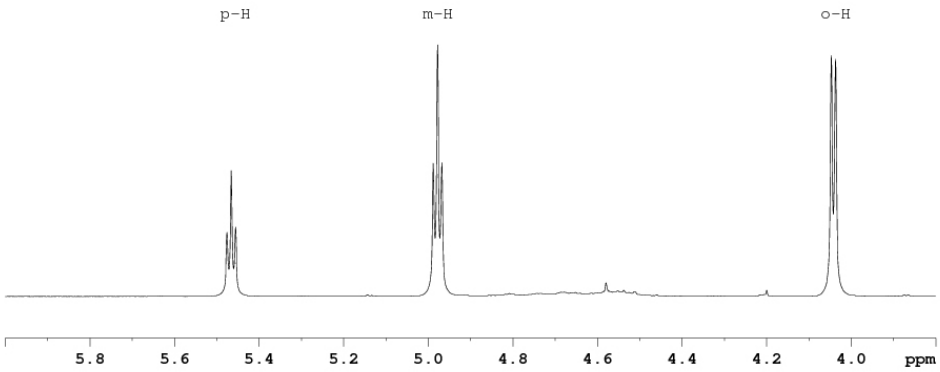

Figure 7-6. ^{1}H NMR spectrum in the region of the arene protons of Ph_2Si[1]MAP (**2c**) at 25 ºC.

Via 2D correlated NMR spectroscopy, ^{13}C NMR signals could be assigned to ortho, meta, and para carbon atoms and, more importantly, the signal of the *ipso*-C atom was detected at δ 32.0. The upfield shift of the resonance of the *ipso*-C atom with respect to the unstrained parent bis(benzene)molybdenum (δ 75.7) clearly supports the conclusion from the proton spectra.

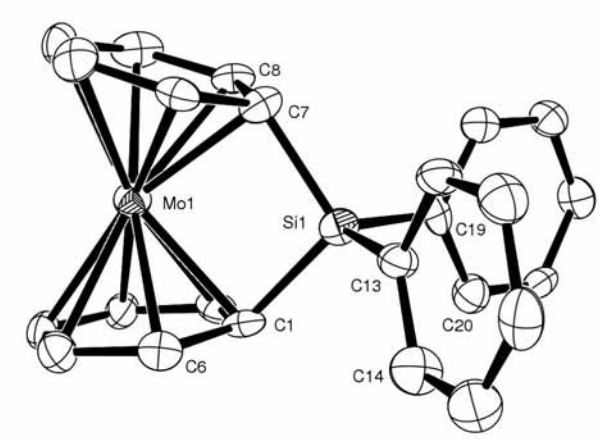

Figure 7-7. Molecular structure of Ph_2Si[1]MAP (**2c**) with thermal ellipsoids at the 50% probability level. H atoms are omitted for clarity. Selected bond lengths [Å] and angles [deg]: Si1–C1 = 1.901(9), Si1–C7 = 1.897(9), Si1–C13 = 1.867(8), Si1–C19 = 1.851(9), C1–Si1–C7 = 102.6(4), C1–Si1–C13 = 111.3(4), C1–Si1–C19 = 111.0(4), C7–Si1–C13 = 111.6(4), C7–Si1–C19 = 109.3(4), C13–Si1–C19 = 110.8(4), α = 20.23(29), δ = 165.29 (see Figure 7-5).

To obtain structural details, a single-crystal X-ray analysis of **2c** was undertaken (Table 7-1 and Figure 7-7). The silicon atom in **2c** is nearly ideally tetrahedrally surrounded by four carbon atoms, which can be illustrated by the narrow range of 102.6(4)–111.6(4)º found for the six C–Si–C angles. Expectedly, the θ angle of 102.6(4)º (C1–Si1–C7) is the most distorted C–Si–C angle. The four Si–C bonds are split into a set of two shorter bonds (Si1–C13 = 1.867(8) and Si1–C19 = 1.851(9) Å) and two longer bonds (Si1–C1 = 1.901(9) and Si1–C7 = 1.897(9) Å). Even though the differences between the two sets are small, they are significant and can be rationalized as being a consequence of the strain exerted on the bonds of silicon to the *ipso*-C atoms of the coordinated phenyl rings. In agreement with this interpretation is the fact that the less strained diphenylsila[1]chromarenophane[19] shows a less pronounced difference between the two sets of Si–C bonds (1.882(4)/1.882(4) Å compared to 1.868(4) / 1.870(5) Å).

The tilt angle α is the most commonly used parameter to illustrate the degree of strain in metallacyclophanes (Figure 7-5). For the aluminum-bridged [1]molybdarenophanes **2a** the α angle of 18.28(17)° means a 55% (6.5°) increase compared to its chromium analogue [$(Me_2Ntsi)Al(C_6H_5)_2Cr$] (α = 11.81(9)°).[12] Similarly, the gallium species **2b** with α = 21.24(10)° shows an increase of 60% (8.0°) with respect to its chromium counterpart (α = 13.24(13)°).[12] Compound **2c** exhibits a tilt angle α of 20.23(29)° which is only a 40% (5.8°) increase compared to its chromium analogue[19] (α = 14.4°). On the basis of the increases found for **2a** and **2b**, a tilt angle between 22–23° would be expected for compound **2c**.

The interest in novel [1]metallacyclophanes is partly driven by their potential usefulness for ring-opening polymerizations (ROPs). However, the known examples of ROPs of strained metallarenophanes are rare. Manners *et al.* had shown that thermal- or anionic co-polymerization of dimethylsila[1]chromarenophane with dimethylsila[1]ferrocenephane can be performed.[20] A

few years later, dimethylsila[1]chromarenophane was polymerized using Karstedt's catalyst, but the poor solubility of the resulting polymers prevented a full characterization.[21] To investigate if a metallarenophane is prone to undergo transition metal mediated ROP, platinum complexes like $[Pt(1,5\text{-cod})_2]$[22,23] and $[Pt(PEt_3)_3]$[23–28] had been used with the intent of isolating a compound in which a PtL_x moiety is inserted into the *ipso*-C bridging-element bond. Compounds of this type have thrown some light on the transition metal mediated ROP.[23] The first isolatable compound was $[Fe(\eta^5\text{-}C_5H_4)_2Pt(PEt_3)_2SiMe_2]$ obtained from dimethylsila[1]ferrocenophane and $[Pt(PEt_3)_3]$.[24,25] On this basis, we intended to find out if the new [1]molybdarenophanes might undergo transition-metal mediated polymerizations and we did a series of experiments with the gallium-bridged species **2b**. Surprisingly, compound **2b** reacts with $[Pt(PEt_3)_3]$ in refluxing benzene to give the new ring-opened product **3b** (Figure 7-8). As deduced from a single-crystal X-ray analysis, **3b** is a platinum-free species (Table 7-1 and Figure 7-8).

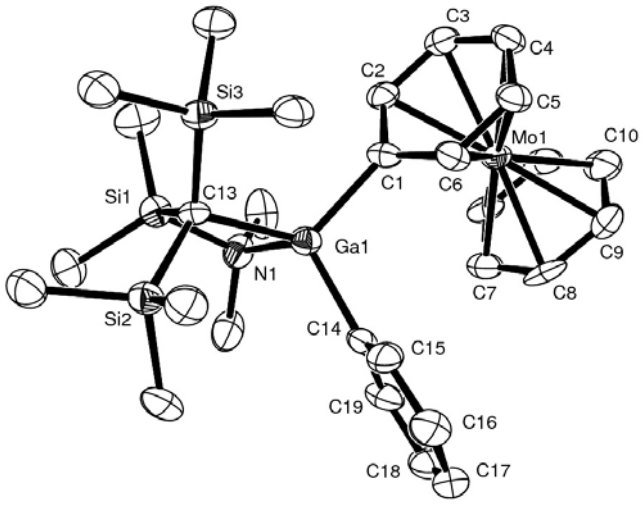

Figure 7-8. Molecular structure of $[(\eta^6\text{-}C_6H_6)Mo\{\eta^6\text{-}C_6H_5[GaPh(Me_2Ntsi)]\}$ (**3b**) with thermal ellipsoids at the 50% probability level. H atoms are omitted for clarity. Selected bond lengths [Å] and angles [deg]: Ga1–N1 = 2.148(6), Ga1–C1 = 2.001(7), Ga1–C14 = 1.994(8), Ga1–C13 = 2.096(7), C1–Ga1–C14 = 109.2(3), C13–Ga1–C14 = 119.9(3), C1–Ga1–C13 = 117.2(3), C14–Ga1–N1 = 112.8(3), C1–Ga1–N1 = 112.2(3), C13–Ga1–N1 = 83.2(3).

Its formation can be rationalized by assuming that benzene reacted with the [1]molybdarenophane **2b** in a 1:1 ratio. We performed a series of NMR experiments to elucidate the role of the platinum complex. ^{1}H NMR experiments with **2b** and [Pt(PEt$_3$)$_3$] in C_6H_6 and C_6D_6, respectively, clearly revealed that the non-substituted benzene ring of the bis(arene)molybdenum moiety of **3b** exclusively comes from the solvent. From a competing experiment between C_6H_6 and C_6D_6 it was shown that both ligands are incorporated into **3b** with the same rate, attesting that C–H activation is not part of a rate determining step. If [Pt(PEt$_3$)$_3$] was not added, the galla[1]molybdarenophane **2b** did not react with benzene at all: the strained species **2b** did not change after heating to 65 ºC in C_6D_6 for 7 days. The reaction of [Pt(cod)$_2$] with **2b** gave also product **3b**. On the basis of these findings, we tested if the platinum complex or just free donor ligands are needed for the transformation. NMR experiments of **2b** in C_6D_6 with 0.3–0.5 equivalent amounts of PEt$_3$, cod, and thf, respectively, all resulted in the formation of **3b**. However, only in the case of thf did the reaction proceed exclusively from **2b** to **3b**, with no signs of any byproducts. For PEt$_3$ and cod the ^{1}H NMR spectra revealed the formation of byproducts, which we could not identify so far. For [Mo(C_6H_6)$_2$] it is known that the benzene ligands are relatively labile what makes the compound a common starting material for half-sandwich complexes.[29,30] However, the substitution of benzene in [Mo(C_6H_6)$_2$] by other arenes requires forcing thermal conditions (160 ºC; 48 h).[31] The respective ligand substitution in the galla[1]molybdarenophane **2b** which yields **3b** is catalyzed by donor species and it seems that the reaction occurs at relatively mild conditions due to the high strain of **2b**.

7.4 Summary and Conclusion

The first [1]molybdarenophanes with aluminum, gallium, and silicon in bridging positions have been synthesized. Surprisingly the gallium species **2b** with an α tilt angle of 21.24(10)º is significantly higher strained than its aluminum counterpart **2a** [α = 18.28(17)]. This is counterintuitive because the slightly smaller Al atom should result in a slightly larger tilt angle α.[32] To date, for all known cases, the tilt angles α are larger for galla than for alumina[1]metallacyclophanes.[10–12] Compounds **2a** and **2b** follow the same trend but show with 3.0º so far the largest difference; the reasons for the structural differences are unknown. In the presence of donor ligands like PEt_3, cod, and thf, respectively, the otherwise thermally robust compound gallium species **2b** adds one equivalent of benzene to give the unstrained complex **3b**. The reaction with thf proceeds very cleanly to give the ring-open product **3b** exclusively, showing that thf acts as a catalyst only. At this point we can only speculate about the mechanism of this catalyzed benzene addition. It seems likely that the σ donor ligand coordinates to the molybdenum atom and weakens the coordination of the phenyl group so that benzene eventually replaces the σ donor ligand and the η^6-phenyl group. This is an unprecedented reactivity of a bis(benzene)molybdenum derivative and a similar ring-opening reaction of [1]metallacyclophanes is not reported in the literature. In contrast to many other [1]metallacyclophanes, the gallium compound **2b** does not insert a PtL_x moiety into E–C(*ipso*) bonds, which might be due to a steric protection of these bonds by two bulky $SiMe_3$ groups.

The first silicon-bridged [1]molybdarenophane (**2c**) shows with α = 20.23(29)° a smaller angle than expected. Our finding that bis(lithiobenzene)molybdenum and Ph_2SiCl_2 results in the targeted sila[1]molybdareanophane **2c** is in contrast to a recent report.[16] The authors reported that 1,1′-disubstituted bis(benzene)molybdenum compounds were formed and speculated that the

targeted [1]molybdareanophanes were thermally instable and, therefore, could not be obtained. We have proven that the most strained [1]molybdarenophane, the gallium-bridged species **2b**, is thermally robust when heated in benzene. Besides the sensitivity towards donor molecules, all [1]molybdarenophanes are very sensitive towards oxygen. In all cases the highest resolved ^{1}H NMR spectra with the smallest peak width were obtained from freshly synthesized samples. Prolonged handling of the species using Schlenk techniques usually resulted in ^{1}H NMR spectra with unstructured and broad signals for the aromatic protons of the coordinated phenyl groups. In extreme cases, these peaks disappeared in the baseline, while all other signals remained undisturbed. These observations can be rationalized by assuming that small amounts of oxygen result in small amounts of paramagnetic Mo(I) cations. A fast electron exchange between the neutral and oxidized [1]molybdarenophanes spreads, on time average, the paramagnetic impurity evenly over all species so that only the aromatic protons are affected. Electron transfer of this type were found for bis(benzene)chromium derivatives before.[12,19,33]

Recently, a novel type of ring-opening polymerization, coined photocontrolled ROP, was described.[34,35] Within this method, a ROP of a sila[1]ferrocenophane is initiated by Cp^{-}, but the polymerization only occurs under irradiation. Photocontrolled ROP is a living polymerization that can be stopped and continued by turning the light off and on, respectively. Photons weaken the Fe–Cp bond allowing the addition of Cp^{-}. It is the only example of ROP where the ring-opening happens at the transition-metal side of the precursor. Based on our findings, it is feasible that one can develop a similar but 'dark' version of the photocontrolled ROP for [1]molybdarenophanes with benzene instead of Cp^{-} as a starter and thf instead of photons as activator.

7.5 Experimental Section

General Procedures. All manipulations were carried out using standard Schlenk techniques. Solvents were dried using a MBraun Solvent Purification System and stored under nitrogen over 4 Å molecular sieves. All solvents for NMR spectroscopy were degassed prior to use and stored under nitrogen over 4 Å molecular sieves. $[Mo(LiC_6H_5)_2]\cdot$tmeda,[15] $AlCl_2[C(SiMe_3)(SiMe_2NMe_2)]$ (**1a**),[36] and $GaCl_2[C(SiMe_3)(SiMe_2NMe_2)]$ (**1b**)[36] were synthesized as described in the literature. $[Pt(PEt_3)_3]$ was prepared from $[Pt(PEt_3)_4]$[37] in situ by heating to 60 ºC under high vacuum in an NMR tube. $[Pt(cod)_2]$ was prepared via a modified procedure by substituting potassium in place of lithium.[38] An improved synthesis of $[Mo(C_6H_6)_2]$ with respect to common method described in reference[39] is reported below. ^{1}H, ^{13}C, and ^{27}Al NMR and spectra were recorded on a Bruker 500 MHz Avance at 25 ºC, unless noted differently. ^{1}H chemical shifts were referenced to the residual protons of the deuterated solvent (C_6D_6 at δ 7.15; C_7D_8 at δ 2.10); ^{13}C chemical shifts were referenced to C_6D_6 at δ 128.00 and C_7D_8 at δ 20.40. ^{27}Al NMR spectra were referenced to $[Al(acac)_3]$ dissolved in C_6D_6. An unequivocal assignment of signals of the bis(benzene)molybdenum moiety of compound **2c** was done with the help of ^{1}H/^{1}H-COSY, HMQC, and HMBC spectroscopy. Mass spectra were measured on a VG 70SE (m/z > 10% are listed for signals of the most abundant ions). Elemental analyses were performed on a Perkin Elmer 2400 CHN Elemental Analyzer using V_2O_5 to promote complete combustion.

Improved Synthesis of $[Mo(C_6H_6)_2]$ (based on ref 39). $MoCl_5$ (7.4072 g, 27.082 mmol), $AlCl_3$ (18.522 g, 138.91 mmol), Al (1.821 g, 67.44 mmol), mesitylene (1.0 mL) and benzene (70 mL) were set to reflux for 76 h. All volatiles were removed in vacuum and the brown solid was broken up into small pieces and added to N_2 saturated aqueous solution (175

mL) containing KOH (51.090 g, 910.60 mmol) and $Na_2S_2O_4$ (11.152g, 64.051 mmol) over 1 h at –20 to –30 ºC. The solution was decanted off and the brown solid was dried on high vacuum. The solid was continually extracted with boiling benzene (150 mL) to give a dark green solution. All volatiles were removed to give a green solid. The solid was washed with hexanes (60 mL) and dried to give a bright green solid (3.2742 g, 48%). 1H NMR (500 MHz): δ 4.58 (s).

Synthesis of [{(Me_2NMe_2Si)(Me_3Si)$_2$C}Al(η^6-C_6H_5)$_2$Mo] (2a). [Mo(C_6H_6)$_2$] (0.7830 g, 3.105 mmol), cyclohexane (30 mL), tmeda (1.875 g, 16.13 mmol), and nBuLi (6.0 mL, 2.6 M in hexanes, 15.6 mmol) were added one after the other and the mixture was heated (2.5 h, 50 ºC) during which the slurry changed color from green to dark red. The solution was syringed off and the remaining red solid was dried in high vacuum to give [Mo(LiC_6H_5)$_2$]·tmeda (0.811 g, 2.13 mmol). A slurry of this compound in benzene (20 mL, 0 ºC) was added to a solution of **1a** (0.770 g, 2.15 mmol) in benzene (10 mL, 0 ºC) and stirred for 1 h at room temperature. LiCl was filtered off, followed by concentration of the filtrate to approximately 5 mL, and crystallization at 6 ºC gave green crystals of **2a**·C_6H_6 (0.969 g, 74%). ^{1}H NMR (500 MHz, C_6D_6): δ = 0.14 (s, 6H, $SiMe_2$), 0.45 (s, 18 H, $SiMe_3$), 1.97 (s, 6H, NMe_2), 3.75 (d, 2H, o-H), 4.43 (d, 2H, o-H), 5.08 (pst, 2H, m-H), 5.16 (pst, 2H, m-H), 5.57 (pst, 2H, p-H). ^{13}C NMR (C_6D_6): 3.0 ($SiMe_2$), 8.1 ($SiMe_3$), 40.5 (NMe_2), 54.4 (*ipso*-C), 74.4 (o-C), 74.5 (o-C), 82.5 (p-C), 83.1 (m-C), 83.8 (m-C). ^{27}Al NMR (C_6H_6): 148 ($w_{1/2}$ = 1800 Hz).MS (70 eV): *m*/*z* (%) 364 (10) [M^+–Mo–C_6H_6–C_6H_5], 295 (14), [M^+–Mo–C_6H_6–2 $SiMe_3$], 246 (60) [MH^+–Mo–Al–C_6H_6–2 C_6H_5–CH_3], 230 (19) [M^+–Mo–Al–C_6H_6–2 C_6H_5–2 CH_3], 219 (18) $[C_9H_{27}Si_3]^+$, 217 (16) $[C_9H_{25}Si_3]^+$, 203 (42) $[C_8H_{23}Si_3]^+$, 154 (31) $[C_{12}H_{10}]^+$, 129 (30) $[C_5H_{13}Si_2]^+$, 102 (34) $[C_4H_{12}NSi]^+$, 91 (12) $[C_7H_7]^+$, 78 (100)$[C_6H_6]^+$, 73 (35) $[C_3H_9Si]^+$, 58 (19) $[C_2H_6Si]^+$. Anal. Calcd for $C_{29}H_{46}AlMoNSi_3$

(615.8603): C, 56.56; H, 7.53; N, 2.27; Found: C, 55.73; H, 7.35; N, 2.62. Crystals of **2a**·½ C_7H_8 suitable for X-ray diffraction were grown from toluene at 6 °C.

Synthesis of [{(Me_2NMe_2Si)(Me_3Si)$_2$C}Ga(η^6-C_6H_5)$_2$Mo] (2b). [Mo(C_6H_6)$_2$] (0.9116 g, 3.615 mmol), cyclohexane (30 mL), tmeda (2.180 g, 18.76 mmol), and nBuLi (7.0 mL, 2.6 M in hexanes, 18 mmol) were added one after another and the mixture was heated (2.5 h, 50 ºC) during which the slurry changed color from green to dark red. The solution was syringed off and the remaining red solid was dried in high vacuum (0.835 g, 2.20 mmol). A slurry of this compound in benzene (30 mL, 0 ºC) was added to a solution of **1b** (0.884 g, 2.20 mmol) in benzene (10 mL, 0 ºC). After stirring for 2 h at room temperature, LiCl was filtered off, the filtrate was concentrated (5 mL), and crystallization at 6 ºC gave green crystals of **2b**·C_6H_6 (0.747 g, 52%). ^{1}H NMR (500 MHz, C_7D_8, –10 ºC): δ = 0.19 (s, 6H, $SiMe_2$), 0.45 (s, 18 H, $SiMe_3$), 1.99 (s, 6H, NMe_2), 3.49 (d, 2H, o-H), 4.09 (d, 2H, o-H), 5.23 (pst, 2H, m-H), 5.32 (pst, 2H, m-H), 5.56 (pst., 2H, p-H). ^{13}C NMR (C_7D_8, –10 ºC) : 2.8 ($SiMe_2$), 7.3 ($SiMe_3$), 11.7 (CSi_3), 41.2 (NMe_2), 44.5 (*ipso*-C), 73.8 (o-C), 73.9 (o-C), 83.6 (p-C), 84.5 (m-C), 85.5 (m-C).MS (70 eV): *m*/*z* (%) 406 (100) [M^+–Mo–C_6H_6–C_6H_5], 361 (22) [M^+–Mo–C_6H_6–C_6H_5–3 CH_3], 292 (13) [M^+–Mo–Ga–C_6H_6–C_6H_5–3CH_3], 246 (87) [MH^+–Mo–Ga–C_6H_6–2 C_6H_5–CH_3], 230 (74) [M^+–Mo–Ga–C_6H_6–2C_6H_5–2CH_3], 223 (13) [$C_{12}H_{10}Ga]^+$, 217 (35) [$C_9H_{25}Si_3]^+$, 203 (31) [$C_8H_{23}Si_3]^+$, 201 (15) [$C_8H_{21}Si_3]^+$, 187 (25) [$C_7H_{19}Si_3]^+$, 175 (14) [$C_8H_{23}Si_2]^+$, 154 (15) [$C_{12}H_{10}]^+$, 128 (28) [$C_5H_{12}Si_2]^+$, 102 (26) [$C_4H_{12}NSi]^+$, 78 (93) [$C_6H_6]^+$, 73 (31) [$C_3H_9Si]^+$. Anal. Calcd for $C_{29}H_{46}GaMoNSi_3$ (658.6017): C, 52.89; H, 7.04; N, 2.13; Found: C, 52.26; H, 7.10; N, 2.37.

Synthesis of [Ph_2Si(η^6-C_6H_5)$_2$Mo] (2c). [Mo(C_6H_6)$_2$] (1.1062 g, 4.387 mmol), cyclohexane (30 mL), tmeda (2.589 g, 22.28 mmol) and *n*BuLi (7.8 mL, 2.86 M, 22.3 mmol) were added one after another and the mixture was heated (2.5 h, 50 ºC) during which the slurry

changed color from green to dark red. The solution was syringed off and the remaining red solid was dried in high vacuum (1.383 g, 3.637 mmol). A slurry of this compound in benzene (30 mL, 0 ºC) was prepared and Ph_2SiCl_2 (0.917 g, 3.622 mmol) was added dropwise during 10 min. The solution was warmed to ambient temperature and stirred for 1 h. An ^{1}H NMR spectrum from an aliquot of the reaction mixture revealed that **2c** had been formed. Crystallization from benzene at 6 ºC gave **2c** as a red-brown crystalline solid (0.415 g, app. 23%), from which a single crystal was used for the X-ray structural analysis. However, according to ^{1}H NMR spectroscopy this crystalline fraction showed an approximate overall purity of 90% (see Supporting Information). ^{1}H NMR (500 MHz, C_6D_6): δ = 4.04 (d, 4H, o-H), 4.98 (pst, 4H, m-H), 5.46 (pst, 2H, p-H), 7.20 (m, 6H, m-H, p-H), 7.97 (pst, 4H, o-H). ^{13}C NMR (C_6D_6): 32.0 (*ipso*-C), 74.1 (o-C), 85.1 (p-C), 85.6 (m-C), 128.9 (p-C), 130.5 (m-C), 134.4 (*ipso*-C), 134.5 (o-C).

Synthesis of [(η^6-C_6H_6)Mo{η^6-C_6H_5[GaPh(Me_2Ntsi)]}] (3b). $Pt(PEt_3)_4$ (0.3751 g, 0.5618 mmol) was placed in a Schlenk flask and heated to 60 ºC under vacuum (10^{-2} torr) to give $Pt(PEt_3)_3$ as a red oil.[37] Benzene (5 mL) and **2b** (0.3698 g, 0.5615 mmol) were added. After stirring for 1 h at ambient temperature, the solution was heated to 65 ºC for 87 h. The mixture was monitored by ^{1}H NMR spectroscopy with a gradual disappearance of **2b** and the appearance of new signals. All volatiles were removed and the resulting black solid was extracted with benzene (5 mL). The benzene was removed and the greenish solid was dissolved in a 1:1 mixture of Et_2O and toluene (5 mL) and kept at –30 ºC to give green crystals (0.105 g, 28%). ^{1}H NMR (500 MHz, C_6D_6): 0.19 (br. s, 6 H, $SiMe_2$) , 0.35 (s, 18H, $SiMe_3$), 2.22 (s, 6H, NMe_2), 4.47 (s, 6H, Ph), 4.53 (br. d, 2H, o-H), 4.60 (br. s, 2H, m-H), 4.67 (pst, 1H, p-H), 7.21 (pst, 1H, p-H), 7.29 (pst, 2H, m-H), 7.68 (d, 2H, o-H).

^{1}H-NMR Experiments with 2b. $[Pt(PEt_3)_3]$ was prepared from $[Pt(PEt_3)_4]$[37] in situ by heating to 60 ºC under high vacuum in an NMR tube. PEt_3 (1.0 M in thf) was purchased from Aldrich. Samples were prepared in glovebox and subsequently flame sealed by freezing the samples in liquid nitrogen and evacuating the tubes under high vacuum (10^{-2} mbar). All NMR tubes were heated for prolonged time at an oil bath temperature of 65 ºC and monitored by ^{1}H NMR spectroscopy.

Tube 1: $[Pt(PEt_3)_4]$ (37.4 mg, 0.0560 mmol) was weighed into a NMR tube and the off white solid was converted to the red oil $[Pt(PEt_3)_3]$ by heating the NMR tube to 60 °C under high vacuum. Compound **2b**·C_6H_6 (37.5 mg, 0.0569 mmol) in C_6D_6 (1 mL) was added to the red oil and the tube was flame sealed. After 1336 h approximately 80% of the starting compound **2b** had been consumed.

Tube 2: PEt_3 (0.016 mL, 1.0 M in thf, 0.016 mmol) was placed in a NMR tube and thf was removed under reduced pressure. Compound **2b**·C_6H_6 (28.6 mg, 0.0434 mmol) in C_6D_6 (1 mL) was added and the tube was flame sealed. After 1168 h the starting compound **2b** had been consumed.

Tube 3: **2b**·C_6H_6 (27.1 mg, 0.0411 mmol) was placed in a NMR tube, C_6D_6 (1 mL) was added, and the tube was flame sealed. After 160 h the starting compound **2b** showed no signs of decomposition or transformation. After 832 h 4% of **2b** had been transformed to **3b**.

Tube 4: **2b**·C_6H_6 (26.4 mg, 0.0401 mmol) and $[Pt(PEt_3)_4]$ (26.6 mg, 0.0398 mmol) were weighed into an NMR tube, C_6D_6 (1.0 mL) was added, and the tube was flame sealed. After 304 h the starting compound **2b** had been consumed.

Tube 5: $[Pt(cod)_2]$ (11.0 mg, 0.027 mmol) was dissolved in C_6D_6 (1.0 mL), compound **2b**·C_6H_6 (15.3 mg, 0.023.2 mmol) was added to the solution, and the tube was flame sealed. After 304 h the starting compound **2b** had been consumed.

Tube 6: **2b**·C_6H_6 (19.4 mg, 0.029 mmol) was placed in a NMR tube, thf (1.2 μL, 0.01 mmol), and C_6D_6 (1.0 mL) were added, followed by flame sealing the tube. After 448 h the starting compound **2b** had been cleanly converted to **3b**.

Tube 7: **2b**·C_6H_6 (25.8 mg, 0.039 mmol) was placed in a NMR tube, cod (2.4 μL, 0.02 mmol) and C_6D_6 (1.0 mL) were added followed by flame sealing the tube. After 448 h the starting compound **2b** had been consumed.

Tube 8: $[Pt(PEt_3)_4]$ (28.3 mg, 0.042 mmol) was converted to $[Pt(PEt_3)_3]$ as described above and **2b**·C_6H_6 (28.1 mg, 0.043 mmol) was added. The compounds were dissolved in C_6H_6 (0.50 mL, 5.6 mmol), and C_6D_6 (0.50 mL, 5.6 mmol) and the tube was flame sealed. After 216 h the reaction was stopped because it was determined that no deuterium isotope effect was present.

Crystal structure determination. The crystal data of **2a–c**, and **3b** were collected at –100 °C on a Nonius Kappa CCD diffractometer, using the COLLECT program.[40] Cell refinement and data reductions used the programs DENZO and SCALEPACK.[41] SIR97[42] was used to solve the structure and SHELXL-97[43] was used to refine the structure. ORTEP-3 for Windows[44] was used for molecular graphics and PLATON[45] was used to prepare material for publication. H atoms were placed in calculated positions with U_{iso} constrained to be 1.2 times U_{eq} of the carrier atom for aromatic protons. U_{iso} is constrained to be 1.5 times U_{eq} for methyl protons. For compound **2a**, a solvent toluene molecule was found disordered around a centre of symmetry. It was modeled with a rigid toluene molecule. The temperature factors of the C atoms of the toluene were allowed to refine, but were restrained by SIMU, DELU and ISOR commands

in the refinement. For compound **2b**, a solvent benzene molecule was found disordered around a centre of symmetry. It was modeled by two rigid benzene molecules with the sum of their occupancies equal to 1.0. The temperature factors of the C atoms of the toluene were allowed to refine, but were restrained by SIMU, DELU and ISOR commands in the refinement.

Compounds **2c** and **3b** gave crystals of poor quality. The maximum observable diffraction angles were low (23.25° and 24.41°) and the merging R values were high (0.159 and 0.13). A full sphere of data was collected in both cases. The presence of a heavy atom (Mo) in both structures contributes strongly to the poor bond precision for the lighter atoms because the Mo atom dominates the scattering. In both structures all non-hydrogen atoms refined anisotropically with no restraints to reasonable positions giving reasonable bond lengths and bond angles, thus clearly establishing the connectivity of the molecules.

Acknowledgement. We thank the Natural Sciences and Engineering Research Council of Canada (NSERC Discovery Grant, J.M.), the Department of Chemistry, the Saskatchewan Structural Sciences Centre, and the University of Saskatchewan for their generous support. We thank the Canada Foundation for Innovation (CFI) and the government of Saskatchewan for funding of the X-ray and NMR facilities in the Saskatchewan Structural Sciences Centre (SSSC).

Supporting Information Available. Crystallographic data for **2a**, **2b**, **2c**, and **3b** in CIF file format; ^{1}H and ^{13}C NMR spectra for **2c**. This material is available free of charge via the internet at http://pubs.acs.org.

7.6 References

(1) Foucher, D. A.; Tang, B. Z.; Manners, I. *J. Am. Chem. Soc.* **1992**, *114*, 6246-6248.
(2) Herbert, D. E.; Mayer, U. F. J.; Manners, I. *Angew. Chem. Int. Ed.* **2007**, *46*, in press.
(3) Elschenbroich, C.; Paganelli, F.; Nowotny, M.; Neumüller, B.; Burghaus, O. *Z. Anorg. Allg. Chem.* **2004**, *630*, 1599-1606.

(4) (a) Tamm, M.; Kunst, A.; Bannenberg, T.; Herdtweck, E.; Sirsch, P.; Elsevier, C. J.; Ernsting, J. M. *Angew. Chem., Int. Ed.* **2004**, *43*, 5530-5534. (b) Tamm, M.; Kunst, A.; Bannenberg, T.; Randoll, S.; Jones, P. G. *Organometallics* **2007**, *26*, 417-424.
(5) Tamm, M.; Kunst, A.; Bannenberg, T.; Herdtweck, E.; Schmid, R. *Organometallics* **2005**, *24*, 3163-3171.
(6) Braunschweig, H.; Lutz, M.; Radacki, K. *Angew. Chem., Int. Ed.* **2005**, *44*, 5647-5651.
(7) Braunschweig, H.; Lutz, M.; Radacki, K.; Schaumloffel, A.; Seeler, F.; Unkelbach, C. *Organometallics* **2006**, *25*, 4433-4435.
(8) Bartole-Scott, A.; Braunschweig, H.; Kupfer, T.; Lutz, M.; Manners, I.; Nguyen, T.-l.; Radacki, K.; Seeler, F. *Chem. Eur. J.* **2006**, *12*, 1266-1273.
(9) Braunschweig, H.; Kupfer, T.; Radacki, K. *Angew. Chem. Int. Ed.* **2007**, *46*, 1630-1633.
(10) Schachner, J. A.; Lund, C. L.; Quail, J. W.; Müller, J. *Organometallics* **2005**, *24*, 785-787.
(11) Schachner, J. A.; Lund, C. L.; Quail, J. W.; Müller, J. *Organometallics* **2005**, *24*, 4483-4488.
(12) Lund, C. L.; Schachner, J. A.; Quail, J. W.; Müller, J. *Organometallics* **2006**, *25*, 5817-5823.
(13) Vogel, U.; Lough, A. J.; Manners, I. *Angew. Chem. Int. Ed.* **2004**, *43*, 3321-3325.
(14) Fischer, E. O.; Stahl, H. O. *Chem. Ber.* **1956**, *89*, 1805-1808.
(15) Green, M. L. H.; Treurnicht, I.; Bandy, J. A.; Gourdon, A.; Prout, K. *J. Organomet. Chem.* **1986**, *306*, 145-165.
(16) Braunschweig, H.; Buggisch, N.; Englert, U.; Homberger, M.; Kupfer, T.; Leusser, D.; Lutz, M.; Radacki, K. *J. Am. Chem. Soc.* **2007**, *129*, 4840-4846.
(17) Sandström, J. *Dynamic NMR Spectroscopy*; Academic Press: London, 1982.
(18) Finckh, W.; Tang, B. Z.; Foucher, D. A.; Zamble, D. B.; Ziembinski, R.; Lough, A.; Manners, I. *Organometallics* **1993**, *12*, 823-829.
(19) Elschenbroich, C.; Hurley, J.; Metz, B.; Massa, W.; Baum, G. *Organometallics* **1990**, *9*, 889-897.
(20) Hultzsch, K. C.; Nelson, J. M.; Lough, A. J.; Manners, I. *Organometallics* **1995**, *14*, 5496-5502.
(21) Berenbaum, A.; Manners, I. *J. Chem. Soc., Dalton Trans.* **2004**, 2057-2058.
(22) Sheridan, J. B.; Temple, K.; Lough, A. J.; Manners, I. *J. Chem. Soc., Dalton Trans.* **1997**, 711-713.
(23) Temple, K.; Jäkle, F.; Sheridan, J. B.; Manners, I. *J. Am. Chem. Soc.* **2001**, *123*, 1355-1364.
(24) Sheridan, J. B.; Lough, A. J.; Manners, I. *Organometallics* **1996**, *15*, 2195-2197.
(25) Reddy, N. P.; Choi, N.; Shimada, S.; Tanaka, M. *Chem. Lett.* **1996**, 649-650.
(26) Temple, K.; Lough, A. J.; Sheridan, J. B.; Manners, I. *J. Chem. Soc., Dalton Trans.* **1998**, 2799-2805.
(27) Chan, W. Y.; Berenbaum, A.; Clendenning, S. B.; Lough, A. J.; Manners, I. *Organometallics* **2003**, *22*, 3796-3808.
(28) Tamm, M.; Kunst, A.; Herdtweck, E. *Chem. Commun.* **2005**, 1729-1731.
(29) R. Davis, L. A. P. Kane-Maguire, in *Comprehensive Organometallic Chemistry, Vol. 3* (Eds.: G. Wilkinson, F. G. A. Stone, E. W. Abel), Pergamon Press, Oxford, **1982**, pp. 1204-1210.
(30) M. J. Morris, in *Comprehensive Organometallic Chemistry, Vol. 5* (Eds.: E. W. Abel, F. G. A. Stone, G. Wilkinson), Pergamon Press, Oxford, **1995**, pp. 529-531.

(31) Asirvatham, V. S.; Ashby, M. T. *Organometallics* **2001**, *20*, 1687-1688.
(32) Al: 1.25 Å and Ga: 1.26 Å (singly bonded, 3-fold coordinated elements) see Holleman-Wiberg *Inorganic Chemistry*; 1. English ed.; Academic Press: San Diego, London, 2001.
(33) Elschenbroich, C.; Zenneck, U. *J. Organomet. Chem.* **1978**, *160*, 125-137.
(34) Chan, W. Y.; Lough, A. J.; Manners, I. *Organometallics* **2007**, *26*, 1217-1225.
(35) Tanabe, M.; Vandermeulen, G. W. M.; Chan, W. Y.; Cyr, P. W.; Vanderark, L.; Rider, D. A.; Manners, I. *Nature Materials* **2006**, *5*, 467-470.
(36) Al-Juaid, S. S.; Eaborn, C.; El-Hamruni, S. M.; Hitchcock, P. B.; Smith, J. D. *Organometallics* **1999**, *18*, 45-52.
(37) Yoshida, T.; Matsuda, T.; Otsuka, S. In *Inorg. Synth.*; Angelici, R. J., Ed.; John Wiley & Sons: New York 1990; Vol. 28, p 120-123.
(38) Spencer, J. In *Inorganic Synthesis*; Shriver, D. F., Ed.; John Wiley & Sons: New York, 1979; Vol. 19, p 213-215.
(39) Silverthorn, W. E. In *Inorganic. Synthesis.*; Mcgraw-Hill: New York; London, 1977; Vol. 17, p 54-57.
(40) *Nonius*; Nonius BV: Delft, The Netherlands: 1998.
(41) Otwinowski, Z.; Minor, W. In *Macromolecular Crystallography, Part A*; Carter, C. W., Sweet, R. M., Eds.; Academic Press: London, 1997; Vol. 276, p 307-326.
(42) Altomare, A.; Burla, M. C.; Camalli, M.; Cascarano, G.; Giacovazzo, C.; Guagliardi, A.; Moliterni, A. G. G.; Polidori, G.; Spagna, R. *J. Appl. Crystallogr.* **1999**, *32*, 115-119.
(43) Sheldrick, G. M.; SHELXL-97; University of Göttingen: Germany: 1997.
(44) Farrugia, L. J. *J. Appl. Crystallogr.* **1997**, *30*, 565.
(45) Spek, A. L.; University of Utrecht, The Netherlands: 2001.

7.7 Supporting Information

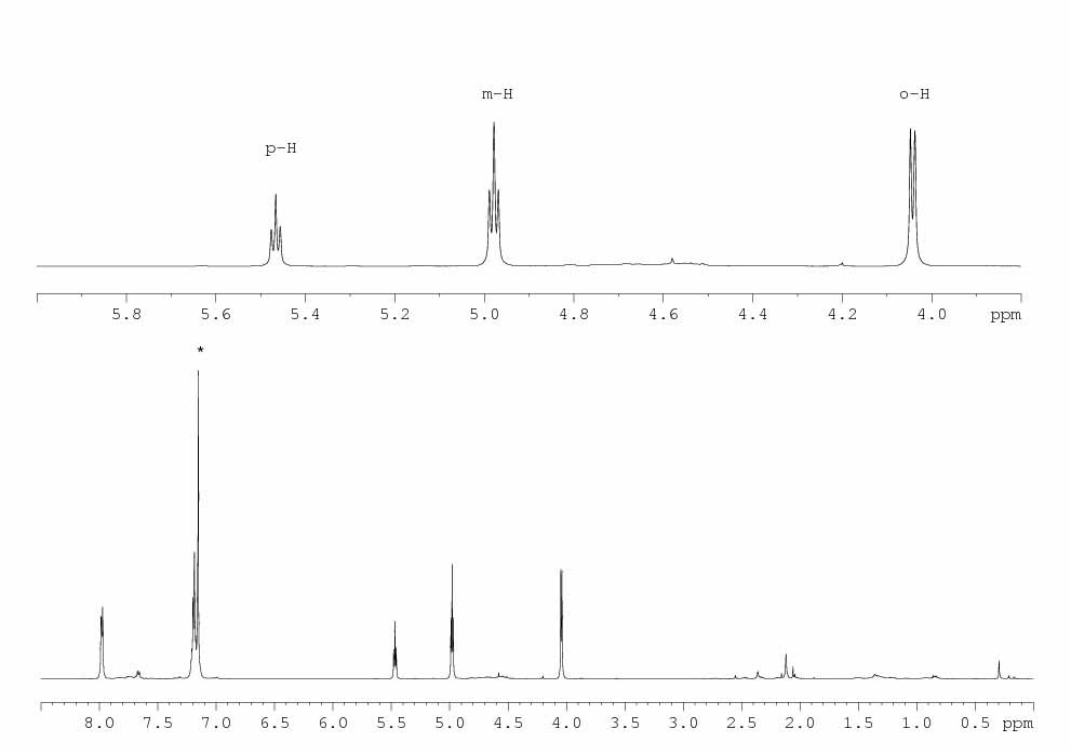

Figure 7-S1. ^{1}H NMR spectrum of Ph_2Si[1]MAP (**2c**) at 25 ºC in C_6D_6 (bottom), and of the arene protons (top). Solvent peak is mark with *.

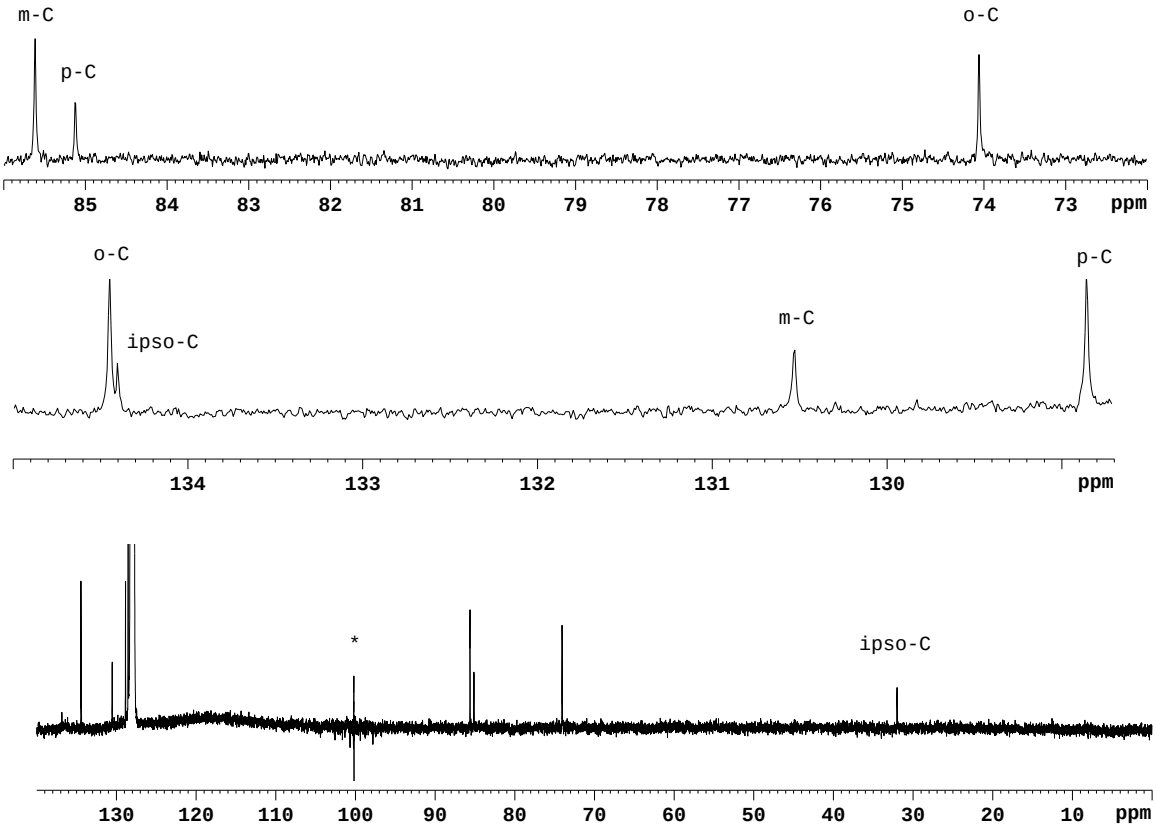

Figure 7-S2. ^{13}C NMR spectrum of Ph_2Si[1]MAP (**2c**) at 25 ºC in C_6D_6 (* spike at the carrier frequency).

CHAPTER 8
PUBLICATION 7

Description

The following chapter is a verbatim copy of an article which was published in *Inorganic Chemistry*[*] in June 2008[†] and describes the synthesis and characterization of the first [1.1]CAPs (**2a**, **4a**, **4b**) and [1.1]MAPs (**5a**, **5b**). The sandwich complexes were bridged by aluminum and gallium equipped with Ar′-like ligands (Figure 1-24). As expected, the [1.1]metallarenophanes were all found to adopt *anti* conformations in the solid state. Electrochemical measurements revealed that the gallium-bridged [1.1]metallarenophanes are Class II molecules according to the Robin–Day classification system. The aluminum-bridged [1.1]metallarenophanes could not be reliably characterized by electrochemical measurements because of their acute sensitivity towards air, moisture and electrolyte.

Author Contributions

My contributions to this publication were the synthesis and characterization of the aluminum- and gallium-bridged [1.1]CAPs and [1.1]MAPs. The co-authors on this paper are Jörg A. Schachner, who provided advice on the electrochemistry measurements and on the purification of the reagents needed for these measurements, Ian J. Burgess, with whom I performed the electrochemical analysis on the title compounds, J. Wilson Quail and Gabrielle

[*] Reproduced with permission from Inorganic Chemistry © 2008 American Chemical Society.
[†] Lund, C. L.; Schachner, J. A.; Burgess, I. J.; Quail, J. W.; Schatte, G.; Müller, J. *Inorg. Chem.* **2008**, *47*, 5992-6000.

Schatte, who performed all single-crystal X-ray analyses, and my supervisor Jens Müller. Written permission was obtained from all contributing authors to include material within this thesis.

Relation of Publication 7 to the Objectives of this Project

The following chapter addresses the third objective of the thesis on hand (Chapter 1.6), namely whether [1.1]metallarenophanes could be synthesized. As stated before, this part of the thesis evolved as a consequence of developments in Müller's group, who had previously reported on the synthesis of group-13-bridged [1.1]FCPs.[‡] Even though the concept of intramolecular stabilization could be used, the ligand Ar′, which was applied successfully for the synthesis of [1.1]FCPs, needed to be altered. The following paper describes the synthesis and characterization of the first [1.1]metallarenophanes, as well as their characterization by cyclic voltammetry.

[‡] Schachner, J. A.; Orlowski, G. A.; Quail, J. W.; Kraatz, H.-B.; Müller, J. *Inorg. Chem.* **2006**, *45*, 454-459.

8. Synthesis and Characterization of Aluminum- and Gallium-Bridged [1.1]Chromarenophanes and [1.1]Molybdarenophanes

Clinton L. Lund,[‡] Jörg A. Schachner,[‡] Ian J. Burgess,[‡] J. Wilson Quail,[§] Gabriele Schatte,[§] and Jens Müller[‡*]

[‡]*Department of Chemistry, University of Saskatchewan, 110 Science Place, Saskatoon, Saskatchewan, Canada, S7N 5C9,* [§]*Saskatchewan Structural Sciences Centre, University of Saskatchewan, 110 Science Place, Saskatoon, Saskatchewan, Canada, S7N 5C9*

Received February 21, 2008

8.1 Abstract

The synthesis and structural characterization of the first [1.1]chromarenophanes and the first [1.1]molybdarenophanes are described. A salt-metathesis reaction of [2-(Me_2NCH_2)C_6H_4]$AlCl_2$ with freshly prepared [$Cr(LiC_6H_5)_2$]·tmeda (tmeda = N,N,N′,N′-tetramethylethylenediamine) resulted in the dialumina[1.1]chromarenophane [{2-(Me_2NCH_2)C_6H_4}Al(η^6-C_6H_5)$_2$Cr]$_2$ (**2a**). The poor solubility of **2a** in organic solvents prompted us to synthesize the new intramolecularly coordinated aluminum- and gallium dichlorides [5-*t*Bu-2-(Me_2NCH_2)C_6H_3]ECl_2 [E = Al (**3a**), Ga (**3b**)] in which the phenyl group was equipped with a *tert*-butyl group. Salt-metathesis reactions of **3a** and **3b**, respectively, with freshly prepared [$M(LiC_6H_5)_2$]·tmeda (M = Cr, Mo) resulted in four new [1.1]metallarenophanes of the general type [{5-*t*Bu-2-(Me_2NCH_2)C_6H_3}E(η^6-C_6H_5)$_2$M]$_2$ [E = Al, M = Cr (**4a**); E = Ga, M = Cr (**4b**); E = Al, M = Mo (**5a**); E = Ga, M = Mo (**5b**)]. **2a**, **4a**,**b** and **5a**,**b** have been structurally characterized by single-crystal analysis [**2a**·½ C_6H_{12}: $C_{48}H_{56}Al_2Cr_2N_2$, monoclinic, $P2_1/c$, a = 9.9117(9) Å, b = 19.9361(16) Å, c = 10.638(2) Å, α = 90°.,β = 112.322(5)°, γ = 90°, Z = 2; **4a**·2 C_6H_6: $C_{62}H_{72}Al_2Cr_2N_2$, monoclinic, $P2_1/c$, a = 10.9626(9) Å, b = 19.3350(18) Å, c =

12.4626(9) Å, α = 90°,β = 100.756(5)°, γ = 90°, Z = 2; **4b**·2 C_6H_6: $C_{62}H_{72}Cr_2Ga_2N_2$, monoclinic, $P2_1/c$, a = 10.8428(2) Å, b = 19.4844(4) Å, c = 12.4958(2) Å, α = 90°, β = 100.6187°, γ = 90°, Z = 2; **5a**·2 C_6H_6: $C_{62}H_{72}Al_2Mo_2N_2$, triclinic, $P\bar{1}$, a = 10.4377(4) Å, b = 11.6510(4) Å, c = 11.6514(4) Å, α = 73.545(3)°,β = 89.318(2)°, γ = 76.120(2)°, Z = 1; **5b**·2 C_6H_6: $C_{62}H_{72}Ga_2Mo_2N_2$, triclinic, $P\bar{1}$, a = 10.3451(5) Å, b = 11.6752(6) Å, c = 11.6900(5) Å, α = 73.917(3)°,β = 89.550(3)°, γ = 76.774(2)°, Z = 1]. All five [1.1]metallarenophanes **2a**, **4a**,**b** and **5a**,**b** crystallize as *anti* isomers with both Me_2N donor groups in *exo* positions (C_i point group symmetry). The new [1.1]metallarenophanes show NMR spectra that can be interpreted as being caused by time-averaged C_{2h} symmetrical species, which is consistent with the findings of their molecular structures in the solid state. Variable temperature ^{1}H NMR measurements for **4a**,**b** and **5a**,**b** (500 MHz; –90 to 90 ºC) revealed only peak broadening in the lower temperature range of –70 to –90 ºC. ^{1}H NMR saturation transfer difference experiment did not show an expected *anti*-to-*anti* isomerization, rendering the new [1.1]metallacyclophanes rigid on the NMR time scale. Electrochemical measurements were performed for **4a**,**b** and **5a**,**b**. However, reproducible cyclic voltammograms could only be obtained for the two gallium species **4b** and **5b** revealing the expected weak communication between the two transition-metal atoms in both compounds (Class II).

8.2 Introduction

Since their first appearance in the literature in 1966,[1] [1.1]ferrocenophanes have been the subject of intensive investigations. The chemistry of the carbon-bridged [1.1]ferrocenophanes was reviewed in 1986 by Mueller-Westerhoff.[2] Usually, carbon-bridged [1.1]ferrocenophanes prefer the *syn* conformation (Figure 8-1, E = C), however, in 1993 the first structural evidence

for the existence of the second isomer, the *anti* isomer (Figure 8-1), was reported.[3] In this particular case, CHMe moieties bridged the two ferrocene units and gave rise to *endo*/*exo* isomers (Figure 8-1). [1.1]Ferrocenophanes are highly dynamic in solution and have been coined "molecular acrobats".[2,4] A distanna[1.1]ferrocenophane (E = $SnBu_2$)[5] was the first hetero-atom-bridged [1.1]ferrocenophane and since its discovery, the group of hetero-atom containing [1.1]ferrocenophanes has grown significantly and is now known for groups 13 (boron,[6] aluminum,[7–9] gallium,[9,10] indium[9]), 14 (silicon,[11,12] tin,[5,13] lead[14]), 15 (phosphorus[15]), and 16 (sulfur[16]).

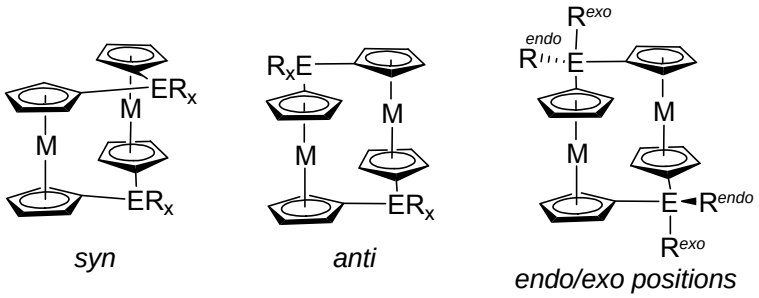

Figure 8-1. Isomerism in [1.1]metallocenophanes.

The knowledge about [1.1]ruthenocenophanes and mixed Ru-Fe [1.1]metallocenophanes is mainly limited to carbon-bridged species, with the knowledge about hetero-atom-bridged [1.1]ruthenocenophane being limited to a $SiMe_2$-bridged species published in 1995 by Herberhold et al.[12]

In the course of our investigation into strained [1]metallacyclophanes with heavier group-13 elements in bridging positions,[17] we found that dilithioferrocene reacts with intramolecularly coordinated group-13 element halides Ar′EX_2 (Ar′ = 2-(Me_2NCH_2)C_6H_4; E = Al,[8,9] Ga,[9] In[9]) to give [1.1]ferrocenophanes. Even though [1.1]ferrocenophanes are unstrained and, therefore, cannot be used for ring-opening polymerizations, they serve as model compounds for the

investigation of metal-metal interactions. Using cyclic voltammetry, we have shown that two isostructural [1.1]ferrocenophanes, a gallium- and a aluminum-bridged species, show distinctively different redox behavior. Whereas the digalla[1.1]ferrocenophane[9] showed the expected Class II[18] behavior (two one-electron oxidation waves) similar to other [1.1]ferrocenophanes, the dialumina[1.1]ferrocenophane[9] showed an unexpected Class I[18] behavior (one two-electron oxidation wave). On the basis of these findings, we wanted to explore reactions of other dilithio sandwich compounds with intramolecularly coordinated alanes and gallanes of the type Ar′EX_2. We were hoping to obtain [1.1]metallacyclophanes to further investigate metal-metal interactions.

In contrast to the large number of [1.1]metallocenophanes, it is surprising that not a single example of a [1.1]metallarenophane is described in the literature. Within this article, we fill this gap by reporting on the synthesis and characterization of the first [1.1]chromarenophanes and the first [1.1]molybdarenophanes.

8.3 Results and Discussion

We started to investigate the reaction of dilithiobis(benzene)chromium with Ar′$AlCl_2$ (**1a**). After several attempts using various reaction conditions, we obtained red crystals from this reaction (equation 8-1). Interestingly, once compound **2a** crystallized, it could not be redissolved in common organic solvents.

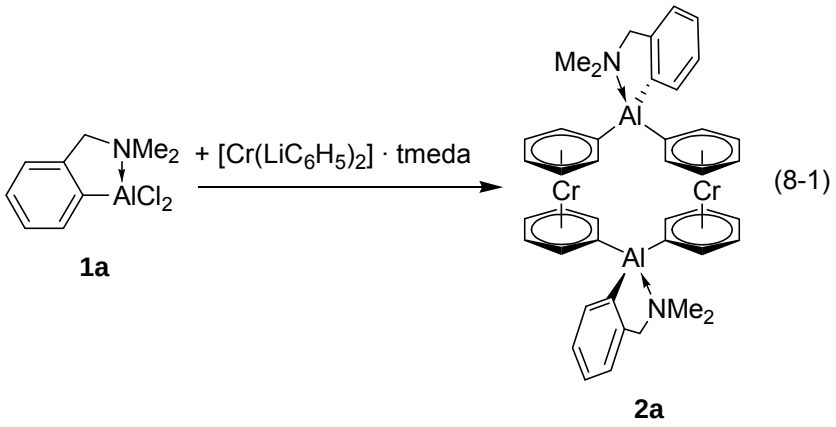

However, the compound is sparingly soluble in thf and a small amount of single crystals of sufficient quality for X-ray single-crystal analysis were obtained from highly diluted thf solution in the presence of cyclohexane (Figure 8-2; Table 8-1). The structural analysis clearly revealed that compound **2a** is a [1.1]chromarenophane. To the best of our knowledge, it is the first [1.1]chromarenophane known to date. **2a** crystallizes as an *anti* isomer with both NMe_2 donor groups in *exo* positions (Figure 8-1 and 8-2). Further structural details will be discussed below.

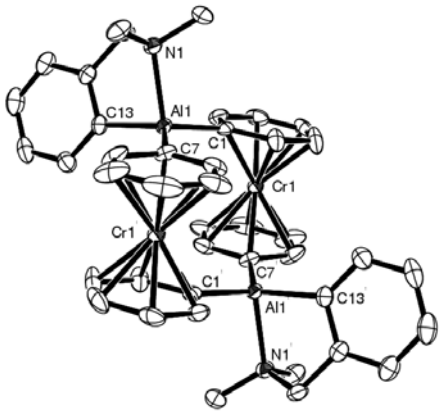

Figure 8-2. Molecular structure of Ar′Al[1.1]CAP (**2a**) with thermal ellipsoids at the 50% probability level. H atoms are omitted for clarity. Selected atom-atom distances [Å] and bond angles [°]: Al1–N1 = 2.072(3), Al1–C1 = 1.972(4), Al1–C7 = 1.962(4), Al1–C13 = 1.978(4), Cr1–Cr1′ = 5.0866(10), C1–Al1–C7 = 121.22(16), N1–Al1–C13 = 85.78(14), C7–Al1–C13 = 120.44(16), C1–Al1–C13 = 113.65(16), C7–Al1–N1 = 103.15(14), C1–Al1–N1 = 101.95(14), α = 4.9(2).

The poor solubility of **2a** made its separation from the simultaneously produced LiCl difficult, and, in addition, prevented investigations into metal-metal interactions in solution, hence, rendering electrochemical methods unsuitable. Therefore, we attempted to increase the solubility of the targeted [1.1]metallacyclophanes by using one-armed phenyl ligands Ar′ equipped with an additional alkyl group on the aromatic ring. From the ample possibilities, we picked an Ar′ derivative with one *t*Bu group para to the donor arm. Starting from commercially available p-(*tert*-butyl)benzylbromide (p-*t*Bu$C_6H_4CH_2Br$) a known two-step synthesis yielded (p-*t*BuAr′Li[19] [p-*t*BuAr′= 5-*t*Bu-2-(Me_2NCH_2)C_6H_3] that was used to synthesize the new intramolecularly coordinated aluminum and gallium dichlorides **3a** and **3b**, respectively (equation 8-2). Expectedly, both species show ^1H and ^{13}C NMR spectra that can be interpreted as being caused by C_s symmetrical species. The ^{27}Al NMR shift of δ 131 for **3a** is very similar to δ 127 reported for the monomeric Ar′$AlCl_2$ (**1a**)[20] and shows that **3a** is a monomeric species with a 4-fold coordinated aluminum atom.

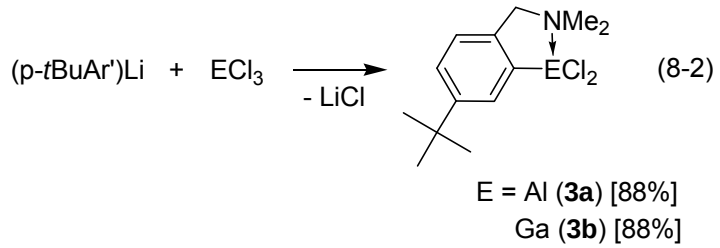

(8-2)

With the alane **3a** and the gallane **3b** in hand, novel [1.1]chromarenophanes and [1.1]molybdarenophanes with improved solubility were prepared through reactions with freshly dilithiated bis(benzene)chromium or -molybdenum (Scheme 8-1). The four [1.1]metallarenophanes **4a**,**b** and **5a**,**b** were isolated and purified by crystallizations from toluene solutions and crystals suitable for single-crystal X-ray crystal analysis were obtained from benzene solutions (Figure 8-3 and 8-4; Table 8-1). According to ^1H NMR measurements of the

reaction mixtures, the formation of the [1.1]metallacyclophanes proceeds relatively cleanly for this type of sensitive chemistry (estimated conversions of 80–90%). In all cases, we detected only small amounts of the parent di(benzene)metal complex among the products. However, N,N,N′,N′-tetramethylethylenediamine (tmeda), which is required for the dilithiation of the parent sandwich compounds, results in the formation of tmeda·LiCl. It is the latter compound that is difficult to separate from the [1.1]metallacyclophanes and, therefore, we isolated pure **4a**,**b** and **5a**,**b** in yields of only 20–30%.

Scheme 8-1. Synthesis of aluminum- and gallium-bridged [1.1]metallarenophanes.

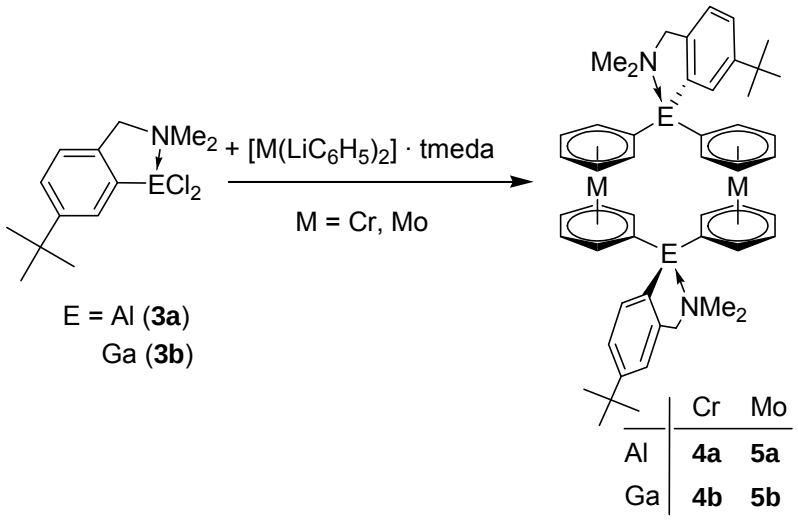

8.3.1 Solid-state structures of 2a, 4a,b and 5a,b. As in the case of the [1.1]ferrocenophanes investigated recently,[8,9] the new [1.1]chromarenophanes **2a** (Figure 8-2) and **4a**,**b** (Figure 8-3, Figure 8-S1) and the new [1.1]molybdarenophanes **5a**,**b** (Figure 8-4, Figure 8-S2) crystallize as *anti* isomers with the two NMe_2 donor groups in *exo* positions (Figure 8-1). All five species exhibit C_i point-group symmetries in the crystal lattice. The geometries around the bridging atoms can be best described as trigonal pyramids, with the three carbon atoms C1, C7, and C13 at the base and the nitrogen atom N1 at the tip of the pyramid. With respect to an ideal tetrahedron, these pyramids are flattened as it can be deduced from the sum

over the three C–E–C angles (E = Al, Ga), which are 355.31 (**2a**), 354.14 (**4a**), 356.25 (**4b**), 354.12 (**5a**), and 355.79° (**5b**). Respective atom–atom distances in **2a**, **4a**,**b** and **5a**,**b** are very similar; for example, the Cr–Cr distances are 5.9866(10), 5.9921(11), and 6.0251(6) Å for **2a**, **4a**, and **4b**, respectively, and the Mo–Mo distances are 5.9983(7) and 6.0277(6) Å for **5a** and **5b**, respectively. These metal–metal distances are larger for the gallium species as compared to the aluminum species, which is partly due to differences in E–C bond lengths: Ga1–C1 and Ga1–C7 bonds being slightly longer than respective Al–C bonds (Figure 8-3 and 8-4). Only the E–N donor bonds are very different for aluminum compared with gallium-bridged species, with Al–N donor bonds being shorter than Ga–N bonds (for **4a** and **4b** the difference is 0.103(4) Å; for **5a** and **5b** it is 0.111(4) Å). Similar differences between E–N donor bond lengths were found for the [1.1]ferrocenophanes[8,9] mentioned before and are a testament of the higher Lewis acidity of aluminum compared with gallium for an amine donor.

For metallacyclophanes, a set of angles can be given to show the distortion with respect to the parent sandwich species.[21] The most illustrative angle is the tilt angle α which is the angle between the two intersecting planes defined by the carbon frameworks of the two coordinated π ligands. Aluminum- and gallium-bridged [1]metallacyclophanes exhibit α angles from 11.81(9)°[22] for an alumina[1]chromarenophane to 21.24(10)°[17] for an galla[1]molybdarenophane. [1.1]Metallacyclophanes are expected to be unstrained sandwich compounds, with tilt angles α close to 0º. For the new complexes **2a**, **4a**,**b** and **5a**,**b**, α angles of 4.9(2), 3.21(14), 2.67(7), 2.7(3), and 2.2(3), respectively, were determined. In all cases, the two planes intersect on the opposite side of the bridging atom, which could be indicated by adding a negative sign to all α angles.

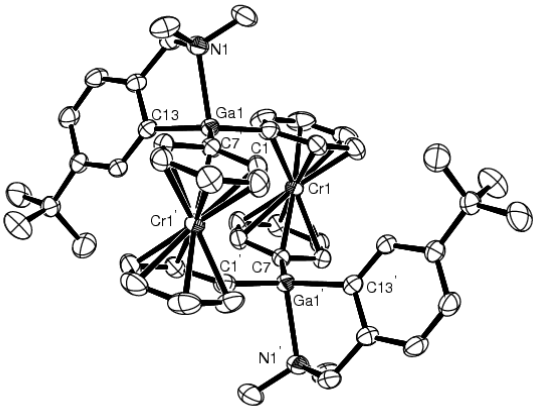

Figure 8-3. Molecular structure of (p-*t*BuAr′)Ga[1.1]CAP (**4b**) with thermal ellipsoids at the 50% probability level. Hydrogen atoms are omitted for clarity. Selected atom–atom distances [Å] and bond angles [°] for **4b**: Ga1–N1 = 2.192(2), Ga1–C1 = 1.980(2), Ga1–C7 = 1.979(2), Ga1–C13 = 1.984(2), Cr1–Cr1′ = 6.0251(6), C1–Ga1–C7 = 121.99(10), N1–Ga1–C13 = 83.41(9), C7–Ga1–C13 = 120.40(9), C1–Ga1–C13 = 113.86(10), C7–Ga1–N1 = 105.71(9), C1–Ga1–N1 = 99.04(9), α = 2.67(7).

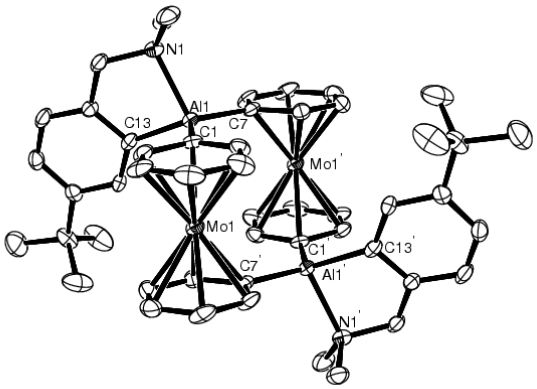

Figure 8-4. Molecular structure of (p-*t*BuAr′)Al[1.1]MAP (**5a**) with thermal ellipsoids at the 50% probability level. Hydrogen atoms are omitted for clarity. Selected atom-atom distances [Å] and bond angles [°] for **5a**: Al1–N1 = 2.096(3), Al1–C1 = 1.968(4), Al1–C7 = 1.968(4), Al1–C13 = 1.981(4), Mo1–Mo1′ = 5.9983(7), C1–Al1–C7 = 120.49(18), N1–Al1–C13 = 85.06(15), C7–Al1–C13 = 120.80(17), C1–Al1–C13 = 112.83(17), C7–Al1–N1 = 106.47(15), C1–Al1–N1 = 101.73(15), α = 2.7(3).

Table 8-1. Crystal and structural refinement data for compounds Ar′Al[1.1]CAP (**2a**), (p-*t*BuAr′)Al[1.1]CAP (**4a**),(p-*t*BuAr′)Ga[1.1]CAP (**4b**), and (p-*t*BuAr′)Al[1.1]MAP (**5a**), (p-*t*BuAr′)Ga[1.1]MAP (**5b**).

	2a · ½ C_6H_{12}	**4a** · 2 C_6H_6	**4b** · 2 C_6H_6	**5a** · 2 C_6H_6[b]	**5b** · 2 C_6H_6[b]
empirical formula	$C_{48}H_{56}Al_2Cr_2N_2$	$C_{62}H_{72}Al_2Cr_2N_2$	$C_{62}H_{72}Cr_2Ga_2N_2$	$C_{62}H_{72}Al_2Mo_2N_2$	$C_{62}H_{72}Ga_2Mo_2N_2$
fw	818.91	1003.18	1088.66	1091.06	1176.54
cryst. size / mm^3	0.20 × 0.20 × 0.12	0.12 × 0.10 × 0.10	0.20 × 0.18 × 0.15	0.13 × 0.13 × 0.10	0.08 × 0.08 × 0.050
cryst. system, space group	monoclinic, $P2_1/c$	monoclinic, $P2_1/c$	monoclinic, $P2_1/c$	triclinic, $P\bar{1}$	triclinic, $P\bar{1}$
Z	2	2	2	1	1
a/ Å	9.9117(9)	10.9626(9)	10.8428(2)	10.4377(4)	10.3451(5)
b/ Å	19.9361(16)	19.3350(18)	19.4844(4)	11.6510(4)	11.6752(6)
c/Å	10.638(2)	12.4626(9)	12.4958(2)	11.6514(4)	11.6900(5)
α/deg	90	90	90	73.545(3)	73.917(3)
β/deg	112.322(5)	100.756(5)	100.6187	89.318(2)	89.550(3)
γ/deg	90	90	90	76.120(2)	76.774(2)
volume/ $Å^3$	1944.6(4)	2595.2(4)	2594.72(8)	1316.82(8)	1318.36(11)
ρ_{calc}/ Mg/m^3	1.399	1.284	1.393	1.376	1.482
temperature/ K	173(2)	173(2)	173(2)	173(2)	173(2)
$\mu_{calc.}$/ mm^{-1}	0.642	0.494	1.477	0.551	1.517
θ range, deg	2.44 to 26.02	3.46 to 25.01	3.32 to 27.47	2.64 to 25.68	3.21 to 27.47
reflns collected/ unique	21561/ 3825	8155/ 4567	41481/ 5916	8528/ 4967	10303/ 6021
absorption correction	ψ-scan	None	ψ-scan	multi-scan	multi-scan
data / restraints / params	3825 / 96 / 273	4567 / 0 / 294	5916 / 0 / 313	4967 / 0 / 312	6021 /0 312
GOF on F^2	1.052	1.032	1.072	1.069	1.059
final R indices [I > 2σ(I)][a]	0.0544	0.0653	0.0368	0.0453	0.0412
wR_2 (all data)[a]	0.1387	0.1452	0.0848	0.1046	0.0941
largest diff. peak and hole, $\Delta\rho_{elect}$/ $Å^{-3}$	0.975 and –0.761	0.278 and –0.304	0.326 and –0.376	0.462 and –0.660	0.690 and –0.801

[a] $R_1 = [\Sigma||F_o|-|F_c||]/[\Sigma|F_o|]$ for $[F_o^2 > 2\sigma(F_o^2)]$, $wR_2 = \{[\Sigma w(F_o^2-F_c^2)^2]/[\Sigma w(F_o^2)^2]\}^{1/2}$ [all data].

[b] These compounds had been crystallized from C_6D_6 (see Experimental Section). The deuterium atoms attached to the benzene solvent molecule were included as hydrogen atoms in the refinement. Chemical formula and derived quantities fw, ρ_{calcd}, μ_{calc}, and *F*(000) were not corrected.

8.3.2 NMR spectroscopy of 2a, 4a,b and 5a,b. ^1H and ^{13}C NMR spectra of compounds **4a**,**b** and **5a**,**b**, measured at ambient temperatures, can be interpreted as being caused by time-averaged C_{2h} symmetrical species. For example, ^1H NMR spectra show one set of signals for the p-*t*BuAr′ ligands and five signals of equal intensities for the η^6-C_6H_5 moieties. In addition to the signal pattern, the ^{13}C NMR spectra show that the chemical shifts of the *ipso*-C atom of the η^6-C_6H_5 moieties at δ 76.0 (**4a**), 79.9 (**4b**), 76.6 (**5a**), and 79.8 (**5b**) are very similar as those of the parent compounds bis(benzene)chromium (δ 74.8)[23] and bis(benzene)molybdenum (δ 75.3)[24].

The absence of an upfield shift clearly shows that the [1.1]metallacyclophanes are unstrained, corroborated by the molecular structures of the species in the solid state. As mentioned earlier, the aluminum-bridged [1.1]chromarenophane **2a** was not soluble in organic solvents anymore once it had crystallized, hence, we could not measure NMR spectra of the isolated product. However, a ^{1}H NMR spectrum was measured from the reaction mixture and showed a comparable pattern as those discussed for compounds **4a**,**b** and **5a**,**b** (see Experimental Section), but the low solubility of **2a** prevented the measurement of reliable ^{13}C NMR data.

Five-membered rings such as those present in the [1.1]metallarenophanes **2a**, **4a**,**b** and **5a**,**b** show envelope conformations in the solid state. In solution these rings would be expected to have conformational flexibility, and fast envelope inversions should result in five-membered rings which are C_s symmetrical on time average. Against this background one expects that a C_i symmetrical [1.1]metallarenophane shows a C_{2h} symmetry in solution, meaning that our NMR results suggest that the molecular structures of **2a**, **4a**,**b** and **5a**,**b** are similar in solution and in the crystal lattice.

As mentioned in the introduction, [1.1]ferrocenophanes had been coined "molecular acrobats".[4] Consequently, we measured the ^{1}H NMR spectra of **4a**,**b** and **5a**,**b** in $C_6D_5CD_3$ in the temperature range of –90 to 90 ºC (500 MHz). Except for small shifts of signals, the high temperature spectra are very similar as those at ambient temperature. In the lower temperature range, a significant broadening of peaks between –70 and –90 ºC occurred. However, even though some peaks are very broad at –90 ºC, the signal pattern is still similar to that at ambient temperature. The low temperature spectra indicate that the molecular dynamics is slowed down with respect to the NMR time scale, but it is still fast enough at the lowest accessible temperature so that only one time-averaged C_{2h} symmetrical species is observed. One feasible dynamic

process for [1.1]metallacyclophanes is a degenerate isomerization of one *anti* isomer to another *anti* isomer; a process comparable to a *chair*-to-*chair* isomerization of cyclohexane. If such a process would be occurring, with saturation transfer difference ^{1}H NMR experiments one should be able to see magnetization transfer from one ortho to the other ortho proton, similarly, from one meta to the other meta proton.[25] However, these experiments gave no indication that an *anti*-to-*anti* isomerization takes place even at temperatures of 80 ºC (Experimental Section for details).

8.3.3 Electrochemistry of 4a,b and 5a,b. Electrochemical measurements were undertaken for the four metallarenophanes to determine the extent of communication between the two transition metal redox centres. In the first attempts we used a small three-neck Schlenk flask with three electrodes inserted through septa (supporting information in reference 9). However, we did not obtain reproducible CVs; in particular, the two aluminum compounds showed only CVs of the parent bis(benzene) complexes, which suggested that moisture had degraded **4a** and **5a**, respectively. Consequently, all subsequent measurements were done inside a glovebox. Extra precautions were taken to dry the solvent thf and the electrolytes used (Experimental Section for details). With these efforts, we obtained reproducible data for the two gallium species **4b** and **5b** (Figure 8-5 and 8-6), but were unsuccessful in obtaining reproducible data for the respective aluminum compounds **4a** and **5a**. The measurements of the latter species indicated that significant amounts of the parent bis(benzene) complexes were always present in solution. Therefore, additional measurements of the aluminum compounds **4a** and **5a** were performed using $[Bu_4N][BF_4]$ instead of $[Bu_4N][PF_6]$ as an electrolyte; however, their CVs varied significantly by this change. Furthermore, it seemed that the concentration of the parent sandwich compounds in a sample of **4a** or **5a** strongly influenced the position and intensities of

the other oxidation and reduction waves and the obtained electrochemical data for **4a** and **5a** were inconclusive.

Figure 8-5 and Figure 8-6 show the CVs of the gallium-bridged species **4b** and **5b**, respectively. Compound **4b** shows two one-electron oxidation and two one-electron reduction waves. The shoulders at lower potential correspond to the redox couple of $[(C_6H_6)_2Cr]$ (asterisk in Figure 8-5). Similarly, species **5b** shows two redox couples which are due to one-electron events (Figure 8-6). As in the case of the chromium compound **4b**, the CV of gallium-bridged molybdenum species **5b** reveals a pair of shoulders corresponding to the presence of $[(C_6H_6)_2Mo]$ (asterisk in Figure 8-6). In contrast to **4b**, however, an additional second reversible redox couple at high cathodic potentials was detected (u_{ox} and u_{red} in Figure 8-6), but we are unable to assign it to a compound. In summary, the two CVs can be interpreted consistently: both compounds, **4b** and **5b**, are oxidized at similar potentials compared to the respective parent sandwich compound $[(C_6H_6)_2M]$ (see Supporting Information). According to the Robin–Day classification[18] both species are Class II compounds.

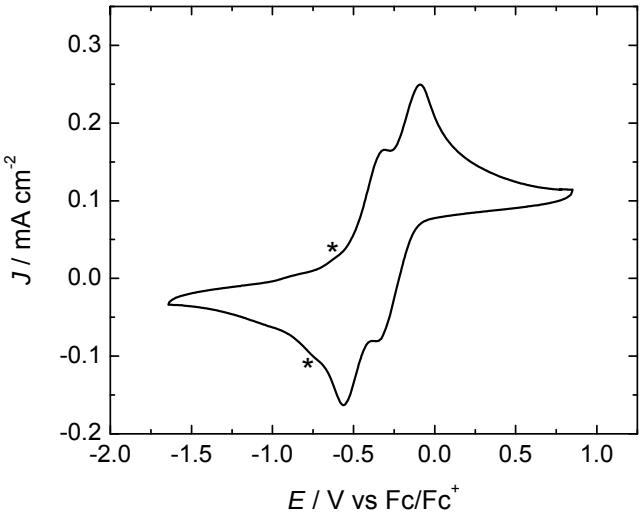

Figure 8-5. Cyclic voltammogram of (p-*t*BuAr′)Ga[1.1]CAP (**4b**) in thf/0.1 M $[Bu_4N][PF_6]$ using a glassy carbon working electrode at a scan rate of 100 mV/s. The measured $E^{o\prime}$ for the two principal peaks are –0.440 and 0.225 V, respectively [$E^{o\prime} = ½(E_{pa} + E_{pc})$].[26] The asterisk denotes a smaller set of voltammetric signals in the CV which is due to small amounts of $[(C_6H_6)_2Cr]$.

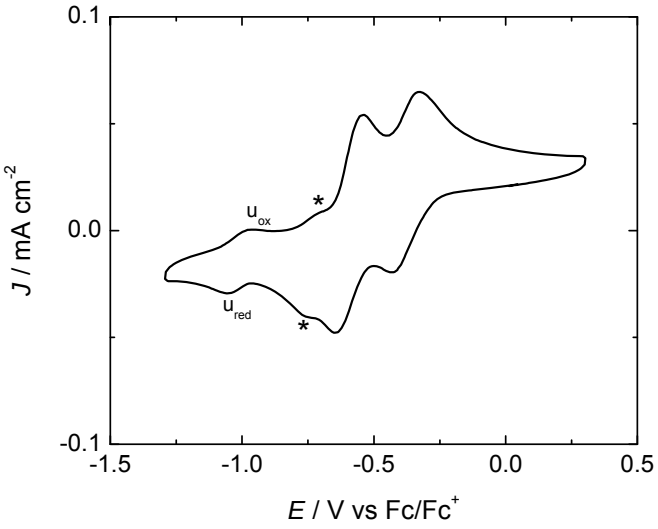

Figure 8-6. Cyclic voltammogram of (p-*t*BuAr′)Ga[1.1]MAP (**5b**) in thf/0.1 M $[Bu_4N][PF_6]$ using a glassy carbon working electrode at a scan rate of 100 mV/s. The measured $E^{o\prime}$ for the two principal peaks is –0.600 and 0.380 V, respectively [$E^{o\prime} = ½(E_{pa} + E_{pc})$].[26] The asterisk denotes a smaller set of voltammetric signals in the CV which are due to small amounts of $[(C_6H_6)_2Mo]$. At very cathodic potentials (ca. –1.0 V), an additional redox process is observed (reversible couple denoted by u_{ox} and u_{red}).

8.4 Conclusion

The first [1.1]metallarenophanes have been synthesized and fully characterized. The aluminum-bridged species (**2a**, **4a**, **5a**) and the gallium-bridged species (**4b**, **5b**) crystallize as *anti* isomers with the dimethylamino groups in *exo* positions (Figure 8-1). Structural parameters like atom–atom distances and bond angles are very similar in all five species. Expectedly, the E–N donor bonds are the only bonds which differ significantly: aluminum as the better Lewis acid for Me_2N donor groups possesses Al–N bonds which are shorter by 0.10 – 0.11 Å compared to the respective Ga–N bonds. ^1H and ^{13}C NMR spectra can be interpreted as being caused by C_{2h} symmetrical compounds. In contrast to their highly dynamic [1.1]metallocenophane cousins, these new [1.1]metallarenophanes do not show *anti*-to-*anti* isomerization in solution. [1.1]Metallacyclophanes can serve as model compounds to investigate metal–metal interactions, however, the extreme sensitivity of the aluminum species **4a** and **5a** prevented us from obtaining reproducible electrochemical data. On the other hand, the gallium-bridged species **4b** and **5b** showed an expected class II behavior.

It is surprising that no other [1.1]metallarenophanes are known in the literature. The most common route for the synthesis of metallacyclophanes is the salt-metathesis between a dilithiated sandwich compound and an element dihalide.[21] In many cases researchers used R_2SiCl_2; these compounds are commercially available and are very reactive towards nucleophilic substitutions. However, silicon in a bridging position of a [1.1]metallacyclophane would dictate approximately a tetrahedral angle for the C*ipso*–Si–C*ipso* linkage. In [1.1]metallacyclophanes there are two pairs of inner α protons which are oriented towards each other (Figure 8-7). If all other structural parameters are kept constant, the distance between those α protons must be larger in [1.1]metallocenophanes, where two five-membered rings are linked, than in

[1.1]metallarenophanes, where two six-membered rings are linked. It might be that, so far, steric repulsion between α protons prevented the formation of silicon-bridged [1.1]metallarenophanes. On the other hand, with aluminum- and gallium moieties in bridging positions the wider C*ipso*–E–C*ipso* angles of around 120º reduce a possible repulsion between the α protons to allow the formation of [1.1]metallarenophanes [C1–E–C7 = 121.22(16) (**2a**), 119.96(19) (**4a**), 121.99(10) (**4b)**, 120.49(**18**) (5a), 122.38(14) (**5b**); see Figure 8-2, 8-3, and 8-4]. A second factor that might have contributed to the lack of reports about [1.1]metallarenophanes might be the low solubility of such compounds; compound **2a** showed unusual solubility properties in organic solvents. One can speculate that other [1.1]metallarenophanes might have been formed in salt-metathesis reactions, but were not identified because of their insolubility.

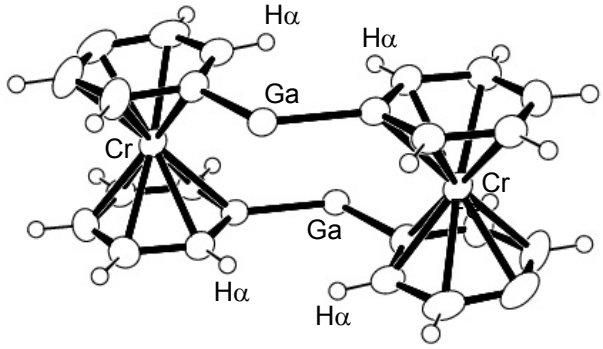

Figure 8-7. Illustration of two pairs of inner α protons pointing towards each other. Drawing is based on the experimentally determined molecular structure of compound (p-tBuAr′)Ga[1.1]CAP (**4b**) (ligand p-*t*BuAr′ removed for clarity).

8.5 Experimental Section

Electrochemistry. A computer controlled system, consisting of a HEKA potentiostat PG590 (HEKA, Mahone Bay, NS, Canada) was used for the cyclic voltammetry experiments. Data was collected using a multifunction DAQ card (PCI 6251 M Series, National Instruments

Austin, Texas) and in-house software written in the *Lab*VIEW environment. Glassy carbon (BAS, 3mm) was used as the working electrode. The quasi-reference electrode (QRE) was a silver wire ($E^{o\prime}$ = 0.645 V vs. Fc/Fc^+ with $E^{o\prime} = ½(E_{pa} + E_{pc})$; Supporting Information). All measurements were made against the QRE and subsequently rescaled to the ferrocene/ferrocenium formal potential[26] $E^{o\prime}$. A loop of gold wire was used as the auxiliary electrode. Before each measurement, 1 mM solutions of **4a**, **4b**, **5a**, and **5b** were freshly prepared in dry thf with 0.1 M $[Bu_4N][PF_6]$ as supporting electrolyte. Extra efforts were undertaken to remove moisture and oxygen from the solvent. thf was first dried using a MBraun Solvent Purification System and then filled into a 1L flask, which was part of a specialty Schlenk line, equipped with greaseless Young valves. To the so pre-dried thf, small amounts of 1,1 diphenylethylene and butyllithium were added, resulting in a red solution, which indicated the absence of moisture. By flask-to-flask condensation under reduced static pressure, a small amount of thf was condensed into a Schlenk tube from the thf reservoir flask. The inert gas (N_2 4.8) used for this Schlenk line was purified by conducting it through two columns before feeding it into the Schlenk line (one column equipped with a copper(I) catalyst and one column equipped with 4Å molecular sieves; both materials purchased from MBraun). A so prepared Schlenk tube filled with freshly condensed thf was moved into the glovebox. The electrolytes were dried overnight under high vacuum ($[Bu_4N][PF_6]$ at 100 °C and $[Bu_4N][BF_4]$ at 70 °C). Unless otherwise specified, the scan rate for all CVs reported was 100 mV/s. All measurements were conducted inside a glovebox and taken at ambient temperature (24 – 25 ºC).

Synthesis. All syntheses were carried out using standard Schlenk techniques. An MBraun glovebox (O_2 < 1 ppm; H_2O < 1 ppm) was used to manipulate the very sensitive bis(benzene) complexes including **2a**, **4a**,**b** and **5a**,**b**. Solvents were dried using a MBraun

Solvent Purification System and stored under nitrogen over 4 Å molecular sieves. All solvents for NMR spectroscopy were degassed prior to use and stored under nitrogen over 4 Å molecular sieves. $[Cr(C_6H_6)_2]$,[27] $[Mo(C_6H_6)_2]$,[17] $[Cr(LiC_6H_5)_2]\cdot$tmeda,[28] $[Mo(LiC_6H_5)_2]\cdot$tmeda,[29] [5-*t*Bu-2-$(Me_2NCH_2)C_6H_3]Li$,[19] and $[2\text{-}(Me_2NCH_2)C_6H_4]AlCl_2$ (**1a**)[20] were synthesized as described in the literature. ^1H, ^{13}C, and ^{27}Al NMR spectra were recorded on a Bruker 500 MHz Avance NMR spectrometer at 25 ºC in C_6D_6, unless noted differently. ^1H chemical shifts were referenced to the residual protons of the deuterated solvent (δ 7.15 for C_6D_6); ^{13}C chemical shifts were referenced to the C_6D_6 signal at δ 128.00; ^{27}Al NMR spectra were referenced to $[Al(acac)_3]$ dissolved in C_6D_6 as an external standard. Mass spectra were measured on a VG 70SE (m/z > 10% are listed for signals of the most abundant ions). Elemental analyses were performed on a Perkin Elmer 2400 CHN Elemental Analyzer using V_2O_5 to promote complete combustion.

For the saturation transfer difference experiments,[25] two spectra were measured, first a control spectrum and then one from a selective irradiation. Subtraction of the second from the first spectrum resulted in a difference spectrum displaying whether any protons exchange with the irradiated one. The pulse sequence used for the saturation transfer experiment was supplied by Bruker. **4b** (C_7D_8) was measured at 25 and 80 ºC and **5b** (C_6D_6) was measured at 25 ºC without any detectable magnetization transfer. Selected parameters include pre-saturation time (d1 = 5.0 s), pulse power (pl14 = 95 dB), and number of data points (TD = 65536). T_1 times [s] for compound **5b** (C_6D_6): o-H = 0.6324; m-H = 1.315; p-H = 1.563; m-H = 1.490; o-H = 1.297.

Synthesis of $[\{2\text{-}(Me_2NCH_2)C_6H_4\}Al(\eta^6\text{-}C_6H_5)_2Cr]_2$ (2a). A slurry of $[Cr(LiC_6H_5)_2]\cdot$ tmeda (1.527 g, 4.541 mmol) in benzene (30 mL, 0 °C) was added to a solution of **1a** (1.016 g, 4.378 mmol) in benzene (10 mL, 0 °C). The cooling bath was removed and the mixture was stirred for 30 min. LiCl was filtered off and the filtrate containing the product was

collected. The product was extracted with an additional (2 × 10 mL) of hot benzene from the LiCl filter cake, and the combined filtrates were reduced in volume to 10 mL during which time a red precipitate formed that was separated by cannula transfer of the filtrate (0.201 g, 0.274 mmol). The mother liquor was stored at 6 ºC to give additional red precipitate (0.138 g, 0.188 mmol). The total yield of **2a** was (0.339 g, 21%). Single crystals for X-ray analysis were obtained from a highly diluted solution of **2a** in 1 mL of cyclohexane and 5 mL of thf at 25 ºC. A ^{1}H NMR spectrum was obtained from the reaction mixture because dissolving the precipitate in common organic solvents was not successful. ^{1}H NMR: δ 1.71 (s, 12 H, NMe_2), 3.37 (s, 4H, CH_2), 4.26 (d, 4H, *o*-H), 4.29 (pst, 4H, *m*-H), 4.45 (pst, 4H, *m*-H), 4.62 (pst, 4H, *p*-H), 5.57 (d, 4H, *o*-H), 7.01 (d, 2H, 3-H), 7.37 (t, 2H, 4-H), 7.48 (t, 2H, 5-H), 8.47 (d, 2H, 6-H). MS(70 eV, EI +): *m*/*z* (%) 208 (21) $[Cr(C_6H_6)2]^+$, 135 (27) $[C_9H_{13}N]^+$, 130 (24) $[C_6H_6Cr]^+$, 91 (15) $[C_7H_7]^+$, 78 (100) $[C_6H_6]^+$, 58 (33). Anal. Calcd for $C_{42}H_{44}Al_2Cr_2N_2$ (734.7674): C, 68.65; H, 6.04; N, 3.81. Found: C, 68.91; H, 6.12; N, 3.59.

Synthesis of [5-*t*Bu-2-(Me_2NCH_2)C_6H_3]$AlCl_2$ (3a). A solution of $AlCl_3$ (2.477 g, 18.58 mmol) in Et_2O (30 mL, –80 ºC) was added to a solution of [5-*t*Bu-2-(Me_2NCH_2)C_6H_3]Li (3.670 g, 18.60 mmol) in Et_2O (20 mL, –80 ºC) followed by stirring at room temperature for 6 h. The suspension was filtered to remove LiCl, the filtrate was collected, and remaining product was extracted with an additional 30 mL of Et_2O from the LiCl filter cake. All volatiles were removed from the combined filtrates and subsequent sublimation of the resulting solid under high vacuum (110 ºC) gave **3a** as a white crystalline solid (4.692 g, 88%). ^{1}H NMR: δ 1.19 (s, 9H, *t*Bu), 1.87 (s, 18 H, 2 $SiMe_3$), 3.05 (s, 6H, NMe_2), 6.73 (d, 1H, 3-H), 7.32 (d, 1H, 4-H), 7.86 (s, 1H, 6-H). ^{13}C NMR: δ 31.5 (*t*Bu), 45.3 (NMe_2), 65.3 (CH_2), 124.4 (3-C), 126.7 (4-C), 133.6 (6-C), 139.9 (2-C, *ipso*-C), 150.5 (5-C, *ipso*-C). ^{27}Al NMR: δ 131 ($w_{1/2}$ = 2500 Hz). MS (70 eV, EI +): *m*/*z*

(%): 287 (26) $[M]^+$, 272 (100) $[M–CH_3]^+$, 191 (45) $[MH–AlCl_2]^+$, 147 (30) $[MH−NMe_2–AlCl_2]^+$, 140 (34), 131 (50) $[M–NMe_2–AlCl_2–CH_3]^+$, 117 (12) $[M–CH_2–NMe_2–AlCl_2–CH_3]^+$, 91 (19) $[C_7H_7]^+$, 58 (52) $[C_4H_{10}]^+$. Anal. Calcd for $C_{13}H_{20}AlCl_2N$ (288.1921): C, 54.18; H, 6.99; N, 4.86. Found: C, 54.11; H, 6.80; N, 5.03.

Synthesis of [5-*t*Bu-2-(Me_2NCH_2)C_6H_3]$GaCl_2$ (3b). A solution of $GaCl_3$ (3.2315 g, 18.352 mmol) in Et_2O (40 mL, –80 ºC) was added to a solution of [5-*t*Bu-2-(Me_2NCH_2)C_6H_3]Li (3.6133 g, 18.319 mmol) in toluene (40 mL, –80 ºC) followed by stirring at room temperature for 16 h. LiCl was filtered off, the filtrate collected, and remaining product was extracted with CH_2Cl_2 (2 x 20 mL) from LiCl filter cake. The combined filtrates were reduced to dryness under vacuum to give a white solid. Subsequent sublimation under high vacuum (120 ºC) gave **3b** as a white crystalline solid (5.331 g, 88%). ^{1}H NMR: δ 1.14 (s, 9H, *t*Bu), 1.88 (s, 18 H, 2 $SiMe_3$), 2.95 (s, 6H, NMe_2), 6.69 (d, 1H, 3-H), 7.26 (d, 1H, 4-H), 7.73 (s, 1H, 6-H). ^{13}C NMR: δ 31.4 (*t*Bu), 45.3 (NMe_2), 64.5 (CH_2), 125.2 (3-C), 126.9 (4-C), 132.5 (6-C), 138.0 (2-C, *ipso*-C), 151.6 (5-C, *ipso*-C). MS(70 eV, EI +): *m*/*z* (%): 314 (10) $[M–CH_3]^+$, 191 (81) $[MH–GaCl_2]^+$, 175 (10) $[MH–CH_3–GaCl_2]^+$, 147 (57) $[MH−NMe_2–GaCl_2]^+$, 132 (20) $[M–CH_2–NMe_2–GaCl_2]^+$, 117 (19) $[M–CH_2–NMe_2–GaCl_2–CH_3]^+$, 105 (11) $[C_8H_9]^+$, 92 (19) $[C_7H_8]^+$, 58 (100) $[C_4H_{10}]^+$. Anal. Calcd for $C_{13}H_{20}AlCl_2N$ (330.9336): C, 47.18; H, 6.09; N, 4.23. Found: C, 46.86; H, 6.19; N, 4.19.

Synthesis of [{5-*t*Bu-2-(Me_2NCH_2)C_6H_3}Al(η^6-C_6H_5)$_2$Cr]$_2$ (4a). A slurry of [$Cr(LiC_6H_5)_2$]·tmeda (1.142 g, 3.396 mmol) in benzene (30 mL, 0 °C) was added to a solution of **3a** (0.976, 3.39 mmol) in benzene (10 mL, 0 °C). The cooling bath was removed and the mixture was stirred for 1 h. All volatiles were removed in vacuum. The product was extracted with toluene (2 × 10 mL), filtered to remove LiCl, and storage of the filtrate at –25 °C led to the

formation of dark red crystals of **4a** (0.425 g, 30%). Single crystals for X-ray analysis were obtained from benzene at 6 ºC. ^{1}H NMR: δ 1.58 (s, 18H, *t*Bu), 1.75 (s, 12 H, NMe_2), 3.42 (s, 4H, CH_2), 4.30 (br. s, 8H, *o*-H, *m*-H), 4.48 (pst, 4H, *p*-H), 4.73 (pst, 4H, *m*-H), 5.77 (d, 4H, *o*-H), 7.05 (d, 2H, 3-H), 7.50 (d, 2H, 4-H), 8.69 (s, 2H, 6-H). ^{13}C NMR: δ 32.1 (*t*Bu), 46.8 (NMe_2), 67.1 (CH_2), 75.0 (*p*-C), 75.6 (*m*-C or *o*-C), 76.0 (*ipso*-C), 76.5 (*m*-C), 80.6 (*o*-C), 81.9 (*o*-C or *m*-C), 123.9 (3-C),124.7 (4-C), 135.0 (6-C), 142.8 (2-C, *ipso*-C), 149.2 (5-C, *ipso*-C). MS(70 eV, EI +): *m*/*z* (%) 208 (43) $[Cr(C_6H_6)_2]^+$, 191 (100) $[C_{13}H_{21}N]^+$, 175 (10) $[C_{12}H_{17}N]^+$, 154 (12), 147 (71) $[C_{11}H_{15}]^+$, 134 (14) $[C_9H_{12}N]^+$, 132 (25) $[C_{10}H_{12}]^+$, 130 (49) $[C_6H_6Cr]^+$, 119 (11), 117 (27) $[C_9H_9]^+$, 105 (11). Anal. Calcd for $C_{50}H_{60}Al_2Cr_2N_2$ (846.9801): C, 70.90; H, 7.14; N, 3.31. Found: C, 70.70; H, 6.98; N, 3.12.

Synthesis of [{5-*t*Bu-2-(Me_2NCH_2)C_6H_3}Ga(η^6-C_6H_5)$_2$Cr]$_2$ (4b). A slurry of $[Cr(LiC_6H_5)_2]$·tmeda (1.072 g, 3.188) in benzene (30 mL) was added to a solution of **3b** (1.073 g, 3.242 mmol) in benzene (10 mL, 0 °C). The cooling bath was removed, and the mixture was immediately warmed to ambient temperature and stirred for 1 h. All volatiles were removed in vacuum. The dark-red product was extracted with toluene (2 × 10 mL) and filtered to remove LiCl. The filtrate was concentrated to 10 mL and kept at –25 ºC to yield dark red crystals of **4b** (0.410 g, 28%). Single crystals suitable for X-ray analysis were obtained from benzene at 6 ºC. ^{1}H NMR: δ 1.57 (s, 18H, 2 *t*Bu), 1.72 (s, 12H, 2 NMe_2), 3.35 (s, 4H, 2 CH_2), 4.28 (pst, 4H, *m*-H), 4.31 (d, 4H, *o*-H), 4.44 (pst, 4H, *p*-H), 4.73 (pst, 4H, *m*-H), 5.73 (d, 4H, *o*-H), 7.08 (d, 2H, 3-H), 7.46 (d, 2H, 4-H), 8.58 (s, 2H, 6-H). ^{13}C NMR: δ 32.1 (*t*Bu), 46.6 (NMe_2), 66.7 (CH_2), 75.0 (*p*-C), 75.8 (*m*-C), 76.6 (*m*-C), 79.9 (*ipso*-C), 80.7 (*o*-C), 81.6 (*o*-C), 124.2 (3-C), 124.4 (4-C), 134.1 (6-C), 142.2 (2-C, *ipso*-C), 149.5 (5-C, *ipso*-C). MS(70 eV, EI +): *m*/*z* (%): 208 (19) $[Cr(C_6H_6)_2]^+$, 191 (100) $[C_{13}H_{21}N]^+$, 175 (10) $[C_{12}H_{17}N]^+$, 147 (71) $[C_{11}H_{15}]^+$, 134 (13)

$[C_9H_{12}N]^+$, 132 (25) $[C_{10}H_{12}]^+$, 130 (22) $[C_6H_6Cr]^+$, 119 (13), 117 (32) $[C_9H_9]^+$, 115 (13), 105 (13). Anal. Calcd for $C_{50}H_{60}Cr_2Ga_2N_2$ (932.463): C, 64.40; H, 6.49; N, 3.00. Found: C, 64.42; H, 5.89; N, 3.02.

Synthesis of [{5-*t*Bu-2-(Me_2NCH_2)C_6H_3}Al(η^6-C_6H_5)$_2$Mo]$_2$ (5a). A slurry of $[Mo(LiC_6H_5)_2]$·tmeda (1.192 g, 3.135 mmol) in benzene (30 mL) was added to a solution of **3a** (0.914 g, 3.17 mmol) in benzene (10 mL, 0 ºC). The cooling bath was removed and the mixture was stirred for 1 h resulting in a red brown solution. All volatiles were removed in vacuum. The product was extracted with toluene (4 × 5 mL), and the solution was filtered to remove LiCl. The filtrate was concentrated to 10 mL and kept at –25 ºC to yield green crystals which were washed with benzene (2 × 3 mL) and dried on high vacuum to give **5a** (0.428 g, 29%). Single crystals for X-ray analysis were obtained from C_6D_6 at 25 ºC from an NMR tube. ^{1}H NMR: δ 1.51 (s, 18H, 2 *t*Bu), 2.01 (s, 9H, 2 NMe_2), 3.45 (s, 4H, 2 CH_2), 4.38 (d, 4H, *o*-H), 4.46 (pst, 4H, *m*-H), 4.86 (pst, 4H, *p*-H), 4.96 (pst, 4H, *m*-H), 5.82 (d, 4H, *o*-H), 6.99 (d, 2H, 3-H), 7.43 (d, 2H, 4-H), 8.24 (s, 2H, 6-H). ^{13}C NMR: δ 32.0 (*t*Bu), 47.1 (NMe_2), 67.3 (CH_2), 74.1 (*p*-C), 76.3 (*m*-C), 76.6 (*ipso*-C), 77.4 (*m*-C), 81.8 (*o*-C), 81.9 (*o*-C), 123.8 (3-C), 124.6 (4-C), 134.7 (6-C), 142.6 (2-C, *ipso*-C), 148.9 (5-C, *ipso*-C). MS(70 eV, EI +): *m*/*z* (%): 191 (100) $[C_{13}H_{21}N]^+$, 190 (88) $[C_{13}H_{20}N]^+$, 175 (10) $[C_{12}H_{17}N]^+$, 154 (16), 147 (73) $[C_{11}H_{15}]^+$, 134 (11) $[C_9H_{12}N]^+$, 132 (25) $[C_{10}H_{12}]^+$, 119 (10), 117 (24) $[C_9H_9]^+$, 105 (12). Anal. Calcd for $C_{50}H_{60}Al_2Mo_2N_2$ (934.8679): C, 64.24; H, 6.47; N, 3.00. Found: C, 64.03; H, 6.33; N, 3.32.

Synthesis of [{5-*t*Bu-2-(Me_2NCH_2)C_6H_3}Ga(η^6-C_6H_5)$_2$Mo]$_2$ (5b). A slurry of $[Mo(LiC_6H_5)_2]$·tmeda (1.071 g, 2.817) in benzene (30 mL) was added to a solution of **3b** (0.917 g, 2.77 mmol) in benzene (10 mL, 0 ºC). The cooling bath was removed and the mixture was stirred for 1 h resulting in a red-brown solution. All volatiles were removed in vacuum. The

product was extracted with toluene (4 × 5 mL) and filtered to remove LiCl. The filtrate was concentrated to 10 mL and kept at –25 ºC to yield green crystals, which were washed with benzene (2 × 3 mL) and dried to give **5b** (0.283 g, 20%). Single crystals for X-ray analysis were obtained from C_6D_6 at 25 ºC from an NMR tube. ^{1}H NMR: δ 1.23 (s, 18 H, 2 *t*Bu), 1.97 (s, 12 H, 2 NMe_2), 3.38 (s, 4H, 2 CH_2), 4.40 (d, 4H, *o*-H), 4.47 (t, 4H, *m*-H), 4.82 (t, 4H, *p*-H), 4.98 (t, 4H, *m*-H), 5.83 (d, 4H, *o*-H), 7.02 (d, 2H, 3-H), 7.39 (d, 2H, 4-H), 8.13 (s, 2H, 6-H). ^{13}C NMR: δ 32.0 (*t*Bu), 46.9 (NMe_2), 66.8 (CH_2), 74.5 (*p*-C), 76.5 (*m*-C), 77.5 (*m*-C), 79.8 (*ipso*-C), 81.5 (*o*-C), 81.7 (*o*-C), 124.1 (4-C), 124.2 (3-C), 133.8 (6-C), 142.0 (2-C, *ipso*-C), 149.2 (5-C, *ipso*-C). MS (70 eV, EI +) *m*/*z* (%): 414 (10) $[C_{25}H_{30}GaN]^+$, 338 (100), 337 (51) $[C_{19}H_{26}GaN]^+$, 336 (93) $[C_{19}H_{25}GaN]^+$, 296 (21), 294 (21), 293 (18) $[C_{17}H_{20}Ga]^+$, 191 (23) $[C_{13}H_{21}N]^+$, 190 (19) $[C_{13}H_{20}N]^+$, 147 (16) $[C_{11}H_{15}]^+$. Anal. Calcd for $C_{50}H_{60}Ga_2Mo_2N_2$ (1020.3508): C, 58.86; H, 5.93; N, 2.75. Found: C, 58.65; H, 5.43; N, 2.49.

Crystal structure determination. Crystal data of **2a**, **4a**,**b** and **5a**,**b** were collected at –100 °C on a Nonius Kappa CCD diffractometer, using monochromated Mo Kα radiation (λ = 0.71073 Å) at –100 °C. An initial orientation matrix and cell was determined φ scans and the X-ray data were measured using φ- and ω-scans.[30] Data reduction was performed with HKL DENZO and SCALEPACK software.[31] Structures were solved by direct methods (SIR-97)[32] and refined by full-matrix least-squares methods on F^2 with SHELX-97.[33] Unless otherwise stated, the non-hydrogen atoms were refined anisotropically; hydrogen atoms were included at geometrically idealized positions but not refined. The isotropic thermal parameters of the hydrogen atoms were fixed at 1.2 times that of the preceding carbon atom. Neutral atom scattering factors for non-hydrogen atoms and anomalous dispersion coefficients are contained in the SHELXTL-NT 6.14 program library.[34] Crystallographic data are summarized in Table 8-1.

ORTEP-3 for *Windows*[35] was used for molecular graphics and PLATON[36] was used to prepare material for publication.

For compound **2a** a disordered cyclohexane molecule in the lattice was modeled with restraints to hold its geometry. The cyclohexane molecule is lying on a symmetry centre in the lattice, which generates the superimposed mirror image of the cyclohexane molecule and results in some very short H···H distances (as short as 1.84 Å) to H atoms in the **2a** molecule. For compound **4b**, the disordered benzene molecule in the structure was modeled as a rigid molecule with anisotropic displacement parameters.

5a,**b** were crystallized from C_6D_6, which was incorporated into their lattices. The deuterium atoms attached to the benzene solvent molecule were included as hydrogen atoms at geometrically idealized positions and were not refined. The chemical formula and the derived quantities fw, ρ_{calcd}, μ_{calcd}, and F(000) were not corrected, to account for the presence of these deuterium atoms.

ACKNOWLEDGMENT. We thank G. A. Orlowski (University of Guelph) and H.-B. Kraatz (University of Western Ontario) for their help with electrochemical measurements in the initial stage of the project. We thank K. Brown (University of Saskatchewan) for NMR measurements. We thank the Natural Sciences and Engineering Research Council of Canada (NSERC Discovery Grant, J.M.), the Department of Chemistry, the Saskatchewan Structural Sciences Centre, and the University of Saskatchewan for their generous support. We thank the Canada Foundation for Innovation (CFI) and the government of Saskatchewan for funding of the X-ray and NMR facilities in the Saskatchewan Structural Sciences Centre (SSSC).

Supporting Information Available. ORTEP plots for compounds **4a** and **5b**; X-ray crystallographic data for **2a**, **4a**,**b** and **5a**,**b** in CIF format; CVs of $[(C_5H_5)_2Fe]$, $[(C_6H_6)_2Cr]$ and

[$(C_6H_6)_2$Mo] with respect to the silver quasi-reference electrode. This material is available free of charge via the internet at http://pubs.acs.org. Crystallographic data for all of the structures in this article have been deposited with the Cambridge Crystallographic Data Centre, under CCDC 675591 (**2a**), CCDC 675592 (**4a**), CCDC 675593 (**4b**) and CCDC 675594 (**5a**), and CCDC 675595 (**5b**). These data can be obtained free of charge from The Cambridge Crystallographic Data Centre via www.ccdc.cam.ac.uk/data_request/cif

8.6 References

(1) Watts, W. E. *J. Am. Chem. Soc.* **1966**, *88*, 855-856.
(2) Mueller-Westerhoff, U. T. *Angew. Chem., Int. Ed.* **1986**, *25*, 702-717.
(3) Löwendahl, M.; Davidsson, Ö.; Ahlberg, P.; Håkansson, M. *Organometallics* **1993**, *12*, 2417-2419.
(4) Löwendahl, M.; Davidsson, Ö.; Ahlberg, P. *J. Chem. Res., Synop.* **1993**, 40-41.
(5) Clearfield, A.; Simmons, C. J.; Withers Jr., H. P.; Seyferth, D. *Inorg. Chim. Acta* **1983**, *75*, 139-144.
(6) Scheibitz, M.; Winter, R. F.; Bolte, M.; Lerner, H.-W.; Wagner, M. *Angew. Chem., Int. Ed.* **2003**, *42*, 924-927.
(7) Schachner, J. A.; Lund, C. L.; Quail, J. W.; Müller, J. *Acta Cryst.* **2005**, *E61*, m682-m684.
(8) Braunschweig, H.; Burschka, C.; Clentsmith, G. K. B.; Kupfer, T.; Radacki, K. *Inorg. Chem.* **2005**, *44*, 4906-4908.
(9) Schachner, J. A.; Orlowski, G. A.; Quail, J. W.; Kraatz, H.-B.; Müller, J. *Inorg. Chem.* **2006**, *45*, 454-459.
(10) (a) Jutzi, P.; Lenze, N.; Neumann, B.; Stammler, H. G. *Angew. Chem., Int. Ed.* **2001**, *40*, 1424-1427; (b) Uhl, W.; Hahn, I.; Jantschak, A.; Spies, T. *J. Organomet. Chem.* **2001**, *637*, 300-303; (c) Althoff, A.; Jutzi, P.; Lenze, N.; Neumann, B.; Stammler, A.; Stammler, H.-G. *Organometallics* **2002**, *21*, 3018-3022; (d) Althoff, A.; Jutzi, P.; Lenze, N.; Neumann, B.; Stammler, A.; Stammler, H. G. *Organometallics* **2003**, *22*, 2766-2774; (e) Althoff, A.; Eisner, D.; Jutzi, P.; Lenze, N.; Neumann, B.; Schoeller, W. W.; Stammler, H.-G. *Chem. Eur. J.* **2006**, *12*, 5471-5480.
(11) (a) Park, J. W.; Seo, Y. S.; Cho, S. S.; Whang, D. M.; Kim, K. M.; Chang, T. Y. *J. Organomet. Chem.* **1995**, *489*, 23-25; (b) Zechel, D. L.; Foucher, D. A.; Pudelski, J. K.; Yap, G. P. A.; Rheingold, A. L.; Manners, I. *J. Chem. Soc., Dalton Trans.* **1995**, 1893-1899; (c) Ni, Y. Z.; Rulkens, R.; Pudelski, J. K.; Manners, I. *Macromol. Rapid Comm.* **1995**, *16*, 637-641; (d) Reddy, N. P.; Choi, N.; Shimada, S.; Tanaka, M. *Chem. Lett.* **1996**, 649-650; (e) MacLachlan, M. J.; Zheng, J.; Thieme, K.; Lough, A. J.; Manners, I.; Mordas, C.; LeSuer, R.; Geiger, W. E.; Liable-Sands, L. M.; Rheingold, A. L. *Polyhedron* **2000**, *19*, 275-289; (f) Calleja, G.; Carré, F.; Cerveau, G. *Organometallics* **2001**, *20*, 4211-4215; (g) Berenbaum, A.; Lough, A. J.; Manners,

I. *Organometallics* **2002**, *21*, 4415-4424; (h) Bao, M.; Hatanaka, Y.; Shimada, S. *Chem. Lett.* **2004**, *33*, 520-521.
(12) Herberhold, M.; Bärtl, T. *Z. Naturforsch. B* **1995**, *50*, 1692-1698 and references therein.
(13) (a) Seyferth, D.; Withers, H. P. *Organometallics* **1982**, *1*, 1275-1282; (b) Dong, T. Y.; Hwang, M. Y.; Wen, Y. S.; Hwang, W. S. *J. Organomet. Chem.* **1990**, *391*, 377-385; (c) Jäkle, F.; Rulkens, R.; Zech, G.; Foucher, D. A.; Lough, A. J.; Manners, I. *Chem. Eur. J.* **1998**, *4*, 2117-2128; (d) Jäkle, F.; Rulkens, R.; Zech, G.; Massey, J.; Manners, I. *J. Am. Chem. Soc.* **2000**, *122*, 4231-4232; (e) Baumgartner, T.; Jäkle, F.; Rulkens, R.; Zech, G.; Lough, A. J.; Manners, I. *J. Am. Chem. Soc.* **2002**, *124*, 10062-10070.
(14) Utri, G.; Schwarzhans, K. E.; Allmaier, G. M. *Z. Naturforsch. B* **1990**, *45*, 755-762.
(15) (a) Brunner, H.; Klankermayer, J.; Zabel, M. *J. Organomet. Chem.* **2000**, *601*, 211-219; (b) Mizuta, T.; Onishi, M.; Miyoshi, K. *Organometallics* **2000**, *19*, 5005-5009; (c) Mizuta, T.; Imamura, Y.; Miyoshi, K. *Organometallics* **2005**, *24*, 990-996.
(16) Ieong, N. S.; Chan, W. Y.; Lough, A. J.; Haddow, M. R.; Manners, I. *Chem. Eur. J.* **2008**, *14*, 1253-1263.
(17) Lund, C. L.; Schachner, J. A.; Quail, J. W.; Müller, J. *J. Am. Chem. Soc.* **2007**, *129*, 9313-9320 and references therein.
(18) Robin, M. B.; Day, P. *Adv. Inorg. Chem. Radiochem.* **1967**, *10*, 247-422.
(19) Cope, A. C.; Gourley, R. N. *J. Organomet. Chem.* **1967**, *8*, 527-533.
(20) Müller, J.; Englert, U. *Chem. Ber.* **1995**, *128*, 493-497.
(21) Herbert, D. E.; Mayer, U. F. J.; Manners, I. *Angew. Chem. Int. Ed.* **2007**, *46*, 5060-5081.
(22) Lund, C. L.; Schachner, J. A.; Quail, J. W.; Müller, J. *Organometallics* **2006**, *25*, 5817-5823.
(23) Elschenbroich, C.; Koch, J. *J. Organomet. Chem.* **1982**, *229*, 139-158.
(24) Measured in C_6D_6 at 25 ºC referenced to the signal at δ 128.00.
(25) Berger, S.; Braun, S. *200 and More NMR Experiments*; 3rd expanded ed.; WILEY-VCH: Weinheim, 2004, page 298.
(26) Bard, A. J.; Faulkner, L. R. *Electrochemical Methods*; 2nd ed.; John Wiley & Sons, Inc.: New York, 2001, chap. 6.
(27) *Synthetic methods of Organometallic and Inorganic Chemistry* Herrmann, W. A., Ed.; Georg Thieme Verlag Stuttgart: New York, 1997; Vol. 8.
(28) Elschenbroich, C.; Hurley, J.; Metz, B.; Massa, W.; Baum, G. *Organometallics* **1990**, *9*, 889-897.
(29) Green, M. L. H.; Treurnicht, I.; Bandy, J. A.; Gourdon, A.; Prout, K. *J. Organomet. Chem.* **1986**, *306*, 145-165.
(30) Nonius *COLLECT*; Nonius BV, Delft, The Netherlands, 1998.
(31) Otwinowski, Z.; Minor, W. In *Macromolecular Crystallography, Part A*; Carter, C. W., Sweet, R. M., Eds.; Academic Press: London, 1997; Vol. 276, p 307-326.
(32) Altomare, A.; Burla, M. C.; Camalli, M.; Cascarano, G.; Giacovazzo, C.; Guagliardi, A.; Moliterni, A. G. G.; Polidori, G.; Spagna, R. *J. Appl. Crystallogr.* **1999**, *32*, 115-119.
(33) Sheldrick, G. M. *SHELXL97-2: Program for the Solution of Crystal Structures*; University of Göttingen, Germany, 1997.
(34) *SHELXTL-NT 6.14: Program Library for Structure Solution and Molecular Graphics*; Bruker AXS, Inc.: Madison, WI, 2000-2003.
(35) Farrugia, L. J. *J. Appl. Crystallogr.* **1997**, *30*, 565.

(36) Spek, A. L. *PLATON, A Multipurpose Crystallographic Tool*; University of Utrecht, The Netherlands, 2001.

8.7 Supporting Information

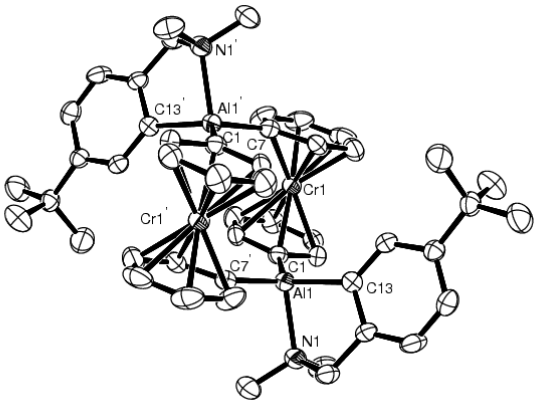

Figure 8-S1. Molecular structure of (p-*t*BuAr′)Al[1.1]CAP (**4a**) with thermal ellipsoids at the 50% probability level. Hydrogen atoms are omitted for clarity. Selected atom-atom distances [Å] and bond angles [º] for **4a**: Al1–N1 = 2.089(4), Al1–C1 = 1.969(5), Al1–C7 = 1.978(5), Al1–C13 = 1.988(4), Cr1–Cr1′ = 5.9921(11), C1–Al1–C7 = 119.96(19), N1–Al1–C13 = 85.09(17), C7–Al1–C13 = 114.0(2), C1–Al1–C13 = 120.18(18), C7–Al1–N1 = 100.59(18), C1–Al1–N1 = 107.54(18), α = 3.21(14).

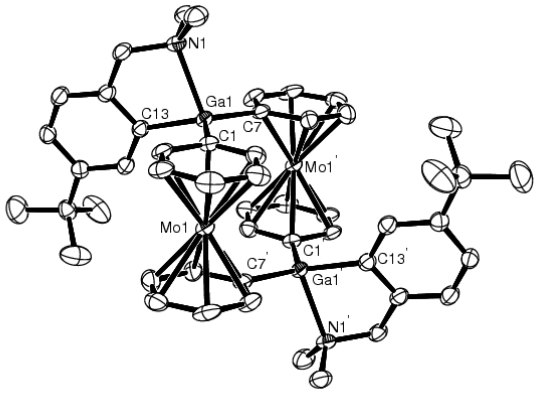

Figure 8-S2. Molecular structure of (p-*t*BuAr′)Ga[1.1]MAP (**5b**) with thermal ellipsoids at the 50% probability level. Hydrogen atoms are omitted for clarity. Selected atom-atom distances [Å] and bond angles [º] for **5b**: Ga1–N1 = 2.207(3), Ga1–C1 = 1.978(3), Ga1–C7 = 1.967(3), Ga1–C13 = 1.983(3), Mo1–Mo1′ = 6.0277(6), C1–Ga1–C7 = 122.38(14), N1–Ga1–C13 = 83.08(13), C7–Ga1–C13 = 120.27(14), C1–Ga1–C13 = 113.14(14), C7–Ga1–N1 = 105.75(12), C1–Ga1–N1 = 100.32(12), α = 2.2(3).

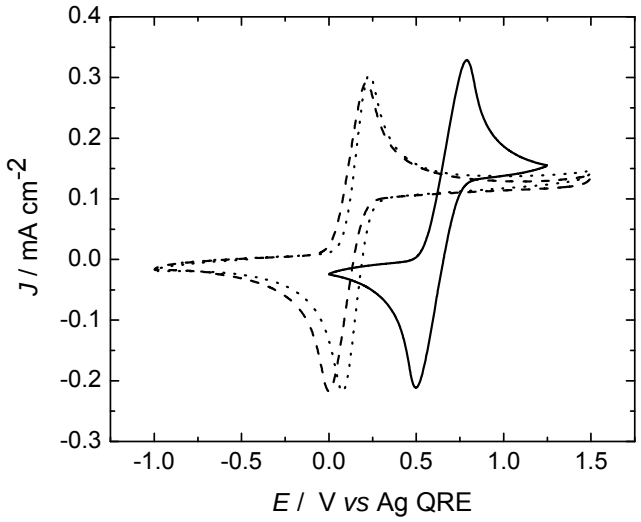

Figure 8-S3. Cyclic voltammogram of $[(C_5H_5)_2Fe]$ (solid line), $[(C_6H_6)_2Cr]$ (dashed line) and $[(C_6H_6)_2Mo]$ (dotted line). CVs were recorded inside a glovebox at 20 mV/s in dry THF (supporting electrolyte was 0.1M $[Bu_4N][PF_6]$) and were used to calibrate the Ag quasi reference electrode (QRE). The $E^{o\prime}$ values are 0.645, 0.105, and 0.150 V for $[(C_5H_5)_2Fe]$, $[(C_6H_6)_2Cr]$, and $[(C_6H_6)_2Mo]$, respectively $[E^{o\prime} = ½(E_{pa} + E_{pc})]$.

CHAPTER 9
PUBLICATION 8

Description

The following chapter is a verbatim copy of an article which was published in *Organometallics*[*] in September 2008[†] and describes the synthesis and characterization of three indium compounds that incorporate the intramolecularly coordinating Me_2Ntsi ligand. The compounds (Me_2Ntsi)$InCl_2$ (**2a)** and (Me_2Ntsi)InI_2 (**2b**) were synthesized and subsequently reacted with dilithioferrocene·2/3 tmeda producing an indium-bridged [1.1]FCP (**3**). Compound **3** was found to adopt an *anti* conformation in the solid state; in solution, variable temperature NMR measurements provided evidence that an equilibrium exists between *anti* and *syn* isomers.

Author Contributions

My contributions to this publication were the synthesis and characterization of the indium compound (Me_2Ntsi)$InCl_2$ (**2a**), the optimization of the synthesis of the indium-bridged [1.1]ferrocenophane **3** and subsequent characterization by variable temperature NMR spectroscopy. The coauthors on this paper are Jörg A. Schachner, who synthesized the indium compound (Me_2Ntsi)InI_2 (**2b**) and carried out the initial synthesis and characterization of **3**, Ian J. Burgess, with whom I performed the electrochemical analysis on the title compound **3**,

[*] Reproduced with permission from Organometallics. © 2008 American Chemical Society
[†] Schachner, J. A.; Lund, C. L.; Burgess, I. J.; Quail, J. W.; Schatte, G.; Müller, J. *Organometallics* **2008**, *27*, 4703-4710.

J. Wilson Quail, who performed all single-crystal X-ray analyses, and my supervisor Jens Müller. Written permission was obtained from all contributing authors to include material within this thesis.

Relation of Publication 8 to the Objectives of this Project

The following publication describes the outcome of a second attempt to synthesize an indium-bridged [1]FCP (first attempt see Chapter 4). This attempt failed to produce a strained sandwich compound, and instead a formal dimer of the targeted species, a [1.1]FCP was obtained. The results described in publication 8, combined with those of publications 5, 6 and 7 (Chapters 6–8), strongly indicate that the bulkiness of the stabilizing ligand attached to the heavier group-13 element plays a crucial role for the outcome of salt-metathesis reactions (see Chapter 9.4 for details). From this viewpoint, the failure described in publication 8 provided a deeper understanding of metallacyclophane chemistry of the heavier group-13 elements.

9. The Dynamic Indium-Bridged [1.1]Ferrocenophane $[(Me_2Ntsi)In(C_5H_4)_2Fe]_2$

Jörg A. Schachner,[‡] Clinton L. Lund,[‡] Ian J. Burgess,[‡] J. Wilson Quail,[§] Gabriele Schatte,[§] and Jens Müller[‡*]

[‡]*Department of Chemistry, University of Saskatchewan, 110 Science Place, Saskatoon, Saskatchewan, Canada, S7N 5C9,* [§]*Saskatchewan Structural Sciences Centre, University of Saskatchewan, 110 Science Place, Saskatoon, Saskatchewan, Canada, S7N 5C9*

Received April 16, 2008

9.1 Abstract

Salt metathesis reaction between Li(thf)(Me_2Ntsi) [Me_2Ntsi = $C(SiMe_3)_2SiMe_2NMe_2$] and InX_3 gave the new indium dihalides (Me_2Ntsi)InX_2 [X = Cl (**2a**), I (**2b**); isolated yields 34% (**2a**) and 44% (**2b**)]. Single-crystal X-ray analysis revealed that **2a** is a Cl-bridged dimer while **2b** is monomeric. Salt metathesis reaction between dilithioferrocene and **2a** and **2b**, respectively, gave the new indium-bridged [1.1]ferrocenophane $[(Me_2Ntsi)In(\eta^5\text{-}C_5H_4)_2Fe]_2$ (**3**). Only when **2a** was used, could analytically pure **3** be isolated (45%). Revealed by a single-crystal X-ray analysis, compound **3** crystallized as an *anti* isomer (C_i symmetry). The diinda[1.1]ferrocenophane **3** revealed fluxional behavior in solution. The proton NMR spectrum of **3** revealed only five singlets at ambient temperature (500 MHz, 25 ºC, C_6D_6 or C_7D_8): one singlet for $SiMe_2$, $SiMe_3$, and NMe_2 each and two singlets for the sixteen Cp protons. These facts can be rationalized by assuming a fast degenerate isomerization from one *anti* isomer to another *anti* isomer (time-averaged D_{2h} symmetry). The two singlets at 4.43 and 4.45 ppm (500 MHz, 25 ºC, C_7D_8) of the α- and β protons broadened at lower temperature and coalesced at 5 ºC. By lowering the temperature further, two sets of signals emerged and became clearly visible at –30

ºC, with each set consisting of four singlets for the Cp protons of equal intensity. Consistent with the splitting of the Cp signals, all other signals split in two sets of 3 singlets, indicating C_s symmetric Me_2Ntsi moieties. These data show that the [1.1]ferrocenophane **3** exists as a mixture of two isomers in toluene solutions (2:1 ratio at –30 ºC). Assuming that the thermodynamically favored isomer was found in the crystal lattice, the most intense set of signals was assigned to the *anti* isomer of **3** while the less intense set of signals was assigned to a *syn* isomer. The already known diinda[1.1]ferrocenophane {[2-(Me_2NCH_2)C_6H_4]In(η^5-C_5H_4)$_2$Fe}$_2$ (**1c**) was revisited. Compound **1c** did not reveal any fluxional behavior in 1D ^{1}H NMR spectra at ambient temperature, but EXSY spectroscopy revealed an occurring *anti*-to-*anti* isomerization of **1c** in solution. Cyclic voltammogram of **3** in thf / 0.1M [Bu_4N][PF_6] showed only an irreversible oxidation. A rationale is given why the reaction of (Me$_2$Ntsi)InX_2 [X = Cl (**2a**), I (**2b**)] with dilithioferrocene gave a [1.1]ferrocenophane, as similar reactions of (Me$_2$Ntsi)ECl_2 (E = Al, Ga) with dilithioferrocene gave strained [1]ferrocenophanes.

9.2 Introduction

[1.1]Ferrocenophanes stepped on the scientific stage when Nesmeyanov and Kritskaya described the first examples in 1956 (Figure 9-1; ER_x = CH_2, CHPh).[1] [1.1]Ferrocenophanes with carbon in bridging positions prefer the *syn* conformation (Figure 9-1; E = C),[2] however, an *anti* isomer was structurally characterized for the first time in 1993.[3]

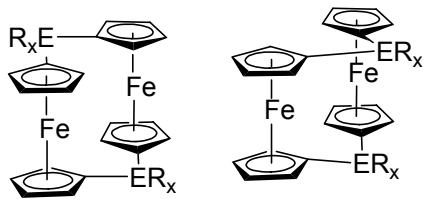

anti-[1.1]FCP *syn*-[1.1]FCP

Figure 9-1. Two different isomers of [1.1]ferrocenophanes.

Since the synthesis of the first hetero-atom-bridged [1.1]ferrocenophane, a $SnBu_2$-bridged species,[4] this family of ferrocene derivatives has grown significantly. To date, [1.1]ferrocenophanes of boron,[5] aluminum,[6–8] gallium,[8,9] indium,[8] silicon,[10,11] tin,[4,12] lead,[13] phosphorus,[14–16], sulfur[17] and mercury [18] are described in the literature. The chemistry of [1.1]ferrocenophanes had been extended to ruthenium: besides reports about carbon-bridged [1.1]ruthenocenophanes and mixed Ru-Fe [1.1]metallocenophanes,[2] to the best of our knowledge, a $SiMe_2$-bridged species[11] is the only heteroatom-bridged [1.1]ruthenocenophane to date. These [1.1]metallacyclophanes are formal dimers of strained [1]metallacyclophanes, which are prone to ring-open polymerize to produce new organometallic materials.[19]

In the course of our investigation of aluminum- or gallium-bridged metallacyclophanes, we discovered that the bulkiness of the ligand that is attached to the bridging group-13 element plays a crucial role. When the bulky *trisyl*-based ligands Pytsi or Me_2Ntsi (Figure 9-2) were applied, strained [1]metallacyclophanes were formed;[20–24] the use of the slimmer "one-armed phenyl" ligand Ar′ or p-*t*BuAr′ (Figure 9-2) resulted in unstrained [1.1]metallacyclophanes.[6,8,25] Among the latter species are the first [1.1]metallacyclophanes of bis(benzene) complexes; i.e., aluminum- and gallium-bridged [1.1]chromarenophanes and [1.1]molybdarenophanes (Figure 9-3).[25]

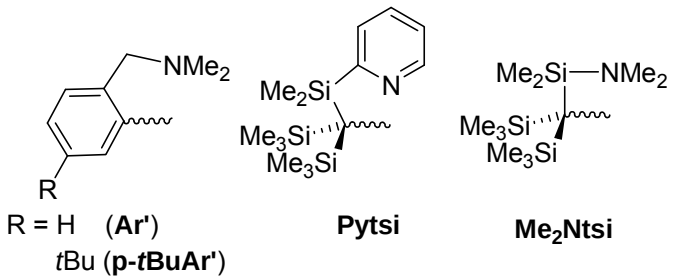

Figure 9-2. Intramolecularly coordinating ligands used for the synthesis of heavier group-13-bridged metallacyclophanes.

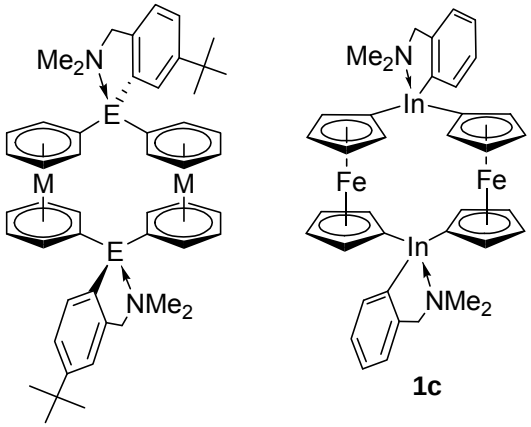

Figure 9-3. The first [1.1]CAPs (M = Cr; E = Al or Ga) and [1.1]MAPsmolybdarenophanes (M = Mo; E = Al or Ga), and the first Ar′In[1.1]FCP (**1c**).[8]

Strained [1]metallacyclophanes with indium in bridging positions are unknown. Our first attempt to get access to an inda[1]ferrocenophane by reacting (Pytsi)InCl$_2$ with dilithioferrocene resulted only in the isolation of the 1,1′-disubstituted ferrocene derivative [{(Pytsi)(μ-Cl)In}C$_5$H$_4$]$_2$Fe.[21] The reaction of Ar′InCl$_2$ with dilithioferrocene gave the unstrained [1.1]ferrocenophane [(Ar′In)(C$_5$H$_4$)$_2$Fe]$_2$ (**1c**; Figure 9-3), which is the only known diinda[1.1]ferrocenophane to date.

Within this report, we describe the outcome of another attempt to prepare an indium-bridged [1]ferrocenophane.

9.3 Results and Discussion

We attempted the synthesis of an indium-bridged [1]ferrocenophane by following the methods that we successfully implemented for aluminum- and gallium-bridged

[1]ferrocenophanes,[22] [1]chromarenophanes,[22] [1]vanadarenophanes,[22] [1]ruthenocenophanes,[23] and [1]molybdarenophanes[24]. In all these cases, the strained metallacyclophane had been synthesized via salt metathesis of dilithiated sandwich complexes with aluminum- or gallium dichlorides; the bridging group-13 element was always equipped with the bulky, intramolecularly coordinating Me_2Ntsi ligand (Figure 9-2). In order to apply this method to indium, we first needed to prepare respective indium dihalides.

9.3.1 Preparation and characterization of indium dihalides 2a and 2b. Salt metathesis reaction between $Li(thf)(Me_2Ntsi)$ and $InCl_3$ and InI_3 gave the new indium dihalides **2a** and **2b**, respectively (equation 9-1). Both compounds were isolated as analytically pure species through crystallization in moderate yields of 34% (**2a**) and 44% (**2b**), respectively.

$$Li(thf)(Me_2Ntsi) + InX_3 \xrightarrow[-\ thf]{-\ LiX} \begin{array}{c} Me_2N{-}SiMe_2 \\ \downarrow \quad | \\ X_2In{-}C(SiMe_3)_2 \end{array} \quad (9\text{-}1)$$

X = Cl (**2a**)
I (**2b**)

Their molecular structures have been determined by single-crystal X-ray structural analysis (Figures 9-4 and 9-5; Table 9-1). Compound **2a** is a chlorine-bridged dimer (Figure 9-4), in which each In atom is in the centre of a distorted trigonal bipyramid. Both bipyramids share one edge between an equatorial and an apical Cl atom to give a centro-symmetric dimer with C_i symmetry. A similar centro-symmetric dimer was found for the $(Pytsi)InCl_2$ (Figure 9-2),[21] and therefore, it is not surprising that the two related species, **2a** and $(Pytsi)InCl_2$[21], show very similar bond lengths and angles. For example, the bond length [Å] in the In_2Cl_4 core of **2a** are (values for $(Pytsi)InCl_2$ in square brackets taken from ref. 21): In1–Cl1 = 2.4521(13) [2.4812(7)], In1–Cl1′ = 2.8363(13) [2.7706(7)], and In1–Cl2 = 2.3530(17) [2.3845(7)]. In contrast to the indium chloride **2a**, the corresponding iodide **2b** is a monomer in the solid state

(Figure 9-5), an expected result, based on the known structure of the related compound (Pytsi)InI$_2$.[26] Again, the Me$_2$Ntsi containing species **2b** is not strikingly different compared to its cousin (Pytsi)InI$_2$.

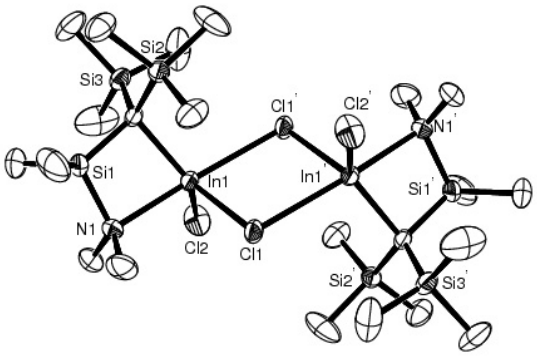

Figure 9-4. Molecular structure of (Me$_2$Ntsi)InCl$_2$ (**2a**) with thermal ellipsoids at the 50% probability level (only one of two dimers is shown). Hydrogen atoms are omitted for clarity. Selected bond length [Å] and angles [º]: In1–Cl1 = 2.4521(13), In1–Cl1′ = 2.8363(13), In1–Cl2 = 2.3530(17), In1–C1 = 2.211(5), In1–N1 = 2.385(4), Cl1–In1–C1 = 128.36(14), Cl2–In1–C1 = 127.74(15), Cl1–In1–Cl2 = 103.75(6), N1–In1–Cl1′ = 171.39(12), N1–In1–C1 = 76.83(17), N1–In1–Cl1 = 94.16(11), N1–In1–Cl2 = 97.91(13), Cl1′–In1–C1 = 103.65(14), Cl1′–In1–Cl2 = 88.59(5), Cl1′–In1–Cl1 = 78.75(4). Symmetry transformations used to generate equivalent atoms: –x+1, –y, –z+1.

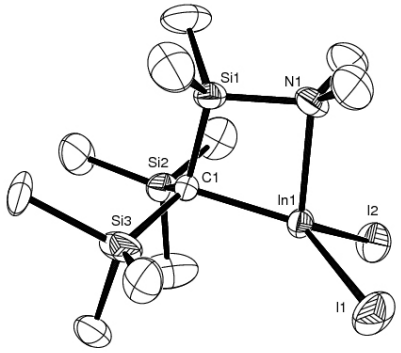

Figure 9-5. Molecular structure of (Me$_2$Ntsi)InI$_2$ (**2b**) with thermal ellipsoids at the 50% probability level. Hydrogen atoms are omitted for clarity. Selected bond length [Å] and angles [º]: In1–I1 = 2.7047(5), In1–I2 = 2.6949(5), In1–N1 = 2.310(4), In1–C1 = 2.215(4), N1–In1–C1 = 78.64(17), N1–In1–I1 = 106.05(12), N1–In1–I2 = 110.65(12), I1–In1–I2 = 103.494(19), I1–In1–C1 = 126.73(12), I2–In1–C1 = 124.86(12).

Compounds **2a** and **2b** show very similar NMR spectra. For example, three singlets in the proton NMR spectra with nearly identical chemical shifts for both species, render **2a** and **2b** C_s symmetric in solution on time average. Based on these data, one can speculate that the chloride **2a** takes part in a fast monomer-dimer equilibrium which lies predominantly on the side of the monomer in benzene solutions.

9.3.2 Synthesis and solid-state structure of diinda[1.1]ferrocenophane 3. In an earlier attempt to prepare an inda[1]ferrocenophane from [(Pytsi)InCl(μ-Cl)]$_2$ and dilithioferrocene, we could only isolate the 1,1′-disubstituted ferrocene [{(Pytsi)(μ-Cl)In}C$_5$H$_4$]$_2$Fe.[21] The indium moieties in this disubstituted ferrocene were similarly bridged by Cl atoms as those of the starting compound [(Pytsi)InCl(μ-Cl)]$_2$. This result left the impression that the dimeric nature of the starting dichloride might prevent the formation of the targeted inda[1]ferrocenophane and that a monomeric starting indium dihalide is required. This was the reason why we synthesized the diiodide **2b** in addition to the dichloride **2a**.

To our surprise, both new indium dihalides react with dilithioferrocene to give a [1.1]ferrocenophane (**3**) and not the targeted [1]ferrocenophane (equation 9-2). However, the isolation of pure **3** turned out to be difficult in both cases and analytical pure product was only obtained from reactions with the dichloride **2a** through crystallization from toluene solutions (yield of 45%).

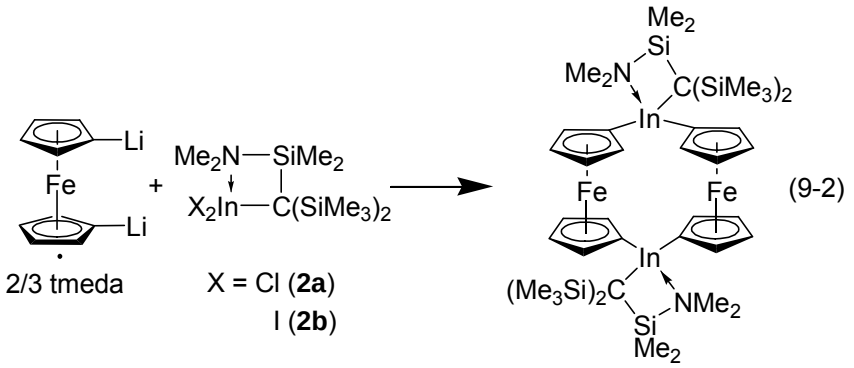

3

The [1.1]ferrocenophane **3** crystallizes in the monoclinic space group $P2_1/c$ (Table 9-1) as a centro-symmetric *anti* isomer (Figures 9-1 and 9-6). The geometry around each In atom can be best described as a flattened trigonal pyramid with C1, C10, and C11 forming the base and N1 at the apex of the pyramid. The sum over the three C–In–C angles of 359.6º indicates that the In atom is almost part of the plane defined by the three C atoms. The In1–N1 bond axis is tilted away from the ferrocene unit, which can be illustrated by the acute angle of 75.09(14)º for C11–In1–N1. The longest bond around indium is the In1–N1 donor bond at 2.437(3) Å. Compound **3** can be best compared to the only other known indium-bridged [1.1]ferrocenophane **1c** (Figure 9-3), which is equipped with the Ar′ instead of the Me$_2$Ntsi ligand (Figure 9-2).[8] The In atoms of **1c** are similarly coordinated as those in **3**; however, the trigonal pyramid is with a sum of 358.0º over the three C–In–C angles slightly less flattened as that in compound **3**.

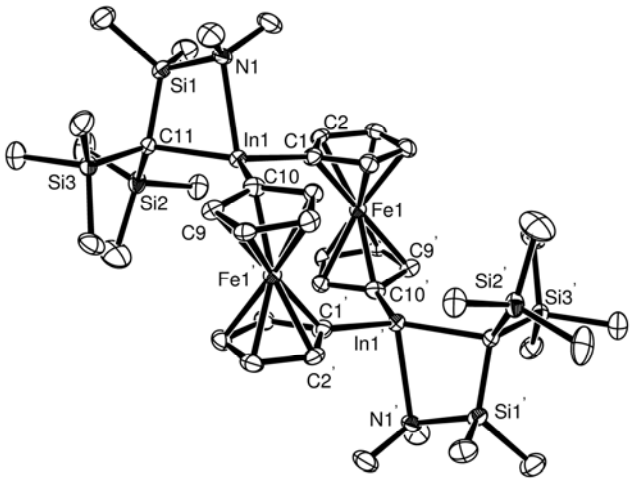

Figure 9-6. Molecular structure of (Me$_2$Ntsi)In[1.1]FCP (**3**) with thermal ellipsoids at the 50% probability level. H atoms are omitted for clarity. Selected bond length [Å] and angles [º]: In1–N1 = 2.437(3), In1–C1 = 2.173(4), In1–C10 = 2.160(5), In1–C11 = 2.291(4), Fe1–Fe1′ = 5.490(1), C1–In1–C10 = 113.07(17), C1–In1–C11 = 125.39(17), C10–In1–C11 = 121.09(17), C1–In1–N1 = 96.96(14), C10–In1–N1 = 106.29(15), C11–In1–N1 = 75.09(14).

Furthermore, the acute C–N–C angle of 77.99(15)º is larger and the In–N bond length of 2.386(4) Å is shorter compared to species **3**.[8] The differences between **1c** and **3** might be mainly a consequence of different ring sizes of the indium-containing cycles; a five-membered compared to a four-membered ring. Presumably, the higher strained four-membered cycle in compound **3** does not allow for an ideal orbital overlap between nitrogen and indium, with the consequence of a lengthened and, hence, weaker In–N donor bond in **3** compared to that of **1c**.

Table 9-1. Crystal and structural refinement data for compounds $(Me_2Ntsi)InCl_2$ (**2a**), $(Me_2Ntsi)InCl_2$ (**2b**), and $(Me_2Ntsi)In[1.1]FCP$ (**3**).

	$(2a)_2$	**2b**	**3**
empirical formula	$C_{22}H_{60}Cl_4In_2N_2Si_6$	$C_{11}H_{30}I_2InNSi_3$	$C_{42}H_{76}Fe_2In_2N_2Si_6$
fw	892.70	629.25	1118.93
cryst. size / mm^3	0.17 × 0.15 × 0.13	0.20 × 0.20 × 0.20	0.10 × 0.04 × 0.02
cryst. system, space group	triclinic, $P\bar{1}$	monoclinic, $P2_1/c$	monoclinic, $P2_1/c$
Z	2	4	2
a/Å	11.0773(4)	8.3419(2)	17.1413(4)
b/Å	12.7834(5)	17.9380(6)	9.5085(3)
c/Å	14.8553(5)	16.5700(4)	16.7639(5)
α/deg	83.170(3)	90	90
β/deg	89.900(3)	116.6581(17)	112.1530(10)
γ/deg	79.024(2)	90	90
volume/$Å^3$	2049.99(13)	2215.91(11)	2530.62(12)
ρ_{calc}/mg/m^3	1.446	1.886	1.468
temperature/ K	173(2)	173(2)	173(2)
$\mu_{calc.}$/mm^{-1}	1.577	4.005	1.634
θ range, deg	2.71 to 26.37	2.70 to 27.48	2.45 to 26.37
reflns collected	27183	8715	40374
Independent/observed reflns	8358 / 6532	5039 / 4282	5170 / 3917
absorption correction	ψ-scan	multi-scan	ψ-scan
data / restraints / params	8358 / 0 / 350	5039 / 21 / 204	5170 / 0 / 254
Goodness-of-Fit on F^2	1.074	1.069	1.052
R_1 indices [I > 2 σ(I)][a]	0.0500	0.0423,	0.0437
wR_2 (all data)[a]	0.1250	0.1044	0.0929
largest diff. peak and hole, $\Delta\sigma_{elect}$/ $Å^{-3}$	2.838 and –0.749	1.175 and –1.605	0.632 and –0.999

[a] $R_1 = [\Sigma||F_o|-|F_c||]/[\Sigma|F_o|]$ for $[F_o^2 > 2\sigma(F_o^2)]$, $wR_2 = \{[\Sigma w(F_o^2-F_c^2)^2]/[\Sigma w(F_o^2)^2]\}^{1/2}$ [all data].

9.3.3 NMR spectroscopy of diinda[1.1]ferrocenophane 3. The proton NMR spectrum of **3** shows only five singlets: one singlet for each of the $SiMe_2$, $SiMe_3$, and NMe_2 moieties and two singlets for the sixteen Cp protons[27] (Figure 9-S1, Supporting Information). The fact that all Cp protons result in only two singlets, directly reveals the presence of a two-fold symmetry element that renders the two halves of the mono-substituted C_5H_4 moieties equivalent. In the solid state, however, compound **3** exhibits C_i symmetry and one would expect that the folded four-membered rings invert fast in solution resulting in a time-averaged C_{2h} symmetric species.

Such a species would give four peaks for the C_5H_4 moieties: two for the inner protons (H_α and H_β) and two for the outer protons (H_α and H_β). A [1.1]ferrocenophane in an *anti* conformation (Figure 9-1) can be looked upon as an expanded cyclohexane in a *chair* conformation; an *anti*-to-*anti* isomerization in [1.1]ferrocenophanes is equivalent to a *chair*-to-*chair* isomerization in cyclohexane.[2,28] If such a degenerate isomerization would occur fast for compound **3** on the NMR timescale, D_{2h} symmetry would result on time average. This process is illustrated in Figure 9-7, where it is shown that inner Cp protons are converted into outer Cp protons and vice versa. Furthermore, this isomerization leads only to identical molecules, if breakage of the In–N donor bonds, rotation of the Me_2Ntsi ligands around In–C bonds, and formation of In–N donor bond on the opposite side of both In atoms are involved. This proposed *anti*-to-*anti* isomerization can explain the measured NMR spectra of species **3** at ambient temperature.

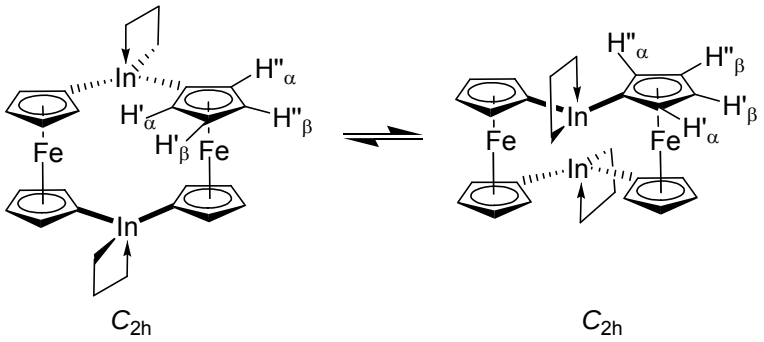

Figure 9-7. Illustration of an *anti*-to-*anti* degenerate isomerization of (Me$_2$Ntsi)In[1.1]FCP (**3**). Inner Cp protons of the left molecule (H′$_\alpha$ and H′$_\beta$) are converted into outer Cp protons of the right molecule (H′$_\alpha$ and H′$_\beta$) and vice versa.

In order to get further insight into the fluxional behavior of the [1.1]ferrocenophane **3**, proton NMR spectra were recorded at low temperatures (25 to –80 ºC). Figure 9-8 depicts the Cp range of selected ^{1}H NMR spectra between 25 and –30 ºC. The two singlets at 4.43 and 4.45 ppm (25 ºC) of the α- and β protons broaden at lower temperature and coalesce at 5 ºC. By lowering the temperature further, two sets of signals emerge and become clearly visible at –30

ºC, with each set consisting of four singlets of equal intensity. Consistent with the splitting of the Cp signals, all other signals split in two sets of 3 singlets, indicating C_s symmetric Me$_2$Ntsi moieties (Figure 9-S2, Supporting Information). These data clearly show that the [1.1]ferrocenophane **3** exists as a mixture of two isomers in toluene solutions in a 2:1 ratio at –30 ºC. Assuming that the thermodynamically favored isomer was found in the crystal lattice, we assigned the most intense set of signals to the *anti* isomer of **3**. The second set of signals can be assigned to the *syn* isomer of **3**, as the minor component. With *syn* isomer we mean an isomer in which the (Me$_2$Ntsi)In moieties are both on the same side of the two ferrocene units (Figure 9-1). In analogy to cyclohexane, such an isomer could be either similar to a *twist-boat* or a *boat* conformation, the latter being a transition state for a *twist-boat-to-twist-boat* isomerization of cyclohexane. Based on the experimental evidence, it is impossible to prove the exact nature of the minor isomer of compound **3**. It might be that the minor isomer has a similar structure as a *twist-boat* conformation of cyclohexane (D_2 symmetry). Compound **3** in a *twist-boat* conformation would exhibit C_2 symmetry, but one can assume that both enantiomers equilibrate fast on the NMR timescale resulting in a time-averaged C_{2v} symmetrical *syn* isomer. In summary, the *anti* and the *syn* both should give the same number of signals with a similar pattern, and that is what was found experimentally.

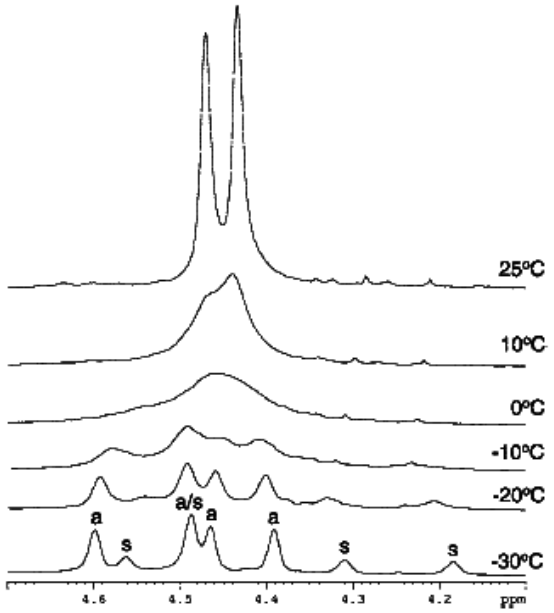

Figure 9-8. Cp region of selected ^{1}H NMR spectra of compound $(Me_2Ntsi)In$[1.1]FCP (**3**) (500 MHz; toluene-d_8). Indication "a" refers to the *anti* isomer of **3**; indication "s" refers to the *syn* isomer of **3** (see text for discussion); "a/s" indicates two coincidently overlapping peaks.

Further support for this interpretation comes from published knowledge of the dynamic behavior of other [1.1]ferrocenophanes. Most of the carbon-bridged [1.1]ferrocenophanes were found as *syn* isomers, however, in 1993 an *anti* isomer was structurally characterized for the first time (Figure 9-1; ER_x = CHMe).[3] Because of their dynamic behavior in solution, [1.1]ferrocenophanes have been coined "molecular acrobats".[2,28,29] With the exception of phosphorus,[15,16] boron[5] and the recently published dithia[1.1]ferrocenophane,[17] all other hetero-atom-bridged [1.1]ferrocenophanes crystallize as *anti* isomers. Interestingly, for a Ph(S)P bridged [1.1]ferrocenophane, both isomers could be characterized by single-crystal X-ray analysis.[16] For the desulfurized [1.1]ferrocenophane (Figure 9-1; ER_x = PhP), only the *syn* isomer crystallized, but both isomers were synthesized and form an equilibrium in toluene solutions.[16] However, the conversion from the *anti*- to the thermodynamically preferred *syn* isomer requires heating, which is in contrast to fast *syn-anti* equilibria known for carbon-bridged

species.[2,28,29] The authors rationalize the slow conversion by the fact that it requires an inversion of one of the two bridging phosphorus atoms.[16]

As already mentioned before, the first diinda[1.1]ferrocenophane (**1c**) was described recently.[8] Similar to its aluminum[6,8] and gallium[8] counterparts, it crystallized as an *anti* isomer. ^{1}H and ^{13}C NMR spectra could be interpreted as being caused by C_{2h} symmetrical molecules, a finding consistent with the structure of **1c** in the solid state; dynamic behavior was not revealed by these one-dimensional NMR spectra. An emerging second signal set at –80 ºC in ^{1}H NMR spectra hinted toward the presence of a second isomer,[8] however, peaks were too broad to be resolved and the identity of the second isomer could not be illuminated. Against the background of the high flexibility of the indium species **3**, we re-examined compound **1c** (Figure 9-9). With a series of NOE measurements all four Cp protons could be assigned to NMR signals. The EXSY spectrum of **1c** reveals with cross peaks between both α- and both β protons that the inner protons exchange their positions with the outer protons, which clearly reveals an occurring *anti*-to-*anti* isomerization of **1c** in solution.

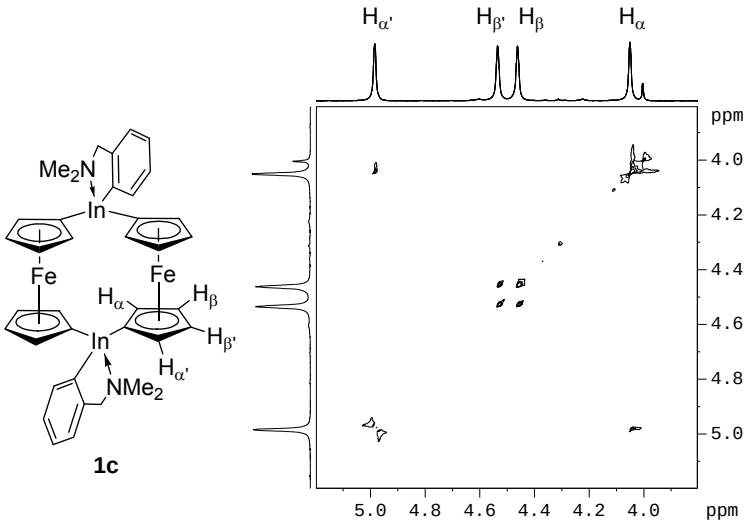

Figure 9-9. Left side: Assignment of Cp protons in Ar′In[1.1]FCP (**1c**) by NOE experiments. Right side: Cp region of an EXSY spectrum of **1c** (small signal at 3.99 ppm corresponds to ferrocene).

9.3.4 Cyclic voltammetry of diinda[1.1]ferrocenophane 3. [1.1]Ferrocenophanes can serve as model compounds to investigate the communication among two linked redox-active metal atoms. Usually, hetero-atom-bridged [1.1]ferrocenophanes show two one-electron redox couples indicating weak interactions of the two iron atoms (class II species).

We attempted to characterize the electrochemical behavior of compound **3** using cyclic voltammetry and 0.1M $[Bu_4N][PF_6]$ in dry thf as an electrolyte. The resulting voltammogram (Figure 9-10) displays a pronounced oxidation wave at approximately 1V *versus* the formal potential of ferrocene. However, this process is completely irreversible as there is no evidence of a reduction half reaction in the cathodic sweep. We have recently reported somewhat similar electrochemical behavior for an aluminum-bridged [1.1]ferrocenophane where both a reversible redox couple and an irreversible wave at more positive potentials were observed.[8] Quartz crystal microbalance studies of that system clearly demonstrated that the irreversible oxidation led to the formation of a passivating film on the working electrode. This is quite consistent with our present work where we observe a steady decrease in the oxidation current upon repeated potential cycling. If our electrode was removed from the cell, mechanically polished, and then returned to the cell, the first potential cycle was identical to the original scan. Unfortunately, unlike our previous electrochemical studies,[8,25] there are no reversible redox couples in the CV of the diinda[1.1]ferrocenophane **3**. For completeness we would like to indicate that additional CV studies of **3** in thf / 0.1M $[Bu_4N][ClO_4]$ revealed a startling dependence on the nature of the electrolyte's anion. In this electrolyte, compound **3** exhibited a quasi-reversible redox couple with an apparent formal potential of ~0.1 V vs Fc/Fc^+ and no evidence of the irreversible wave at positive potentials (Figure 9-S3, Supporting Information). However, the similarity of this CV to the voltammogram of pure ferrocene/ferrocenium and the absence of the redox couple in 0.1M

[Bu$_4$N][PF$_6$] is quite suspicious. It seems that either the perchlorate ion, or perhaps trace amount of chloride ions, led to a degradation of the metallocenophane into a ferrocene-like compound.

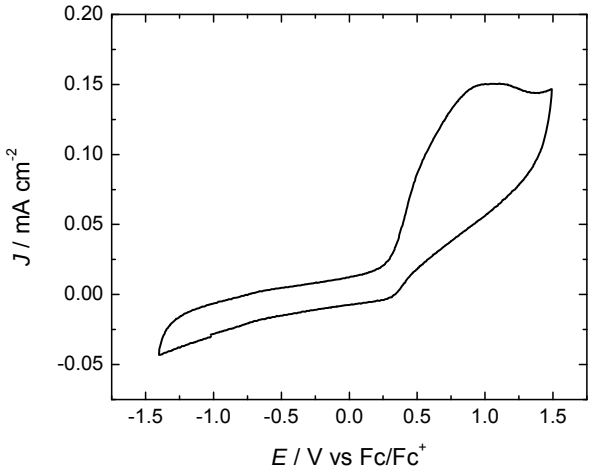

Figure 9-10. Cyclic voltammogram of (Me$_2$Ntsi)In[1.1]FCP (**3**) in thf / 0.1M [Bu$_4$N][PF$_6$] using a glassy carbon working electrode at a scan rate of 100 mV/s. The potential was measured *versus* a silver quasi reference electrode and subsequently re-referenced to the formal potential of ferrocene in 0.1M [Bu$_4$N][PF$_6$].

9.4 Conclusion

The new diinda[1.1]ferrocenophane **3** was obtained by reaction of dilithioferrocene with an indium dihalide (Me$_2$Ntsi)InX$_2$ (**2a** or **2b**; equation 9-2). Compound **3** is only the second known indium-bridged [1.1]ferrocenophane to date. The diinda[1.1]ferrocenophane **3** is fluxional in solution and its NMR spectra at room temperature can be interpreted by assuming a fast degenerate *anti*-to-*anti* isomerization. Upon cooling to –30 ºC the proton NMR spectrum reveals two similar signal patterns indicating the presence of an *anti*- and a *syn* isomer of **3**. [1.1]Ferrocenophanes are known to be highly dynamic in solutions and some carbon-bridged species were thoroughly investigated.[2,28] Most of the hetero-atom-bridged [1.1]ferrocenophanes show fast degenerate isomerizations, however, to the best of our knowledge, VT-NMR measurements had only been applied to a lead-bridged [1.1]ferrocenophane (Figure 9-1, ER$_x$ =

$PbPh_2$).[13] This diplumba[1.1]ferrocenophane, which was assumed to crystallize as an *anti* isomer, showed a significant broadening of the one of the two Cp proton signals at –89 ºC (300 MHz; CD_2Cl_2), but a coalescence temperature could not be reached.[13]

Recently, we had shown that the steric requirements of the ligand that is attached to the group-13 element plays an important role for aluminum- and gallium-bridged metallacyclophanes. While the bulky *trisyl*-based ligands Pytsi and Me_2Ntsi (Figure 9-2) stabilized strained [1]metallacyclophanes,[20–24] the slimmer "one-armed phenyl" ligand Ar′ or p-tBuAr′ (Figure 9-2) resulted exclusively in unstrained [1.1]metallacyclophanes (Figure 9-3).[6,8,25] Against this background it was a surprise that a [1.1]ferrocenophane **3** instead of an expected [1]ferrocenophane was formed (equation 9-2). How can this result be rationalized?

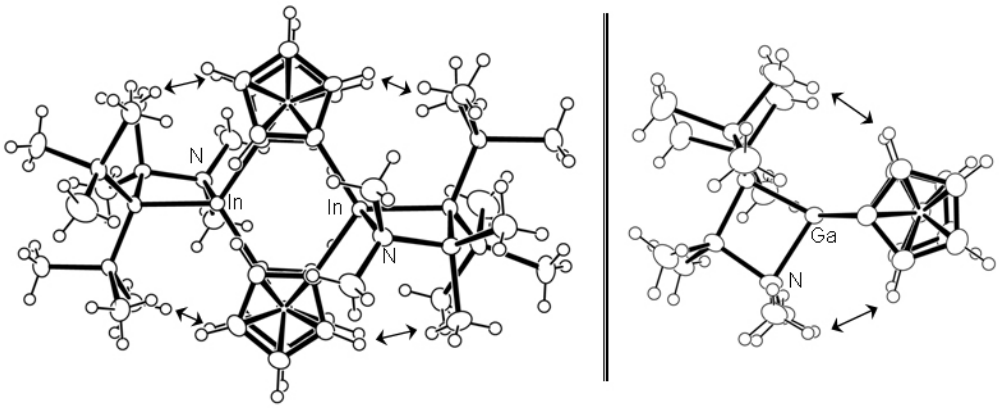

Figure 9-11. Illustration of the proximity between methyl groups of the Me_2Ntsi ligand and α protons of the ferrocene moieties (see double-headed arrows) in the (MeN_2tsi)In[1.1]FCP (**3**) (left side) and the galla[1]ferrocenophane $[(Me_2Ntsi)Ga(\eta^5\text{-}C_5H_4)_2Fe]$[22] (right side). H···H distances[30] in **3** are 2.15, 2.35, 2.36 and 2.38 Å ($SiMe_3$---αH); H···H distances[30] in $[(Me_2Ntsi)Ga(\eta^5\text{-}C_5H_4)_2Fe]$ are 2.28 and 2.44 Å ($SiMe_3$···α-H) and 2.35 and 2.53 Å (NMe_2···α-H).

Figure 9-11 illustrates steric interactions of a Me_2Ntsi moiety in a [1.1]ferrocenophane and a [1]ferrocenophane. The drawings are based on the crystallographic data of compound **3** (left side) and that of the published galla[1]ferrocenophane $[(Me_2Ntsi)Ga(\eta^5\text{-}C_5H_4)_2Fe]$[22] (right side). In both types of compounds the closest H···H contacts[30] are found between the α-H atoms

of the ferrocene moieties and Me groups of the Me$_2$Ntsi ligand (double-headed arrows in Figure 9-11). If these types of steric repulsions are reduced or even absent, which presumably is the case for Ar′ or p-tBuAr′ containing species (Figure 9-2 and 9-3), then the unstrained [1.1]metallacyclophane is formed as the thermodynamically preferred species.[6,8,25] However, for a four-fold coordinated group-13 element in a bridging position there is less space available around that element in a [1.1]metallacyclophane compared to a [1]metallacyclophane. Therefore, if the bulkiness of ligands start playing a role, then a [1.1]metallacyclophane is thermodynamically disfavored over a [1]metallacyclophane. These speculations are based on the observation that Pytsi and Me$_2$Ntsi equipped Al- and Ga moieties exclusively yielded [1]metallacyclophanes;[20–24] [1.1]metallacyclophanes were not formed. Aluminum and gallium have with 1.25 Å and 1.26 Å nearly the same covalent radii, whereas indium with 1.44 Å is significantly larger (singly bonded, 3-fold coordinated elements).[31] This increase in size translates into significant longer E–C bonds for indium species, as evident from a comparison of the three In–C bond lengths of 2.173(4) (In1–C1), 2.160(5) (In1–C10), and 2.291(4) Å (In1–C11) for **3** compared with the respective values of 2.008(3), 2.017(3), and 2.048(3) Å for the galla[1]ferrocenophane [(Me$_2$Ntsi)Ga(η^5-C$_5$H$_4$)$_2$Fe][22] (Figure 9-11). The longer the E–C bonds are, the weaker the steric repulsion between the ligand and the α-H atoms, with the result that for the (Me$_2$Ntsi)E bridging moiety with E = In the unstrained [1.1]ferrocenophane, but with E = Al[22] or Ga[22] strained [1]ferrocenophanes are the thermodynamically favored species. All these argument are based on proposed thermodynamic stabilities of [1]metallacyclophanes compared to [1.1]metallacyclophanes. All Al- and Ga-bridged metallacyclophanes were prepared through salt metathesis reactions and one must assume that these are not equilibrium reactions, which means that the formation of a particular product is kinetically controlled. With respect to the

formation of ferrocenophanes from intramolecularly stabilized group-13 dichlorides $RECl_2$, the first intermediate will be an asymmetrically substituted ferrocene in which one Cp ring carries the group-13 element moiety RECl while the other Cp ring is still lithiated. An *intramolecular* reaction will result in a [1]ferrocenophane whereas further *intermolecular* reactions will lead to a [1.1]ferrocenophane. Both these reaction routes will involve nucleophilic substitutions of Cl^- by a $C_5H_4^-$, which is a part of a ferrocene derivative, and one can assume that for the rate determining steps steric interactions between α-H atoms and intramolecularly coordinating ligands (Figure 9-2) play a key role. That means, the same arguments used for the ground-state structures (Figure 9-11) can be used for transition states.

9.5 Experimental Section

9.5.1 General Procedures. All manipulations were carried out using standard Schlenk techniques, if not noted differently. Solvents were dried using an MBraun Solvent Purification System and stored under nitrogen over 4 Å molecular sieves. C_6D_6 and C_7D_8 were prepared through freeze-pump-thaw procedures and stored under nitrogen over 4 Å molecular sieves. ^1H and ^{13}C NMR spectra were recorded on a Bruker 500 MHz Avance spectrometer at 25 °C, unless noted differently. ^1H chemical shifts were referenced to the residual protons of the deuterated solvent (C_6D_6: δ 7.15; C_7D_8: δ 2.10); ^{13}C chemical shifts were referenced to δ 128.00 (C_6D_6). Mass spectra were measured on a VG 70SE and were reported in the form M (%I) [F], where M is the mass observed, %I is the intensity of the peak relative to the most intense peak in the spectrum and F is the molecular ion or fragment. Mass peaks with intensities of >10% are reported. Elemental analyses were performed on a Perkin Elmer 2400 CHN Elemental Analyzer; samples were prepared in a glovebox and V_2O_5 was added to promote combustion.

The following compounds were purchased and use as received: $InCl_3$ (99.99%; Alfa Aesar), InI_3 (99.999%; Alfa Aesar), and MeLi (1.0 M in thf / cumene; Aldrich). $Li(thf)(Me_2Ntsi)$ was either freshly prepared, as in the case of **2a**, or isolated through crystallization, as in the case of **2b**.[32] The acronym Me_2Ntsi stands for $[(Me_2N)Me_2Si](Me_3Si)_2C$ (Figure 9-2). $[(LiC_5H_4)_2Fe]\cdot 2/3$ tmeda was synthesized as described in the literature.[33]

Compound **1c** was investigated by NMR Exchange Spectroscopy (EXSY) (Figure 9-9). First, a series of gradient 1D NOESY experiments were conducted to assign each peak in the Cp range to a proton. Then the relaxation times T1 of the Cp protons were measured in order to optimize the mixing times for the EXSY experiment.[34] Relaxation times for the Cp protons were in the range of 0.8–1.0 s. Then a series of 2D NOE experiments with mixing times (d2) of 0.4, 0.8 and 1.2 s were performed and checked for positive cross-peaks. Only for the last case (where d2 > T1) two positive cross-peaks were identified as shown in Figure 9-9.

9.5.2 Electrochemistry. A computer controlled system, consisting of a HEKA PG590 potentiostat (HEKA, Mahone Bay, NS, Canada) was used for the cyclic voltammetry experiments. Data was collected using a multifunction DAQ card (PCI 6251 M Series, National Instruments Austin, Texas) and in-house software written in the LabVIEW environment. Glassy carbon (BAS, 3mm) was used as the working electrode. The quasi-reference electrode (QRE) was a silver wire (E = 0.645 V vs the formal potential, E$^{o\prime}$, of 0.1 mM Fc/Fc^+). All electrochemical measurements were made using the QRE and subsequently rescaled to the ferrocene/ferrocenium formal potential[35]. A loop of gold wire was used as the auxiliary electrode. Before each measurement, a 1 mM solution of **3** was freshly prepared in dry thf with 0.1 M of supporting electrolyte ($[Bu_4N][PF_6]$, $[Bu_4N][BF_4]$, or $[Bu_4N][ClO_4]$). Extra efforts were undertaken to remove moisture and oxygen from the solvent thf. The solvent was first dried

using an MBraun Solvent Purification System and then filled into a 1L flask, which was part of a specialty Schlenk line, equipped with greaseless Young valves. To the so pre-dried thf, small amounts of 1,1-diphenylethylene and butyllithium were added resulting in a red solution, which indicated the absence of moisture. By flask-to-flask condensation under reduced static pressure, a small amount of thf was condensed into a Schlenk tube from the thf reservoir flask. The inert gas (N_2 4.8) used for this Schlenk line was purified by conducting it through two columns before feeding it into the Schlenk line (one column equipped with a Cu(I) catalyst and one column equipped with 4Å molecular sieves; both materials purchased from MBraun). A so prepared Schlenk tube filled with freshly condensed thf was moved into the glovebox. The electrolytes were dried under high vacuum ([Bu$_4$N][PF$_6$] overnight at 100 °C; [Bu$_4$N][BF$_4$] overnight at 70 °C; [Bu$_4$N][ClO$_4$] for 3 days at 25 °C). Unless otherwise specified, the scan rate for all CVs reported was 100 mV/s. All measurements were conducted inside a glovebox and taken at ambient temperature (24 – 25 ºC).

Synthesis of dichlorido{[(dimethylamino)dimethylsilyl]bis(trimethylsilyl)methyl-*κ*2C,N}indium(III) (2a). MeLi (20.2 mL, 1.0 M in thf/cumene) was added to a solution of Me$_2$NtsiH (5.172 g, 19.80 mmol) in thf (10 mL) and heated for 24 h at 45 °C. All volatile materials were removed in vacuo to leave a yellow solid behind. The solid was dissolved in Et$_2$O (30 mL) and the solution was added dropwise to a slurry of InCl$_3$ (4.205 g, 18.96 mmol) in Et$_2$O (20 mL) at 0 °C and subsequently stirred for 16 h. All volatiles were removed in vacuum from the resulting yellow solution to a give yellow solid which was then dried at 60 °C under high vacuum. The product was extracted with benzene (4 × 10 mL). The combined benzene phase was filtered, the filtrate was reduced in volume to 20 mL and stored at 6 °C to yield colorless crystals (2.347 g). After the mother liquor was concentrated to 10 mL and stored at 6 °C,

additional colorless crystals were obtained (0.496 g) (combined crystal fractions: 2.843 g, 34%). A single crystal for X-ray structural analysis was picked from the first fraction of crystals. ^{1}H NMR (C_6D_6, 500.13 MHz): δ 0.01 (s, 6H, $SiMe_2$), 0.31 (s, 18H, $SiMe_3$), 2.05 (s, 6H, NMe_2). 13C NMR (C_6D_6, 125.76 MHz): δ 2.02 ($SiMe_2$), 6.51 ($SiMe_3$), 41.19 (NMe_2), one C obscured. MS (70eV, EI+) *m*/*z* (%): 430 (30) [M^+–Me], 250 (13), 230 (100) [$Me_2NSiC(SiMe_3)_2^+$], 207 (11), 201 (17) [$(Me_3Si)_2C(SiMe)^+$], 187 (38) [$(Me_3Si)_2CSiH^+$], 129 (36) [$C_5H_{13}Si_2^+$], 115 (19) [In^+], 102 (22) [$Me_2SiNMe_2^+$], 73 (69) [$SiMe_3^+$], 59 (38) [$C_2H_7Si^+$]. anal. calcd. for $C_{11}H_{30}Cl_2InNSi_3$ (446.35): C, 29.60; H, 6.78; N, 3.14. Found: C, 29.73; H, 6.89; N, 3.09.

Synthesis of {[(dimethylamino)dimethylsilyl]bis(trimethylsilyl)methyl-κ^2C,N}diiodidoindium(III) (2b). Li(thf)(Me_2Ntsi) (3.43 g, 10.1 mmol) dissolved in toluene (20 mL) was added dropwise to a slurry of InI_3 (5.00 g, 10.1 mmol) in toluene (30 mL) at 0 °C and stirred for 2 h. The red solution was filtered and reduced in volume to ~10 mL. At –25 °C colorless crystals of analytically pure **2b** were obtained (2.76 g, 43%). A single crystal for X-ray structural analysis was picked from this fraction. ^{1}H NMR (C_6D_6, 500.13 MHz): δ 0.03 (s, 6H, $SiMe_2$), 0.34 (s, 18H, $SiMe_3$), 2.06 (s, 6H, NMe_2). ^{13}C NMR (C_6D_6, 125.76 MHz): δ 3.27 ($SiMe_2$), 6.95 ($SiMe_3$), 43.20 (NMe_2), one C obscured. MS (70eV, EI+) *m*/*z* (%): 347 (100) [$C_9H_{26}InNSi_3^+$], 203 (53) [$(Me_3Si)_2C(SiMeH_2)^+$], 115 (35) [In^+], 73 (55) [$SiMe_3^+$]. anal. calcd. for $C_{11}H_{30}I_2InNSi_3$ (629.25): C, 21.00; H, 4.81; N, 2.23. Found: C, 21.82; H, 5.13; N, 2.16.

Synthesis of bis{[(dimethylamino)dimethylsilyl]bis(trimethylsilyl)methyl-κ^2C,N}bis(μ-ferrocen-1,1′-diyl)diindium(III) (3). Compound **2a** (1.337 g, 2.995 mmol) was dissolved in toluene (15 mL) and chilled to –20 °C. A suspension of $[(LiC_5H_4)_2Fe]\cdot 2/3$ tmeda (0.826 g, 3.00 mmol) in toluene (15 mL) was added dropwise via tubing. After stirring for 2 h, the color of the solution had changed to red. Subsequently, the reaction mixture was filtrated,

and concentrated to 5 mL. Crystallization at –25 °C gave analytically pure **3** as red crystals (0.758 g, 45%). A single crystal for X-ray structural analysis was picked from this fraction. ^{1}H NMR (C_6D_6, 500.13 MHz): δ 0.21 (s, 6H, $SiMe_2$), 0.44 (s, 18H, $SiMe_3$), 2.04 (s, 6H, NMe_2), 4.43, 4.45 (s, 8H, C_5H_4). ^{13}C NMR (C_6D_6, 125.76 MHz): δ 3.26 ($SiMe_2$), 7.95 ($SiMe_3$), 42.19 (NMe_2), 70.41, 76.33 (C_5H_4), 77.88 (*ipso*-C, C_5H_4), one C is obscured. Low temperature 1H NMR (C_7D_8, 500.13 MHz, –30 °C): *Anti* isomer: 0.42 (s, 12H, $SiMe_2$), 0.51 (s, 36H, $SiMe_3$), 1.93 (s, 12H, NMe_2), 4.36, 4.43, 4.45, 4.57 (s, 16H, Cp); *syn* isomer: 0.20 (s, 36H, $SiMe_3$), 0.23 (s, 12H, $SiMe_2$), 2.14 (s, 12H, NMe_2), 4.15, 4.28, 4.45, 4.53 (s, 16H, Cp). MS (70eV, EI+): *m*/*z* (%): 1118 (5) [M^+], 857 (28) [M^+–$C(SiMe_3)(SiMe_2NMe_2)$–H], 560 (74) [$(C_5H_5)Fe(C_5H_4)In$–$[C(SiMe_3)(SiMe_2NMe_2)]^+$], 544 (22) [$C_{20}H_{35}FeInNSi_3^+$], 300 (80) [$(C_5H_5)Fe(C_5H_4In)^+$], 261 (17) [$HC(SiMe_3)(SiMe_2NMe_2)^+$], 230 (100) [$Me_2NSiC(SiMe_3)_2^+$], 217 (59) [$SiHMe_2C(SiMe_3)_2^+$], 186 (75) [$(C_5H_5)_2Fe^+$]. anal. calcd. for $C_{42}H_{76}In_2Fe_2N_2Si_6$ (1118.93): C, 45.08; H, 6.85; N, 2.50. Found: C, 45.09; H, 6.76; N, 2.27.

X-ray structural analysis for 2a, 2b and 3. All measurements were made on a Nonius KappaCCD 4-Circle diffractometer using monochromated Mo Kα radiation (λ = 0.71073 Å) at –100 °C. An initial orientation matrix and cell was determined from 10 frames using ϕ scans (1º per frame, 20 s exposures per degree for a 10° rotation).[36] Data were measured using ω-scans.[36] Data reduction was performed with the HKL DENZO and SCALEPACK software.[36] Absorption corrections were applied (see Table 6-1). The structures were solved using direct methods (SIR-97)[37] and refined by full-matrix least-squares method on F^2 with SHELXL97-2.[38] The non-hydrogen atoms were refined anisotropically. Hydrogen atoms were included at geometrically idealized positions (C–H bond distances 0.95/0.98/1.00) and were not refined. The isotropic thermal parameters of the hydrogen atoms were fixed at 1.5 times for methyl hydrogen atoms in

compounds **2a** and **3**, and 1.2 times that of the preceding carbon atom for all other hydrogen atoms. The asymmetric unit of **2a** consists of two half dimer units that are not crystallographically equivalent. The two half dimers are structurally very similar. In the structure of **2b** the carbon atoms [labeled as C(5A), C(6A), C(7A), C(5B), C(6B), C(7B)] of the methyl groups attached to Si(3) were disordered over two positions. Geometrical (SAME) and rigid body restraints (DELU and SIMU) were used to model the disorder in SHELXL97-2.[38] The refined site occupancy factors are 0.61(3) [C(5A), C(6A), C(7A)] and 0.39(3) [C(5B), C(6B), C(7B)], respectively.

ACKNOWLEDGMENT. We thank G. A. Orlowski (University of Guelph) and H.-B. Kraatz (University of Western Ontario) for their help with electrochemical measurements in the initial stage of the project. We thank the Natural Sciences and Engineering Research Council of Canada (NSERC Discovery Grant, JM), the Department of Chemistry, the Saskatchewan Structural Sciences Centre, and the University of Saskatchewan for their generous support. We thank the Canada Foundation for Innovation (CFI) and the government of Saskatchewan for funding of the X-ray and NMR facilities in the Saskatchewan Structural Sciences Centre (SSSC).

Supporting Information Available. Crystallographic data for **2a**, **2b** and **3** in CIF file format; ^{1}H NMR spectra of **3** (C_6D_6; 25 ºC and C_7D_8; –30 ºC); CV of **3** and ferrocene (thf / 0.1M [Bu_4N][ClO_4]). This material is available free of charge via the internet at http://pubs.acs.org. Crystallographic data for all of the structures in this article have been deposited with the Cambridge Crystallographic Data Centre, under CCDC 684585 (**2a**), 684586 (**2b**), and 684587 (**3**). Copies of this information may be obtained free of charge from The Director, CCDC, 12 Union Road, Cambridge CB2 1EZ, U.K. (fax, +44-1223-336033; e-mail, deposit@ccdc.cam.ac.uk; web, http://www.ccdc.cam.ac.uk).

9.6 References

(1) Nesmeyanov, A. N.; Kritskaya, I. I. *Bull. Acad. Sci. USSR, Div. Chem. Sci. (Eng. Transl.)* **1956**, 243-244.
(2) Mueller-Westerhoff, U. T. *Angew. Chem., Int. Ed.* **1986**, *25*, 702-717.
(3) Löwendahl, M.; Davidsson, Ö.; Ahlberg, P.; Håkansson, M. *Organometallics* **1993**, *12*, 2417-2419.
(4) (a) Seyferth, D.; Withers, H. P. *Organometallics* **1982**, *1*, 1275-1282; (b) Clearfield, A.; Simmons, C. J.; Withers Jr., H. P.; Seyferth, D. *Inorg. Chim. Acta* **1983**, *75*, 139-144.
(5) Scheibitz, M.; Winter, R. F.; Bolte, M.; Lerner, H.-W.; Wagner, M. *Angew. Chem., Int. Ed.* **2003**, *42*, 924-927.
(6) Braunschweig, H.; Burschka, C.; Clentsmith, G. K. B.; Kupfer, T.; Radacki, K. *Inorg. Chem.* **2005**, *44*, 4906-4908.
(7) Schachner, J. A.; Lund, C. L.; Quail, J. W.; Müller, J. *Acta Cryst.* **2005**, *E61*, m682-m684.
(8) Schachner, J. A.; Orlowski, G. A.; Quail, J. W.; Kraatz, H.-B.; Müller, J. *Inorg. Chem.* **2006**, *45*, 454-459.
(9) (a) Jutzi, P.; Lenze, N.; Neumann, B.; Stammler, H. G. *Angew. Chem., Int. Ed.* **2001**, *40*, 1424-1427; (b) Uhl, W.; Hahn, I.; Jantschak, A.; Spies, T. *J. Organomet. Chem.* **2001**, *637*, 300-303; Althoff, A.; (c) Jutzi, P.; Lenze, N.; Neumann, B.; Stammler, A.; Stammler, H.-G. *Organometallics* **2002**, *21*, 3018-3022; (d) Althoff, A.; Jutzi, P.; Lenze, N.; Neumann, B.; Stammler, A.; Stammler, H. G. *Organometallics* **2003**, *22*, 2766-2774; (e) Althoff, A.; Eisner, D.; Jutzi, P.; Lenze, N.; Neumann, B.; Schoeller, W. W.; Stammler, H.-G. *Chem. Eur. J.* **2006**, *12*, 5471-5480.
(10) (a) Park, J. W.; Seo, Y. S.; Cho, S. S.; Whang, D. M.; Kim, K. M.; Chang, T. Y. *J. Organomet. Chem.* **1995**, *489*, 23-25; (b) Zechel, D. L.; Foucher, D. A.; Pudelski, J. K.; Yap, G. P. A.; Rheingold, A. L.; Manners, I. *J. Chem. Soc., Dalton Trans.* **1995**, 1893-1899; (c) Ni, Y. Z.; Rulkens, R.; Pudelski, J. K.; Manners, I. *Macromol. Rapid Comm.* **1995**, *16*, 637-641; (d) Reddy, N. P.; Choi, N.; Shimada, S.; Tanaka, M. *Chem. Lett.* **1996**, 649-650; (e) MacLachlan, M. J.; Zheng, J.; Thieme, K.; Lough, A. J.; Manners, I.; Mordas, C.; LeSuer, R.; Geiger, W. E.; Liable-Sands, L. M.; Rheingold, A. L. *Polyhedron* **2000**, *19*, 275-289; (f) Calleja, G.; Carré, F.; Cerveau, G. *Organometallics* **2001**, *20*, 4211-4215; (g) Berenbaum, A.; Lough, A. J.; Manners, I. *Organometallics* **2002**, *21*, 4415-4424; (h) Bao, M.; Hatanaka, Y.; Shimada, S. *Chem. Lett.* **2004**, *33*, 520-521.
(11) Herberhold, M.; Bärtl, T. *Z. Naturforsch. B* **1995**, *50*, 1692-1698.
(12) (a) Dong, T. Y.; Hwang, M. Y.; Wen, Y. S.; Hwang, W. S. *J. Organomet. Chem.* **1990**, *391*, 377-385; (b) Jäkle, F.; Rulkens, R.; Zech, G.; Foucher, D. A.; Lough, A. J.; Manners, I. *Chem. Eur. J.* **1998**, *4*, 2117-2128; (c) Jäkle, F.; Rulkens, R.; Zech, G.; Massey, J.; Manners, I. *J. Am. Chem. Soc.* **2000**, *122*, 4231-4232; (d) Baumgartner, T.; Jäkle, F.; Rulkens, R.; Zech, G.; Lough, A. J.; Manners, I. *J. Am. Chem. Soc.* **2002**, *124*, 10062-10070.
(13) Utri, G.; Schwarzhans, K. E.; Allmaier, G. M. *Z. Naturforsch. B* **1990**, *45*, 755-762.
(14) Brunner, H.; Klankermayer, J.; Zabel, M. *J. Organomet. Chem.* **2000**, *601*, 211-219.
(15) Mizuta, T.; Onishi, M.; Miyoshi, K. *Organometallics* **2000**, *19*, 5005-5009.
(16) Mizuta, T.; Imamura, Y.; Miyoshi, K. *Organometallics* **2005**, *24*, 990-996.

(17) Ieong, N. S.; Chan, W. Y.; Lough, A. J.; Haddow, M. R.; Manners, I. *Chem. Eur. J.* **2008**, *14*, 1253-1263.
(18) (a) Lemenovskii, D. A.; Urazowski, I. F.; Baukova, T. V.; Arkhipov, I. L.; Stukan, R. A.; Perevalova, E. G. *J. Organomet. Chem.* **1984**, *264*, 283-288; (b) Kuzmina, I. G.; Struchkov, Y. T.; Lemenovsky, D. A.; Urazowsky, I. F. *J. Organomet. Chem.* **1984**, *277*, 147-151.
(19) (a) Herbert, D. E.; Mayer, U. F. J.; Manners, I. *Angew. Chem. Int. Ed.* **2007**, *46*, 5060-5081; (b) Bellas, V.; Rehahn, M. *Angew. Chem. Int. Ed.* **2007**, *46*, 5082-5104.
(20) (a) Schachner, J. A.; Lund, C. L.; Quail, J. W.; Müller, J. *Organometallics* **2005**, *24*, 785-787; (b) Schachner, J. A.; Quail, J. W.; Müller, J. *Acta Cryst.* **2008**, *E64*, m517.
(21) Schachner, J. A.; Lund, C. L.; Quail, J. W.; Müller, J. *Organometallics* **2005**, *24*, 4483-4488.
(22) Lund, C. L.; Schachner, J. A.; Quail, J. W.; Müller, J. *Organometallics* **2006**, *25*, 5817-5823.
(23) Schachner, J. A.; Tockner, S.; Lund, C. L.; Quail, J. W.; Rehahn, M.; Müller, J. *Organometallics* **2007**, *26*, 4658-4662.
(24) Lund, C. L.; Schachner, J. A.; Quail, J. W.; Müller, J. *J. Am. Chem. Soc.* **2007**, *129*, 9313-9320.
(25) Lund, C. L.; Schachner, J. A.; Burgess, I. J.; Quail, J. W.; Schatte, G.; Müller, J. *Inorg. Chem.* **2008**, *47*, 5992-6000.
(26) Lund, C. L.; Schachner, J. A.; Quail, J. W.; Müller, J. *Acta Cryst.* **2005**, *E61*, m2063-m2065.
(27) Often the Cp protons appear as pseudotriplets, however, in the case of **3**, the triplet structure is not resolved and they appear as singlets.
(28) Löwendahl, J.-M.; Håkansson, M. *Organometallics* **1995**, *14*, 4736-4741 and references therein.
(29) Löwendahl, M.; Davidsson, Ö.; Ahlberg, P. *J. Chem. Res., Synop.* **1993**, 40-41.
(30) H···H distances are only taken as an indication of possible steric interactions. The absolute values are not important as they do not reflect the real H···H distances, however, the comparison of H···H distances in two similar structures are meaningful.
(31) Holleman-Wiberg *Inorganic Chemistry*; 1. English ed.; Academic Press: San Diego, London, 2001, page 1756.
(32) Al-Juaid, S. S.; Eaborn, C.; Hitchcock, P. B.; Hill, M. S.; Smith, J. D. *Organometallics* **2000**, *19*, 3224-3231.
(33) Butler, I. R.; Cullen, W. R.; Ni, J.; Rettig, S. J. *Organometallics* **1985**, *4*, 2196-2201.
(34) Berger, S.; Braun, S. *200 and More NMR Experiments*; 3rd expanded ed.; WILEY-VCH: Weinheim, 2004, page 430 and 445.
(35) Bard, A. J.; Faulkner, L. R. *Electrochemical Methods*; 2nd ed.; John Wiley & Sons, Inc.: New York, 2001.
(36) Otwinowski, Z.; Minor, W. In *Macromolecular Crystallography, Part A*; Carter, C. W., Sweet, R. M., Eds.; Academic Press: London, 1997; Vol. 276, p 307-326.
(37) Altomare, A.; Burla, M. C.; Camalli, M.; Cascarano, G.; Giacovazzo, C.; Guagliardi, A.; Moliterni, A. G. G.; Polidori, G.; Spagna, R. *J. Appl. Crystallogr.* **1999**, *32*, 115-119.
(38) Sheldrick, G. M. *SHELXL97-2: Program for the Solution of Crystal Structures*; University of Göttingen, Germany, 1997.

9.7 Supporting Information

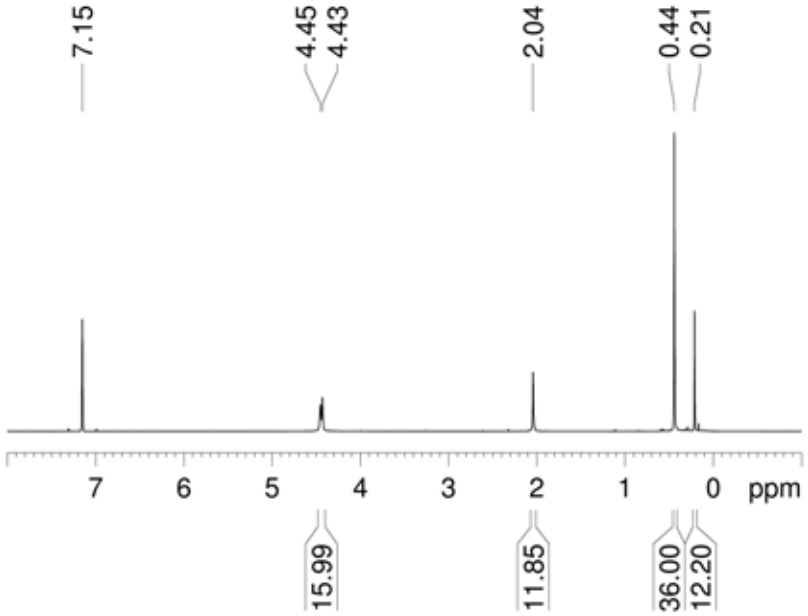

Figure 9-S1. ^{1}H NMR spectrum of compound (MeN$_2$tsi)In[1.1]FCP (**3**) at 25˚C (C$_6$D$_6$; 500 MHz). See experimental section for chemical shifts.

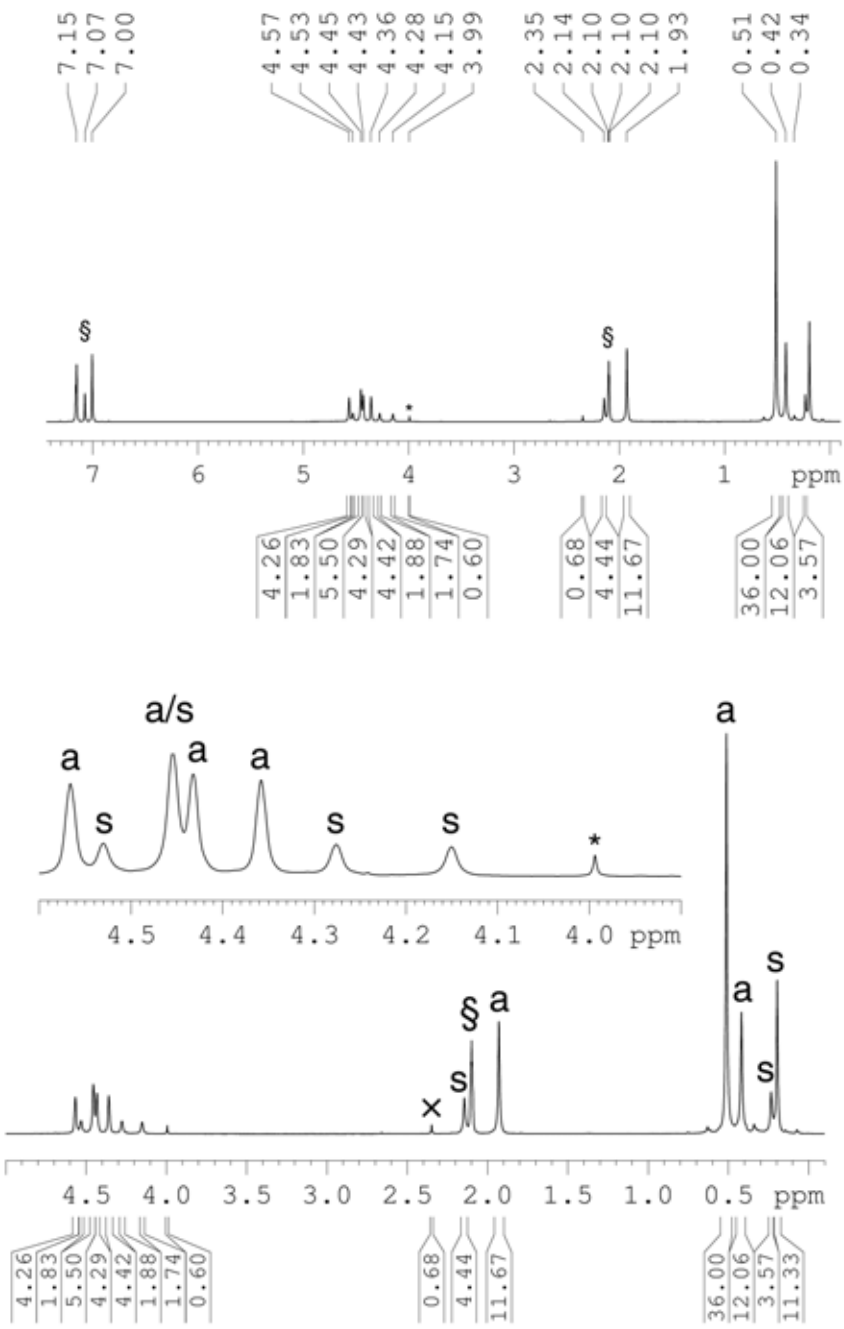

Figure 9-S2. ^{1}H NMR spectrum of compound (MeN$_2$tsi)In[1.1]FCP (**3**) at –30˚C (C_7D_8; 500 MHz). See experimental section for chemical shifts. § denotes solvent signals (C_7D_8), * denotes the resonance of $FeCp_2$, × denotes an unknown impurity, and "a" and "s" refers to the *anti*- and *syn* isomer, respectively.

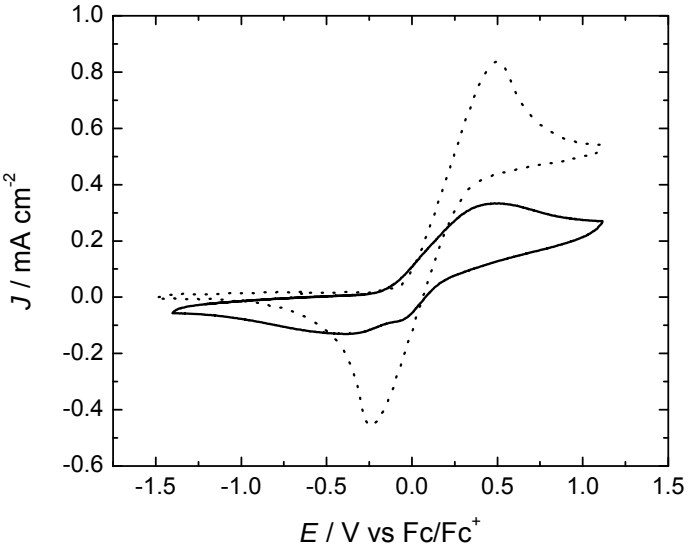

Figure 9-S3. Cyclic voltammogram of compound (MeN$_2$tsi)In[1.1]FCP (**3**) (solid line) and ferrocene (dotted line) in thf / 0.1M [Bu$_4$N][ClO$_4$] using a glassy carbon working electrode at a scan rate of 100 mV/s. The potential was measured versus a silver quasi reference electrode and subsequently re-referenced to the formal potential of ferrocene in 0.1M [Bu$_4$N][PF$_6$].

CHAPTER 10
SUMMARY and CONCLUSIONS

In-line with the first objective of this Ph.D. project, aluminum, gallium and indium compounds equipped with intramolecular coordinating ligands such as Pytsi, Me_2Ntsi, Me_2NCH_2tsi, Ar′, or p-*t*BuAr′ were synthesized (Figure 10-1). The ligands incorporate amine or pyridine donors with differing degrees of steric protection to satisfy the Lewis-acidic group-13 element.

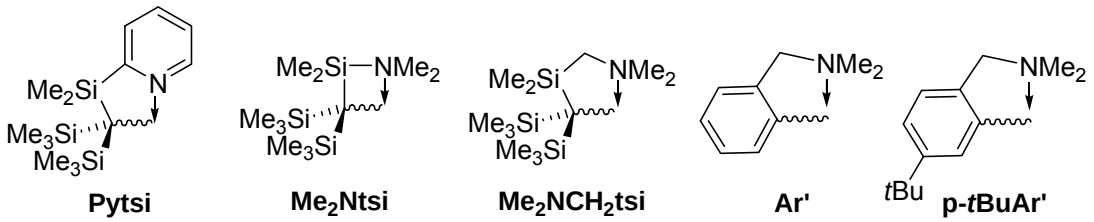

Figure 10-1. Intramolecular coordinating ligands utilized in this Ph.D. project.

By first targeting compounds with Pytsi-type ligands (Chapters 2, 3 and 4, pages 92-157; Figure 10-2), I was able to establish a foundation to build upon, comprised of well-defined group-13 compounds. Though I was never able to employ these species in preparing metallarenophanes, these compounds provided the groundwork for others to succeed in their respective projects. For example, (Pytsi)$AlMe_2$ (Figure 10-2a) was utilized by Olimpiu Stanga in preparing a reactive, cationic aluminum compound (Chapter 2, pages 92-112) and compounds of the type (Pytsi)EX_2 (Figure 10-2b) were employed by Jörg Schachner in the synthesis of strained aluminum- and gallium-bridged [1]FCPs (Chapter 4, pages 136-157). Pytsi-like compounds

featuring ortho-substituents on the pyridine ring (Figure 10-2a) were targeted as precursors for preparing aluminum cations because they offer considerably more steric protection than the parent compound (Pytsi)$AlMe_2$. This additional steric protection could possibly allow for stable cations to be generated (Chapter 3, pages 113-135).

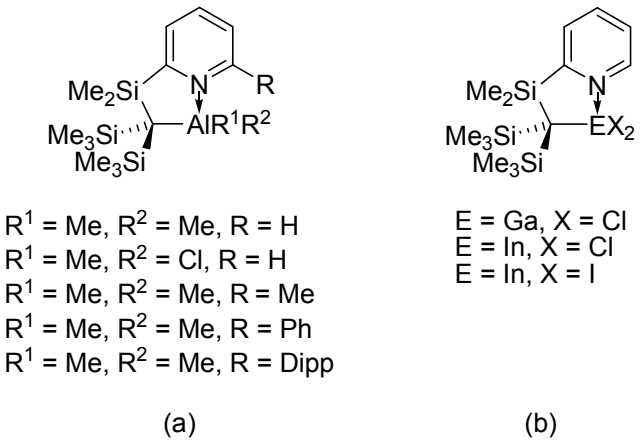

Figure 10-2. Novel compounds equipped with Pytsi-type ligands prepared during this Ph.D. project: (a) compounds incorporating AlMe moieties; (b) compounds incorporating EX_2 moieties.

As mentioned earlier, compounds of the type (Pytsi)EX_2 can be used to prepare [1]FCPs, albeit in low to moderate yields. Therefore, I targeted and prepared (Pytsi)$InCl_2$ (Chapter 4, pages 136-157), for the synthesis of an inda[1]FCP. However, (Pytsi)$InCl_2$ turned out to be a dimer in the solid state, with each five-fold coordinate indium atom bridged by two chlorine atoms and bound with two terminal chlorine atoms *trans* to each other (Figure 4-6, page 146). When (Pytsi)$InCl_2$ was reacted with dilithioferrocene, a ferrocenophane bridged by a In–$(\mu\text{-Cl})_2$–In moiety was produced (Figure 4-7, page 148). This bridging In–$(\mu\text{-Cl})_2$–In unit was similar to the one observed in the starting (Pytsi)$InCl_2$, which suggested that a monomeric indium dihalide was required to produce indium-bridged [1]metallacyclophanes. For this reason, I synthesized (Pytsi)InI_2 which was found to be a monomer with an unusual coordination geometry in the solid

state (Chapter 5, pages 158-167). The indium atom is in a four-fold coordinate environment, surrounded by a carbon, a nitrogen and by two iodine atoms (Figure 5-1, page 163). The geometry around the indium can be described as a trigonal bypyramid with one apical site unoccupied. Encouraged by the fact that (Pytsi)InI_2 was a monomer, it was anticipated that (Pytsi)InI_2 could be used to prepare [1]metallacyclophanes, but reactions of (Pytsi)InI_2 and dilithioferrocenes have only produced unidentifiable mixtures, to date.

Even though (Pytsi)EX_2 (E = Al, Ga) gave access to [1]FCPs, reactions of dilithiobis(benzene)metal complexes and (Pytsi)EX_2 did not produce [1]metallarenophanes, but only produced complex mixtures (Scheme 10-1) for unknown reasons.

Scheme 10-1. Unsuccessful synthesis of [1]metallarenophanes using (Pytsi)ECl_2.

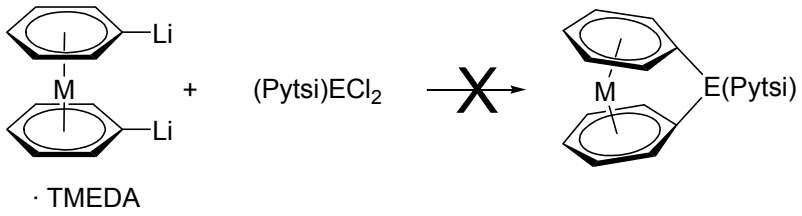

It was envisioned that a small alteration to the Pytsi ligand might allow for group-13-bridged [1]metallarenophanes to be prepared. Of the ample number of *trisyl*-based derivatives in the literature, I targeted the known compounds (Me_2Ntsi)ECl_2 with E = Al and Ga (Figure 10-1), because of their ease of preparation from the readily available $HC(SiMe_3)_2(SiMe_2Br)$, which had been used in the synthesis of the compounds of the type (Pytsi)EX_2.

By utilizing (Me_2Ntsi)$AlCl_2$ and (MeNtsi)$GaCl_2$, the first aluminum- and gallium-bridged [1]CAPs, [1]VAPs and [1]MAPs were prepared and isolated in moderate yields (Chapters 6 and 7, pages 168-220; Figure 10-3), thus reaching the primary goal of this Ph.D. project. These compounds represent the first examples of heavier group-13-bridged [1]metallarenophanes. I would like to point out that the [1]MAPs are the first strained bis(benzene)molybdenum species.

For this reason, diphenylsila[1]MAP was synthesized and characterized (Chapter 7, pages 193-220; Figure 10-3).

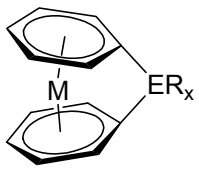

M = Cr, ER_x = Al(Me_2Ntsi)
M = Cr, ER_x = Ga(Me_2Ntsi)
M = V, ER_x = Al(Me_2Ntsi)
M = V, ER_x = Ga(Me_2Ntsi)
M = Mo, ER_x = Al(Me_2Ntsi)
M = Mo, ER_x = Ga(Me_2Ntsi)
M = Mo, ER_x = $SiPh_2$

Figure 10-3. Novel [1]metallarenophanes prepared during this Ph.D. project.

All [1]metallarenophanes were fully characterized by X-ray crystallography, revealing highly-tilted molecules (Table 10-1). In all cases, for any given [1]metallarenophane, the gallium-bridged [1]metallarenophanes have larger tilt angles compared to the analogous aluminum-bridged [1]metallarenophane for reasons that remain unknown (Chapter 8.4, pages 237-238). This difference becomes very pronounced when comparing the aluminum- and gallium-bridged [1]MAPs. On the basis of only the covalent radii of aluminum (1.25 Å) and gallium (1.26 Å),[1] a slightly larger tilt angle would be expected for an aluminum-bridged species in comparison with the respective gallium-bridged compound.

[1] Holleman-Wiberg *In Inorganic Chemistry*, 1st English ed.; Wiberg, N., Ed.; Academic Press: San Diego, 2001, 1756-1759.

Table 10-1. Tilt angles α determined from the solid-state structures of [1]metallarenophanes synthesized during this Ph.D. project.

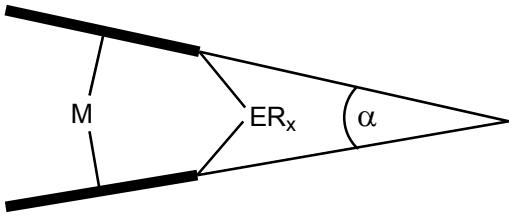

M	ER_x	α (°)
Cr	$Al(Me_2Ntsi)$	11.81(9)
Cr	$Ga(Me_2Ntsi)$	13.24(13)
V	$Al(Me_2Ntsi)$	14.65(14)
V	$Ga(Me_2Ntsi)$	15.63(14)
Mo	$Al(Me_2Ntsi)$	18.28(17)
Mo	$Ga(Me_2Ntsi)$	21.24(10)
Mo	$SiPh_2$	20.23(29)

Based on the successful use of aluminum and gallium compounds equipped with Me_2Ntsi ligands in the synthesis of [1]metallarenophanes, $(Me_2NCH_2tsi)AlCl_2$ was synthesized (Chapter 6, pages 168-192; Figures 10-1 and 10-4). However, it proved to be unreactive towards dilithium sandwich complexes.

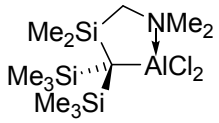

Figure 10-4. Compound $(Me_2NCH_2tsi)AlCl_2$ prepared during this Ph.D. project.

[1]Metallarenophanes synthesized during this Ph.D. project (Figure 10-3) were evaluated as possible monomers for producing organometallic polymers by ROP (Chapter 1.3, pages 29-49). ROP methodologies that have been applied to [1]metallarenophanes include thermal, anionic and transition-metal catalyzed ROP, with the latter methodology having found the most wide-spread success. To determine if the gallium-bridged [1]MAP is prone to undergo transition-metal catalyzed ROP, $[Pt(PEt_3)_3]$ was added with the expectation that a $[Pt(PEt_3)_2]$

moiety would insert into the strained C–Ga bond. However, from this reaction, the only isolable product was [(η^6-C_6H_6)Mo{η^6-C_6H_5[GaPh(Me_2Ntsi)]}] (Figure 7-8, page 206). Through a series of NMR tube experiments it was determined that the ring-opening reaction was catalyzed by donor molecules like thf, PEt_3 or cod, with solvent benzene being incorporated in the isolated molecule. This is an unprecedented reactivity of a bis(benzene)molybdenum derivative and a similar ring-opening reaction of [1]metallacyclophanes is not reported in the literature. All attempts to utilize these donor molecules as initiators for ROP of [1]metallarenophanes have not been successful, to date. Therefore, the aluminum- and gallium-bridged [1]metallarenophanes were resistant to transition-metal catalyzed ROP with steric congestion at the bridging element being a possible cause (Chapter 7, pages 193-220).

To succeed at the third objective of synthesizing group-13-bridged [1.1]metallarenophanes, I adopted an approach used before in the preparation of group-13-bridged [1.1]FCPs (Chapter 1.4.2, pages 54-58).[2,3] A reaction of Ar′$AlCl_2$ (Figure 10-1) with [$Cr(C_6H_5Li)_2$]·tmeda produced the first [1.1]CAP (Figure 10-5). The poor solubility of this [1.1]CAP in organic solvents, prompted me to synthesize new intramolecularly coordinated compounds, (p-*t*BuAr′)$AlCl_2$ and (p-*t*BuAr′)$GaCl_2$ (Figure 10-1). The salt-metathesis reactions of these group-13 dihalides with [$M(C_6H_5Li)_2$]·tmeda (M = Cr, Mo) resulted in the formation of four new [1.1]metallarenophanes with improved solubility (Figure 10-5).

[2] Braunschweig, H.; Burschka, C.; Clentsmith, G. K. B.; Kupfer, T.; Radacki, K. *Inorg. Chem.* **2005**, *44*, 4906-4908.
[3] Schachner, J. A.; Orlowski, G. A.; Quail, J. W.; Kraatz, H.-B.; Müller, J. *Inorg. Chem.* **2006**, *45*, 454-459.

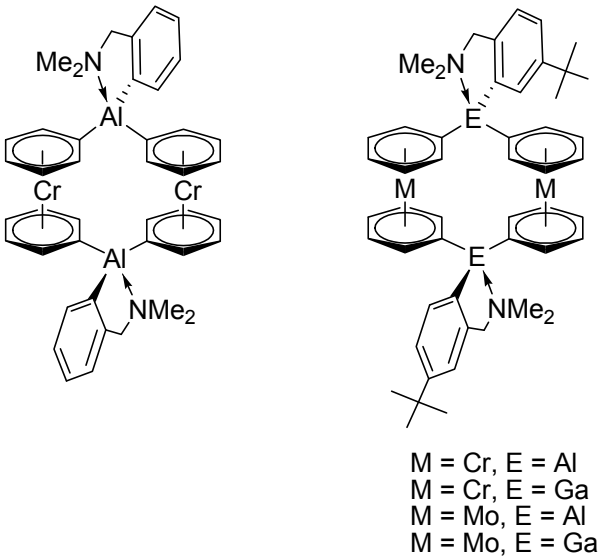

Figure 10-5. Novel [1.1]metallarenophanes prepared during this Ph.D. project.

All [1.1]metallarenophanes were characterized by single-crystal X-ray analysis. The solid-state structures of the [1.1]metallarenophanes revealed molecules in *anti* conformations with Me_2N groups occupying *exo* positions. The electronic communication between the metal centres in these [1.1]metallarenophanes, bridged by group-13 elements equipped with p-*t*BuAr′ ligands, were investigated by cyclic voltammetry. Whereas the gallium-bridged species turned out to be Class II compounds (Figures 8-5 and 8-6, page 236), the results for the respective aluminum species were inconclusive possibly due to their sensitivity towards air, moisture and electrolytes used.

After successfully preparing aluminum- and gallium-bridged [1]- and [1.1]metallarenophanes, another attempt to synthesize an inda[1]metallacyclophane was undertaken. Based on earlier results, it was envisioned that the reaction of an indium dihalide, equipped with the Me_2Ntsi ligand, and a dilithium metal complex should produce a metallacyclophane. For this reason, I synthesized (Me_2Ntsi)$InCl_2$ (Figure 10-6). Interestingly,

when $(Me_2Ntsi)InCl_2$ was added to dilithioferrocene·2/3 tmeda, a diinda[1.1]FCP was obtained (Figure 9-6, page 261). This [1.1]FCP crystallized as an *anti* isomer with the Me_2N groups occupying *exo* positions.

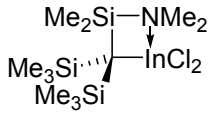

Figure 10-6. Compound $(Me_2Ntsi)InCl_2$ synthesized during this Ph.D. project.

Several conclusions can be drawn from this Ph.D. work. First, the steric requirements of the ligand bound to a group-13 dihalide has a dramatic influence on whether [1]metallacyclophanes or [1.1]metallacyclophanes will be produced from reactions of these dihalides with dilithium sandwich complexes. The Me_2Ntsi ligand stabilized strained aluminum- and gallium-bridged [1]CAPs, [1]VAPs and [1]MAPs, allowing them to be isolated (Chapters 6 and 7, pages 168-220). When the "slimmer" Ar′ and p-*t*BuAr′ ligands were bound to aluminum or gallium dichlorides, unstrained [1.1]CAPs or [1.1]MAPs could be isolated from salt-metathesis reactions (Chapter 8, 221-250). Surprisingly, when indium was bound to Me_2Ntsi and reacted with dilithioferrocene, an unstrained [1.1]FCP was formed (Chapter 9, pages 251-281). All these results can be rationalized by assuming that potential steric interactions between α-protons of the sandwich complex and H atoms of the respective stabilizing ligand bound to the bridging element are of major importance. In short, salt metathesis reactions described in this Ph.D. thesis are kinetically controlled and either give [1.1]metallacyclophanes or [1]metallacyclophanes. The available space between α-protons and H atoms of the ligand backbone is more restricted in a [1.1]metallacyclophane than in a [1]metallacyclophane. Therefore, as soon as these H-H interactions start to play a prominent role, the formation of a

[1.1]metallacyclophane is prevented and a strained [1]metallacyclophane is formed. For a detailed discussion see Chapter 9.4 (pages 268-271).

The tilt angles α were found to be larger for a galla[1]metallarenophane when compared to an analogous alumina[1]metallarenophane. For example, the gallium-bridged [1]MAP with an α tilt angle of 21.24(10)º is significantly higher tilted than its aluminum counterpart [α = 18.28(17)°] (Chapter 7, pages 193-220). One can assume that a larger tilt angle also means a higher degree of strain, such that the gallium-bridged [1]metallacyclophanes are more strained than their aluminum counterparts. This is counterintuitive because the slightly smaller Al atom should result in a slightly larger tilt angle α. A similar but less pronounced difference was observed for the [1]CAPs and [1]VAPs (Chapter 6, pages 168-192); the reasons for the structural differences are unknown.

The group-13-bridged [1]metallarenophanes prepared during this thesis were surprisingly resistant to transition-metal catalyzed ROP, presumably due to steric overprotection at the bridging element–*ipso* carbon bond. The thermally robust gallium-bridged [1]MAP could be ring-opened in the presence of donor ligands like PEt_3, cod, and thf, respectively, adding one equivalent of solvent benzene to give the unstrained complex $[(\eta^6\text{-}C_6H_6)Mo\{\eta^6\text{-}C_6H_5[GaPh(Me_2Ntsi)]\}]$ (Chapter 7, pages 193-220). The reaction with thf proceeds very cleanly giving this unstrained complex exclusively, showing that donor molecules catalyze this ring-opening reaction. This allows benzene to eventually replace the σ donor ligand and the η^6-phenyl group. As mentioned earlier, this is an unprecedented reactivity of a [1]metallacyclophane. [1]MAPs are not thermally labile, contrary to earlier reports (Chapter 1.1.4, pages 13-14). [1]Metallarenophanes prepared during this thesis project can potentially be

converted to organometallic polymers via ROP. It remains to be seen what interesting and unique properties these anticipated polymers will possess.